DEVELOPMENT OF POLY(METHYL METHACRYLATE-CO-METHACRYLIC ACID) BASED ELECTROLYTES WITH SYNTHESIZED AND COMMERCIAL IONIC LIQUIDS FOR DYE SENSITIZED SOLAR CELLS

VHAISSNAVI SUNDARARAJAN

FACULTY OF SCIENCE
UNIVERSITI MALAYA
KUALA LUMPUR

2021

Universiti Malaya

DEVELOPMENT OF POLY(METHYL METHACRYLATE-CO-METHACRYLIC ACID) BASED ELECTROLYTES WITH SYNTHESIZED AND COMMERCIAL IONIC LIQUIDS FOR DYE SENSITIZED SOLAR CELLS

VHAISSNAVI SUNDARARAJAN

THESIS SUBMITTED IN FULFILMENT OF THE REQUIREMENTS FOR THE DEGREE OF DOCTOR OF PHILOSOPHY

DEPARTMENT OF PHYSICS
FACULTY OF SCIENCE
UNIVERSITI MALAYA
KUALA LUMPUR

2021

Universiti Malaya

UNIVERSITI MALAYA

ORIGINAL LITERARY WORK DECLARATION

Name of Candidate: **VHAISSNAVI SUNDARARAJAN**

Matric No: **SVA170044**

Name of Degree: **DOCTOR OF PHILOSOPHY**

Title of Thesis:

DEVELOPMENT OF POLY (METHYL METHACRYLATE-CO METHACRYLIC ACID) BASED ELECTROLYTES WITH SYNTHESIZED AND COMMERCIAL IONIC LIQUIDS FOR DYE SENSITIZED SOLAR CELLS

Field of Study**: ADVANCED MATERIALS**

I do solemnly and sincerely declare that:

(1) I am the sole author/writer of this Work;
(2) This Work is original;
(3) Any use of any work in which copyright exists was done by way of fair dealing and for permitted purposes and any excerpt or extract from, or reference to or reproduction of any copyright work has been disclosed expressly and sufficiently and the title of the Work and its authorship have been acknowledged in this Work;
(4) I do not have any actual knowledge nor do I ought reasonably to know that the making of this work constitutes an infringement of any copyright work;
(5) I hereby assign all and every rights in the copyright to this Work to the University of Malaya ("UM"), who henceforth shall be owner of the copyright in this Work and that any reproduction or use in any form or by any means whatsoever is prohibited without the written consent of UM having been first had and obtained;
(6) I am fully aware that if in the course of making this Work I have infringed any copyright whether intentionally or otherwise, I may be subject to legal action or any other action as may be determined by UM.

Candidate's Signature Date:

19 February 2021

Subscribed and solemnly declared before,

Witness's Signature Date: 19/02/2021

Name:

Designation:

University of Malaya

DEVELOPMENT OF POLY(METHYL METHACRYLATE-CO-METHACRYLIC ACID) BASED ELECTROLYTES WITH SYNTHESIZED AND COMMERCIAL IONIC LIQUIDS FOR DYE SENSITIZED SOLAR CELLS

ABSTRACT

A persistent challenge for expanding global population and soaring economic progress has always been ensuring everyone has enough access to energy supply. At present, the high dependency on fossil fuel derived energy has led to a crisis that necessitated a shift of attention towards greener energy sources like solar. Solar energy serves as the most consistent back up energy and the best option for environmental conservation. Among the listed solar harvesters, dye sensitized solar cells (DSSCs) bring about vast potential in efficient conversion of solar to electrical energy. The fact that this discovery has not reached its pinnacle and every constituent of the cell still needs working on, a popular research interest would be the replacement of liquid electrolytes with gel polymer counterparts. Being a hybrid, gel polymer electrolytes (GPEs) retain the cohesive nature of solid electrolytes and stay diffusive as liquid electrolytes producing reasonable ionic conductivity and maintains good contact between components within the DSSCs., In that perspective, this work examines a series of poly(methyl methacrylate-co-methacrylic acid) P(MMA-co-MAA) based PE system for DSSCs. Initial sample preparation steps were modified by varying the ratio of I_2/I_3^- redox mediator from a sodium salt, copolymer and solvent used. As a part of secondary electrolyte systems studied, novel quinolinium based ionic liquids (ILs) were incorporated to the best single salt system. Great care was taken during the synthesis and purification of N-butyl-6-methylquinolinium bis(trifluoromethylsulfonyl) imide [C_4mquin][NTf_2] and N-butyl-6-methylquinolinium iodide [C_4mquin][I] ILs in order to achieve low impurity levels. Exploring the new cation-anion combined IL for the purpose of DSSCs was necessary to achieve better and more sustained electrolyte conductivity. Subsequently, the prepared electrolyte mixtures

Universiti Malaya

were tested with a standard DSSC configuration of glass/FTO/TiO_2/N719 dye/electrolyte/Pt/FTO/glass with active area of 0.3 cm^2. The single salt system samples were able to achieve highest ionic conductivity and power conversion efficiency (PCE) of 1.07 mS cm^{-1} and 2.34%, respectively. Remarkably, upon the addition of the quinolinium IL, the ionic conductivity and PCE had increased to 2.26 mS cm^{-1} and 5.67%, respectively for [C_4mquin][NTf_2] and 2.64 mS cm^{-1} and 4.98%, respectively for [C_4mquin][I] at its optimum concentration. As to emphasis the role of novel quinolinium based IL containing electrolytes in DSSCs, the efficiency of these cells were compared with DSSCs assembled with a commercialized a used imidazolium IL, [C_6mim][I] which recorded a maximum ionic conductivity of 2.23 mS cm^{-1} with PCE of 5.30%. The developed polymer electrolyte samples were also characterized with X-ray diffractometer (XRD), Fourier transform infrared spectroscopy (FTIR) and Thermogravitimetry Analyzer (TGA). As an additional diagnosis to understand the performance and electrochemical properties of PEs in DSSCs, electrochemical impedance studies were conducted to elucidate charge transfer processes occurring at interfacial within the cell. The performance of the quinolinium containing DSSCs has been improved by enhanced electron transport properties, reduced charge recombination and increased electron lifetime. Overall, the quinolinium based PEs prepared have performed better than anticipated, considering the sole participation with a single salt system, the bulkiness of cation present and quasi-solid nature unlike most commercially available ILs.

Keywords: ionic liquid, polymer electrolyte, dye-sensitized solar cells.

Universiti Malaya

DEVELOPMENT OF POLY(METHYL METHACRYLATE-CO-METHACRYLIC ACID) BASED ELECTROLYTES WITH SYNTHESIZED AND COMMERCIAL IONIC LIQUIDS FOR DYE SENSITIZED SOLAR CELLS

ABSTRAK

Perkembangan populasi global dan kemajuan ekonomi yang pesat telah menimbulkan suatu cabaran yang berterusan untuk sentiasa memastikan setiap manusia mempunyai akses kepada bekalan tenaga yang mencukupi. Pada masa ini, ketergantungan yang tinggi pada tenaga hasil daripada bahan pembakaran fosil telah menyebabkan krisis yang mendesak peralihan perhatian ke arah sumber tenaga yang lebih hijau seperti solar. Tenaga solar adalah tenaga yang paling konsisten dan pilihan terbaik untuk pemeliharaan alam sekitar. Antara sel solar yang disenaraikan, sel solar sensitif pewarna (DSSC) amat berpotensi dan cekap dalam penukaran tenaga suria kepada tenaga elektrik. Hakikatnya, penemuan ini masih belum mencapai kemuncaknya dan setiap komponen sel masih perlu dikaji, jadi, salah satu fokus penyelidikan adalah penggantian elektrolit jenis cecair dengan elektrolit gel berasaskan polimer (GPE). GPE bersifat hibrid dan boleh mengekalkan sifat kohesif seperti elektrolit pepejal serta kekal difusif sebagai elektrolit cecair. Ia mampu menghasilkan kekonduksian ionik. Dari perspektif itu, kajian ini meneliti serangkaian sistem elektrolit polimer berasaskan poly(methyl methacrylate-co-methacrylic acid) P(MMA-co-MAA) untuk digunakan dalam DSSCs. Langkah-langkah penyediaan sampel awal diubahsuai dengan mengubah nisbah bahan redoks I_2/I_3^-daripada garam natrium, kopolimer dan pelarut yang digunakan. Sebagai sebahagian daripada sistem elektrolit sekunder yang dikaji, cecair ionik (IL) berasaskan quinolinium telah ditambahkan ke dalam sistem elektrolit asas yang terbaik. Sintesis IL N-butyl-6-methylquinolinium bis(trifluoromethylsulfonyl) imide $[C_4mquin][NTf_2]$ dan N-butyl-6-methylquinolinium iodide $[C_4mquin][I]$ diberi perhatian tambahan untuk memastikan tahap impuriti yang rendah. Penerokaan IL yang mempunyai kombinasi kation– anion

Universiti Malaya

yang baru bagi tujuan DSSC perlu untuk mencapai kekonduksian elektrolit yang lebih baik dan lebih mantap. Seterusnya, campuran elektrolit yang telah disediakan diuji dengan konfigurasi piawai DSSC iaitu kaca /FTO /TiO_2/pewarnaN719/elektrolit/Pt/FTO/kaca dengan keluasan aktif bernilai 0.3 cm^2.Sampel sistem asas dengan hanya garam dan tanpa IL dapat mencapai kekonduksian ionik tertinggi bernilai 1.07 mS cm^{-1} dan kuasa penukaran fotovoltaik (PCE) 2.34%. Tambahan pula, dengan penambahan IL quinolinium, kekonduksian ionik dan kecekapan PCE meningkat kepada 2.26 mS cm^{-1} dan 5.67% untuk [C_4mquin][NTf_2] serta 2.64 mS cm^{-1} dan 4.98%, untuk [C_4mquin][I] pada kepekatan optimumnya. Sebagai penekanan kefungsian elektrolit yang mengandungi IL quinolinum, kecekapan sel ini dibandingkan dengan DSSC yang mengandungi elektrolit dengan IL imidazolium, [C_6mim][I] yang mencatatkan kekonduksian ionik maksimum 2.23 mS cm^{-1} dengan kecekapan penukaran kuasa sebanyak 5.3%. Sampel-sampel GPE yang dihasilkan turut dikaji ciri-cirinya dengan kajian difraksi sinar- X (XRD), transformasi Fourier inframerah (FTIR) dan analisis termogravimetri (TGA). Sebagai diagnosis tambahan untuk memahami prestasi dan sifat elektrokimia GPE dalam DSSC, kajian impedans elektrokimia telah dijalankan untuk menjelaskan proses pemindahan caj yang berlaku pada peantaraan komponen dalam sel. Prestasi DSSCs yang mengandungi IL quinolinium berjaya dipertingkatkan kerana pengangkutan elektron bertambah, penggabungan cas berkurang dan jangka hayat electron meningkat. Secara keseluruhannya, GPE berasaskan quinolinium yang disediakan telah menunjukkan prestasi yang lebih baik daripada yang dijangkakan memandangkan penyertaan tunggal bersama sistem garam, kationnya yang besar dan sifat separa pepejalnya yang tidak seperti kebanyakan IL yang boleh didapati secara komersil.

Kata kunci: cecair ionik, elektrolit polimer, sel solar sensitif pewarna.

Universiti Malaya

ACKNOWLEDGEMENTS

எல்லா புகழும் இறைவனுக்கே. Penning down this humble note of thanks after several months of intensive thesis writing brings much content as I reflect on the support and help I received from many kind souls in the course of this endeavour.

First and foremost, I thank both my supervisors Prof. Dr. Ramesh T Subramaniam and Assoc. Prof. Dr. Ramesh Kasi for rewarding me with a gratifying postgraduate study experience through their research group. Thank you for giving me invaluable advice, insightful suggestions, intellectual freedom, financial support as well as the push in meeting high standard of work in all my accomplishments.

Next, I extend my heartfelt appreciation to my constant lab-mates, Dr. Hon Ming, Dr. Fatin, Dr. Shahid, Khuzaimah, Shahira, Maryam and Surender for their friendship, support and kindness in helping me at many instance. I am also indebted to Gowri from UTP for her valuable help and insights for this research. Without all their involvement, completing this work would not have been possible.

My PhD journey has been an intense period of learning not only in science but also very much at a personal level. I owe a heartfelt gratefulness to my whole family and in-laws for their selfless help, good thoughts and unwavering support. This endeavour would not have been possible without them. And to my husband, I thank you so much, thou it does not suffice your positive impetus on me that brought me this far.

Finally, my heartiest gratitude to the most divine and precious relation in my life, my mother, my guardian angel-Kamala, whom I believe have been the light that guided me from within. I dedicate this milestone to you ***Amma.***

Universiti Malaya

TABLE OF CONTENTS

Universiti Malaya

Universiti Malaya

Universiti Malaya

Universiti Malaya

Universiti Malaya

LIST OF FIGURES

Universiti Malaya

Universiti Malaya

Universiti Malaya

Universiti Malaya

Universiti Malaya

LIST OF TABLES

Universiti Malaya

Universiti Malaya

Universiti Malaya

LIST OF SYMBOLS AND ABBREVIATIONS

η	:	photovoltaic conversion efficiency
J_{sc}	:	short-circuit current density
V_{oc}	:	open circuit voltage
DSSC	:	dye sensitized solar cells
EIS	:	electrochemical impedance spectroscopy
FF	:	fill factor
FTIR	:	Fourier Transform Infrared
GPE	:	gel polymer electrolyte
HMImI	:	1-hexyl-3-methylimidazolium iodide
NaI	:	sodium iodide
PCE	:	power conversion efficiency
P(MMA-co-MAA)	:	poly(methyl methacrylate-co-methacrylic acid)
Pt	:	platinum
TGA	:	Thermogravimetry Analysis
XRD	:	X-ray Diffractometer

Universiti Malaya

LIST OF APPENDIX

Universiti Malaya

CHAPTER 1- INTRODUCTION

1.1 Motivation

The pressing challenge for global development has always been ensuring everyone has enough access to energy systems. It is indeed undeniable that the historical and current energy schemes rely heavily on fossil fuels (coal, oil and natural gas). Thus, human wellbeing is challenged between economic development and environmental impacts. The 2019 BP statistical review on world energy, claims that we are falling short in achieving the transition envisaged by the Paris Agreement signed by 195 participating countries in 2015 to lower their carbon emission as a way to reduce greenhouse effect and curb accelerated global warming (BP Statistical Review of World Energy, 2019). This unsustainable path demands a growth in renewable generation of energy to decarbonize the power sector. One way would be to pursue the omnipresent solar energy.

Solar energy is the most consistent backup energy owing to its high reliability with almost no pollutant release. Besides, this truly renewable energy source is not only restricted to generate electricity but also supplies thermal energy for clean water supplies. Most importantly, the constant technology advancement and improvements in the solar power industry, be it in quantum physics, chemistry or nanotechnology, see the potential increase in effectiveness of solar power systems through the increase in electricity input in the coming years. Other common forms of renewable resources include wind, geothermal, bioenergy and hydroelectric. Despite their own advantages, a common shortfall among these listed resources are the difficulty in producing the same and consistent amount of electricity that are as large as conventional fossil fuel sources.

Malaysia, a country known for its strategic geographical location and its equatorial position allows the country to see 365 days of sunlight. However, only 2% of Malaysia`s electricity is generated by cumulative renewable resources and the nation is still highly

Universiti Malaya

dependent on its limited fossil fuel reserves to meet demands (Chu, 2019). At current, our government aims to increase the nation's dependency on renewable energy mix from 2% to 20% in the next 10 years by targeting commercial and industrial buildings to fix photovoltaic devices. Utilizing solar energy in Malaysia from fitted photovoltaic devices is foreseen to yield a whopping 34,200 MW electricity at an instance. This value significantly surpluses the current total electricity production of 24,000 MW.

On the downside, installation of solar panels or creation of solar farms use solar harvesting devices that are mostly made of silicon hence, the exorbitant initial cost is less favoured by its consumers. Besides, the efficiency of a solar cell depends on weather as well. Yes, solar energy can be still harvested during rainy or cloudy days, but efficiency is significantly affected (Islam, 2009). Thus, this has motivated extensive research around the world to develop a much affordable and effective alternative for conventional silicon solar cells.

1.2 Research Objectives

This research aims to achieve the objectives listed below:

1. To develop poly(methyl methacrylate-co-methacrylic acid) P(MMA-co-MAA) based gel polymer electrolytes (GPEs) with the addition of an iodide salt suitable for the fabrication of dye sensitized solar cells (DSSCs).
2. To characterize the prepared P(MMA-co-MAA) based GPEs using various techniques namely Electrochemical Impedance Spectroscopy (EIS), Fourier Transform Infrared spectroscopy (FTIR), X-ray Diffraction spectroscopy (XRD) and Thermogravimetric analysis (TGA).
3. To formulate GPEs by incorporating novel synthesized and commercial ionic liquids.

Universiti Malaya

4. To evaluate the performance of the ionic liquid based P(MMA-co-MAA) GPEs in terms of physical, structural, thermal and electrical properties.
5. To fabricate DSSCs using the developed P(MMA-co-MAA) based GPEs and investigate the efficiency of the synthesized and commercial ionic liquids.

1.3 Novelty

Poly(methyl methacrylate), PMMA based polymeric conductors have been widely prepared and investigated as electrolytes in the photovoltaic industry. Previous works concentrate mainly on PMMA blend polymer electrolytes like PVdF–HFP/PMMA, PVA/PMMA, PVAc/PMMA and PVdC-AN/PMMA for the use of DSSCs (Mathew, Kesavan, & Rajendran, 2015; Park, Lee, Park, & Choi, 2007). These polymer blends have shown ionic conductivity up to ~10^3 S cm^{-1}. However, blend systems are very much subjected to phase separation over a period of time. Up to date, there is no report on the use of a co-polymer of PMMA containing methacrylic acid except the work by Li et al.,

on lab cooked P(MMA-co-MAA)/PEG blends which cannot be deemed analogous (Li, Wu, Huang, Hao, Lan, Li, & Kang, 2007). On top of this, the effect of ionic liquids in P(MMA-co-MAA) electrolytes is also investigated throughout this research. Two novel ionic liquids which are N-butyl-6-methylquinolinium bis(trifluoromethylsulfonyl) imide [C_4mquin][NTf_2] and N-butyl-6-methylquinolinium iodide [C_4mquin][I] were separately added into P(MMA-co-MAA) polymer electrolytes in this work. A comparative research was necessary to study the effect of ion diffusion in the polymer electrolytes. Besides, the P(MMA-co-MAA) polymer electrolytes and ionic liquid–added polymer electrolytes are also applied in the DSSC fabrication to study the potential application in photovoltaic technology.

Universiti Malaya

1.4 Research scope

The research scope covers the listed research fundamentals made to achieve the research goal.

1. Development of novel polymer electrolytes to improve DSSC efficiency.

The electrolyte mixtures were prepared and the most suitable electrolyte composition for optimum performances was determined. The iodide/iodine ratio was altered to test the effect of iodine on ionic conductivity and the DSSC performance. The most appropriate electrolyte was selected to include ionic liquid and further tested the effect on DSSC performance.

2. Characterization of DSSCs

DSSCs were assembled with the developed electrolytes and the conversion efficiency of the cell was evaluated. The cell stability was also examined to confirm efficient conversion of solar energy to electrical energy for longer time. Solar cell performance was monitored through current-voltage measurements and electrochemical impedance spectroscopy. The effect of addition of ionic liquids on DSSC performance was equally analysed.

Universiti Malaya

1.5 Thesis outline

This thesis collocates into six chapters as briefed below.

1. Chapter One outlines research background, objectives and research scope.
2. Chapter Two gives an overview of milestones achieved and recent developments in utilizing polymer electrolytes and ionic liquids in improving overall performance in DSSCs.
3. Chapter Three discourses all conducted experimental methodologies in this research.
4. Chapter Four discusses all experimental results obtained in this research.
5. Chapter Five compares the photovoltaic performance of the systems presented in Chapter Four and summarizes them.
6. Chapter Six concludes the findings of this research and their importance. Suggestions for prospective research are also included.

Universiti Malaya

CHAPTER 2: LITERATURE REVIEW

2.1 Introduction to chapter

This chapter discusses on the cardinal development of polymer based electrolytes for DSSCs. Firstly, the fundamental theories in DSSCs, major components present and the general working mechanism is introduced. This is followed by, a brief comparison of DSSC with other 3rd generation solar cells. Thirdly, the use of polymer electrolytes in DSSCs is comprehensively deliberated. This includes the transport mechanism occurring and strategies used to improve overall performance of GPEs as applied in DSSCs. Finally, reasons for research choice will be summarized.

2.2 Dye Sensitized Solar Cells (DSSCs)

The role of converting solar energy directly to electrical power has been successively done by photovoltaic devices like silicon-based, organic, inorganic and hybrid solar cells. Silicon solar cells still dominate the solar market but with their high module costing and complex assembly, extensive domestic use is limited. Thus, research resorts to organic solar cells which are relatively cheaper and easy to fabricate in order to make this technology available to everyone.

In 1991, O`Reagan and Gratzel built a tiny cell comprising of dye-coated nanoporous semiconductor and a metal electrode separated by a thin layer of redox electrolyte in the middle (Oregan & Gratzel, 1991). Thus, came the name dye-sensitized solar cell or shortly DSSC. The cell was able to produce photoelectric power conversion efficiency exceeding 7% which was approximately 80% photon to electric current conversion. In terms of costing, the simple set up was only 20% of a mainstream silicon crystalline panel price (Jacoby, 2016). Efficient conversion of solar energy to electrical energy alike photosynthesis in plants, along with low costing technology stirred continuous research

Universiti Malaya

on DSSCs ever since its discovery. At current, based on National Renewable Energy Laboratory (NREL) data on confirmed conversion efficiencies for a range of photovoltaic technologies, DSSC marks a highest value of 12.3% as shown in figure below.

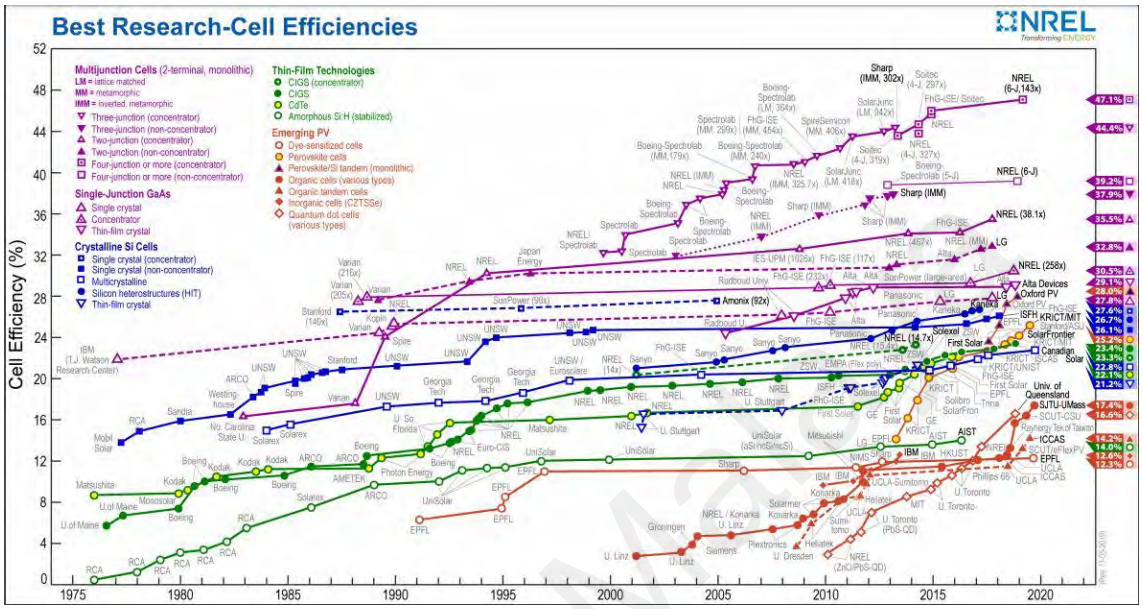

Figure 2.1: Efficiencies for various photovoltaic technologies till present. This plot is courtesy of the National Renewable Energy Laboratory, Golden, CO.

DSSCs can be deemed as a revolution in the solar harvesting industry. In comparison to silicon solar wafers, DSSC have relatively cheaper starting materials and production cost. The light weighted materials used in DSSCs do not require special protection thus, making them an easy to handle device. The mechanical robustness DSSC provides is a key factor that prolongs the life time of the cell. Besides, DSSCs offer versatility in the terms structure and flexibility as they come in different sizes and some with bending ability.

Generally, silicon solar cells are more susceptible to internal heating due to mechanically driven electron flow which requires coolants in a glass box to prevent cell damage due to overheating. This is an unlikely scenario with DSSCs as they are made with thin layer plastics that are capable of radiating heat. The lesser internal heat, the better power conversion efficiency (Rhee et al., 2014).

Universiti Malaya

In contrast to traditional solar cells, the ability of DSSC to function under dim-light condition is another drawing factor that gains great research interest. The profound capability of DSSC to work under illumination below normal ranges is due to the dye used which absorbs both fluorescent lights and diffused sunlight. Nevertheless, less impact was found on power conversion efficiencies making DSSC suitable for use in cloudy weather and poor sunlight areas. Hence, DSSCs are a boon to the countries with climates where conventional solar cells would fail.

With about 11% power production efficiency commercially, DSSCs make good candidates for low-density indoor applications. Despite not having a remarkable efficiency compared to other solar harvesting devices, DSSCs remain superlative in terms of price-to-power ratio.

2.2.1 Competitors and commercialization of DSSC.

Currently, the development and commercialization of photovoltaic (PV) technology marks into a third generation of devices. Unlike its predecessors, the third generation of PV cells look ahead to produce optimize energy conversion efficiencies on a decreased cost which includes organic solar cells, quantum dot solar cells, perovskite sensitized solar cells and of course, DSSCs. By far, majority of the listed PV devices are still in the research step. These 3rd generation of cells vary extensively based on the materials used to construct, working principles and production techniques. (Mozaffari et al. 2017)

In terms of overall cell efficiency, perovskite sensitized cells top the list with remarkable efficiency improvement to 22% in a span of 7 years. This new kind of solar cell has amazed researchers with its performance nevertheless falls short in competing in the green energy market. These cells rely heavily on environmentally hazardous heavy metals and have minimal to no tolerance to moisture. Besides, the lifetime of these cells under outdoor condition is still uncertain. Unless these key issues can be resolved in near

Universiti Malaya

future, DSSCs are considered as the most prospective and greenest 3rd generation PV device. According to Professor Michael Gratzel theoretical efficiency calculation for DSSCs revealed an achievable power conversion efficiency of 32% which is far superior than operating perovskite sensitized solar cells or even the previous generation of solar cells. (GCell, n.d.)

If that's so, why isn't DSSCs are extensively commercialized? The attempt is still being postponed due to the relatively lower achievement in cell efficiency and poor long term outdoor stability caused mainly by the use of liquid electrolytes. Alternatives like ionic liquid and polymer gel based electrolytes have been tested upon, however the lower efficiency recorded hinders further progress. The slow progress and difficulty in scaling up does foster an impression that DSSCs have failed to fulfil needs. Conversely, G24 Power from Wales is commercializing DSSC technology with few products available under the brand name GCell. However, there is no information on the nature of electrolytes used in these devices. The alluring opportunities for DSSC market in foreseen in the near future for building integrated photovoltaic system along with indoor and portable applications. Portable charging is likely to lead the application wing of DSSC market. As for regional marketing prospects, Europe held the largest share for DSSC commercialization in 2017. This trend is now changing with Asia Pacific being estimated as multi-opportunist market due to the growth in sustainable energy usage. It is worth noting that there is an extensive list of key operative players in the global DSSC market like Fujikura Ltd., Konica Minolya, Sensing Europe B.V, 3GSolar Photovoltaics, Dyesol Ltd., Solaronix, G24 Power Ltd. and Solaris Nanoscience Corporation.

The current world leader in manufacturing DSSCs, G24 Power along with Texas Instruments conducted a comparative study on performance between DSSCs, amorphous silicon (a-Si) and organic solar materials (OPV). They were convinced that, DSSC under indoor conditions for energy harvesting applications is a better candidate than a-Si and

Universiti Malaya

OPV in terms of maximum power density (Sridhar & Freeman, 2011). Similarly, a comparative study between DSSC and a-Si modules by Dyesol Co. Ltd showed a significant increase in DSSC performance by 10% on peak sunny days and 20% increase during cloudy days compared to a-Si solar modules. Unlike the other discovered solar cells, DSSC uniquely performs better in midmorning and midevening settings. On top of this, DSSC performance again is less affected by light incidence angle though an increase in angle does boost conversion efficiencies (Roslan et al., 2018). Indeed the price of Silicon photovoltaic have considerably dropped but still the manufacturing process is tedious and expensive compared to DSSCs. From the Malaysian perspective, the façade of photovoltaic devices has been always growing towards building integrated photovoltaic implementation as we do give equal importance in harnessing sunlight for heating purposes. As such, a recent study by Hamed et al. on performance comparison between silicon solar panel and dye-sensitized solar panel in Malaysia context revealed the distribution of data supports that the dye sensitized solar panel is much better and is very sensitive to heat throughout the day and not only high output on midday (Hamed et al., 2017)

Overall, despite a minimal market appearance as compared to first generation of photovoltaic devices, DSSCs are still actively pursued due to its superior low-light performance that brings to expanded operating hours, flexibility and easy integration like being in cohabitation with greenhouses and shaded regions in buildings as well as prospects for lower cost for greater power density.

2.2.2 Components of a DSSC

DSSC is categorized as a thin film solar cell. A typical built includes four main elements, namely, photoanode, dye, electrolyte and cathode. Based on literature readings, a schematic diagram of DSSC along with the constructive electron route is shown in Figure 2.2. The details on working mechanism is discussed in the upcoming subsections.

Universiti Malaya

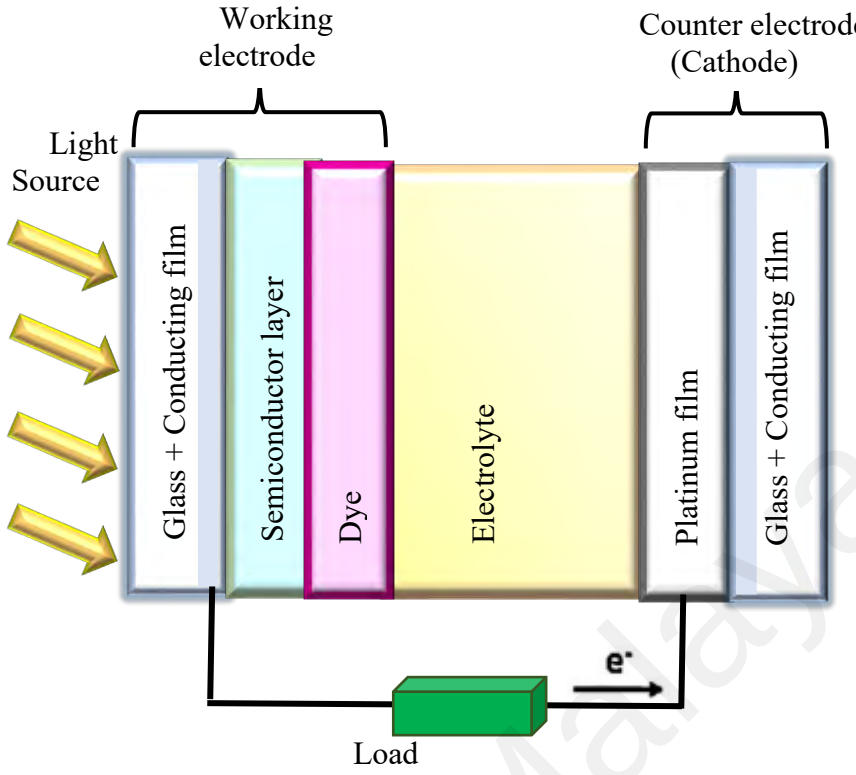

Figure 2.2: A schematic diagram of DSSC assembly.

2.2.2.1 Transparent conducting Films

Transparent conducting films (TCFs) are vital components of DSSC. Both working electrodes and counter electrodes are built on them. TCFs are transparent thin films carrying electrically conductive materials. As for photovoltaic applications, TCFs have been fabricated from both organic and inorganic materials. Organic layers developed include carbon nanotube networks and graphene whilst inorganic layers are typically transparent conducting oxide (TCO) coats. Popular TCOs are fluorine doped tin oxide (FTO) and indium-doped tin oxide (ITO). These forms of TCOs are widely used in DSSC technology due to their ability to provide electrical contacts with minimal resistance without blocking light.

FTO coated glasses have the ability to transmit about 70-80% light in the visible region (Yang 2008). In terms of performance, ITO coats performs marginally better than FTOs.

Universiti Malaya

However, substantial DSSC research is carried out with FTO because ITO`s electrical properties have been found to degrade in the presence of oxygen at high temperatures, i.e during the annealing process. Furthermore, FTO is more affordable, thus a better preliminary choice.

2.2.2.2 Working electrodes

Working electrode, also known as photoanodes, be made of a mesoporous nanostructure layer of semiconductor on a TCF and becomes functional once immersed in dye. In DSSC, the most common semiconducting oxide used is titanium dioxide (TiO_2) which was utilised by Oregan himself in 1991. Anatase- type TiO_2 nanoparticles are known for their photocatalytic activity. The valence and conductive band gap of 3.2 eV is considerably large and promotes high conduction band energy (Hagfeldt et al., 2010). Other studied semiconductors include both simple to complex oxides namely ZnO, Nb_2O_5, SnO_2 and NiO (Park & Kim, 2008; Lenzmann et al., 2001; Zhang & Cao, 2011). Nevertheless, TiO_2 has become a common research model for DSSC due to its abundance, environmentally friendly nature, inexpensive to obtain, stability and good deal of photo-corrosion resistance.

Quantum physics explains that an electron from the valence band of the semiconductor is able to hop on into the conduction band when the energy of photo matches or exceeds the band gap. This phenomenon results in an electron hole at the valence band which is transferred to the external circuit to generate electrical current (Hoffmann et al., 1995). A high performing semiconductor should be able to provide high surface for dye adsorption, allow effective mass transport via diffusion and possess a band gap that matched with most sensitizer for effective electron injection and transport (Lau et al., 2014). Ideally, agglomeration of TiO_2 nanocrystals in colloids applied on TCF have average sizes of 15-30 nm with usual coat thickness ranging from 1-15 μm.

Universiti Malaya

Growing research on photoanode fabrication even allows metal oxides to be chemically grown on conducting substrates (Sinha et al., 2018). Nevertheless, popular deposition methods for thin semiconductor layer still remain as screen printing and doctor blading techniques owing to its cost-effectiveness and scalability. In brief, doctor blading is done by spreading a colloidal mixture of metal oxide using a smooth glass rod or even slides to required thickness assisted by a tape frame. Once the coat is satisfactory, sintering is done at high temperatures of 450- 500 ^{o}C to allow nanoparticles to interconnect and form a nano-porous layer which provides large surface area for dye adsorption.

2.2.2.3 Sensitizers

Dye or sensitizers are light absorbers with ability to inject electrons into the conduction band of semiconductors. A good sensitizer should possess important features like: (i) strong and broad absorption spectrum covering the whole visible region and parts of near-infrared region; (ii) contain anchoring groups namely, carboxylate, phosphate and sulfonates to bind strongly with the semiconductor surface; (iii) good reversibility in oxidized and excited state for effective regeneration of dye molecules; (iv) suitable highest occupied molecular orbital (HOMO) and lowest unoccupied molecular orbital (LUMO) to allow efficient charge injection into the semiconductor; (v) have hydrophobic sides to minimize direct contact with electrolytes as well as reduce water-induced distortion of dyes; and (vi) good photo-, electrochemical- and thermal stability for long term use (Shalini et al., 2016). In this regard, most efficacious sensitizer are still based on Ruthenium (Ru)-complexes like (N3-cis-di (thiocyanato) bis (2,2-bipyridine-4,4-dicarboxylate) ruthenium) (N3 dye), (di-tetrabutyl ammonium cis-bis (isothiocyanato) bis (2,2′-bipyridyl-4,4′- dicarboxylato) ruthenium (II)), (N719 dye) and black dye (N749 dye) despite the known disadvantages of high production cost and toxic nature (Sekar & Gehlot, 2010).

Universiti Malaya

Thus, many Ru-free dyes have been developed and can be categorized into the following types: (i) metal-free organic dyes; (ii) quantum dot sensitizers; (iii) perovskite-based; and (iv) natural dyes (Ito, 2011). At current, quantum-dot sensitized solar cell, (QDSSC) and perovskite-based solar cells have emerged as new type of photovoltaic device and considered to be hybrids of DSSC, organic photovoltaics and thin film solar cells (Ahmed et al., 2015).

As for organic alternatives like coumarine, porphyrin, indoline and carbazole along with natural dyes, still remain inferior to conventional Ru-dyes in terms of conversion efficiencies (Prabavathy et al., 2017; Sharma et al., 2018). Nonetheless, advantages like lower cost, facile synthesis, higher molar extinction coefficient, tunable energy levels and stable under prolonged illumination still boost research interest to explore new dyes that render good stability and efficiency. Success relies in understanding the mechanism of dye aggregation and their tunable physicochemical properties fully in order to compete with the performance of Ru dyes.

N719 is actually an intentionally modified version of the N3 dye, founded by replacing four H^+ counterions of N3 dye by teoo TBA^+ and two H^+ counterions, and is proven to improve the V_{oc} of the cell. The comparative structures of N719 and N3 are shown in Figure 2.3. To date, from the table, N719 dye by far is the most successful dye applied in DSSCs owing to improved dye absorption at molecular level due to reduced electrostatic repulsion between dye molecules compared to N3 dye whereas N749 has lower absorption coefficient. N719 is commonly employed with co-absorbents like chenodeoxycholic acid (CDCA) to prevent aggregation of dye over the TiO_2 surface and form stable linkage that limits recombination reactions (Bandara et al., 2016; Aghazada & Nazeeruddin, 2018).

Universiti Malaya

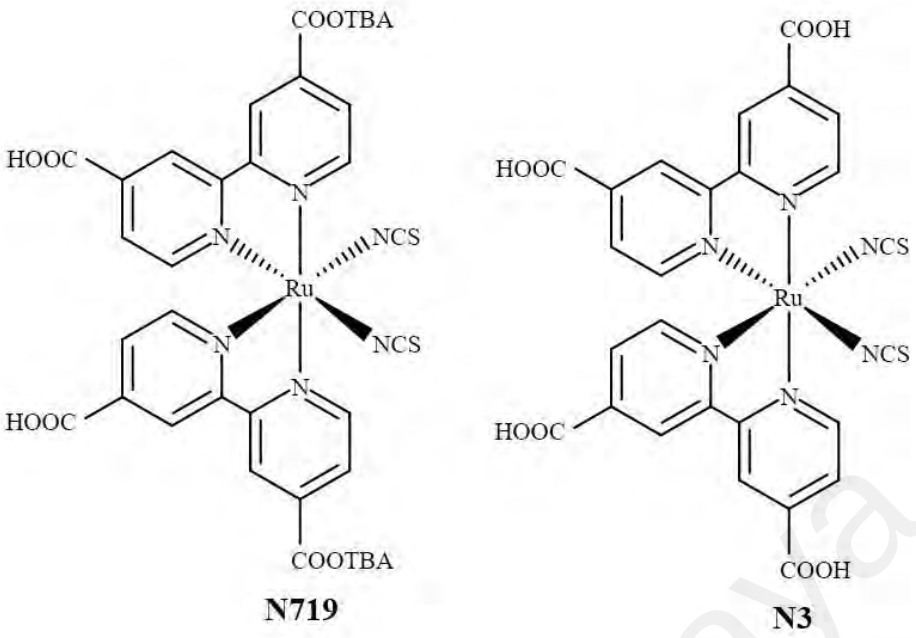

Figure 2.3: Chemical structures of Ruthenium complexes used as dyes.

2.2.2.4 Counter Electrodes

The term counter electrodes were first coined by Gratzel himself in his pioneering DSSC paper in 1991(Oregan & Gratzel, 1991). With respect to function, counter electrodes are sometimes referred as cathodes to indicate electron entering and reduction occurs at the electrode. In order to maintain the electrical continuity in DSSC, counter electrodes convert oxidised redox couple present in electrolyte to the original state which in return promotes dye regeneration. The reducing role of counter electrodes comes from the ability to collect electrons from the external circuit. Literature reviews claim that a good electrode should possess high catalytic activity as well as good electrical conductivity (Wu et al., 2015). Initial research on DSSC, utilised platinum (Pt) deposited on FTO conducting glass as its electrocatalytic properties improves the reduction of triiodide ions, I_3^- to iodide, I^-. Despite having a good catalytic activity, the primary disadvantage of material scarcity for such rare metal hinders commercialisation. Large area production of DSSCs would require high fabrication cost. Moreover, some reports also prove that Pt electrodes are prone to corrosion when assembled with iodide

Universiti Malaya

containing electrolytes generating complexes like PtI_2 (Lee et al., 2017). Thus, research on other desirable Pt-free materials are intensively studied, with carbonaceous material topping the list. Other materials include conductive polymers and transition metal compounds. The advantage and disadvantages of alternative counter electrode materials are listed in Table 2.1.

Table 2.1: Three main classes of Pt-free counter electrode materials and their respective pros and cons.

	Advantages	Disadvantages
Carbon based	Low cost, simple preparation, good stability	Low conductivity and catalytic activity
Conductive polymers	Depends on polymers used- establishing a balance of cost and performance offered is the key	
Transition Metal Compounds	Material diversity, easy preparation and modification	Lower performance due to low conductivity and electron transfer

Overall, Pt counter electrode is the most frequently used as it well satisfies all requirements. Platinum film is highly reflective and this improves the light harvesting efficiency of dye molecules absorbed onto the semiconductor. This in return contributes to an enhanced cell performance. Thus, it is not surprising that most highly efficient systems reported are based Pt counter electrodes.

2.2.2.5 Electrolytes

Electrolytes in DSSCs are conducting components carrying a redox mediator, commonly the I^-/I_3^- redox couple. Electrolyte acts as shuttles transporting charge carriers between working electrodes and counter electrodes which assists the regeneration of oxidised dye molecules. Interaction of electrolytes with both electrode interfaces make

Universiti Malaya

electrolytes very important in governing the overall power conversion efficiency and lifetime of DSSCs. Details on parameters affecting cell efficiency is discussed in Section 2.2.3. Electrolytes can be divided into 3 main categories namely liquid, solid-state and quasi-solid electrolytes based on their physical features and composition. Wu et al. went a step further and classified these electrolytes into 11 sub-types on the basis of formation mechanisms (Wu et al., 2015).

Generally, a good electrolyte for the application of DSSCs should contain abilities like

i) Permits fast diffusion and effective transport of charge carriers between the photoanode and counter electrode.
ii) Match the dye redox potential in order to reduce the oxidised dye to its ground state rapidly before non-radiative decay process occurs.
iii) Able to sustain a long term with good electrochemical, thermal and interfacial stability
iv) Prevents desorption and degradation of dye on the semiconductor surface as well as corrosion on the counter electrode
v) Exhibit no or minimal absorption in the visible light region.

For the case of liquid electrolytes, solvent leakages and evaporation must be prevented (Pandikumar & Ramaraj, 2018). Besides, most DSSC electrolytes utilizes I^-/I_3^- redox couple and I_3^- is capable absorbing some light itself and can react with injected electrons from oxidized dye which increase dark current. Hence, optimization of I^-/I_3^- concentration is equally vital in electrolyte preparation.

Alternatively, bromide/tribromide (Br^-/Br_3^-) and psedohalogens like thiocyanate/trithiocyanate (SCN^-/SCN_3^-) and selenocyanate/triselenocyanate ($SeCN^-/SeCN_3^-$) redox couples have been also used. Undoubtedly, I^-/I_3^-redox shuttles remain popular owing to the high solubility, assist dye regeneration efficiently and has

Universiti Malaya

fairly slower recombination kinetics between electrons in the photoanode conduction band with oxidised dye molecules and triiodide in the electrolyte (Boschloo & Hagfeldt, 2009).

Normally, electrolyte containing I^-/I_3^- redox couple is formulated by adding iodide salts with iodine. To date, the study on various iodide salts is capitalized by introducing different cation sizes. Small cation contributors include lithium (Li), sodium (Na) and magnesium (Mg) salts, whereas common large cations studied are caesium (Cs), ammonium (NH_4^+), guanidium (G) and tetrapropylammonium iodide (TPAI) (Kumari, Senadeera, & Dissanayake, 2017). Along with iodide salts, additives like room temperature ionic liquids (RTIL) are also added, as they are proven to improve conductivity of electrolytes (Bhattacharya et al., 2009). Combination of different additives and salts in electrolytes alter the energetics at the photoanode/ electrolyte interface at which dye regeneration takes place.

By far, liquid electrolytes have been offering good interface affinity and high ionic conductivity resulting in remarkable power conversion efficiency in lab- sized DSSC. A decent increase from 7% in 1991 to the current record of 14.3% in 2015 is noteworthy (Kakiage et al., 2015).

Besides, liquid electrolytes are also historical on the basis of electrochemical device research and industrial market. Apart from DSSCs, liquid electrolytes are widely used in rechargeable and redox flow batteries, supercapacitors and supercapatteries. Typical examples of liquid electrolytes include aqueous, organic, ionic liquid electrolytes and molten salts electrolytes (Xia et al., 2017). These electrolytes share many advantages like high working voltage and ultra-fast electrode charge transfer kinetics but also carry limitations mainly on cell stability, safety concerns and cost. The short shelf-life by virtue of leakages is a major bane. Detailed drawbacks of liquid electrolytes include low safety performance and operating temperature range as organic solvents are mostly flammable,

Universiti Malaya

encapsulating difficulties while manufacturing and high possibility of internal short circuit (Ng et al., 2017 ; Venkatesan et al., 2016).

Thus, a defined idea was utilising solid-state electrolytes which possess contrasting physical properties. All solid-state electrolyte for DSSC was first revealed by Tennakonne et al. in 1995 by casting copper iodide solution to form a complete hole-transporting layer, to establish conduction (Li et al., 2006). Solid-state electrolytes have energy density, ease of application and more flexible geometry, higher operating temperatures, hardly any electrolyte leakages and tops the list on safety. However, they fall short on ionic conductivity due to the high crystallinity, exhibit poor photoanode/ electrolyte contact and significantly lower cell performance. An intermediate of both solid and liquid electrolyte would be a semi-solid state; i.e quasi-solid electrolyte.

Quasi solid electrolyte are cohesive in nature like solids electrolytes on top of being diffusive as liquid electrolytes thus, better long-term stability can be realised without compromising much on ionic conductivity.

Quasi- solid electrolytes are commonly prepared by solidifying liquid electrolytes using organic polymers or inorganic gelators. Based on the resulting features and physical properties, Wu et al. further classified quasi- solid electrolytes into 4 sub types namely, thermoplastic polymer electrolytes, thermosetting polymer electrolytes, composite polymer electrolytes and ionic liquid electrolytes (Wu et al., 2008). Polymer based electrolytes will be discussed further in section 2.3.

Currently, worldwide research on the design and synthesis of novel electrolytes for DSSCs is still in its way and targeted to prepare a non-volatile redox mediator with high charge carrier transporting abilities and possess adaptability to sustain for a good period. On a commercial viewpoint, a cheaper membrane cost with superior ionic conductivity and enhanced mechanical stability is the challenge to meet.

Universiti Malaya

2.2.3 Working mechanism

The working mechanism of DSSCs differs extensively from the previous generation of solar cells and is frequently referred as to mimic photosynthesis. Light absorption initiates charge carrier transport that is performed by the different components present. The details on processes occurring in DSSC is shown in Table 2.2 and schematically illustrated in Figure 2.4.

Upon light irradiation, the processes that occur include:

1. Sensitizer present on the surface of the semiconductor is photoexcited to produce excited dye.
2. Excited electrons are injected into the conduction band of semiconductor resulting in the formation of oxidized dye.
3. Electrons are transported through semiconductor to conducting substrate and flow towards the counter electrode via external circuit.
4. Oxidized redox couple is regenerated by accepting the electrons arriving at counter electrode
5. Oxidized dye is regenerated by receiving electrons from the reduced redox couple.
6. Photo-injected electron recombination with oxidized dye.
7. Photo-injected electron recombination with oxidized redox couple.

Sequential processes (1)-(5) are essential to generate electric from light. Since this is done without undergoing any permanent changes chemically, DSSCs can be classified as a regenerative photoelectrochemical cell. However, processes (6) and (7) are possible dark reactions resulting in charge recombination which reduces the overall efficiency of DSSCs. Wu et al. claims the undesirable effect of charge recombination to be less significant due to slower reaction rate compared to the main reactions (Wu et al., 2017).

Universiti Malaya

Table 2.2: Summary of reaction in an operating DSSC.

Equations	Reactions	
$D + h\nu \longrightarrow D^*$	Photo-excitation	(1)
$D^* \longrightarrow D^+ + e^-$	Electron-injection	(2)
$I_3^- + 2e^- \longrightarrow 3I^-$	Reduction	(4)
$2D^+ + 3I^- \longrightarrow 2D + I_3^-$	Dye regeneration	(5)
$I_3^- + 2e^- \longrightarrow 3I^-$	Recapture	(6)
$D^+ + e- \longrightarrow D$	Recombination	(7)

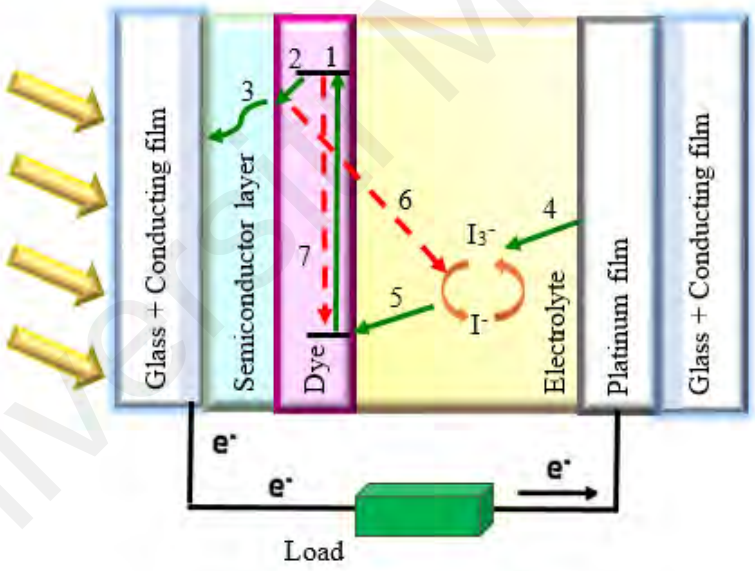

Figure 2.4: Schematic diagram on reactions pathway in a DSSC.

2.2.4 Evaluation of performances

The performances of DSSCs are evaluated based on four parameters that is open circuit voltage (V_{oc}), short circuit current density (J_{sc}), fill factor (FF) and energy conversion efficiency (η).

University of Malaya

V_{oc} is the highest cell voltage measured at zero current within the cell. This happens to be the difference between the electrolyte redox potential and the quasi- fermi level of electrons in the conduction band of semiconductor. High V_{oc} is possible when a redox couple with more positive redox potential is used. J_{sc} is the maximum photocurrent measured at zero potential over an active cell area. Photocurrent is obtained by generation and collection of charge with the cell. Improving J_{sc} values require dye sensitizers that can absorb broad sunlight covering not only the visible region but as well the near infrared range of the spectrum (Wei, 2011).

FF essentially signifies how well the DSSC is performing under subjected cell resistance and resistance of the materials used. *FF* is calculated as the ratio of maximum power output to the theoretical power value calculated based on short circuit photocurrent and open circuit voltage as shown in *Equation 2.1*.

$$FF = \frac{P_{max}}{P_{theo}} = \frac{J_{max} \times V_{max}}{J_{sc} \times V_{oc}} \tag{2.1}$$

FF can be depicted as the largest rectangle obtained in a *J-V* curve as shown as the shaded region in Figure 2.5.

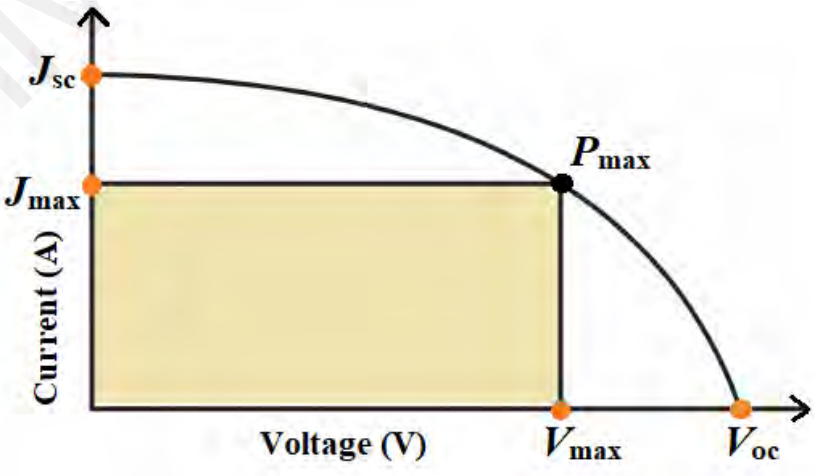

Figure 2.5: Characteristic *J-V* curve to evaluate DSSC performance.

Universiti Malaya

η *which* is also the external quantum efficiency is a function of V_{oc} , $J_{sc,}$ and *FF* calculated based on the ratio of output energy over the input energy of the cell as presented in *Equation 2.2*.

$$\eta = \frac{\boldsymbol{J_{sc} \times V_{oc} \times FF}}{\boldsymbol{P}_{\text{in}}} \text{ x } 100\% \tag{2.2}$$

Thus, any improvement to the energy conversion efficiency is a result of optimizing the above mentioned parameters. It is also important to note that, η also depends on the incident radiation power which is usually denoted in experiment findings. All these parameters depend largely on the properties of materials and physical process that occurs within the device.

Besides current voltage measurements, electrochemical impedance is also measured to evaluate the performance of DSSC. A typical DSSC has three main spatial boundaries i.e. conducting glass-semiconductor, photoanode- electrolyte, and electrolyte-counter electrode interfaces where impedance is measured as a function ac electrical current at a certain angular frequency when certain ac voltage is applied. Prior to analysis, the system is retained in a steady state and measurements are done by applying constant constrains like illumination intensity. Generally, a frequency sweep ranging from mHz to 10MHz is done to measure impedance. This usually results in 5-10 readings per region forming a semicircle figure.

The three interfaces stated is translated as three characteristic semicircles in the Nyquist spectra. The peak frequency of semicircle in the lowest frequency region corresponds to diffusion occurring within the electrolyte, while the mid-range frequency it reflects the properties of photoinjected electrons at the semiconductor surface. Finally, the peak frequency at the high frequency region corresponds to charge transfer at the counter electrode. The impedance data of a DSSC translates into reliable values of

Universiti Malaya

parameter relating to electron transport, fundamental for improving cell efficiency, among which are the ohmic serial resistance (R_s),charge transfer resistance at Pt counter electrode/ electrolyte interface (R_{Pt}), charge recombination resistance at TiO_2/ electrolyte interface (R_{CT}), electron transport resistance in TiO_2 (R_w), effective lifetime of electrons(τ_{eff}), effective electron diffusion coefficient (D_{eff}) and effective rate constant for recombination with tri-iodide (k_{eff}).

Adachi et al. worked on determining parameters of electron transport in DSSC through EIS is a comprehensive study that unifies preceding descriptions proposed by Kern et al. and Bisquert et al. in terms of electron transport and charge recombination in the nanocrystalline semiconductor. Despite the extensive use of coined term R_{CT}, Adachi`s procedure demonstrates the use of R_k to represent charge recombination resistance. The development of a reliable equation to retrieve fundamental information to improve cell efficiency was possible by Adachi et al. with detailed characterization and clarification of the spectra measured by electron impedance spectroscopy. Determination of parameters of electron transport from an Nquist plot was possible with the following equations.

$$\boldsymbol{k_{eff} = \omega_{max}} \tag{2.3}$$

$$\boldsymbol{R_{dc} = \frac{1}{3} R_w + R_k} \tag{2.4}$$

$$\boldsymbol{D_{eff} = (\frac{R_k}{R_w}) L^2 k_{eff}} \tag{2.5}$$

Firstly, the peak frequency of the second-semicircle, ω_{max} is estimated to the rate constant of recombination, k_{eff}. Next, the direct current resistance, R_{dc} at $\omega = 0$ is given as a function of both electron transport resistance and charge transfer resistance related to recombination. Lastly, D_{eff} is a product of resistance ratio, thickness of TiO_2 film, *L* and $k_{eff.}$ The requisite for making highly efficient DSSC is highlighted as having a high

Universiti Malaya

electron diffusion coefficient, low recombination rate constant, higher recombination resistance than electron diffusion resistance and high electron density (Kern et al., 2002; Adachi et al., 2006; Bisquert, 2010).

2.3 Polymer Electrolytes

For a very long time, synthetic polymers were mainly used as electrical insulators. In 1973, the Fenton group from UK, successfully measured ionic conductivity on crystalline polyethylene oxide (PEO) polymer membrane upon doping with alkali salt that produced conductivity in the range of 10^{-3} S cm^{-1} at high temperatures above the glass transition temperature of PEO (Fenton et al., 1973).

Conducting polymers fascinated many research groups as they envisaged the potential application in energy storage devices. For instance, the Armand research group devoted on exploring various solid polymer electrolytes for electrochemical devices. Though the reported ionic conductivities are lower than conventional liquid electrolytes systems, the application of these new materials suited applications that consumed low currents (Hallinan & Balsara, 2013). Likewise, they show good compatibility with devices like batteries, capacitors and DSSCs. The popularity polymer electrolytes have gained over the years is also due to the safety it offers mainly to the less likely to leak feature and high molecular weight polymers are mostly non-volatile and inert to ignition. By contrast, the organic solvents utilized in general liquid electrolytes are highly flammable and prone to leaking if not sufficiently sealed.

Polymer electrolytes are unique as polymer matrices solvate ions and the segmental motion of polymer backbone navigates the movement of ions causing ionic conductivity. Polymer electrolytes are mostly utilized as solid-state electrochemical components. Initial research on polymer electrolytes focused mainly on utilizing synthetic polymers. Among the most studied linear polymer electrolytes as complexes containing metal salts and

Universiti Malaya

polymers include polyethylene oxide (PEO), polymethyl methacrylate (PMMA), poly acrylonitrile (PAN), poly(vinylidene fluoride-co-hexafluoropropylene) (PVdF-HFP), polyvinyl alcohol (PVA) and polyvinylpyrrolidone (PVP) (Pandikumar & Ramaraj, 2018). On the other hand, growing environmental concerns mooted the conception of biopolymer electrolytes. The budding research on less dependency on petroleum- derived plastics explores polymer fibres from both plants and animals. Agar, carrageenan, pectin, chitin, starch and gums are the few to mention (Singh et al., 2016; Bella et al., 2017).

Solid - state polymer electrolytes be it both synthetic and bio-derived have shown to produce low ionic conductivities by only incorporating metal salts. In general, the average conductivities ranges from 10^{-7} S cm^{-1} to 10^{-4} S cm^{-1} and some systems have reached 10^{-2} S cm^{-1} usually in the presence of water (Singh et al., 2013). The performance of solid polymer electrolytes are largely poor owing to the low ionic conductivity due to restricted motion and possible crystallization of ionic salts in the absence of solvent.

Thus, polymer electrolytes are either plasticized with solvents, blend with other polymers or doped with additives and fillers to improve ionic conductivity at room conditions. This gives rise to 4 main groups of polymer electrolytes classified based on their preparation practice and physical features as shown in Figure 2.6. All four classes of polymer electrolytes are intensively studied with liquid crystals being the newest type of polymer electrolytes learned. A brief summary in the progress of polymer electrolyte usage in DSSCs is tabulated in Table 2.3 (Aziz et al., 2018).

Universiti Malaya

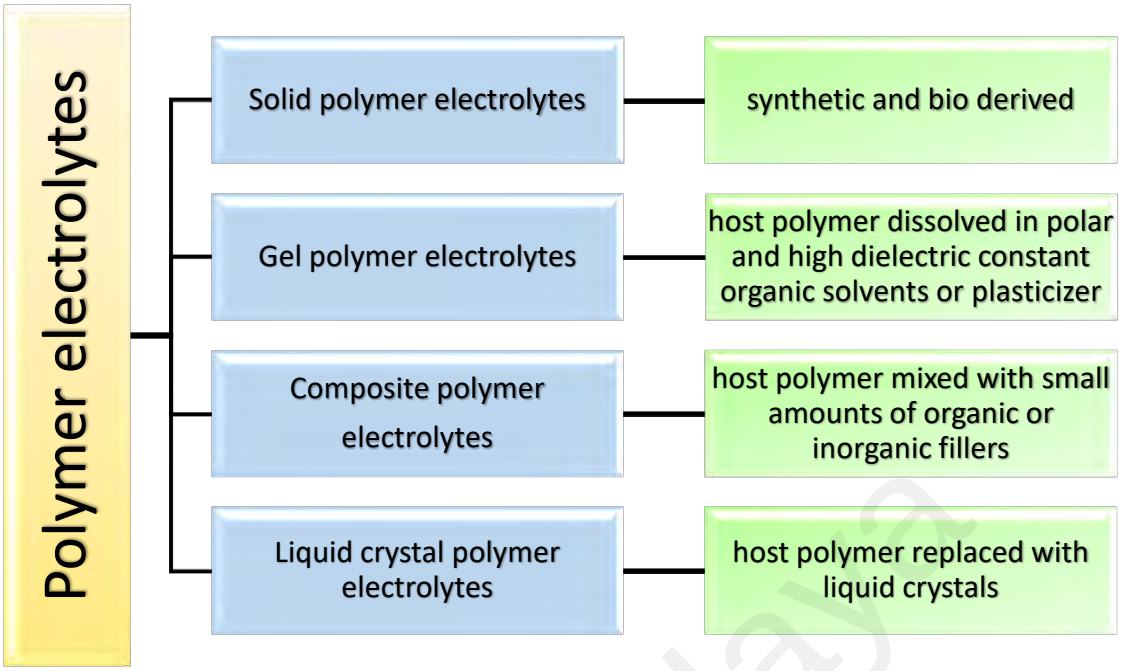

Figure 2.6: Main classes of polymer electrolyte.

Table 2.3: A partial list of literature study on DSSCs with polymer electrolytes.

Year	Research Objective	Results Obtained	Reference
2008	Yang et al. demonstrated the study on emulsion polymerized PMMA based GPE using NaI/ I_2 redox couple	It was observed that the DSSC possessed good stability with PCE of 4.78% under 1 sun solar stimulation	(Yang et al., 2008)
2010	Chen et al. fabricated a gel-state electrolyte by using poly(acrylonitrile -co-vinyl acetate) (PAN–VA) as the gelator of an 3-methoxypropionitrile (MPN)-based liquid electrolyte.	The power conversion efficiency of the DSSC containing gel-electrolyte was recorded at 8.34%, which is 97% the value 8.63% of the liquid-state cell.	(Chen et al., 2011)

Universiti Malaya

Table 2.3, continued.

Year	Research Objective	Results Obtained	Reference
2011	Noor et al. studied a plasticized polymer electrolyte system composed PVDF-HFP containing KI/I_2 redox couple and equal weight of EC and PC	The optimized electrolyte showed best performance with a short-circuit current density of 8.16 mA cm^{-2}, open-circuit voltage of 0.76 V, fill factor of 0.35, and photoconversion efficiency of 2.2%.	(Noor et al., 2011)
2014	Salvador et al. synthesized a cellulose based electrolyte.	The optimized gel bio polymer had maximum PCE of 3.33% and open circuit voltage of 0.67 V at 100 $mWcm^{-2}$	(Salvador et al., 2014)
2015	Rudhziah et al. investigated a blend bio-polymer containing kappa- carrageenan and cellulose derivatives.	It was observed that the combination of bio-polymers yielded light to electrical energy conversion of 2.32% with open circuit voltage of 0.5 V at 100 $mWcm^{-2}$	(Rudhziah et al., 2015)
2017	Buraidah et al. studied phthaloylchitosan based GPE by varying the amount of iodide salt and ionic liquid	The maximum PCE of the optimized system was found to be 9.47% with open circuit voltage of 0.71V	(Buraidah et al., 2017)

Universiti Malaya

Table 2.3, continued.

Year	Research Objective	Results Obtained	Reference
2018	Tan et al. prepared a gel state DSSC based on poly(vinyl alcohol-co-ethylene), P(VA-co-PE) using NaI/ I_2 redox couple	It was found that the light to electrical energy conversion efficiency of the copolymer is up to 3.32%.	(Tan et al., 2018)
2019	Farhana et al. prepared a GPE containing a terpolymer P(VB-co-VA-co-VAc) with TPAI as dopant salt for DSSCs.	The PCE of 4.62% was achieved with an open circuit voltage of 0.678 V 40 wt% TPAI salt.	(Farhana et al., 2019)

The choice of polymer host for a specific electrolyte is governed by two factors, that is, (1) ability to solvate salts present and (2) glass transition temperature, T_g of the polymer. A polymer is able to solvate salt if it contains polar bonds that can form interaction with dissociated salt cations. Generally salts with lower lattice dissolves easily in polymer matrix. Hence, it's equally important to select the appropriate salt. Besides, polymers with low T_g, allow better segmental motion that facilitates ion conduction with ease.

2.3.1 Gel Polymer Electrolytes (GPE)

Polymer based quasi-solid electrolytes otherwise known as gel polymer electrolytes (GPEs) or plasticized- polymer electrolytes are the most studied owing to its distinct preparation methods and adaptability (Ramesh & Bing, 2012). GPEs utilize polymeric cages to entrap liquid electrolytes. A wide-reaching practice is by dissolving polymer host and doping salts in polar organic solvents with high dielectric constants (Rajendran

Universiti Malaya

et al., 2008). Apart from gelation of liquid electrolyte, quasi-solid electrolytes can be also prepared via swelling and *in situ* sol-gel technique.

Among the widely used solvent cum plasticizers to obtain GPEs are carbonate ester such as propylene carbonate (PC), ethylene carbonate (EC), dibutyl phthalate (DBP), diethyl carbonate (DEC) as well as N,N–dimethyl formamide (DMF) and γ–butyrolactone with very high dielectric constant (Ponrouch et al., 2012; Ramesh et al., 2011). The effect of plasticizer are significantly noted in literatures. Table 2.4 lists popular aprotic solvents and their physical properties. Plasticizers tend to reduce both inter-and intramolecular forces between polymer backbones. Addition of plasticizer, also alter glass transition temperatures of polymer electrolytes as a result of reducing three-dimensional rigidity. The changing mechanical properties guarantees better salt dissociation. The ion conduction is supported by the wide disordered network of polymer host present. As such, the degree of freedom achieved in GPEs at atomic levels during polymer relaxation is sometimes analogous to liquid electrolytes (Ramesh & Liew, 2013).

Overall, GPEs inherit many advantages, for instance, improved ionic conductivity with small portion of plasticizer added, better electrolyte/electrode contact that reduces interfacial resistance, exhibit good flexibility which allows easy fabrication into preferred size and shape as well as lower assembly cost. On an electrochemical viewpoint, GPEs have wider operating temperatures than liquid electrolytes with less chances of leakage. Thus, safety is definitely another attractive feature of GPEs (Wen, 2011).

Table 2.4: Selected aprotic solvents and their dielectric constants.

Solvents	Molecular weight (g mol^{-1})	Boiling point (^{o}C)	Dielectric constant
EC	88.06	243.0	89.8
PC	102.09	240.0	64.9
DMSO	78.13	189.0	47.0

Universiti Malaya

Table 2.4, continued.

Solvents	Molecular weight (g mol^{-1})	Boiling point (^oC)	Dielectric constant
Acetonitrile	41.05	81.6	38.0
DMF	73.09	153.0	37.0
DBP	278.34	340.0	6.4
DEC	118.13	126.0	2.8

Solvent choices for polymer electrolytes are greatly influenced by their physical properties like high boiling points and dielectric constant along with low melting point and viscosity that assist in dissociating the salt. From systematic reviews of the literature, it is clearly understood that the increase in ionic high level addition of plasticizers is due to conductivity due to better dissociation ion-pairs into free cations and anions but this reduces mechanical properties in polymer electrolytes as they become more viscous fluid-like. Apart for that, the polar solvents added also show reactivity with metal electrodes and are prone to volatility (Pandey et al., 2013 ; Kumar, Singh, & Sekhon, 2005).

On the other hand, gelation of polymers with liquid electrolytes are subjective towards the nature of host polymer and electrolyte. Some polymers are capable of gelating well but others go out of phase with time. As such, the photovoltaic performances and stability of DSSCs are at risk. The resulting polymer mesh can obstruct smooth movements of ions present. Phase separation is also possible if the polymers have reacted other compounds present in the electrolyte like salts and additives, instead of being only a mobility aid.

The disadvantages that GPEs carry require alternative interventions that would boost mechanical strength and electrochemical stability without compromising much on ionic conductivity. In a combined systems containing polymer, salts and plasticizers, the electrochemical property is largely determined by the plasticizer component whereas

Universiti Malaya

safety and mechanical morphology is defined by the polymer matrix used (Baskoro et al., 2019).

Ideally, the first cut-off factor of a good polymer electrolyte for the use of DSSCs would be retaining an ionic conductivity higher than 10^{-3} S cm^{-1} at room temperature. Despite the absence of an exact benchmarking for development of polymer electrolytes for DSSCs, achieving high conductivity and stability- in days or possibly years, should be a good criterion to embark new inventions. This disparity can be due to the vast difference in operating technology with the well establish second generation solar cells. It would be wiser to comprehend the factors influencing ionic conductivity in gel polymer electrolytes and their influence towards photovoltaic performance before applying general strategies to improve the overall performance of DSSCs.

2.4 Ionic Conduction in Polymer Electrolytes.

Conductivity in organic polymer membranes can be postulated as follows: 1) electronic conduction whereby semiconductor behaviours are observed with large energy gap, 2) aqueous conduction of ions if polymers are present in aqueous environment and 3) ionic conduction with an active diffusion process (Cherry et al., 1972). Ionic conductivity relies on the transport of one or more types of ions across a material. In an electrolyte, diffusion of mobile charge carriers occur when a potential is applied across the cell. In crystalline phase, this migration happens along the direction of electric field. Ideal crystals have minimal space for ions to diffuse and only vibrate continuously around its equilibrium position. Migration of ions, i.e. ion conduction can only occur if these ions are able to overcome the potential barrier present in fixed lattices positions in order to diffuse or transport themselves (Raghavan, 2011). Most long chain polymers usually present themselves in non-crystalline form or semi-crystalline form owing to disorder in chain arrangement. Close-packing and alignment promote by mechanical works increases

Universiti Malaya

crystallinity. As such, there are two probable mechanism that illustrates ion diffusion in polymer electrolytes namely, vacancy mechanism and interstitial mechanism. These mechanism form the basis of the Arrhenius and Vogel−Tammann−Fulcher (VTF) models for ion transport (Baskoro et al., 2019; Aziz, Woo, et al., 2018).

2.4.1 Ionic Transport Mechanism in Polymer Electrolytes

It is indeed undeniable that ionic transport mechanism in polymer electrolyte is a significantly intricate phenomenon owing to the various contributing factors. The listed factors are salt cation size, dielectric constant of host polymer, occurrence of ion pairing, amorphous phase character and mobility of both anion and cation, i.e-charge carriers present (Baskoro et al., 2019). At current, proposing a reliable mechanism of ion transport inside polymer electrolyte is still a challenge for many research groups. As polymer electrolytes are made from dissolving low lattice energy salts in polar polymer matrix, cations present take responsible for ionic conductivity (Aziz et al., 2018). Subsequently, the number of mobile ions available is strongly influenced by the degree of dissociation of salts in the polymer matrix. Theoretically, in high molar mass polymer electrolytes, cations are able to dissociate between adjacent coordinating sites of either polymer host or neighbouring entities. Abraham et al., were one to earliest to envisage this concept in PEO polymer matrix (Abraham, 1996). The cations can be presumed to form a temporary bond with polar groups present on the polymer backbone and moves via polymer segmental motion.

Generally, most polar polymers used in making polymer electrolytes consist of both amorphous and crystalline subdivisions in which above their glass transition temperature, ionic migration occurs in the amorphous region. Thus, it is clear that ionic transportation in polymer electrolytes are strongly thermal activated.

Universiti Malaya

The vacancy mechanism relates closely to a hopping motion of an ion from its original position to an adjacent empty space. This mechanism is based on the vibrational cum thermal energy of ions sufficient enough to break the coordination bonds and jump to an adjacent vacant side. Similarly interstitial mechanism is also temperature dependent. However, mobile charge carriers move through the void present called interstices. Interstitial diffusions are normally more rapid than vacancy diffusion due to the higher probability of interstices present than empty sites as well as lower energy requirement to shift. As a result, two alkali cations end up sharing the same negatively charged cationic site which is usually a non-bridging oxygen atom. This entity is equivalent of a Frenkel defect as is justified an Arrhenius behaviour. This mechanism is visualized in Figure 2.7(b). Above glass transition temperature (T_g), interstitial diffusion in polymer electrolytes create free volume, thus giving it the name free volume mechanism. Free volume mechanism involves polymer movement along with interstitial mechanism. This cooperative mechanism involves transfer of moving species between neighbouring and adjourned "charge-cages" upon random density fluctuation or by polymer chain movements which creates so called "free" volume without any enthalpic cost (Souquet et al., 2012). Figure 2.7 illustrates the cation movement trough polymer matrix through the three mechanism discussed above.

Universiti Malaya

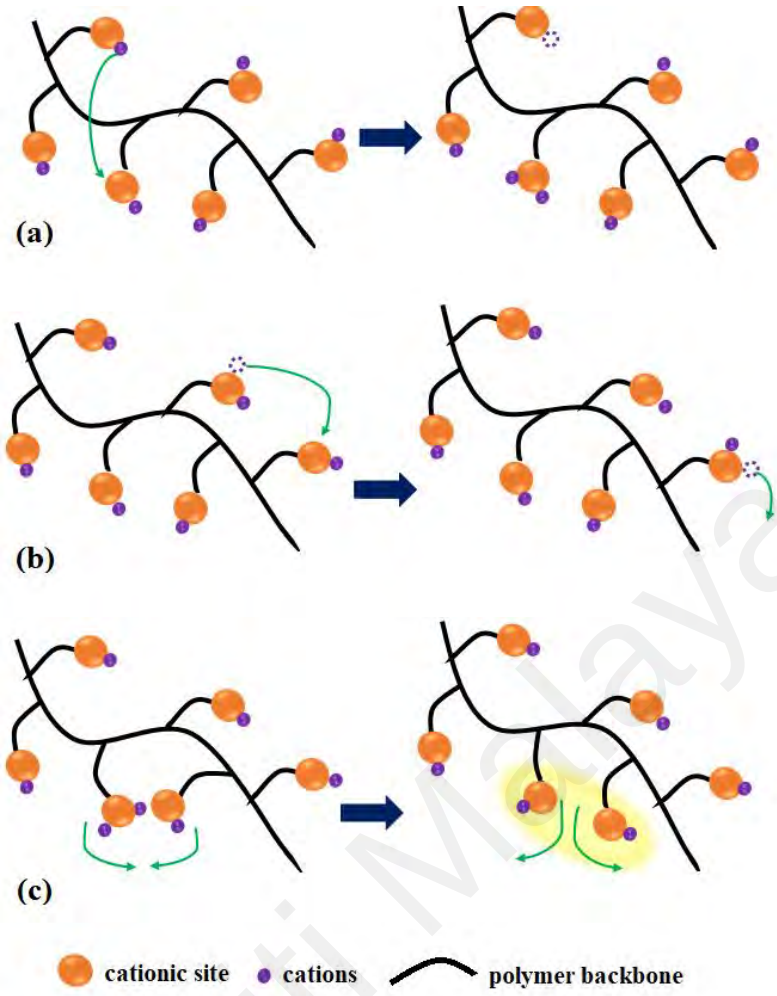

Figure 2.7: Schematic representation of conduction mechanism. (a) Vacancy mechanism. (b) Interstitial mechanism (c) Free volume mechanism.

2.4.2 Ionic Carrier Generation in Polymer Electrolytes

Efficient ionic conduction is not only affected by ion mobility but also by the number of charge carriers. The number of carrier ions present consequently increases with an increase in salt or ionic liquid concentration however, it is unlikely of a directly proportional relationship owing to the ability to dissociate. High concentrations of salts a very less likely to dissociate completely in solvents of low polarity. When salts are added, one should anticipate the possibility of free moving ions which function as charge carriers and also the presence of aggregated ions. Inclusively, the number of charge carriers present is highly influenced by the type of salt used, the concentration,

Universiti Malaya

temperature, solvent dielectric constant and the polymer structure (Watanabe & Ogata, 1988). Thus, the ionic conductivity in polymer electrolytes can be expressed as follows.

$$\boldsymbol{\sigma(T) = \sum n_i q_i \mu_i} \tag{2.6}$$

whereby ionic conductivity, σ the sum product of n_i- the number of charge carriers type of i, q_i - the charge on ions, and μ_i is the mobility of ions type of *i*. The equation illustrates that concentration of ions has a direct effect on the ionic conductivity of the electrolytes when charge and mobility of ions remains constant and vice versa. However, it's worth noting that, the mobility of ions can never be fixed for all polymer electrolyte samples as polymer network and electrolyte crystallinity varies which in return largely affects ion motion.

High degree crystallinity in polymer electrolytes implies a low amorphousness present in the structure. By definition, crystalline refers to a solid structure where atoms, ions or even molecules are arranged in orderly manner whereas amorphous state in polymers refers to the atoms, ions or molecules present at random and unorganized (Zallen et al., 2008).

It is fairly difficult to transport ions through crystalline region and allow ionic conduction unless crystallographic defects present. Comparatively, migration of ions occur at a higher rate in amorphous regions. No one polymer is 100% crystalline or 100% amorphous. In fact, it is kinetically impossible to create a fully crystalline polymer. Polymer electrolytes undergo significant segmental chain motion in the amorphous region upon subjected to heat. At T_g, physical transition occurs from a hard –brittle state to a soft-rubbery state. The elastomeric property after T_g is associated with long range molecular motion in polymers. This increase in polymer degree of rotational freedom assist movement of atoms or ions along the chain better. Besides, polymers electrolytes with high dielectric constant support ion dissociation, prevent aggregation of ions and

Universiti Malaya

allow better ion diffusion, thus improving the rate of ion transport mechanism. Much emphasis is also given to the flexibility of polymer chains which forms interactive bond with solvated ions and therefore, dissociated them with more ease. As a result, ionic conduction is improved in the polymer electrolytes (Aziz & Abidin, 2013).

As temperature increases, the amorphous region in polymer electrolytes gradually swells, allowing increased segmental motion in polymer chains. The faster internal modes which accelerated bond rotation promotes ionic motion to take pace as a dynamic hopping motion in both intra- and inter-chain (Gadjourova et al., 2001; Rajiv Kumar & Sekhon, 2013).

2.5 Strategies to Enhance Ionic Conduction in Polymer Electrolytes

Continuous investigation of ionic conduction and performance of GPEs in DSSCs, leads us to achieve more information on what factors affect and how to improve the properties of GPEs. Every component that makes up the GPE is an influencer to the overall ionic conductivity. On a specific note, polymer type and concentration, type of iodide salt and concentration, organic solvent used and temperature has an impact. Thus, research groups usually study on all combinatory possibilities. With various studies come various solutions to improve physical and electrochemical properties of GPEs according to the needs of application. Two agreed strategies would be to incorporate co-polymers and ionic liquids in preparing GPEs.

2.5.1 Usage of co-polymers

Polymers are macromolecules that are made up repeating units called monomers. The term co- is inserted when a minimum of two different monomers are used to make polymers. The arrangement of monomers during polymerisation results in either linear or branched co-polymers. Thus, co-polymers are usually classified as four main types as shown in Figure 2.8. For most cases, monomers present in co-polymer are not in 1:1 ratio

Universiti Malaya

unless they have equal reactivity. However, 1:1 ratio is possible by understanding monomer reactivity and changing concentration while polymerisation. This type of co-polymers are identified as alternating polymers. On the contrary, co-polymers can be also formed by random arrangement of monomers. Next, block co-polymers represent themselves as to homopolymers joined together at ends. Lastly, graft polymers have one monomer grafted on the backbone of the other monomer via reaction of the functional groups present. The second monomer usually dangles along the long chain of the first monomer (Feng et al., 2017).

Copolymerisation became necessary to introduce new properties and meet specific needs like improving mechanical properties, modifying glass transition temperatures and increase polymer solubility. For instance, in order to reduce the brittleness of polystyrene particles, polystyrene is grafted on rubbery chains of polybutadiene. The resulting high-impact polystyrene has combined properties of both.

In context of electrolytes, J. Przytuski et al. in 1992 demonstrated that ethylene oxide-propylene oxide copolymers combine with alkali salts showed highly amorphous nature and good ambient temperature conductivity along with wide temperature stability range better than original EO polymers (Przytuski & Wieczorek, 1992). Research on co-polymer electrolytes have come long way since then. Its application on DSSCs also shows promising outcomes like Chen et al. prepared poly(acrylonitrile-co-vinyl acetate) containing GPE and achieved a remarkable of 8.34% energy conversion efficiency (Chen et al., 2011). The vinyl acetate section of the copolymer was essential for dissolution in a nitrile based liquid electrolyte whereas, the acrylonitrile segment helped enough to improve the mechanical strength to form gel state. Likewise, the Ramesh research group have worked on studying the conductivity and dielectric properties of other co-polymers like poly(1-vinylpyrrolidone-co-vinyl acetate), poly(vinyl alcohol-co-ethylene), poly(acrylamide-co-acrylic acid), poly(vinylidene fluoride-co-hexafluoro propylene) and its

Universiti Malaya

performance as employed in DSSCs (Ng et al., 2015; Zebardastan et al., 2017; Kumaran et al., 2018; Tan et al., 2018). A concluding remark from all these research was the utilisation of co-polymer boost ionic conductivity in their own way and show good electrochemical properties.

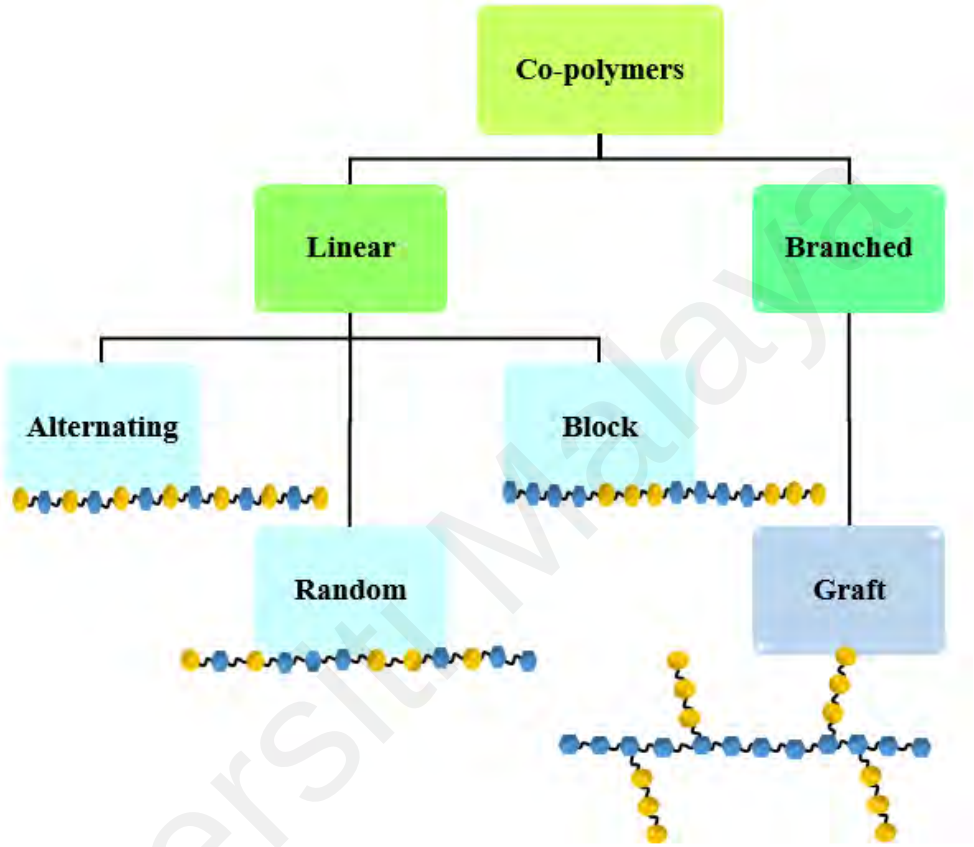

Figure 2.8 Schematic representation of various copolymer assembly.

Polymers with methacrylic ester group are among the most studied host polymers owing to excellent properties they offer such as high chemical resistance, surface resistivity and mechanical properties. PMMA in particular surpluses in non-tacking and optical abilities like high transparency. Highly conducting polymers require flexible backbones and PMMA is able to offer this requirement due to the large pendant group present. The presence of polar carbonyl (C=O) and ether (C-O-C) function groups in PMMA exhibit high affinity towards small cations like Li^+, Na^+ and Mg^{2+} forming significant polymer- ion interaction that leads to ionic conduction. Copolymerisation with

Universiti Malaya

methyl acrylic acid results in PMMA-co-MAA which has better flexibility and impact strength than unmodified PMMA (Ali et al., 2015).

This study utilises P(MMA-co-MAA) as the polymer backbone in electrolytes. Following the co-polymer structure as shown below in Figure 2.9, both PMMA and PMAA regions are amorphous with PMMA being slightly more crystalline. For this reason, the combination of both polymers is foreseen to assist in improving mechanical strengths of the electrolytes without compromising much on electrical performances. Besides, MAA has good affinity for polar solvents and capable to facilitate electrolyte swelling, whereas, MMA with the lesser affinity can maintain the structural integrity. At current, PMMA-co-MAA is a copolymer that is yet to be explored in the electrochemical field. Thus, the selection of this particular polymer is anticipated to produce fruitful outcomes to the polymer-electro industry.

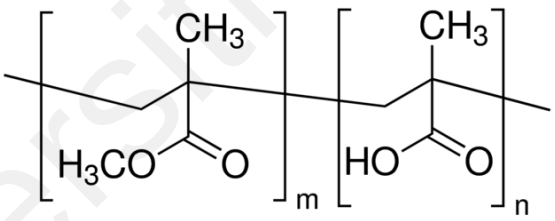

Figure 2.9: General structure of P(MMA-co-MAA).

2.5.2 Usage of Ionic Liquids

Ionic liquid is an exclusive term given to organic salts that melt below 100 ºC unlike the usual ionic compounds which are known for their high melting points. In literatures, room-temperature ionic liquids (RTIL) are also addressed as molten organic salts, fused organic salts, non-aqueous ionic liquid and neoteric solvents (Freemantle, 2010). The earliest reported use of ionic liquids back dates to 1914, however, it has been an active

Universiti Malaya

part of DSSC research only since the early 2000s. This major academic leap can be owed to the introduction of moisture and air stable ionic liquids.

The characteristics exhibited by an ionic liquid is accustomed to the organic cation and any selected anion that makes the compound. Cations present are huge highly flexible organic chains with low charge densities and possess weak intermolecular forces that loosely fit anions around themselves. Cations often influence the stability of ionic liquids whereas, anions has stronger effect on chemical functionality. It is believed that, with the wide choice of cations and anions available, customisation would allow formation of 10^{18} ionic liquids theoretically. Essentially, by altering cations and anions, huge variance in fundamental properties like solubility can be achieved making ionic liquids more sought after.

Other distinguishing characteristics of ionic liquid include good thermal stability and non-flammability, high electrochemical stability, capability to dissolve in numerous organic and inorganic solvents, excellent ionic conductivity, wide operating electrochemical window, readily recycled as solvents or catalyst for reactions and most importantly, have negligible vapour pressure. These greener credentials attract extensive use of ionic liquids in DSSCs. Organic solvent volatility and ionic conductivity of electrolytes have always been the practical problem in constructing and maintaining the durability of DSSC devices. For that reasons, non- volatile ionic liquids are usually incorporated, either partially or as whole, in preparing electrolytes for the DSSC.

Successful ionic liquid polymer electrolytes combo carry critical requirements like high ionic conductivity, good mechanical and dimensional stability with high composition retention even after long-term operation. Common cations used in the making of ionic liquids include imidazolium, pyridinium, pyrrolidinium, ammonium, phosphonium, and sulfonium. As for anions, it can be selected from a wide range of

Universiti Malaya

inorganic and organic atoms as well as polyatoms. Figure 2.10 displays the structurally diverse cations and anions commonly used to formulate ionic liquids.

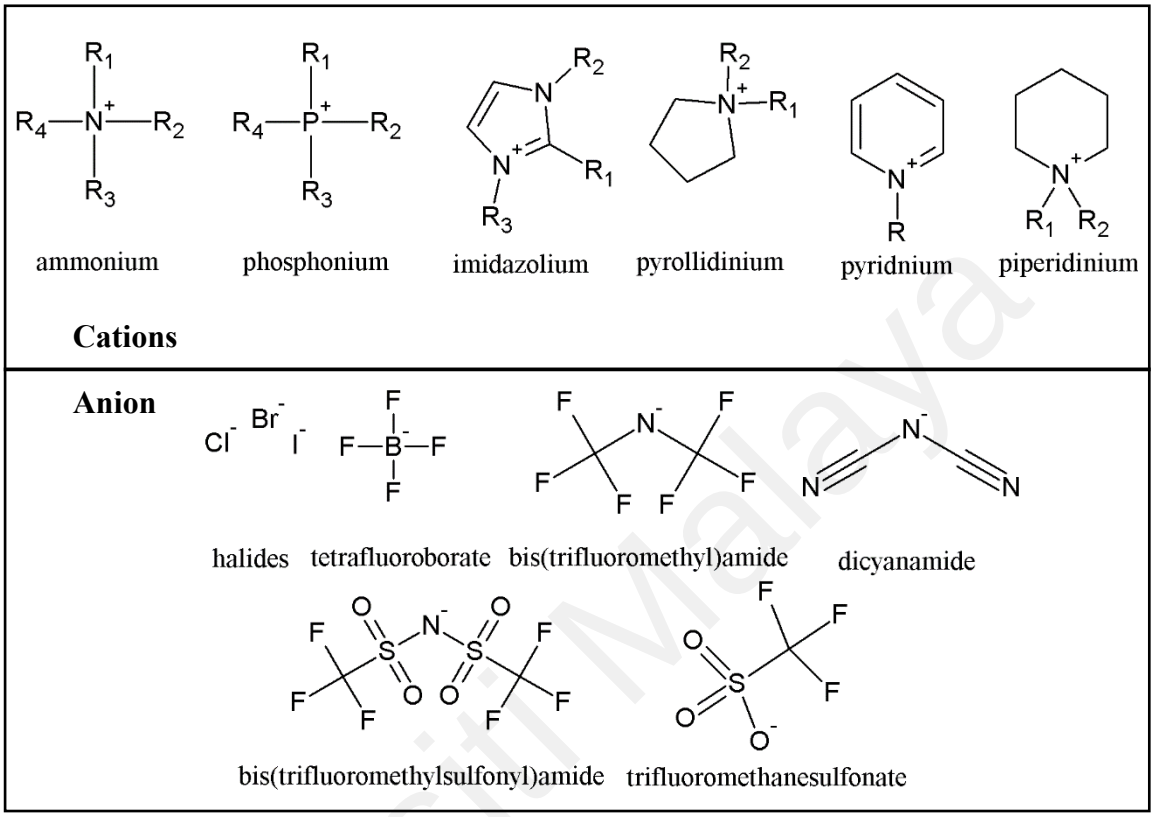

Figure 2.10: Examples of cations and anions commonly used in ionic liquids.

Prior to designing a highly performing ionic liquid-gel polymer electrolyte, it is essential to focus on the miscibility of the select a polymer matrix and the ionic liquid. Morphological impact on membrane properties and electrochemical device performance are real, thus, the expansion in pursuing copolymer and network polymer in creative ways to combine with different ionic liquid is done to yield optimized electrolytes (Ye et al., 2013).

2.5.2.1 Imidazolium Ionic Liquids

To date, literature describes about 1000 ionic liquids and roughly 300 are available commercially. An easy classification would be to separate these ionic liquids into

Universiti Malaya

imidazolium and non-imidazolium based. This section focuses on performances of imidazolium based ionic liquids which dominate the DSSC polymer electrolyte research. Imidazolium derived ionic liquids have shown persistent superiority in establishing high ionic conductivity and stability to oxidative and reductive conditions in the long run compared to other listed cations. A more physical attraction would be its low melting points and viscosity and ease of synthesis (Handy, 2005).

Besides, previous studies claim that imidazolium cations contain functional groups that efficiently hinder charge recombination at photoanode/electrolyte interface. Modified imidazolium cations in particularly with alkyl chains were reported to prolong electron lifespan in DSSCs (Kambe et al., 2002; Kubo et al., 2001). The overall conversion efficiency and stability of ionic liquid containing electrolytes are affected by factors like viscosity, interaction with electrodes, redox mediator and dye molecules along with additives.

Prior to the year 2000, power conversion efficiency utilising ionic liquids in DSSCs were less than 5%. In 2002, Wang et.al. combined poly(vinylidenefluoride-co-hexafluoropropylene)(PVdF–HFP) copolymer with 1-methyl-3-propylimidazolium iodide [MPIm][I] to produce a gel polymer electrolyte with 5.3% efficiency (Wang et al., 2002). Costa et al. reported the improvisation in ionic conductivity on poly(ethylene glycol) dimethyl ether (PEGdME) from 10^{-6} S cm^{-1} 10^{-3} S cm^{-1} upon addition 1-butyl-3-methylimidazolium hexafluorophosphate ([bmim]PF_6) ionic liquid (Costa et al., 2007). An important finding that several research groups agreed on was significant improvement on room temperature ionic conductivity upon using low viscosity ionic liquid as dopants (Singh et al., 2013; Ramesh et al., 2011; Buraidah et al., 2010).

Most research improvisations done by the same research group. The Ramesh research group from University Malaya has extensive track record on utilising various imidazolium based ionic liquids with polymer. Table 2.5 below shows some of their

Universiti Malaya

recent achievements utilising commercially available imidazolium ionic liquids in polymer electrolytes.

Table 2.5: Incorporation of various imidazolium ionic liquids with polymers.

Polymer	Ion source	Ionic liquid (wt. %)	η (%)	Reference
Polyethylene oxide	NaI/1-hexyl-3-methylimidozium iodide	9%	7.87%	(Syairah et al., 2018)
Agar	KI/1-methyl-3-propylimidazolium iodide	-	2.16%	(Nadia et al., 2016)
Poly(propylene) carbonate	NaI/1-butyl-3-methylimidozium	60%	6.14%	(Farhana et al. 2017)
Rice starch	NaI/1-methyl-3-propylimidazolium iodide	20%	2.09%	(Khanmirzaei et al., 2015)
	NaI/1-hexyl-3-methylimidozium iodide	20%	3.42%	

Very recently, Denizalti et al. synthesized five novel imidazolium ionic liquids with varying substituents from butyl to decyl aliphatic chains and incorporating ions for the sole purpose of DSSC application. The highest efficient was obtained by utilising butyl-butyl side chains to the imidazolium salt as electrolytes with J_{sc} of 17.60 mA cm^{-2}, V_{oc} of 0.60 V, *FF* of 0.49 and overall power conversion efficiency of 5.17 % Denizalti concluded that improvement on charge transport capability and inhibition of charge recombination benefits photovoltaic performances (Denizalti et al., 2018).

2.5.2.2 Non- imidazolium ionic liquids.

Alongside imidazolium cations, ionic liquid research also extends to the use of other cations like quaternary ammonium, sulfonium, quaternary phosphonium, pyyrolidium, pyridinium and piperdinium. The research on other cations was mainly due to the high

Universiti Malaya

viscosity of imidazoilium iodides, and, as a consequence, limitation in mass transport occurs. Restricted transport usually slows down ion diffusion and higher concentrations of triiodides are required to improve power conversion efficiencies in DSSCs (Yang et al., 2010). Despite the lower conversion efficiencies recorded by the listed cations in comparison to imidazolium containing ionic liquids, some positive prospects are also seen over the years. For example, phosponium containing salts are considerably inexpensive to manufacture on industrial scale and easy to be recycled. Besides, phosponium salts even have an edge with imidazolium salts in terms of thermal stability. These cations also provide wide electrochemical window for operation despite being highly viscous.

On the other hand, ammonium containing ionic compounds carry special features like low-melting points and viscosity. Their chemical and electrochemical stability ease development of ionic liquids for the safe use in high density devices (Handy, 2005). Another factor to diversify ionic liquid research was to possibly replace imidazolium derivatives to less toxic and more biodegradable cations. For example, pyridinium cation containing ionic liquids showed higher biodegradability potential compared to their imidazolium counterparts (Phuong et al. 2010). Petkovic et al. claimed that the anion present in ionic liquids presented a less predictable effect and often concluded as less significant on toxicology measures (Petkovic et al., 2011). Nevertheless, Palomar and team highly concluded that ionic liquid cytotoxicity cannot be systematically assessed from summing the independent contribution of cation and anion toxicity (Palomar et al., 2010).

On the other hand, quinolinium containing ionic liquids are among the rarely studied groups. The only reported application of quinolinium in polymer derivatives applied in DSSC technology was from Huang et al. who developed poly (acrylonitrile-*co*-styrene) polymer electrolyte containing *N*-methyl-quinoline iodide and iodine as redox source with 1,2-propanediol carbonate, dimethyl carbonate and ethylene carbonate as mixture

Universiti Malaya

solvents. Their novel polymer electrolyte recorded a best performance of 4.04% conversion efficiency by using only 0.6 M *N*-methyl-quinoline iodide (Huang et al., 2007).

Quinolinium derivatives are highly polar and show significantly different Abraham`s constant of solvation from the previously known imidazolium and pyridinium based ionic liquids. More obvious differences are observed in the π–π interactions and hydrogen bond acidity. The higher hydrogen bond acidity may be explained by a higher number of hydrogen atoms per molecule compared with other monocationic ionic liquids (Shashkov & Sidelnikov, 2019). Two alkylquinolinium containing ionic liquids were synthesized for this research by varying the anions present. Quinolinium cation was chosen for this study owing to its fused benzene and pyridine rings that possibly would supply the electrolyte system with higher electron density. Two different anions were incorporated with a common cation to study the possibility of coordinating properties by anions as much assumptions claim all ionic liquids behave like non-coordinating solvents.

In general, ionic liquids with halide anions particularly iodide tend to have higher viscosity due to high polarity of ion and more localised charge density. Pursue on non-halide ionic liquids have become increasingly favourable with halides being replaced with some weakly coordinating anions. On top of lowered viscosity, binary ionic liquids composed of anions like BF_4^-, PF_6^- and NTf_2^- are more stable thermally than their halide complements. High viscosity of ionic liquids restrict fast ion transport in electrolytes. Permissibly, higher I_3^- concentration is required to compensate their slow diffusion. Thus, incorporation of ionic liquids with halide salts is another popular approach to boost conductivity in electrolytes. Incorporation of ionic liquids with volatile solvents is also necessary as the diffusion coefficients of I_3^- in solely ionic liquid electrolytes are still about 1–2 orders of magnitude lower (Yang et al., 2010; Wasserscheid & Welton, 2008).

Universiti Malaya

2.6 Summary

This literature review addresses the current concerns in the DSSC industry, whereby there is a constant need in improvisation particularly in producing more sustainable electrolytes. Despite the high conversion efficiencies produced by liquid electrolytes consisting mainly of organic solvents, the cells carry low stability owing to volatility and flammability issues. Toxicity is also another area of concern. Polymers have been able to resolve the issue of cell leakage by gelling liquid electrolytes. Yet, polymer based electrolytes have underperformed when compared to their liquid electrolyte counter parts. In order to improve the conversion efficiency, ionic liquids are added in mixtures to address conductivity issues and promote the need of using lesser organic solvents that disrupt cell stability and safety.

This work will address the problem by incorporating novel ionic liquids to polymer electrolytes in the most viable combination. The methodologies of the preparation and characterization of polymer electrolytes with and without ionic liquids will be discussed in the following chapter.

Universiti Malaya

CHAPTER 3 – MATERIALS AND METHODOLOGY

3.1 Introduction

This chapter begins with the detailed list of materials and chemicals used in this research. Next, the comprehensive methodology employed in this research is clearly outlined. The first half of this research involves on the preparation of purified ILs and the second part focuses on the development of polymer electrolytes, fabrication of DSSCs and electrochemical analysis.

3.2 Materials

The complete list of materials utilized in this work is shown in the table below.

Table 3.1: Purchase details of materials used in this research.

	Materials	Purchased from
Ionic liquid precursor	6-Methylquinoline (98%) 1-iodobutane (99%)	Sigma Aldrich
Host copolymer	Poly (methyl methacrylate-co-methacrylic acid) [P(MMA-co-MAA)]	Sigma Aldrich
Inorganic Salt	Sodium iodide (NaI)	Friedemann Schmidt Chemical
Redox contributor	Iodine (I_2)	Friedemann Schmidt Chemical
Commercialized Ionic liquid	1-hexyl-3-methylimidazolium iodide [C_6mim][I]	Sigma Aldrich

Universiti Malaya

Table 3.1, continued.

	Materials	Purchased from
Solvents	Acetonitrile Ethyl acetate Ethylene Carbonate (EC) Propylene Carbonate (PC)	Merck
Dye	N719 (*Ditetrabutylammonium cis-bis(isothiocyanato)bis(2,2'-bipyridyl-4,4'dicarboxylato)ruthenium(II))*	Sigma Aldrich
Semiconductors	Titanium dioxide (TiO_2) P25 and P90	Degussa Germany

3.3 Research Layout

Four different iodide based polymer electrolytes were prepared. Initially, the novel copolymer P(MMA-co-MAA) was homogenized with various weight ratio of a single salt sodium iodide (NaI). This step was necessary to study the compatibility between the host polymer and the inorganic salt as well as to discover the electrochemical and physical properties. Then, the best conducting sample was incorporated with three different ionic liquids, again, at different weight ratios to produce a system with best conduction ability and mechanical strength. The ionic liquid utilized were novel N-butyl-6-methylquinolinium bis (trifluoromethylsulfonyl) imide [C_4mquin][NTf_2], novel N-butyl-6-methylquinolinium iodide [C_4mquin][I] and commercially available 1-hexyl-3-methylimidazolium iodide [C_6mim][I]. The polymer electrolytes prepared are as below.

1. P(MMA-co- MAA) –NaI
2. P(MMA-co- MAA)- NaI- [C_4mquin][NTf_2]

Universiti Malaya

3. P(MMA-co- MAA)- NaI-[C_4mquin][I]
4. P(MMA-co- MAA)- NaI-[C_6mim][I]

Figure 3.1 recapitulates the main steps carried out in this research.

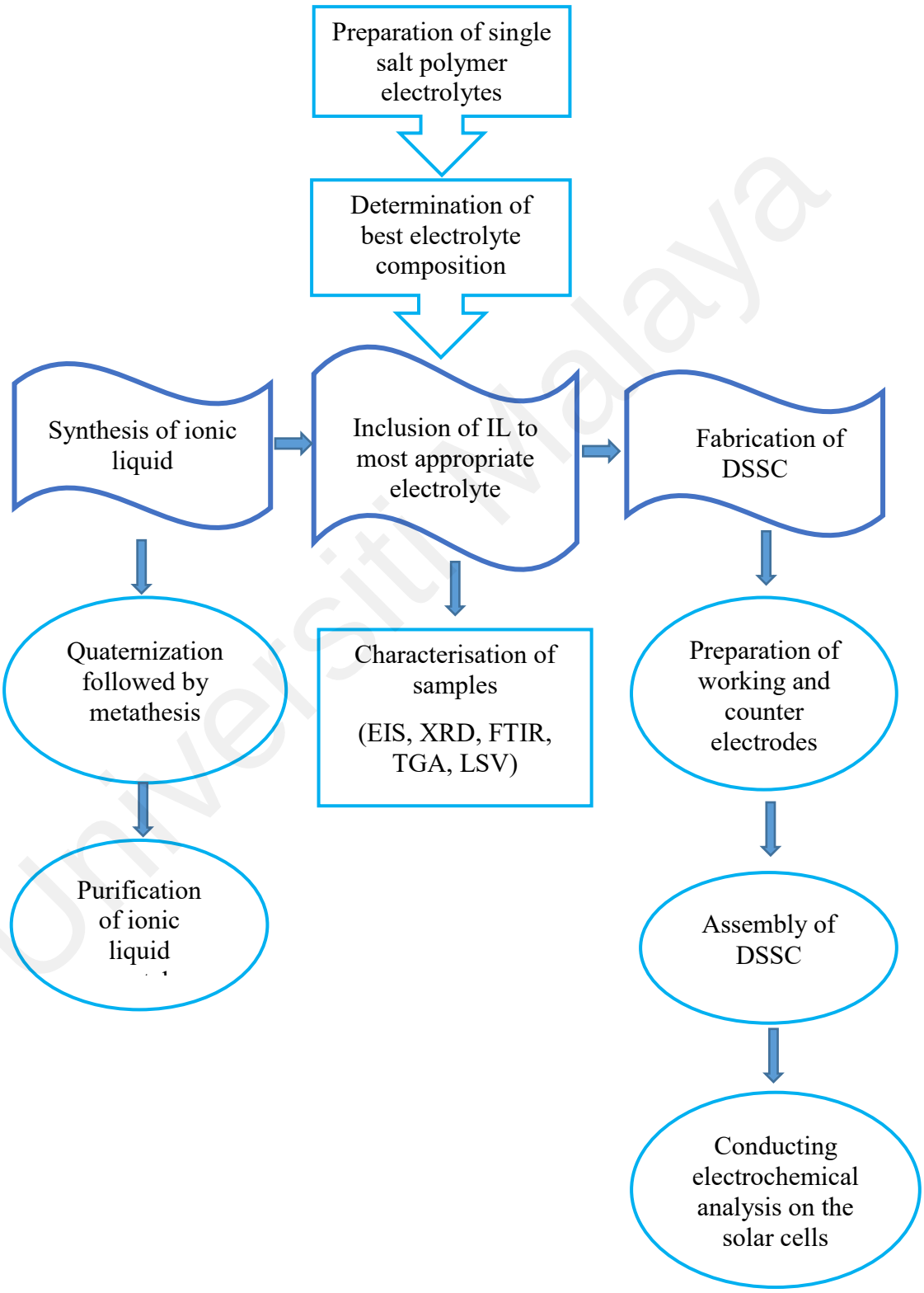

Figure 3.1: Summary of research outline.

University Malaya

3.4 Synthesis of Ionic Liquids (ILs)

This work utilized two novel ILs namely, [C_4mquin][I] and [C_4mquin][NTf_2]. The synthesis of the ILs can be divided into 3 major steps that is, precursor quaternization, and metathesis and product purification. Prior to synthesis, all starting materials were also purified following a standard designation by Ionic team in Universiti Teknologi Petronas (UTP) (Selvaraj, 2017).

3.4.1 Synthesis of [C_4mquin][I]

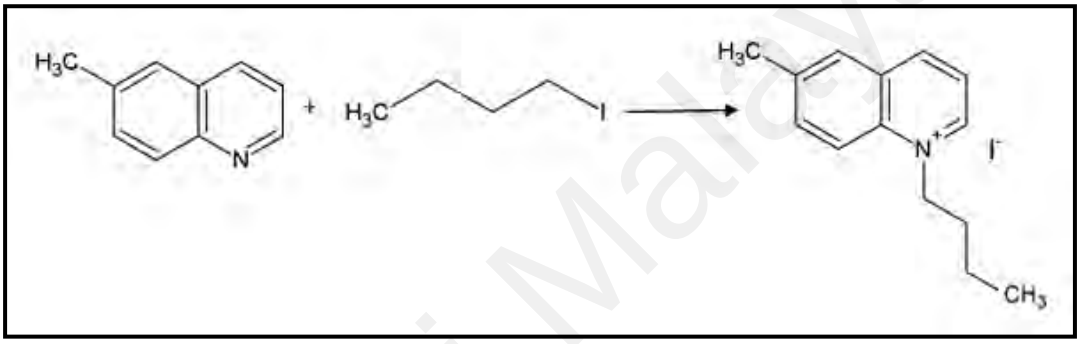

Figure 3.2: Synthetic route on the formation of [C_4mquin][I].

6- methylquinoline (50.02 g, 0.35 mol) was dissolved in 50 ml of acetonitrile. Next, 1-iodobutane (75.45 g, 0.41 mol) was added drop-wise to the precursor solution and stirred vigorously at 75 ^oC under inert condition. The reaction mixture was maintained under refluxed for 5 days before washing with ethyl acetate (5 x 30 ml). After repeated washing process, the sample was dried under vacuum. [C_4mquin][I] was crystallized using 1:1 ratio of acetonitrile and ethyl acetate. The solution was gradually boiled for 20 minutes before cooling down to room temperature. Subsequently, the sample was placed overnight in a freezer. Any traces of solvent was removed by drying under vacuum. The resulting bright yellow crystals of N-butyl-6-methylquinolinium iodide [C_4mquin][I] was characterized using ^{1}H NMR to confirm the presence of quinolinium derivative in the IL (Selvaraj, 2017).

Universiti Malaya

3.4.2 Synthesis of [C4mquin][NTf2]

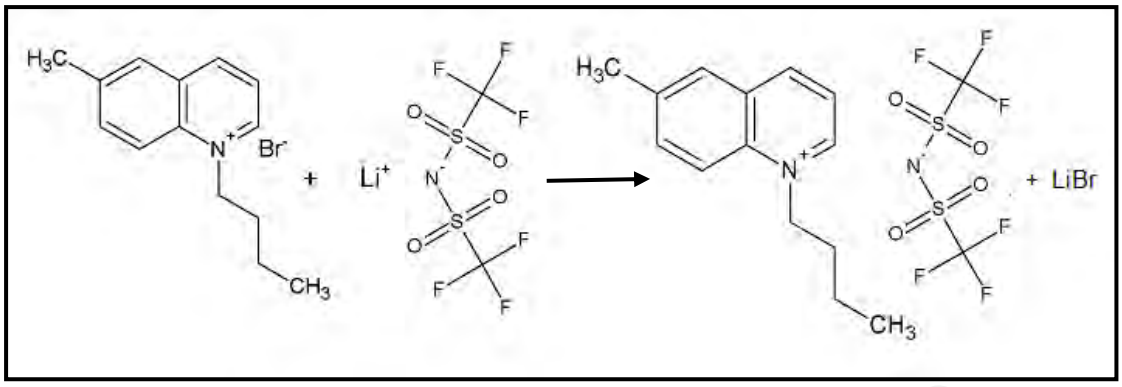

Figure 3.3: Synthetic route of the formation of [C4mquin][NTf2].

[C4mquin][Br] (10.00 g, 0.035 mol) was dissolved in deionized water and was stirred at 700 rpm with heating at 50 ºC. Next, lithium bis(trifluromethanesulfonyl) imide (10.05 g, 0.035 mol) was slowly added to the mixture and stirred for 3 hours. Lithium bromide precipitate formed was filtered off. The resulting mixture was washed with cold deionized water (5 x 20 ml) and dried under vacuum to crystal out the light red crystals of *N*-butyl-6-methylquinolinium bis(trifluoromethanesulfonyl) imide (Selvaraj, 2017).

3.4.3 Characterization of ionic liquids.

Characterization of the novel ionic liquid was necessary to confirm the structure, physical and thermal properties. Among the listed characterization done were Nuclear Magnetic Resonance (NMR) study, Fourier Transform Infrared (FTIR) study, thermogravimetric analysis (TGA), differential scanning calorimetry (DSC) and moisture content test. ^{1}H, ^{13}C and ^{19}F NMR were measured using Bruker 400 MHz spectrometer with DMSO-D6 as solvent. FTIR was recorded using Perkin Elmer Spectrum One. The measurements were made between the ranges of 4000 to 400 cm^{-1} at resolutions of 1 cm^{-1}. TGA was conducted with Perkin Elmer STA 6000 under nitrogen flow of 20 ml/min at 10 ºC/min. and DSC was carried out with Mettler Toledo DSC 1 Star System under inert nitrogen flow at heating and cooling rates of 10 °C/min. In addition to DSC testing, melting point of the ionic liquid was also determined using conventional melting point

Universiti Malaya

apparatus. Finally, the water content was determined using Mettler Toledo DL39 Karl Fisher Coulometer.

3.5 Preparation of Polymer Electrolytes

The four polymer electrolyte systems made as mentioned in Section 3.3 utilized the materials listed in Table 3.1. The amount of solvent, EC: PC, used was maintained at 1:1 weight ratio for all samples.

The only redox contributor tested in this work was the iodide/triiodide (I_2/I_3^-) pair. The weight of I_2 added was calculated to be one-fifth of the total molar weight of iodine added. A total of 24 electrolyte samples were prepared including a primary system of 6 without ionic liquids. Overall, polymer electrolytes of different weight percentage ratio of polymer and redox couple along with ionic liquids were prepared following the composition listed in tables below.

Table 3.2: Designation for P(MMA-co-MAA)-NaI gel polymer electrolytes.

Designation	Polymer: NaI (wt. %) Composition
PS0	100:0
PS10	90:10
PS20	80:20
PS30	70:30
PS40	60:40
PS50	50:50

Universiti Malaya

Table 3.3: Designations for P(MMA-co-MAA)-NaI- ionic liquid gel polymer electrolytes.

Designation			P:NaI:I_2:X (wt. %) (X = $[C_6mim][I]$, $[C_4mquin][I]$, $[C_4mquin][NTf_2]$)
P:NaI: $[C_6mim][I]$	P:NaI:$[C_4mquin][I]$	P:NaI: $[C_4mquin][NTf_2]$	
Hm5	Qi5	Qt5	49.4:38:7.6:5
Hm10	Qi10	Qt10	46.8:36:7.2:10
Hm15	Qi15	Qt15	44.2:34:6.8:15
Hm20	Qi20	Qt20	41.6:32:6.4:20
Hm25	Qi25	Qt25	39.0:30:6.0:25
Hm30	Qi30	Qt30	36.4:28:5.6:30

In order to prepare the primary electrolyte system, corresponding amounts of NaI salt was added to EC: PC in a glass vial and magnetically stirred for at 80 ^oC until complete dissolution is seen. Then, the iodine pellets were added and stirred together. Finally, upon noticing a homogenous solution, P(MMA-co-MAA) copolymer was added gradually to ease stirring. Temperature was raised to around 105 ^oC and stirring was continued for 2 hours until complete homogeneity is noticed. The same procedure was carried out in preparing the secondary electrolyte system which contained ionic liquids. However, prior to the addition of copolymer, the appropriate amounts of ionic liquid was added in stir. The resulting thick liquid-like mixture was allowed to cool down to room temperature allowing it to form gel consistency. All gel polymer electrolyte samples were kept in desiccators to prevent moisture attack.

Several studies have been conducted on the optimized GPEs namely:

Universiti Malaya

1. Electrochemical impedance spectroscopy (EIS) – Ionic conductivity studies and ion conduction mechanism
2. Fourier Transform Infrared Spectroscopy (FTIR)
3. X-ray Diffraction Spectroscopy (XRD)
4. Thermogravimetric Analysis (TGA)
5. Linear Sweep Voltammetry (LSV)

3.5.1 Electrochemical Impedance Spectroscopy (EIS)

The ionic conductivity of all GPEs made was studied using computer interfaced HIOKI 3532-50 LCR Hi-Tester. Readings were taken over a frequency range of 50 Hz to 5 MHz at room temperature 27±1 ºC. The samples were placed on a coin disc of 1.6 cm in diameter and sandwiched between two stainless steel blocking electrodes. The sweep of frequency through the sample generates a set of complex impedance, Z* value which is a contribution of real impedance, Z′ and imaginary impedance, Z″ values. The corresponding values was calculated using the formula below.

$$\boldsymbol{Z'} = |\, \boldsymbol{Z(\omega)} \,|\, \boldsymbol{\sin\theta} \tag{3.1}$$

$$\boldsymbol{Z''} = |\, \boldsymbol{Z(\omega)} \,|\, \boldsymbol{\cos\theta} \tag{3.2}$$

The resulting Z* values can be also derived as a relation of Z′ and Z″ with a constant i.

$$\boldsymbol{Z^* = Z' - iZ''} \tag{3.3}$$

The data obtained was transformed into a Cole- Cole impedance plot that displays variation of Z' and Z'' as function of frequency. An archetype Cole-Cole plot for polymer electrolyte sample is shown in Figure 3.4. The presence of two distinct regions, namely linear (low- frequency) and semicircle (high frequency) is clearly shown. Extrapolation of the semicircle intercepts the Z′ x-axis at value corresponding to bulk resistance, R_b.

Universiti Malaya

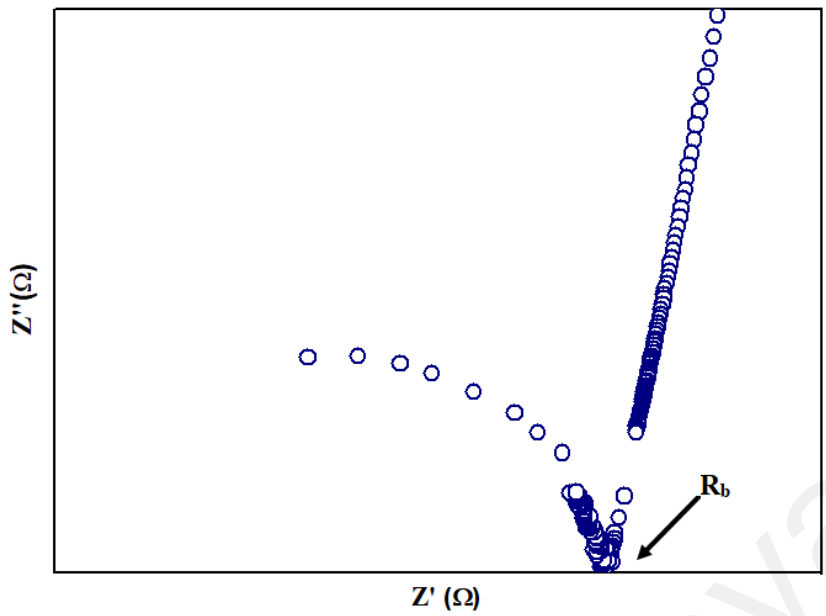

Figure 3.4: Typical Cole-Cole impedance plot for gel polymer electrolytes.

Essentially, the ionic conductivity, σ of GPE samples are measured using the following equation:

$$\boldsymbol{\sigma = l/R_bA} \tag{3.4}$$

which employs R_b values in Ω as well as thickness of the sample placed in coin cell, l and surface area, A of the stainless-steel electrodes in cm^2. These dimensions of the coin cell holding the GPE was measured using a micrometre screw gauge.

3.5.2 Fourier Transform Infrared (FTIR) Analysis

Infrared based spectroscopy provides valuable information to assess the molecular structures in the polymer mixture. Upon infrared irradiation, GPE samples are capable of absorbing light at specific wavelengths corresponding to normal mode vibration frequencies characteristic to the functional groups present. In this work, FTIR study is vital, as not only polymer- ion complexation is monitored, but polymer-ion and solvent-ion interaction were also captured as a function of varying salt concentration.

Universiti Malaya

Samples were scanned between the regions of 4000 cm^{-1} to 500 cm^{-1} at resolutions of 1 cm^{-1} with data recorded under transmittance mode using Thermo Scientific Nicolet ISIO Smart ITR. All infrared spectra collected were after doing a background correction.

3.5.3 X-Ray Diffraction Spectroscopy (XRD) Analysis

The working principles of XRD involves collection of reflected monochromatic X-ray beams that were directed to the GPEs. The interaction of incident rays with the polymer samples results in constructive interference and diffraction which can be explained using the Bragg`s equation stated as below.

$$\boldsymbol{2d\,sin\theta = n\lambda} \tag{3.5}$$

Where d, θ, n, λ are spacing distance between atomic planes, incident angle, integer and wavelength, respectively.

The relationship between X-ray wavelength and diffraction angle gives insight to lattice spacing present in crystalline samples. XRD diffraction patterns are essential to determine the relative abundance of crystallinity in homogenous polymeric mixture like GPEs. It can be also compared with reference materials. However, it does not convey information about chemical composition of the tested material. X- ray diffraction is a non-destructive technique and only small sample quantity is required. In this work, the investigation of crystallinity and amorphous nature of electrolytes made was done using PANanalytical Empyrean diffractometer with Cu $K\alpha$ radiation of wavelength λ = 1.54056 Å. Scanning was done at Bragg angles (2θ) ranging from 5º to 80º with a step size of 0.0260º at ambient temperature.

3.5.4 Thermogravimetric Analysis (TGA)

Thermogravimetric analysis (TGA) is a thermoanalytical technique which the mass of a substance is measured as a function of temperature while a reference sample is subjected to a controlled temperature program. The consequential mass loss plotted as percentage

Universiti Malaya

loss against temperature gives valid information regarding thermal stability and initial composition of the sample, possible intermediates formed upon heat treatment and remaining solid residue if any.

Initially, the sample is placed into a silica TGA sample holder then placed on a sensitive balance and finally into the high temperature chamber. The mass of the sample is weighed at room temperature and the mass changes is monitored with gradual increase in heat. The TGA was done on a Perkin Elmer Pyris Diamond TG/DTA Instrument Universal. The sample was heated from 25 ºC to 850 ºC at a heating rate of 50 ºC min^{-1} under inert nitrogen atmosphere. In addition to inferring thermal stability, the weight losses observed in TGA can be quantified to predict degradation pathway.

3.5.5 Linear Sweep Voltammetry (LSV)

Symmetrical cell steady-state current measurements were done using linear sweep voltammetry techniques provided by NOVA software connect with Metrohm Autolab potentiostat (PGSTAT128N) to calculate the triiodide diffusion coefficient. The estimation of electrochemical window stability utilized Pt/electrolyte/Pt configuration with a hole area of 0.2 cm^2 and spacer thickness of 0.047 mm, the symmetrical cells containing GPE were scanned on a voltage sweep from − 0.7 to 0.7 V with 10 mV s^{-1} scan rate conducted at room temperature. LSV voltammograms contain current response plotted as a function of voltage.

3.6 Fabrication of DSSC

3.6.1 Preparation of Electrodes

Fluorine doped conducting glass plates (FTO) with average surface resistance of 12 Ω cm^{-2} were used in the preparation of both working and counter electrodes. All FTO substrates were cleaned using distilled water and ethanol prior to use. Working electrode, also known as photoanode, was prepared by depositing two layers of mesoporous

Universiti Malaya

titanium dioxide (TiO_2) nanoparticles of different size (P-25 and P-90). The first layer was made by spin coating a slurry of P-90 in nitric acid (pH-1) at 2350 rpm for 50 seconds. The resulting coat was sintered at 450 ^oC for 30 minutes and left to cool to room temperature to form a thin compact layer. A compact initial layer is essential for better adhesion of TiO_2 to the FTO plate. Besides, contact between redox electrolytes and conducting glass substrate is also minimized which is crucial to prevent electron recombination in DSSC (Kovash et al., 2012). Next, a second layer consisting of P-25 made slurry in nitric acid with few drops of Triton-X was applied on top of the first layer by doctor blading technique. Sintering process was done at similar conditions as first layer. For the purpose of this study, anatase type TiO_2 is utilized due to its ability to allow adsorption of large amount of dye molecules with its high surface area. Nevertheless, we fear an increase in the rate of recombination. Thus, as suggested a multilayer coated is done to improve overall cell performance.

The dual coated working electrode was immersed in an ethanolic dye solution containing ruthenium, N719 ((Di-tetrabutylammoniumcis-bis(iso-thiocyanato) bis (2,2-bipyridy 4,4'dicarboxylato)ruthenium(II)) 24 hours before use.

In order to fabricate the counter electrode, an aqueous solution with 1:1 weight ratio of chlorplatinic acid solution (H_2PtCl_6) in isopropyl alcohol (C_3H_7OH) was prepared and spotted over a pre-cleaned FTO. After spotting, the setup was sintered at 450 ^oC for 30 minutes. Subsequently, the counter electrode is rinsed with ethanol and the same steps were repeated 2 to 3 times to produce a dense reflective Pt coated counter electrode.

3.6.2 Assembly of DSSCs

The prepared working and counter electrodes were assembled as shown in Figure 3.5. A small amount of polymer electrolyte made was applied on the surface of the dye sensitized TiO_2 layer. Next, the Pt counter electrode was placed on-top, creating a

University Malaya

sandwich type cell and clipped together. This assembly was possible since the electrolytes were in gel form and no leakages were noticed. Using a black tape, an active area of 0.3 cm^{-2} was set. Performance of each polymer electrolyte made was determined by conducting current density –voltage measurement for three different replicated cell of the same electrolyte composition. Along with this, electrochemical impedance spectroscopy of the DSSC was also studied.

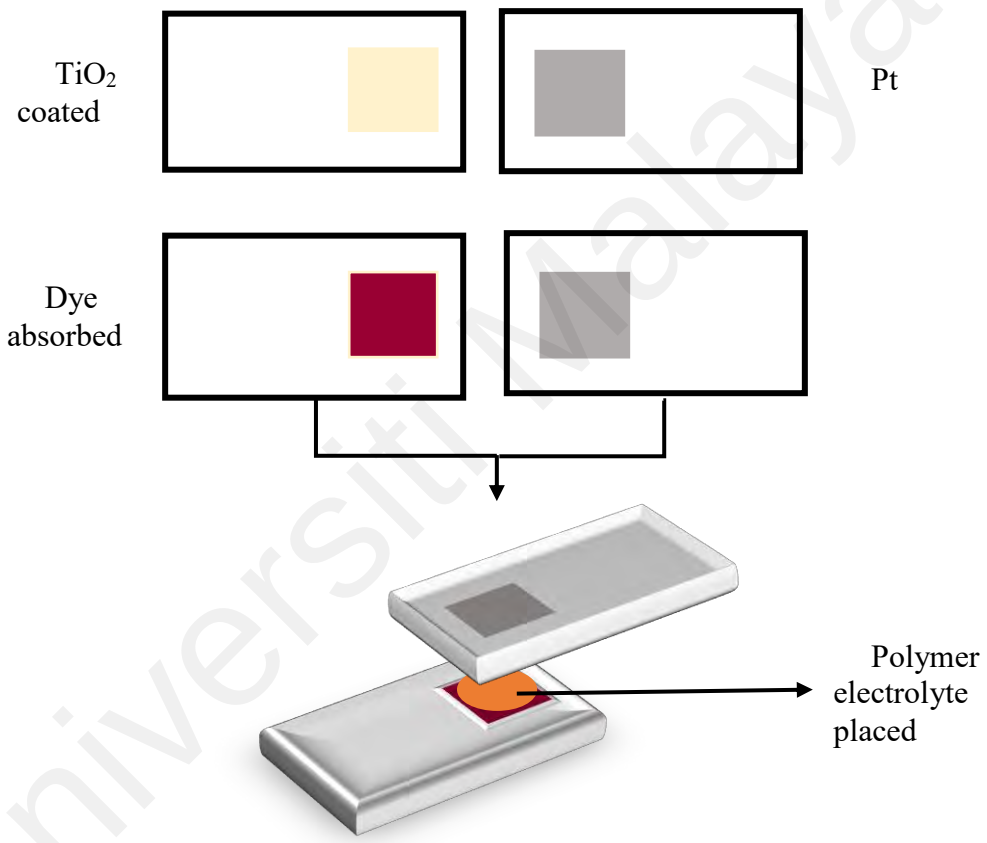

Figure 3.5: Schematic summary of DSSC fabrication.

3.6.3 Current- Voltage measurements

The DSSC`s cell efficiency was determined by measuring photocurrent density-voltage characteristics under 1 sun illumination that is, at a stimulated solar spectrum of air mass 1.5 (1.5 AM) and intensity of 100 mW cm^{-2} (P_{in} = 1.0). Under normal lab atmosphere, there is an offset of sunlight reaching the DSSCs. Hence, a calibrated lamp

Universiti Malaya

source from the solar stimulator was set to make sure the incident light has pass 1.5 times longer in air before hitting the surface of the DSSCs.

The assembled cell was placed directly under the solar stimulator and was connected to the data analyser using crocodile clips. The current density- voltage characteristics produced by each DSSC was studied by an external load sweep from zero to infinity or in other words, from short circuit conditions to open circuit conditions. The sweep was repeated until stable readings were achieved. Metrohm Autolab potentiostat (PGSTAT128N) automatically calculates P_{max}, J_{max}, $V_{max,}$ FF and η and the resulting data is presented as a J-V curve as shown in Figure 2.5. The parameters are defined following the equations listed in section 2.2.4. The maximum power is generated at maximum current density and voltage given as J_{max} and V_{max} respectively as shown below.

$$\boldsymbol{P_{max} = J_{max} \times V_{max}} \tag{3.6}$$

3.6.4 Electrochemical Impedance Spectroscopy

Electrochemical impedance analysis of the assembled DSSC was carried out using Metrohm Autolab potentiostat (PGSTAT128N) in a frequency range of 0.1 Hz – 100 kHz with AC potential of 10 mV under no light conditions. The impedance spectra obtained for each electrolyte system was analysed using Metrohm Autolab Nova software by the means of fitting suitable equivalent circuits.

Universiti Malaya

CHAPTER 4- RESULTS AND DISCUSSION 1: CHARACTERIZATION OF POLYMER ELECTROLYTES.

4.1 Introduction

This chapter discusses the results and findings obtained in this research. The first section discusses on the synthesis of two novel ionic liquids along with their characterization. The second part consists the discussion of the physical, thermal, electrochemical properties of four P(MMA-co-MAA) based gel polymer electrolytes with and without ionic liquids based on the studies mentioned in Section 3.5

4.2 Synthesis and Characterization of Novel Ionic Liquids.

The synthesis of *N*-butyl-6-methylquinolinium iodide and precursor N-butyl-6-methylquinolinium bromine from 6-butylquinoline involves the quaternization reaction of amine with a corresponding alkyl halide. The reaction is initiated by mixing and heating the reactants for a prolonged period. Mechanistically, this is a bimolecular nucleophilic substitution, SN_2 reaction that involves the rear-side attack of a nucleophile occurring simultaneously with the parting of the leaving group (Wilkinson, 1997). This is shown in Figure 4.1 below. With bonding electrons present on 6-methylquinoline, it acts as the nucleophile and attacks the electrophilic carbon-halogen bond in 1-iodobutane forming a bond. Both reactant species are involved in rate determining step to form the transition state. A generalized SN_2 rate equation for this reaction would be, rate = k [6-methylquinoline][1-iodobutane].

Universiti Malaya

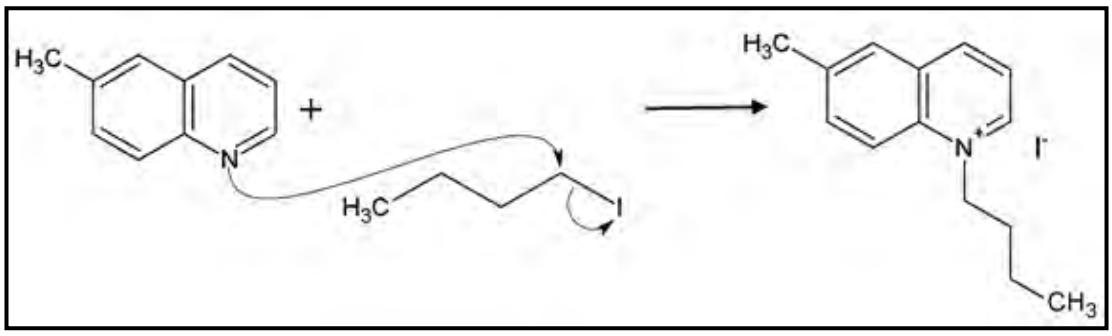

Figure 4.1: The SN_2 mechanism showing the quaternization of 6-methylquinoline with 1-iodobutane.

Reaction rates involving SN_2 reactions rely on the alkyl halide used and are generally more efficient with primary halides like 1-iodobutane that possess minimal steric hindrance. Polar solvents were required for the solvation of precursors, thus, acetonitrile was the chosen as the most suitable instead of other solvents like ethyl acetate and DMSO, owing to high solubility of 6-methylquinoline, 1-iodobutane and N-butyl-6-methylquinolinium iodide in it. The nucleophile stability is further enhanced and becomes more available in the presence of polar aprotic solvents like acetonitrile (Parker, 1969). This reaction required an optimal reaction of 5 days which generated the highest yield of 82% for N-butyl-6-methylquinolinium iodide. The formation of a second generation, non-iodide, ionic liquid *N*-butyl-6-methylquinolinium bis(trifluoromethanesulfonyl) imide involved the ion exchange reaction between N-butyl-6-methylquinolinium bromide and lithium bis(trifluromethanesulfonyl) imide. The yield recorded was 87%.

Both pure ionic liquids were a result of multiple steps synthesize that worked very efficiently. The methodology includes purification of starting materials primarily to remove moisture, optimization of reaction conditions like solvent suitability and ideal reaction time, recrystallization and vacuum drying. The revised procedure was successfully done by a team from UTP and was adapted for the purpose of this research (Selvaraj, 2017). The essential characterization listed previously was done to confirm the structure and determine their physical and thermal properties of the novel ionic liquids.

Universiti Malaya

The FTIR data revealed information regarding conversion of reactants completely into products. All vibrational frequencies were justified based on literature findings. Reactant 1-iodobutane contained strong C-H stretching peaks around 2950 cm^{-1} and bending peaks around 1460 cm^{-1} due to the alkane chain present whereas, C-I stretching are commonly found less than 600 cm^{-1}. As for 6-methylquinoline, aromatic C-H stretches show around 3150-3050 cm^{-1} (William E. Acree, Jr., n.d.). As for the products, [C_4mquin][I] FTIR data displayed strong peaks corresponding to the C-H and C-C behaviour in the *N*-butyl-6-methylquinolinium cation as shown in Figure 4.3. As for [C_4mquin][NTf_2], general C-H stretches were noticed from Figure 4.2 along with some distinctive peaks corresponding to the additional functional groups present. Table 4.1 shows exact vibrational frequencies for the two ionic liquids.

Table 4.1: Vibrational frequencies of [C_4mquin][NTf_2] and [C_4mquin][I] based on Figure 4.2 and 4.3.

	Wavenumber (cm^{-1})	Vibration description	Contributing group
[C_4mquin][NTf_2]	1340	S=O	Sulfoxide
	1191	C-F	
	1134	S=O	Sulfoxide
	1052	S-N	Sulfonamide
[C_4mquin][I]	3495	O-H stretch	Water
	3029	=C-H stretch	Alkene
	2959	C-H stretch	Alkane
	1591 - 1460	C-C stretch	Aromatic

Universiti Malaya

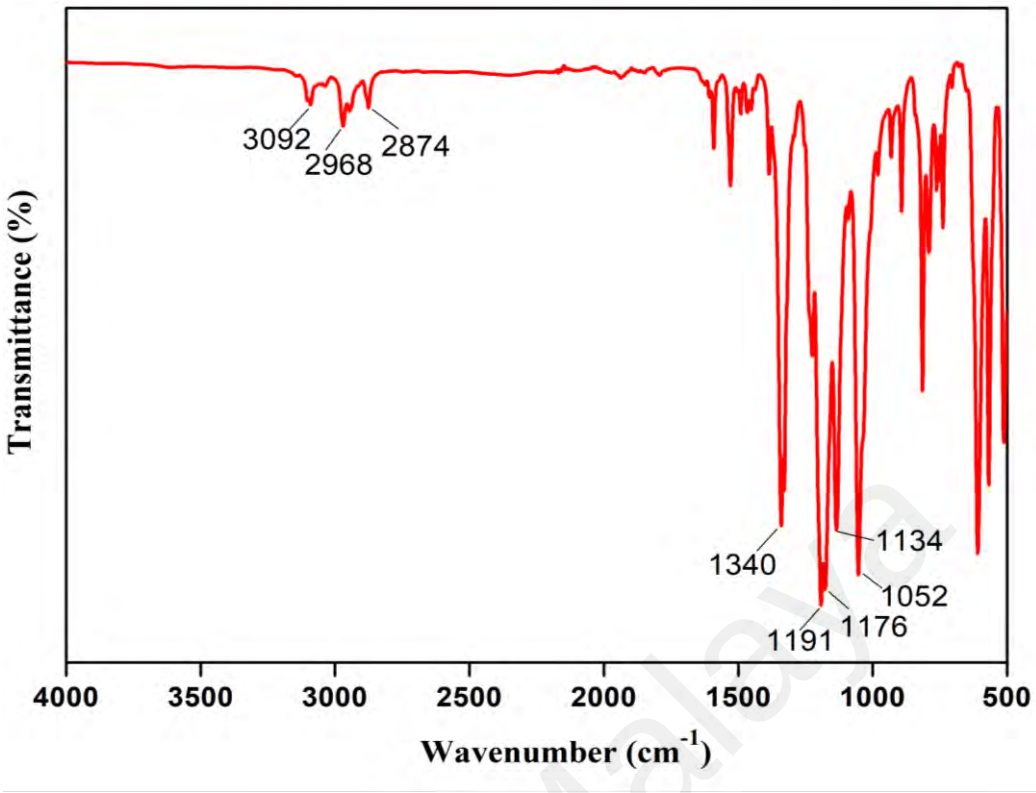

Figure 4.2: FTIR spectrum of pure [C4mquin][NTf2].

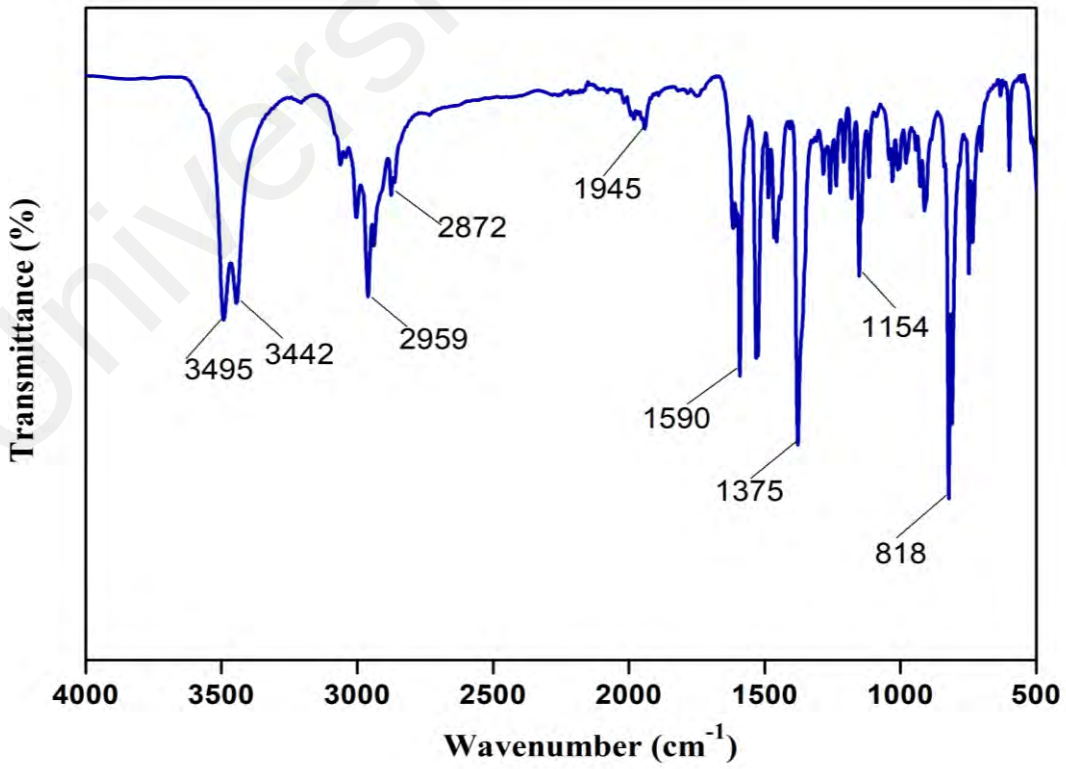

Figure 4.3: FTIR Spectrum of pure [C4mquin][I].

Universiti Malaya

In order to further elucidate structure of ionic liquids and monitor progress in product formation, ^{1}H and ^{13}C NMR analysis has been used. Additionally, the ^{19}F NMR was utilized for the synthesis of [C_4mquin][NTf_2] only. Both ionic liquids showed good dissolution in deuterated dimethyl sulfoxide (DMSO-d_6), deuterated methanol and water. However, despite being hygroscopic and high in viscosity, DMSO-d_6 was used as the solvent to obtain the spectra which had shown good peak resolution. As such, the solvent peak shows well around 2.6 ppm with multiple splitting. Split patterns and position found in ^{1}H and ^{13}C NMR for [C_4mquin][NTf_2] and [C_4mquin][I] are almost analogous indicative of the correct formation of the desired product despite [C_4mquin][NTf_2] being a second generation ionic liquid. The detail on peak splitting and its position for both ionic liquid is as listed below.

N-butyl-6-methylquinolinium bis(trifluoromethylsulfonyl)imide (7.44 g, 87 %);

^{1}H NMR δ 0.90–0.93 (t, J = 7.4 Hz, 3H), 1.35–1.43 (m, 2H), 1.90–1.97 (m, 2H), 2.61 (s, 3H), 5.04–5.07 (t, J = 7.6 Hz, 2H), 8.12–8.16 (m, 2H), 8.26 (s, 1H), 8.54–8.56 (d, J= 9.1 Hz, 1H), 9.18–9.19 (d, J = 8.3 Hz, 1H), 9.52–9.54 (d, J = 4.9 Hz, 1H); ^{13}C NMR δ 13.9, 19.6, 21.3, 33.0, 57.5, 119.2, 122.6, 129.6, 130.35, 136.4, 138.1, 140.7, 147.0, 149.0; ^{19}F NMR δ -78.73 (Selvaraj, 2017).

N-butyl-6-methylquinolinium iodide (25.52 g, 82 %);

^{1}H NMR δ 0.92–0.95 (t, J =7.4 Hz, 3H), 1.37–1.44 (m, 2H), 1.91–1.97 (m, 2H), 2.63 (s, 3H), 5.04–5.07 (t, J = 7.5 Hz, 2H), 8.13–8.17 (m, 2H), 8.27 (s, 1H), 8.54–8.56 (d, J = 9.1 Hz, 1H), 9.17–9.19 (d, J = 8.3 Hz, 1H), 9.48–9.50 (d, H = 6.9 Hz, 1H); 13C NMR δ 13.9, 19.6, 21.3, 32.0, 57.6, 119.2, 122.6, 129.6, 130.4, 136.4, 138.1, 140.7, 147.0, 149.0 (Selvaraj, 2017).

Complete ^{1}H, ^{13}C and ^{19}F NMR spectra are presented under appendix.

Universiti Malaya

The thermogravimetric analysis was able to convey information regarding the overall thermal stability of the ionic liquids. Neither [C_4mquin][NTf_2] nor [C_4mquin][I] had decomposed below 200 ^oC which is ideal to be incorporated into electrolytes of DSSC. However, the ionic liquid containing the NTf_2 group showed better thermal stability. This can be owed to the hydrophobicity of the large anion and halide ions in general record a lower thermal stability than non-halide anions (Huddleston et al., 2001). TGA curves in Figure 4.4, show absence of multistep degradation for both ionic liquids. The thermal stability of analogous ionic liquids with varying anions depends on the nucleophicity and basicity of the anions. Halides significantly reduce thermal stability since they possess both a relatively high nucleophilic and basic character (Maton et al., 2013). Single step degradation is a favourable result as it indicates that the cationic and anionic interaction is not altered with varying temperature. An SN_2 thermal degradation character is probable for halide ionic liquids with multiple simultaneous homolytic cleavage and proton transfer of the hydrocarbon fragments occurring between 200 ^oC- 300 ^oC. As for [C_4mquin][NTf_2] a slight shouldering degradation is noticed above 400 ^oC which is probable of a degradation of the perfluorinated NTf_2 organic anion. Ionic liquids carry a wide liquid range with the lower limit being the glass transition temperature and upper limit as the decomposition temperature. Differential scanning calorimetry technique showed the glass transition temperature (T_g) values of the ionic liquids as depicted in Figure 4.5 and 4.6. Table 4.2 tabulates the physical and thermal properties for both ionic liquids. Halide functionalized ionic liquids tend to have higher glass transition temperatures than their non-halide counterparts and not surprisingly, [C_4mquin][I] had a higher T_g value than [C_4mquin][NTf_2]. The lower T_g value noted is due to the larger charge delocalization which causes weaker inter-ion contacts. Glass transition temperature value are important in the design of ionic liquids as it reveals more noticeable changes in heat capacity and thermal expansivity which usually happens in the

Universiti Malaya

solidification of viscous liquid during cooling (Alireza et al., 2012). [C_4mquin][I] and [C_4mquin] [NTf_2] formed crystals upon cooling and their melting temperatures below 80 ^oC makes them ideal to be incorporated to develop quasi-solid polymer electrolytes.

In order to reduce the moisture content in the crystalized ionic liquid, repeated vacuum drying was done and this technique was able to reduce the moisture content of the sample to a very low level of less than 0.05%. This was remarkable as iodide are somehow hydrophilic and bis(trifluoromethylsulfonyl) imide is noted to be hygroscopic, that its, capable of absorbing moisture from air. Both ionic liquids were sensibly stored in neutral alumina contained desiccators.

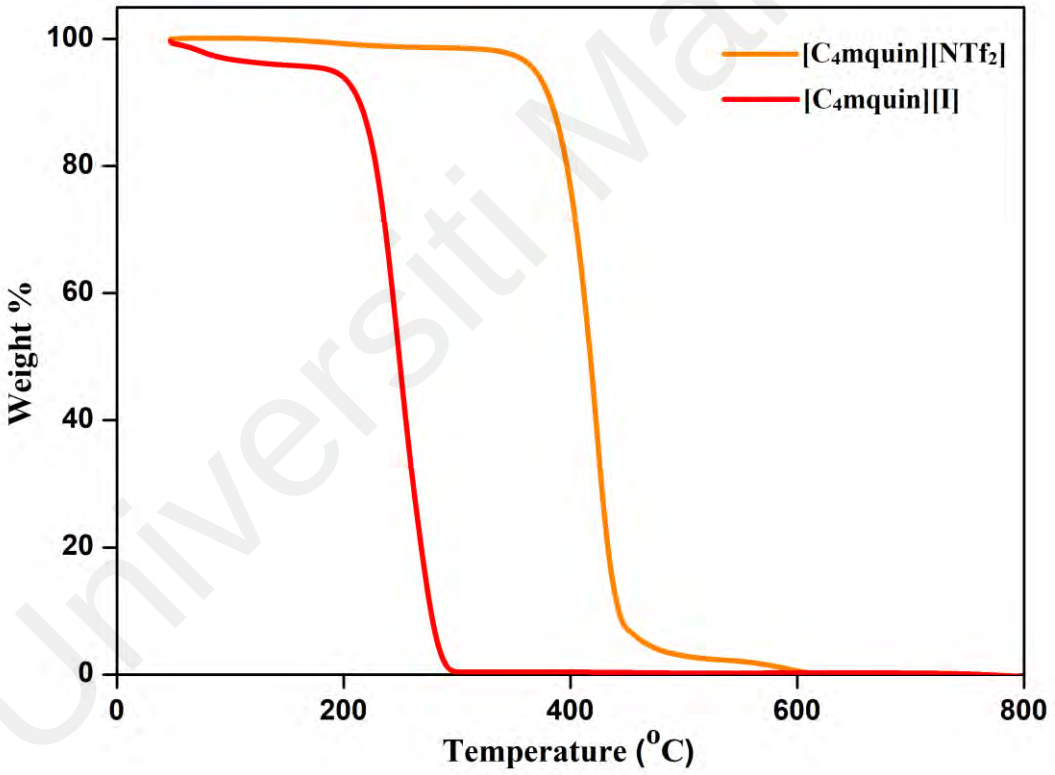

Figure 4.4: TGA curves for [C_4mquin][NTf_2] and [C_4mquin][I].

Universiti Malaya

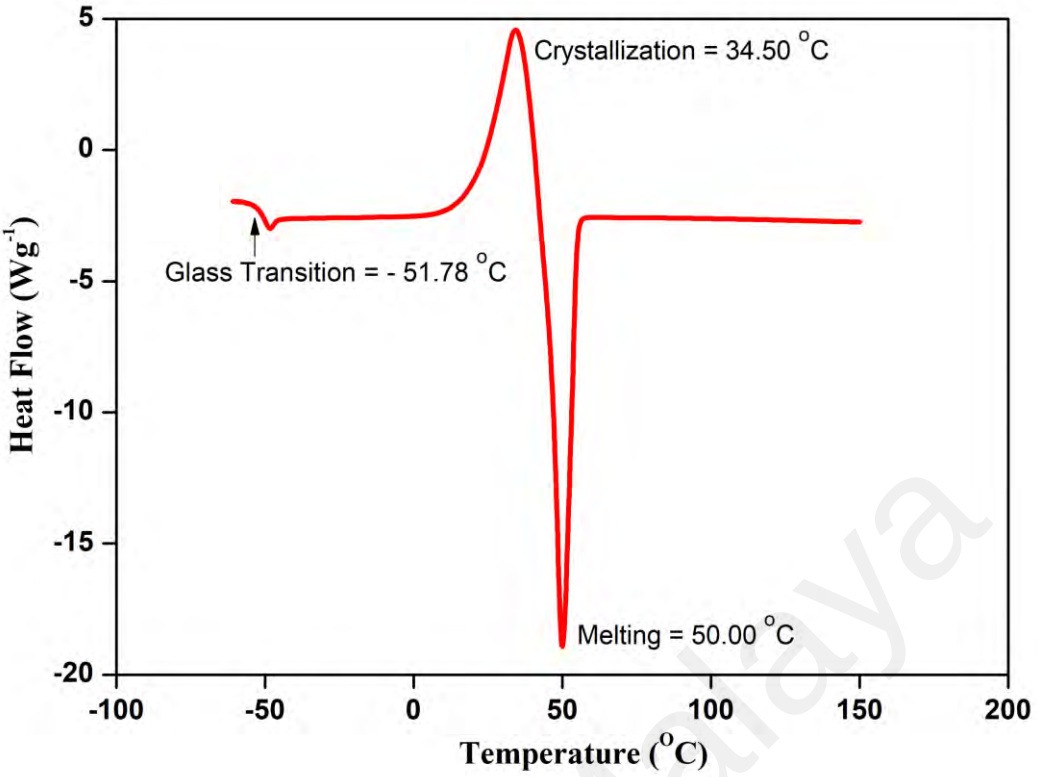

Figure 4.5: DSC curve for [C4mquin][NTf2].

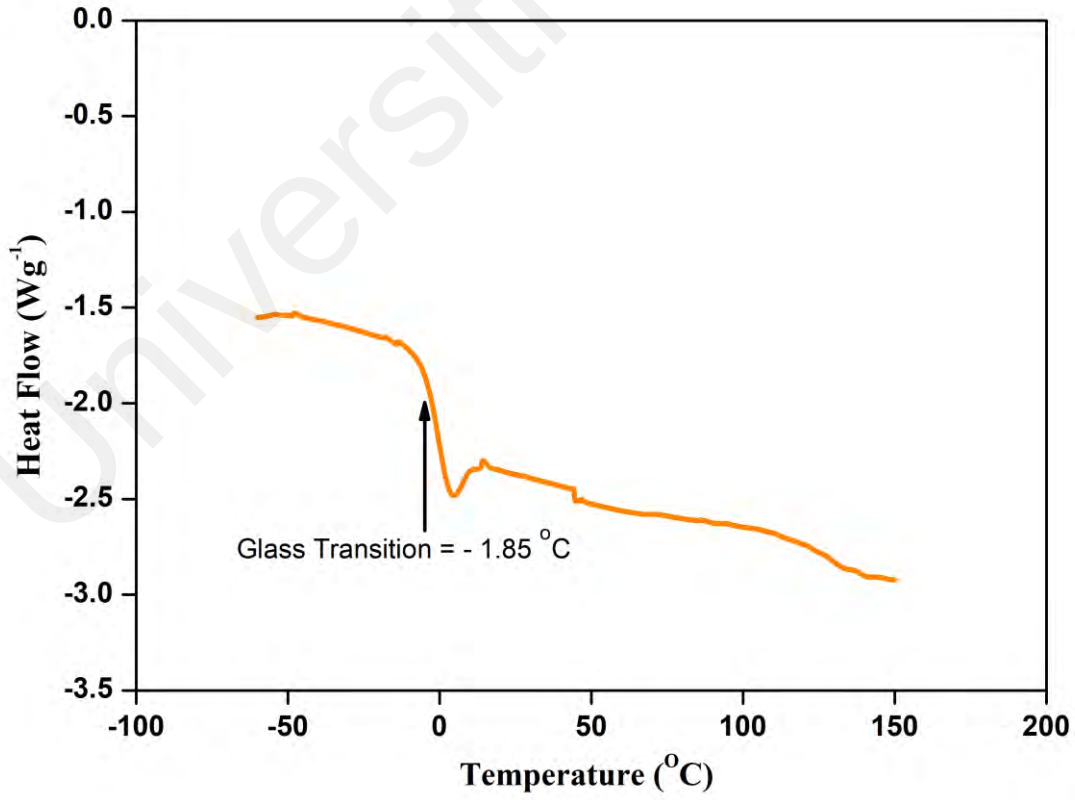

Figure 4.6: DSC curve of [C4mquin][I].

Universiti Malaya

Table 4.2: Thermal properties of ionic liquids.

Ionic liquid	Molecular weight (g/mol)	Density (g/ml)	Onset T_d (^oC)	T_m (^oC)	T_g (^oC)
$[C_4mquin][I]$	327.20	1.21	219.93	76.90	-1.85
$[C_4mquin][NTf_2]$	480.45	1.07	390.00	47.40	-51.78

T_d - decomposition temperature, T_m - melting point, T_g - glass transition temperature.

XRD diffractograms display in Figure 4.7 depicts the highly crystalline nature of both ionic liquids as significant amount of scattering is present. The narrow sharp peaks are sufficient to confirm that the ionic liquids made form crystalline solids upon cooling and are not amorphous.

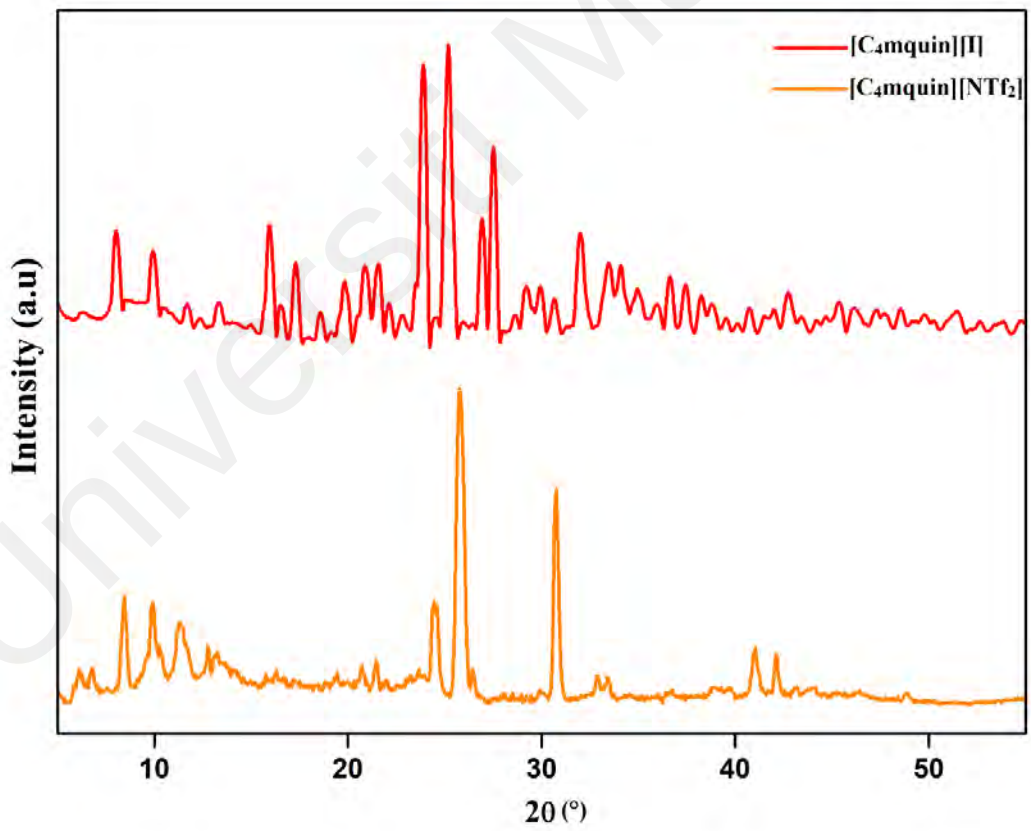

Figure 4.7: XRD diffractograms of pure $[C_4mquin][NTf_2]$ and $[C_4mquin][I]$.

Universiti Malaya

4.3 P(MMA-co-MAA)-NaI Gel Polymer Electrolyte.

Electrochemical impedance spectroscopy gives character to the changes that occur at boundaries or surfaces under specific system parameters. With reference to frequency, impedance can reveal underlying chemical processes. As such, it is used as tool to measure the dielectric and transport properties in materials.

As previously discussed, polymers themselves are mainly inert towards electronic and ionic conduction. P(MMA-co-MAA) is no different. Hence, a chosen ionic salt is added to P(MMA-co-MAA) forming an electrolyte that supports ionic conduction, which in this study is NaI. NaI is listed among the smaller sized salt. NaI was particularly chosen than the commonly used LiI in DSSC studies owing to several reason. Based on literary exhaustion, NaI is found capable of producing comparable total conductivity with LiI and is available commercially at a cheaper price. The photovoltaic performances of NaI-based cells also overtook their potassium iodide (KI) counterparts (Lee et al., 2010; Bella et al., 2016). Since Na^+ cation (227 ppm) is slightly larger than the lithium cation (182 ppm), better charge separation is anticipated between the cation and anion as electrostatic force of attraction would be lower. Indeed, Li^+ ions are found to have better cationic conductivity than Na^+, however it should be noted that performance of DSSC depends primarily on the anionic conductivity. Besides, NaI has also shown better solubility in the solvents used in this study as compared to KI. The ionic conductivity obtained is discussed in this section and the improvement in conductivity observed with ionic liquids are discussed later in this chapter.

4.3.1 Ambient temperature ionic conductivity studies

Diffusion of ions through polymer free volume results in ionic conduction. As the number of free moving ions increase, the higher the achieved ionic conductivity. Prior to the addition of NaI, the observed ionic conductivity of pure P(MMA-co-MAA) dissolved

Universiti Malaya

in EC:PC was in the order of 10^{-5} S cm^{-1}. Pure polymers contain tightly bound electrons and in the absence of free moving ions results in very low conductivity value. The ionic conductivity measured for ionic liquid–free polymer electrolytes with regard to different concentration of NaI was a lead-in step to determine the most suitable mass ratio of P(MMA-co-MAA) to NaI be used for ionic liquid–added polymer electrolytes in next step. Figure 4.8 displays the ionic conductivity of polymer electrolytes without addition of ionic liquids as a function of different mass fraction of NaI.

On the other hand, the impedance plot, Cole- Cole plot, shown in Figure 4.9 for samples with increasing salt wt. % highlights the presence of a linear and pseudo semicircle region at the low and high frequency region respectively. Initial impedance observed at low frequency is due to ion conduction in bulk and as the frequency surges, a linear residual tail indicates the occurrence of blocking effect at the electrolyte/electrode boundary (Subramania et al., 2013). An equivalent circuit representation would link a resistor and a capacitor in parallel to denote ion migration throughout the polymer matrix and the bulk polarisation of the immobile polymer chain respectively (Abarna & Hirankumar, 2017). The disappearance of semicircle at higher frequency regions is a good indication that current carriers are predominantly ions (Selamat et al., 2017). Hence, the conductivity obtained for this system is greatly influenced by free moving ions rather than movement of electrons. Besides, a single semicircle obtained indicates the absence of interference which is a result of excellent contact between the electrodes and polymer electrolytes.

The numbers beside each polymer electrolyte sample is the wt. % of salt present in the mixture. Interception of the extrapolated semicircle on the x-axis gives bulk resistance, R_b values. Based on the Cole-Cole plot in Figure 4.9, the R_b values obtained for each GPE samples is used to calculate ionic conductivity using *Equation 3.4*. The variation in ionic conductivity is shown in Figure 4.8 along with the exact value in Table 4.3.

Universiti Malaya

Based on the results, R_b values decreased with increasing salt content of up to 40 wt. % of NaI denoted as PS40. This basic system recorded a highest ionic conductivity of 1.07 mS cm^{-1} at room temperature for 40 wt. % NaI. When ions were introduced gradually at different wt%, a significant increase in ionic conductivity is observed before a rapid decrease at 50 wt. % NaI (PS50). Generally, the mobility of the redox couple I^-/ I_3^- governs the ionic conductivity which is described by the *Equation 2.6*.

The equation clearly depicts that concentration of ions has a direct effect on the ionic conductivity of the electrolytes when charge and mobility of ions remain constant. Nevertheless, in the present electrolyte system, ion mobility is hardly fixed for all samples as varying polymer network and electrolyte crystallinity largely affects motion. Plasticizer cum solvent like EC/PC is capable of promoting ion mobility, owing to their high dielectric constant (Kumaran et al., 2018). Increasing salt concentration and lowering polymer content shows improvement in ionic conductivity as crystallinity is reduced. Conductive channels are free to allow ion percolation which is usually hindered in crystalline region. In order to create an amorphous region, a 1:1 ratio is maintained between the plasticizer. Previous studies have clearly noted that the particular composition yielded good conductivity and sample sustainability as compared to other blend ratios (Khiar & Arof, 2010).

All samples prepared contained a maximum of 50 wt. % of EC/PC to prevent disruption of desired structural integrity. Progression in ionic conductivity with increasing salt concentration does not apply beyond saturation point. The observed drop in ionic conductivity at 50% weight ratio of salt is an end-result of neutral pair reservoir owing to agglomeration of excess ions along with reduction in polymer chain dynamics.

Universiti Malaya

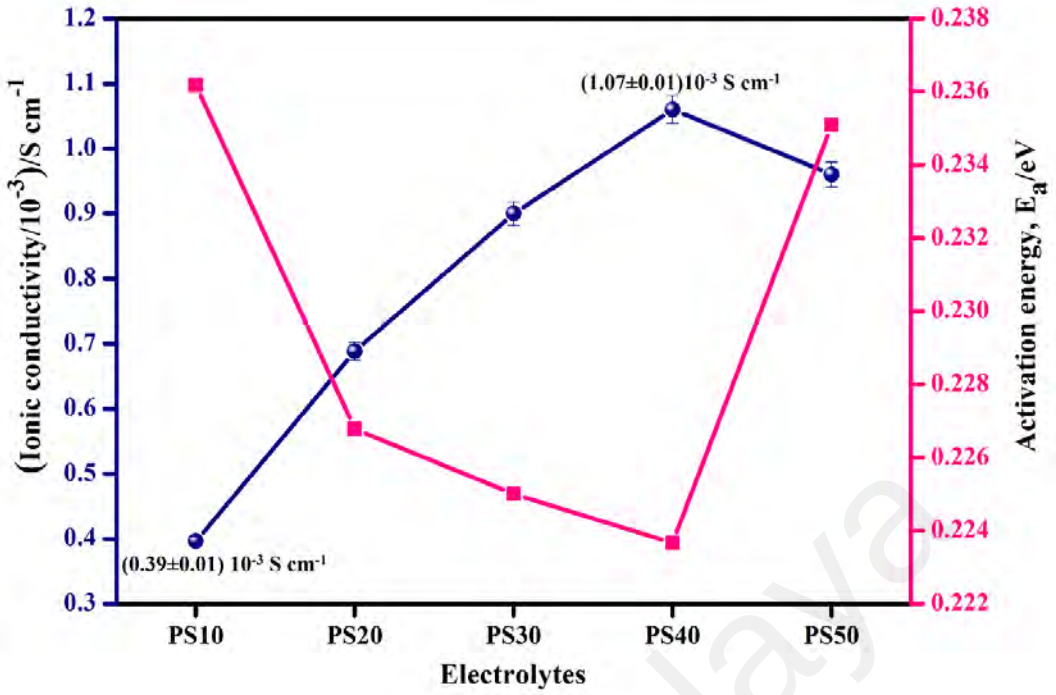

Figure 4.8: Variation in ionic conductivity of the GPE samples with different NaI concentration at room temperature.

Table 4.3: Ionic conductivity values for P(MMA-co-MAA)-NaI GPE samples at room temperature.

Electrolytes	Average R_b (Ω)	Ionic conductivity (mS cm^{-1})	Activation Energy (eV)
PS10	320.0	0.39±0.01	0.236
PS20	184.4	0.68±0.01	0.227
PS30	140.3	0.84 ± 0.02	0.225
PS40	118.9	1.07±0.01	0.224
PS50	132.5	0.96 ±0.01	0.235

Universiti Malaya

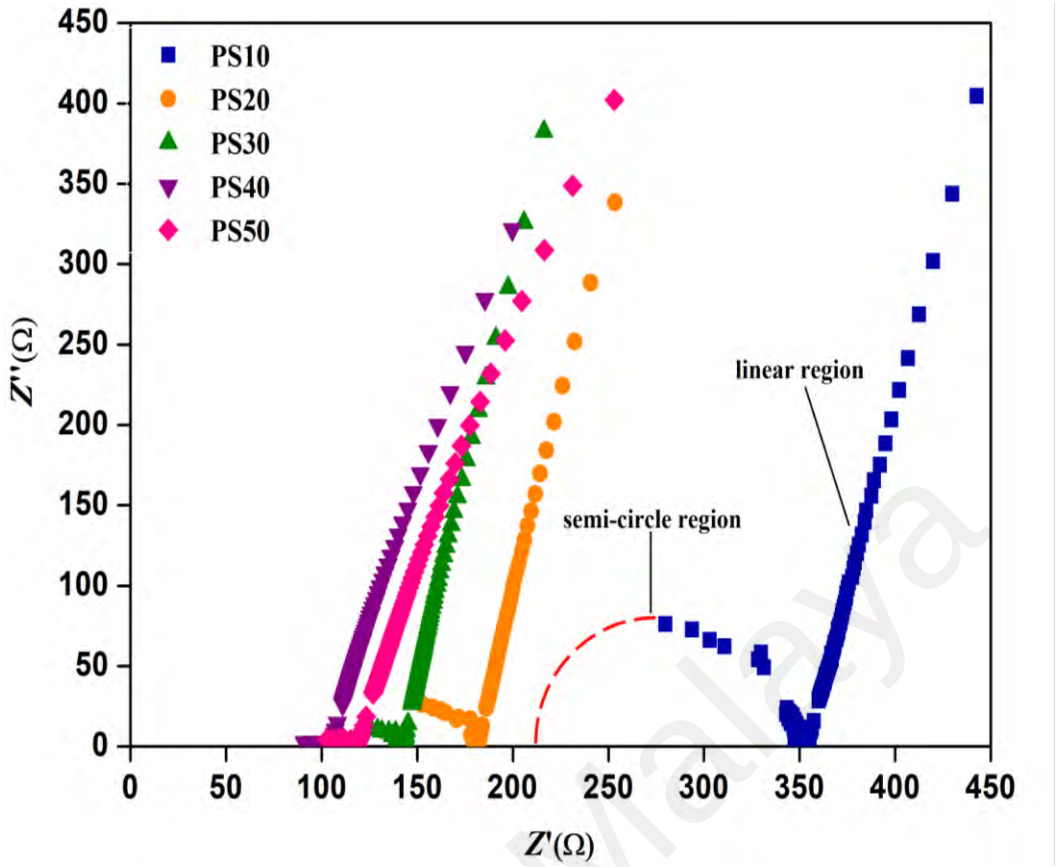

Figure 4.9: Impedance plot of P(MMA-co-MAA)-NaI GPE samples at room temperature.

4.3.2 Temperature dependent ionic conductivity studies

In addition to ion concentration that boost ionic conductivity, segmental motion of polymer chain is also crucial in transporting ions throughout the electrolyte by creating disorder. Thermal treatment on polymer electrolytes allows better understanding of ion dynamic mechanism pertaining to ions. The GPEs were subjected to a variation in temperature ranging from 30 °C to 100 °C. Undoubtedly, a hike in the ionic conductivities was seen and is summarized as an Arrhenius relationship in Figure 4.10. Faster ion movement at higher temperatures is a result of faster vibration modes in polymer chain affecting both intra- and interchain motions. Thermal expansion are likely to occur in GPE and create more free volume for ion migration as shown in Figure 4.11. Besides, the availability for more conduction pathways is also possible at higher temperatures (Petrowsky & Frech, 2009). Regression values approaching 1 on the temperature

Universiti Malaya

dependence plot is highly indicative of samples obeying Arrhenius relationship for the range of temperature tested. Expression of the Arrhenius theory is as per below.

$$\boldsymbol{\sigma = \sigma_o[\frac{-E_a}{kT}]} \tag{4.1}$$

whereby σ is the ionic conductivity, σ_0 is the pre-exponential factor, T is the temperature, k is the Boltzmann constant and E_a is the activation energy.

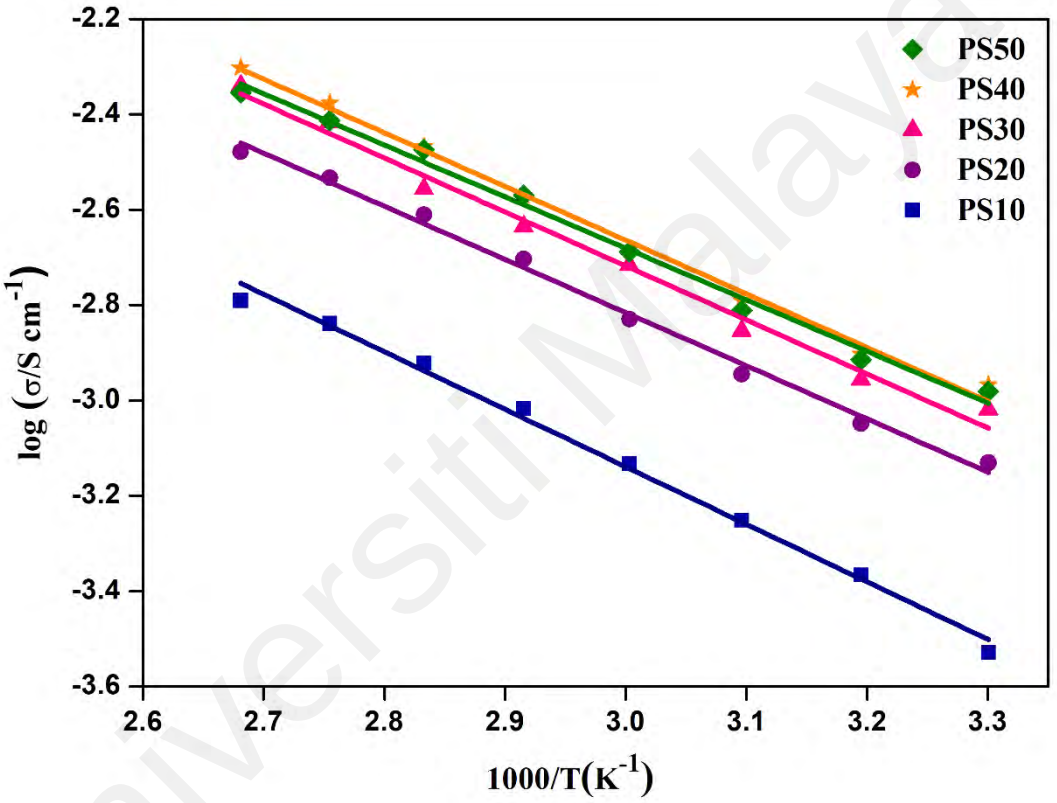

Figure 4.10: Arrhenius plots showing conductivity of the GPE samples for temperature range 303K to 373K.

Complying with Arrhenius theory means that the movement of sodium ions as such that they hop on to occupy vacant sites at an increasing rate with increasing polymer segmental motion at higher temperature and this occurs at a lower activation energy. Linear plots on Figure 4.10 are also the indication of no phase transition occurring during temperature increment and samples are generally amorphous.

Universiti Malaya

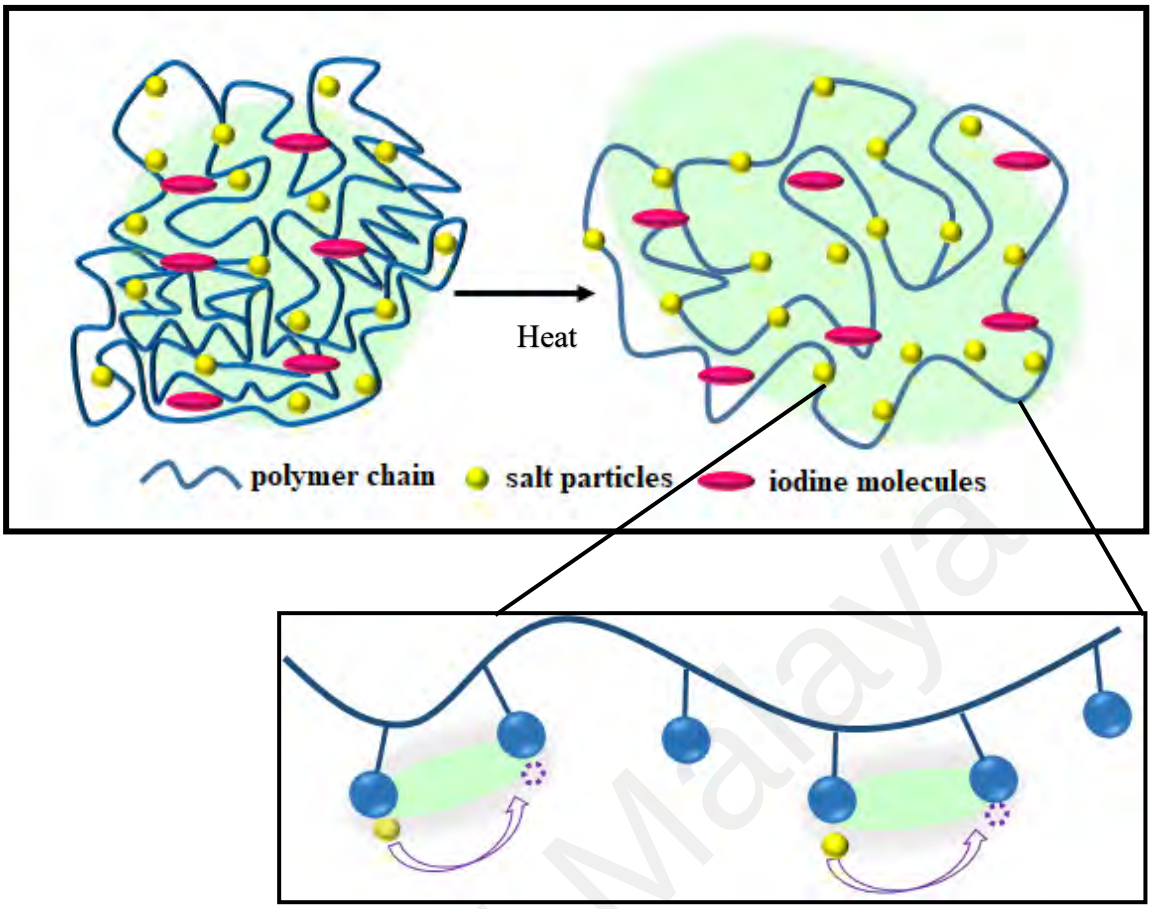

Figure 4.11: Schematic representation thermal expansion of GPE creating more free volume and of salt ion (yellow sphere) hopping to occupy vacant sites along the polymer backbone.

4.3.3 FTIR

FTIR results were essential to confirm the multiple occurrence of different degrees of coordination between the co-polymer, plasticizer and salt moieties. For instance, the different vibrational modes observed were compared between precursor data and electrolytes to further understand complexation between materials. Changes in vibrational shifts and peak intensity are expected with varying concentration of components added in making the polymer electrolytes. Figure 4.12 depicts the FTIR spectra of pure P(MMA-co-MAA), 1:1 ratio of EC/PC and pure NaI. The assignment of EC/PC peaks are listed in Table 4.4 following elucidation from literature. It can be observed that most bands found are of close match to pristine EC and PC FTIR spectra (Tommasini et al., 2018; Kanamura et al., 2001; Deepa et al., 2004; Ali et al., 2007;

Universiti Malaya

Ikezawa & Nishi, 2008). This is a good indication that EC and PC have mixed well and can be utilized as a binary plasticizing solvent.

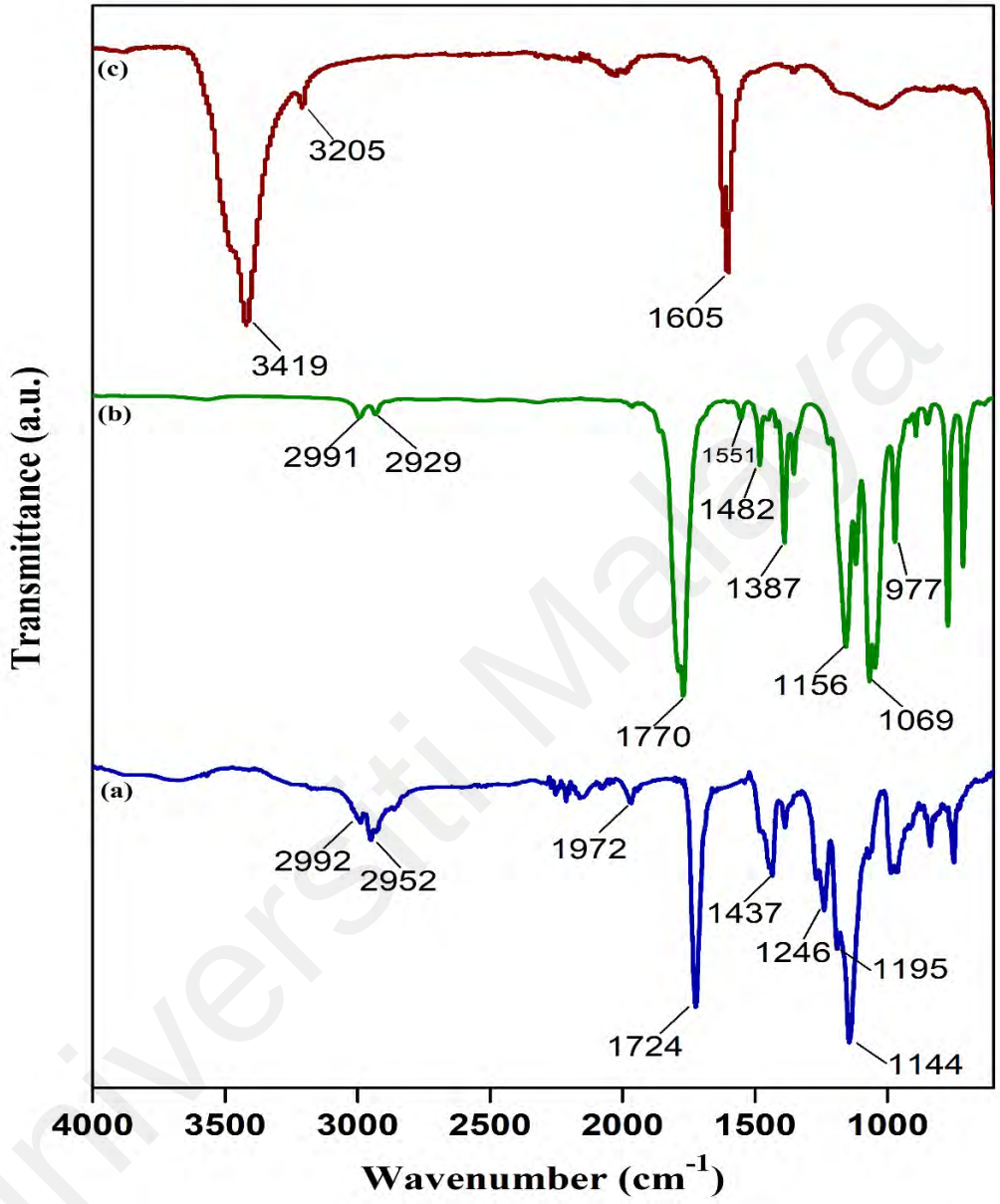

Figure 4.12: FTIR spectra of (a) pure P(MMA-co-MAA; (b) EC/PC and (c) pure NaI.

Universiti Malaya

Table 4.4: FTIR parameters for ethylene carbonate and propylene carbonate as well as the 1:1 blend.

Description of vibrational modes	Wavenumber (cm^{-1})		
	EC:PC	Pure EC	Pure PC
CH_3 asymmetric stretching	2991	-	2989
CH_2 asymmetric stretching	2929	-	2935
C=O stretching	1770	1772, 1796	1777
CH_2 bending	1482	1479	1450
CH_2 wagging	1387	1390	1386
CH_2 scissoring	1156	1154	1485
Ring breathing	1551, 1069, 977	1067, 890	1557, 957

P(MMA-co-MAA) consists of MMA and MAA chemical structures which are very similar, hence, all characteristic absorption bands are summarized in Table 4.5 based on comparative literature interpretation. According to the FTIR spectra, characteristic peak of at 1724 cm^{-1} can be an overlapped peak because the carbonyl group absorption bands of the carboxylic acid and the methyl ester appear around 1710–1760 cm^{-1} and 1740–1750 cm^{-1} respectively (Ulu et al., 2016, Tommasini et al., 2018). The interaction of polymer-salt is expected to occur at this carbonyl functional group of P(MMA-co-MAA). The absorption band values obtained for pure P(MMA-co-MAA) was the point of reference in confirming polymer-ion complexation in the polymer electrolytes.

Universiti Malaya

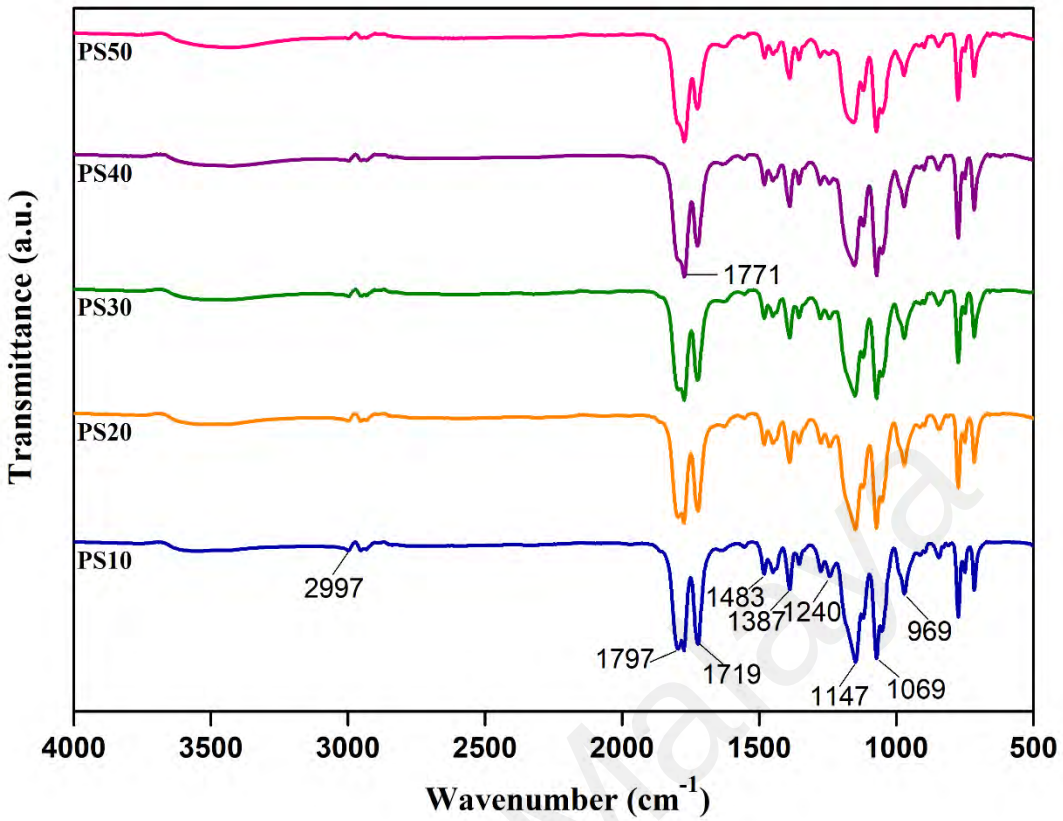

Figure 4.13: FTIR spectra for P(MMA-co-MAA)-NaI GPEs with varying NaI wt.%- PS10, PS20, PS30, PS40 and PS50.

As for the P(MMA-co-MAA)- EC/PC- NaI based polymer electrolytes, the resulting FTIR spectra in Figure 4.13 was used to study interaction behaviour, changes to peak position and intensity due to cation-polymer interaction sites. Plus, deconvolution of main peaks was done to unveil probable hidden peaks due to other ion-polymer interaction present in the electrolyte as illustrated in Figure 4.14 (Yusuf et al., 2016).

Two significant coordination environments in the polymer electrolytes is the C-O-C, ether, (1000-1200 cm^{-1}) and C=O, carbonyl, (1700-1850 cm^{-1}) group observed in the FTIR spectrum. Apart from the prominent carbonyl group region, these C-O-C groups are also possible complexation site for the cation of the salt.

Universiti Malaya

Table 4.5: IR parameters for pure P(MMA-co-MAA) and GPEs PS10- PS50.

Description of vibrational modes	Wavenumber cm $^{-1}$					
	P(MMA-co-MAA)	PS10	PS20	PS30	PS40	PS50
C-H stretching mode in CH_3 group	2992	2995	2995	2995	2995	2995
C-H stretching mode in CH_2 group	2952	-	-	-	-	-
C=O stretching	1724	1797, 1776, 1719	1771, 1723	1771, 1723	1771, 1723	1771, 1723
C-H bending mode in CH_3 group	1437	1483	1483	1483	1480	1480
α-methyl group vibration	1246	1240	1240	1240	Slight shoulder presentation	
Characteristic PMMA absorption band	1145	1147	1147	1150	1153	1153

.

Universiti Malaya

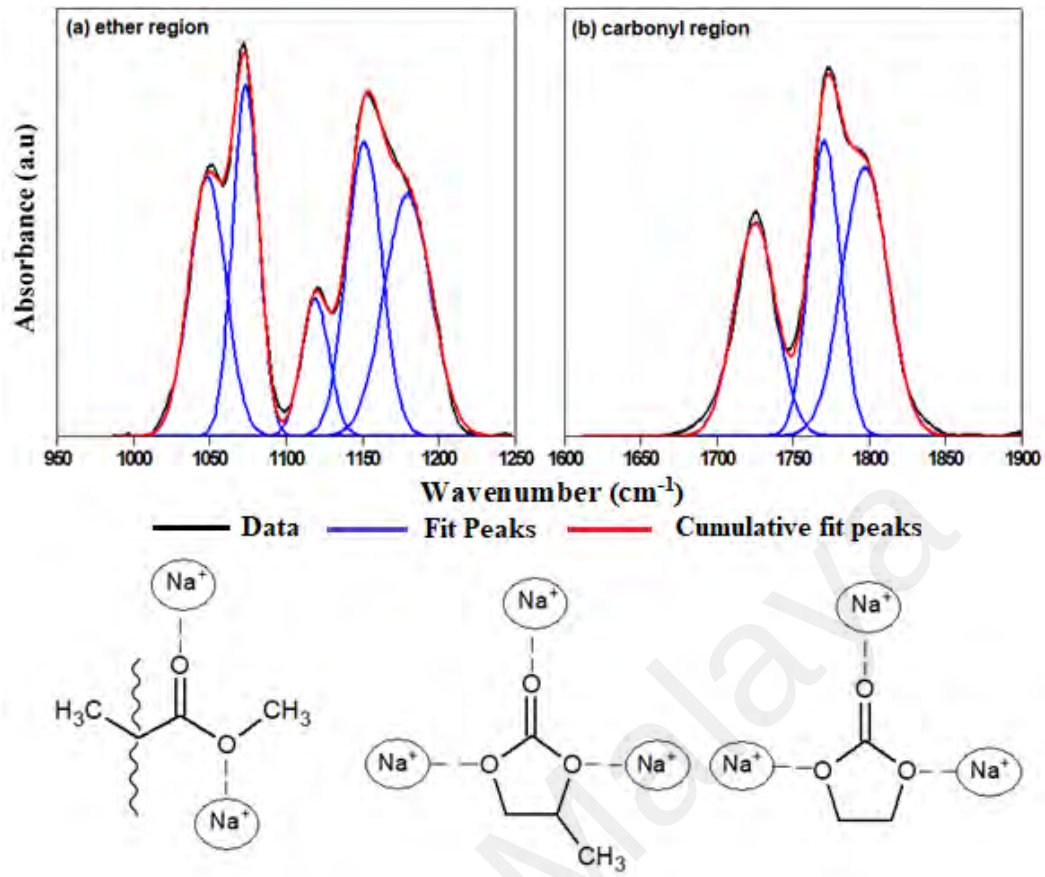

Figure 4.14: Deconvolution of individual FTIR regions: (a) ether (1000–1200 cm^{-1}) and; (b) carbonyl (1700–1840 cm^{-1}) showing interaction between NaI with the ether and carbonyl functional group present in polymer matrix EC and PC solvent.

Unaltered P(MMA-co-MAA) showed peak at 1246 cm^{-1}corresponding to symmetrical ν(C-O-C) vibrations respectively (Mas Harris et al., 2010). However, on addition of plasticizers and salts, strong absorption peaks in the ether region is observed about 1070 cm^{-1} and 1150cm^{-1}. Deconvolution of the peaks show other contributing peaks which are present in varying intensity. Bar graph in Figure 4.15 shows the resulting peak area in percentage of the peaks. The five peak positions identified are not only attributed by the interaction of C-O-C group present in P(MMA-co-MAA) with Na^+ ions but can be also the consequence of EC: PC interaction with the salt cation. The peak at 1073 cm^{-1} is assigned to the coordination of Na^+ ions with the C-O-C with peak intensity was found highest for PS40. As previously mentioned, increasing cation concentration beyond PS40 results in accumulation of ions forming neutral pairs, thus, the drop in intensity is mostly

Universiti Malaya

likely as less Na^+ ions are available to coordinate with the C-O-C group present. Stretching vibrations of free C-O-C present in the amorphous region can be assigned to peak at 1119 cm^{-1} which gradually decreases with decreasing polymer content from PS10 to PS50. Besides, the peak intensity was the lowest for PS40 at 1151cm^{-1} whereas the opposite was true at 1179 cm^{-1}. At these regions, the difference in intensity values doesn't fall far which suggest the complexation of the Na^+ cation with the polymer/EC: PC is less likely influenced by the flux in ion concentration.

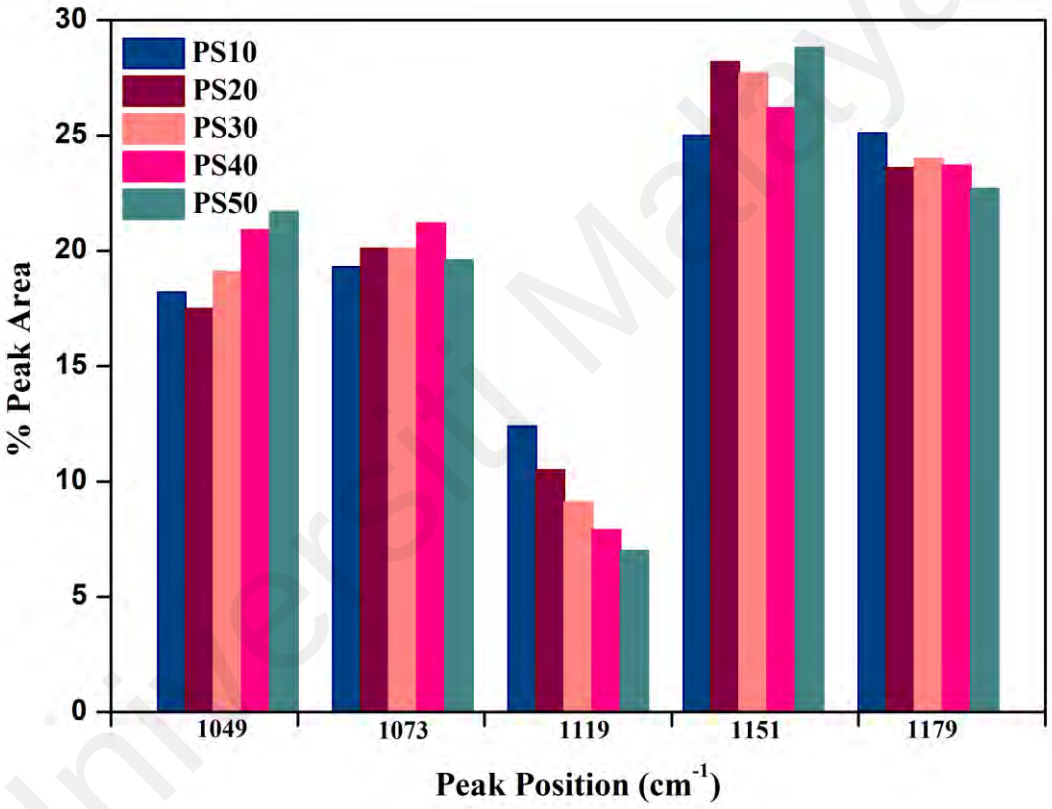

Figure 4.15: Relative FTIR band percentage area in the range of 1000 to 1200 cm^{-1}.

Alternatively, the percentage area of the deconvoluted peaks in the carbonyl region is displayed in Figure 4.16. C=O absorption peaks present are probable from cation interaction with both the copolymer and plasticizer. Peak at 1724 cm^{-1} is a characteristic feature of P(MMA-co-MAA) which is also present in the GPE FTIR. Deconvolution showed a gradual decrease in this peak area from PS10-PS50 as the wt. % of the polymer also decreases with addition of salt. Similar trend is also observed for the peak at 1797

Universiti Malaya

cm^{-1}. However, this peak was originally present as a shoulder at 1790 cm^{-1} in the EC: PC spectrum which has now shifted to a higher wavenumber indicating strengthening of the C=O owing to overall interaction present between the plasticizers and the Na^+ ion. The larger peak area percentage indicates a higher contribution of interaction between the cation and plasticizers. The most intense peak present at 1771 cm^{-1} also belongs to the carbonyl group present in EC: PC. Increasing peak area with increasing salt content can be due to improved flow of plasticizers that allows better accessibility to coordinate with the carbonyl site. Significant interaction of Na^+ ion with EC: PC is seen as 50 wt. % of the GPE is made up of plasticizers. Finally, the slight broad peak at about wavenumber 3500 cm^{-1} is probable of water traces trapped at the surface of GPEs maybe owing to some sweating during electrolyte preparation.

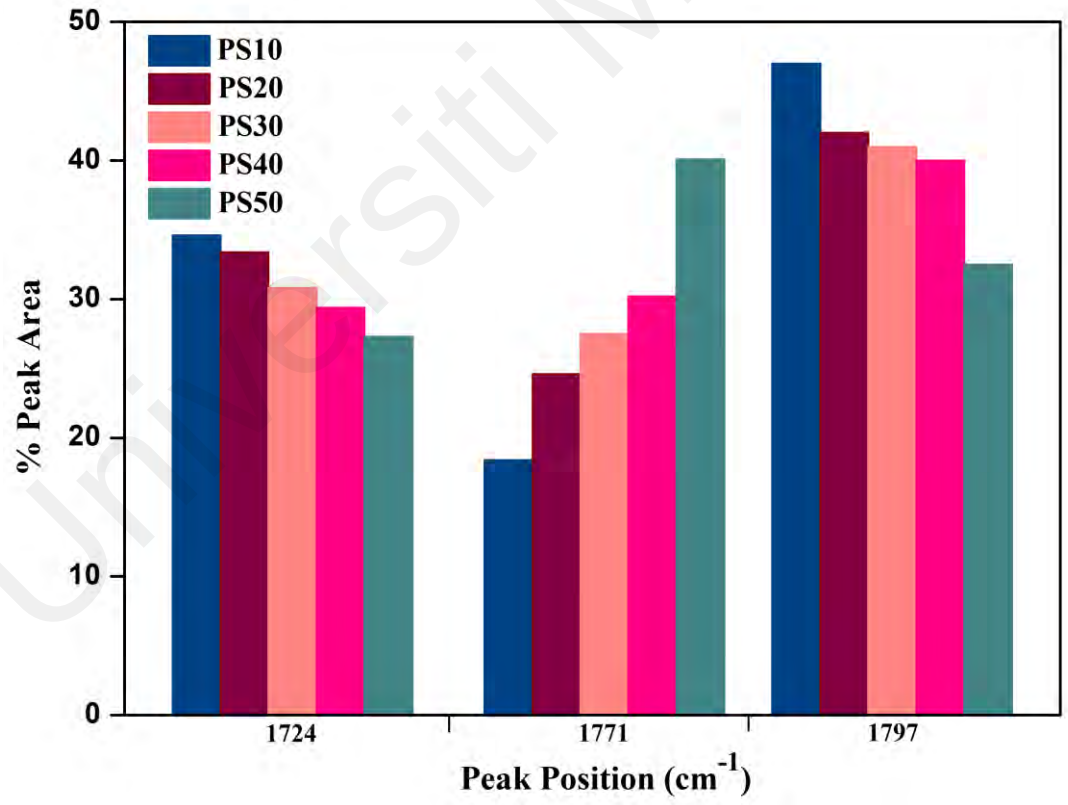

Figure 4.16: Relative FTIR band percentage area in the range of 1700 to 1840 cm^{-1}.

Universiti Malaya

4.3.4 XRD

XRD investigations were necessary to investigate the extent of crystallinity in the polymer electrolyte systems. The increase or decrease in crystallinity or otherwise amorphous nature is a vital area to explore as such nature can affect the conductivity demonstrated by polymer electrolytes. The XRD diffractogram of pure P(MAA-co-MAA) in Figure 4.17 shows the presence of characteristic peaks at 2θ value of 14.26º, 30.34º and 43.85º. The peaks noted are of close match with Jayakumar`s work on PMMA which had broad band peaks at 13.85°, 30.09° and 42.06° (Jayakumar & Srinivasan, 2015). The similarity in XRD pattern obtained at 2θ range between 10º and 50º without any sharp diffraction peaks thereby confirms the non-crystalline nature of PMMA which dominates the composition of the co-polymer. It is mentioned in literatures that, broad peaks found on pure polymer XRD patterns is a result of interchain segment scattering in the amorphous state (Thakur et al., 2016).

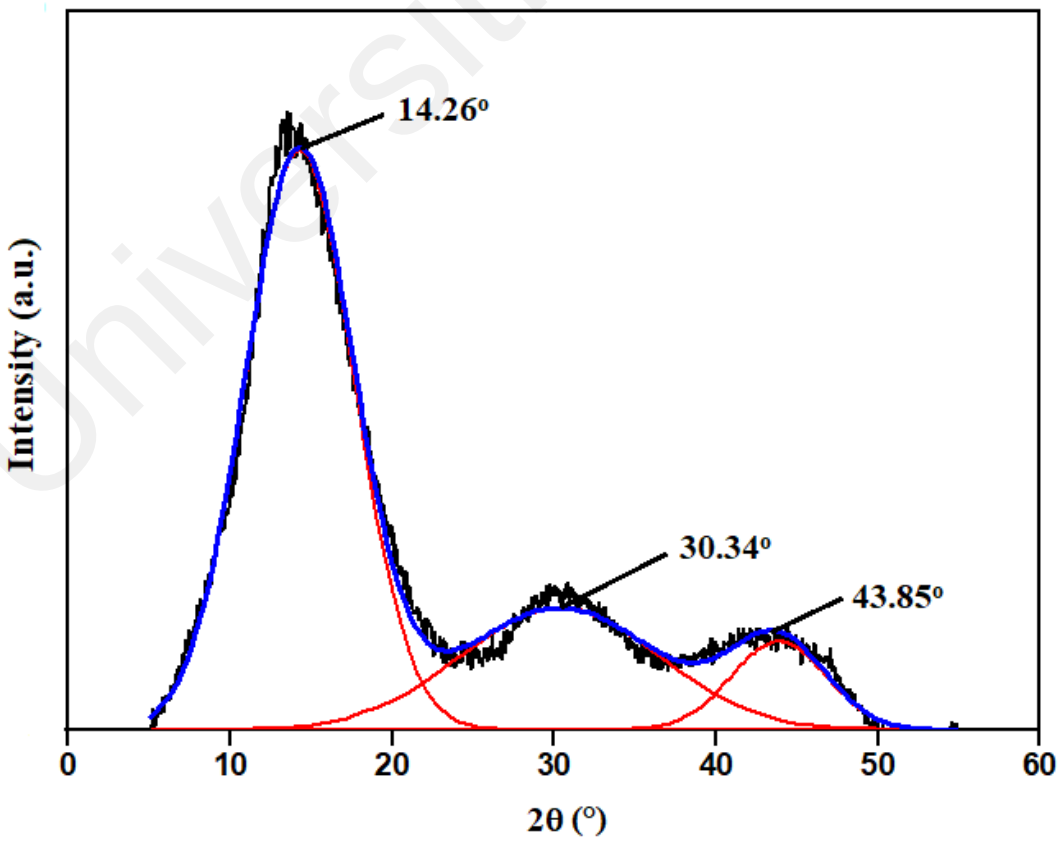

Figure 4.17: XRD pattern of pure P(MMA-co-MAA).

Universiti Malaya

Figure 4.18 portrays the difractograms of polymer-salt complexes. Peak analysis revealed broad peaks observed around 20.0º and the height of peak decreasing with increasing amount of NaI. This is good indication of complexation within the samples and the polymer electrolytes are mostly amorphous. The small peaks observed on the spectra suggest there might be minimal crystals present owing to NaI. High density narrow peaks arise from periodic crystalline atom arrangement, whereas when crystallinity decreases, scattering of X-rays results in wider peak at the 2θ range as shown in Figure 4.18. Decreasing polymer content and increasing NaI promotes salt-polymer interaction that further causes disorder in the polymer electrolyte crystallinity (Selvanathan et al., 2018). Although visibly the most amorphous polymer electrolytes was found to be PS50, but the favourable amorphous nature is observed for sample PS40 as it coincides with highest conductivity. It should be also noted that the three peaks found on pure PMMA-co-MAA XRD spectra is now absent, instead a single peak is present at a shifted 2θ. This phenomena is possibly a result of larger interchain spacing in the electrolyte sample than that of the pure polymer.

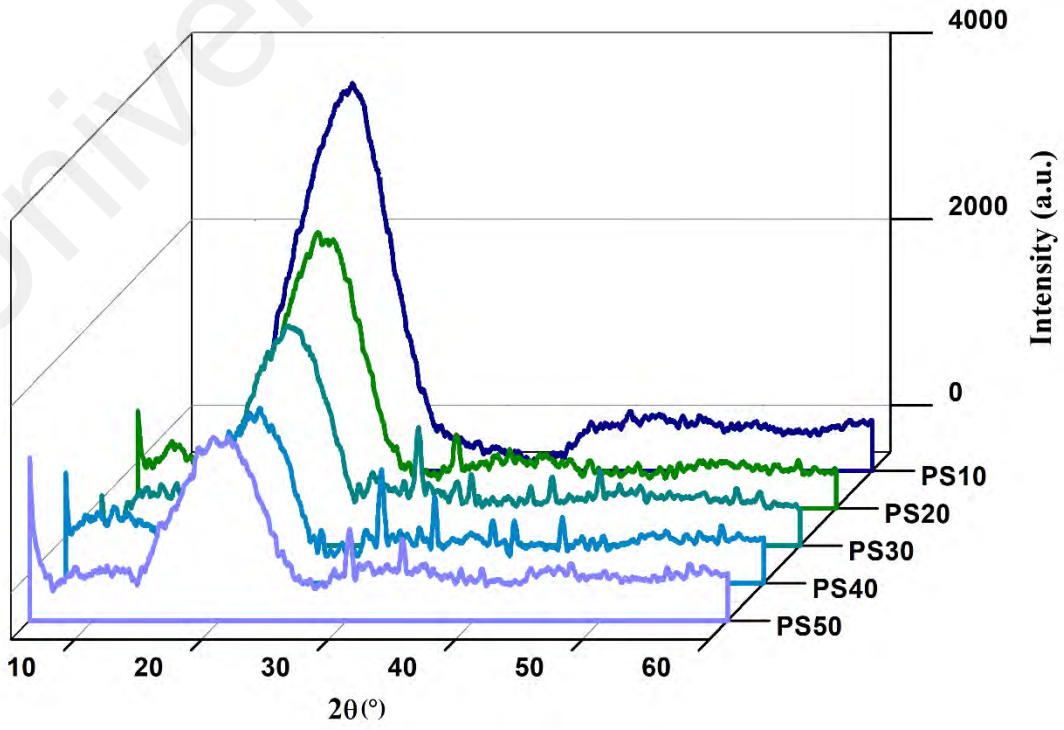

Figure 4.18: XRD spectra of P(MMA-co-MAA)- NaI GPEs at varying salt wt. %.

In order to quantify the crystallinity or amorphous nature of the electrolytes, all five diffractograms were deconvoluted using the OriginPro 8.1 software. Deconvolution revealed the decrease in intensity with increasing full width half maximum (FWHM) of the noticed peak. A correlation between the intensity of the peak and degree of crystallinity can be established by the Hodge criterion. Hodge et al. summoned an equation that determines the degree of crystallinity by calculating the area under the crystalline peak per area under the curves of all the peaks (Hodge, 1996; Genova et al., 2013). Since only one broad peak is clearly notice in the diffractograms, the degree of crystallinity of the polymer electrolytes is correlated with coherence length, *T*, quantitatively expressed by the Scherer formula as below:

$$\boldsymbol{T = \frac{0.9\lambda}{\beta \cos\theta}} \tag{4.1}$$

where λ is the X-ray wavelength (1.5406 Å), β is the full width at half maximum, and θ is the angle of the peak. The details of 2θ, FWHM, and crystallinity variation for all of the polymer electrolyte sample is tabulated in Table 4.6.

Table 4.6: Significant parameters obtained from peak deconvolution on XRD spectra of ionic liquid free GPEs.

Electrolytes	2θ(°)	FWHM (Å)	*T* (Å)
PS10	19.02	8.095	0.174
PS20	20.07	8.071	0.174
PS30	20.23	7.179	0.196
PS40	19.94	8.216	0.171
PS50	20.35	7.092	0.199

Universiti Malaya

The *T* values have found did not show a clear trend after the addition of NaI into the host polymer. However, the smaller the value of *T*, the lower the degree of crystallinity present in the sample. As such, PS40 contains the lowest *T* value and manifests itself as the most amorphous polymer electrolytes sample which in turn aided the most efficient ion transport for this system.

4.3.5 TGA

The TGA curves of pure PMMA-co-MAA, P0 and salt added polymer electrolytes are present in Figure 4.20. Thermal degradation of pure copolymer shows one significant degradation step at a peak range around 320- 420 ºC indicating the degradation of the polymer main chain. The TGA curve obtained for P(MMA-co-MAA) in our work is similar to that reported for PMMA by Costache et al. (Costache et al., 2006). This indicates the dominant contribution from the MMA monomer than the MAA monomer during polymerization as stated by Sigma Aldrich in their feed ratio. Upon further heating, it was completely degraded at around 450 °C leaving no solid residue. This can be due to the volatile methyl methacrylate (MMA) and methyl acrylic acid (MAA) monomers are formed as the sole products. Polymer degradation occurs as a result of random scission mechanism occurring at various locations in the polymer chain. The prevalent mechanism produces free radicals via homolysis of the C-C bonds along the polymer backbone as shown in Figure 4.19.

As for P0, three degradation steps are observed. The initial weight loss noted up till 200 ºC (~ 18 wt. %) is very much probable to the release of moisture from the sample along with some ethylene carbonate and propylene carbonate. The first main stage degradation with 30 % mass loss in P0 occurred between 200- 270 ºC was mainly due to the anhydride formation reaction. Anhydride formation was possible between the carboxyl group of MMA and the carboxyl group of MAA with the carboxyl groups of EC and PC. Ulu et al. highlighted the likelihood of anhydride formation between the polymer

Universiti Malaya

branches, i.e- among the carboxyl group of MAA and the carboxyl group of MMA, however, this interaction was not considered in this weight loss transition as prior degradation of pristine P(MMA-co-MAA) did not exhibit such observation (Ulu et al., 2016). It was interesting to note that all degradation related to EC/ PC exhibited a cumulative mass loss of 50 % which was in agreement to the formulation of P0 with 1:1 ratio of polymer: EC/PC.

Upon addition of salts, a drastic weight loss of 57 % and 59 % corresponding to temperature range 140- 250 ^{o}C and 100- 246 ^{o}C are attained for PS40 and PS50 respectively instead of a stepwise degradation like in P0. Again, a three staged degradation is observed with insignificant water weight loss up until 100 ^{o}C. Since a 50 wt. % of EC/PC was maintained in preparing all polymer electrolytes, the weight loss in this region is mainly because of the plasticizers and iodine present. The additional contributor in this thermal decomposition stage is suggestive of the degradation of the methoxycarbonyl side group. Scissoring of side chains are deemed much easier with the increasing salt concentration with growing interaction between the delocalised electrons in the carboxylate functional group with the sodium ions present.

As can be seen, PS40 depicts slightly higher decomposition temperature than PS50 which implies better thermal stability than other polymer complexes. A further 7% weight loss was noticed around 300 ^{o}C probable of decarboxylation reactions accompanied with the removal of CO_2 (Schild, 1993). Upon further heating, polymer degrades at 430 ^{o}C with a noticeable mass loss of 14% and 16% for PS40 and PS50, respectively. Beyond this stage, the residual mass belongs to the ionic salts present whereby NaI only melts around 800 ^{o}C (Broström et al., 2013). Hence, PS40 with a higher residual mass is a promising candidate as polymer electrolyte owing to its higher first decomposition temperature.

Universiti Malaya

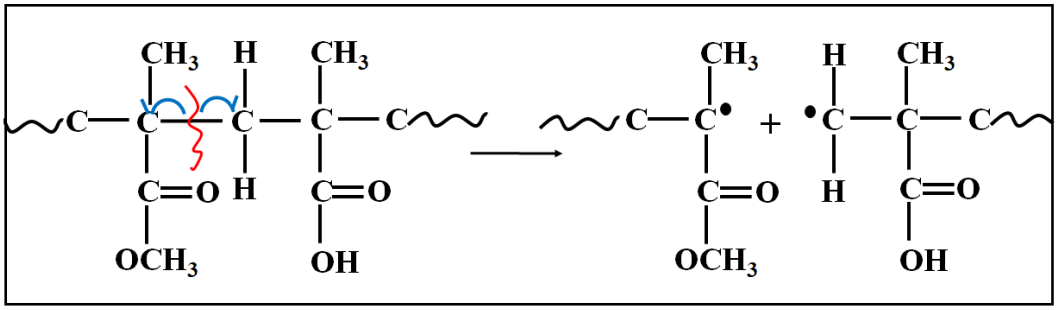

Figure 4.19: Decomposition of P(MMA-co-MAA) through random scission.

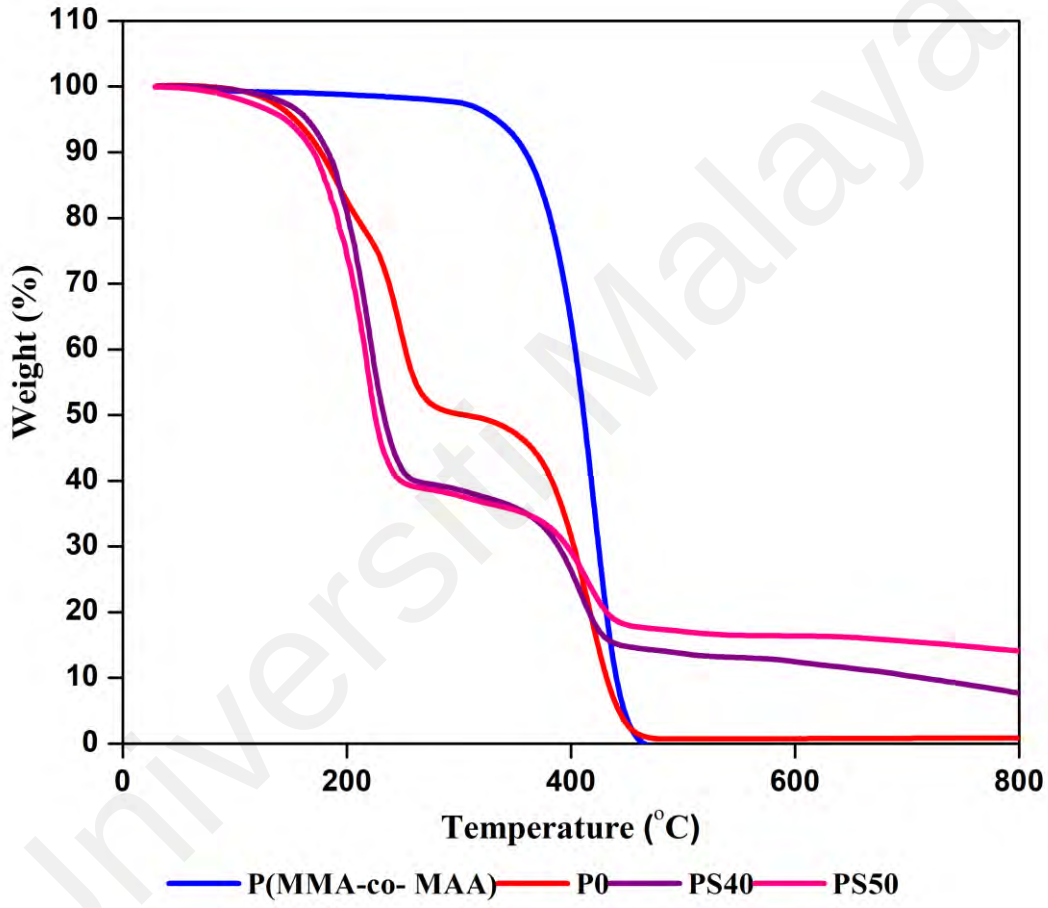

Figure 4.20: TGA analysis of P(MMA-co-MAA), P0, PS40 and PS50.

4.3.6 Apparent diffusion study of I_3^-

Diffusion of I^- and I_3^- ions through the electrolyte produces current upon an applied voltage. Linear sweep voltammetry (LSV) technique was applied to measure the limiting current (J_{lim}) at steady state. Usually, electrolyte compositions contains higher concentration of iodide than iodine which implies that the limiting current attained is for

the triiodide ions. Thus, J_{lim} value is solely employed to determine the diffusion coefficient of triiodide ions according to the equation below (Zistler et al., 2006):

$$\boldsymbol{D}_{\mathbf{I_3}^-} = \frac{\boldsymbol{J}_{\text{lim}}\mathbf{2\delta}}{\mathbf{2nFC}_{\mathbf{I_3}^-}} \tag{4.3}$$

where the meaning of symbols are as listed: J_{lim} the limiting current, δ half the thickness of the electrolyte, F is the Faraday constant and $C_{I_3^-}$ is the concentration of I_3^- ions. The value of n is 2 as it is the number of electrons required for the reduction of triiodide. The triiodide diffusion coefficient in electrolytes in DSSC is an essential parameter to detect the limiting short-circuit current which perchance relates the energy conversion efficiency of DSSCs.

Based on Figure 4.21, an increment in voltage results in an increase in current until saturation occurs about 0.3 V. The hump noted implies the inability of I_3^- flux at the electrode to keep up with the growth of diffusion layer above the electrode. Table 4.7 lists the J_{lim} and $D_{I_3^-}$ values for the polymer electrolytes. The limiting current observed increases with increasing wt. % of salt till reaching a maximum for PS40 then dropping slightly after. Higher J_{lim} values denote faster rate of charge-transfer process with varying potential. Thus, it is not surprising to observe similar behaviour in conductivity in these electrolytes. However, the $D_{I_3^-}$ values are seen to depreciate upon increasing salt content which does not correspond to the trend observed in ionic conductivity in samples. Similar findings were also reported by Buraidah's group on their work using TPAI salts (Buraidah et al., 2017). This phenomena can be linked to a notion that at certain I_2/I^- concentration, the attraction between the anion and cations is significant to reduce the gap for diffusion of the I_3^- ions to occur. Low diffusion coefficient values is viewed as declining triiodide ion supply at the counter electrode, which in return would lessen reduction process of triiodide to iodine but the ionic conductivity is seen less likely influenced by the diffusivity rate of I_3^- but increases with higher number density of I^- ions present.

Universiti Malaya

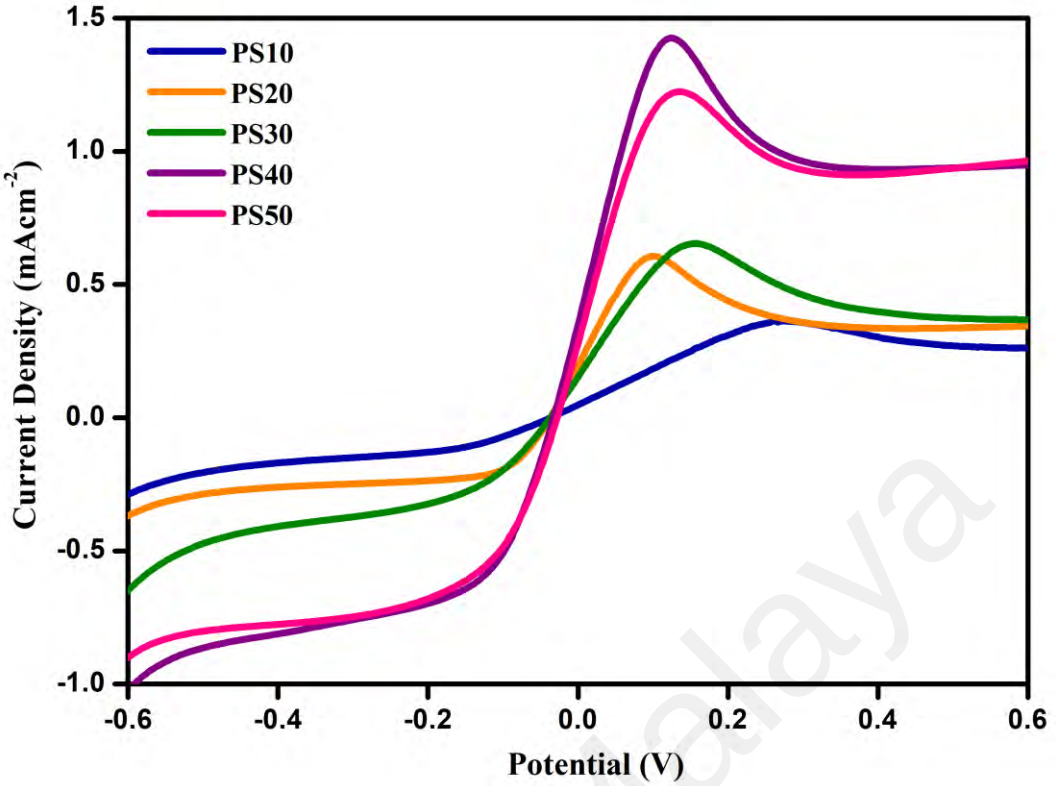

Figure 4.21: Linear sweep voltammograms of salt only GPEs from PS10 to PS50.

Table 4.7: Diffusion coefficient values calculated using steady state current measurement for PS10- PS50.

Electrolyte	J_{lim} (mA cm^{-2})	$D_{I_3^-}$ (x 10^{-8} cm^{2}s^{-1})
PS10	0.26	1.60
PS20	0.35	1.09
PS30	0.43	0.90
PS40	0.95	1.51
PS50	0.93	1.16

Universiti Malaya

4.3.7 Summary

The most suitable ratio of P(MAA-co-MAA)-NaI blend to serve as electrolyte host has been examined using several characterization techniques. The electrolyte with 60 wt. % polymer and 40 wt. % NaI, PS40 is deemed the most amorphous upon XRD analysis. FTIR analysis confirmed the complexation of components present in the electrolyte and good thermal stability was noted upon TGA analysis. Further confirmation on the conductivity capability of the electrolyte was confirmed by LSV studies with PS40 having the highest triiodide diffusion coefficient contributing to the highest ionic conductivity and power conversion efficiency achieved. Thus, PS40 has been chosen as the electrolytes host for further characterization with ionic liquids.

4.4 P(MMA-co-MAA)-NaI- [C_4mquin][NTf_2] Gel Polymer Electrolyte.

4.4.1 Ambient temperature ionic conductivity studies.

The comparative ionic conductivity results of the GPE samples containing ionic liquid [C_4mquin][NTf_2] to PS40 is illustrated in Figure 4.22. The figure highlights the gradual increase in conductivity as the wt. % of ionic liquid was increased. A significant hike in ionic conductivity at 25 wt. % of [C_4mquin][NTf_2] is seen which undoubtedly relates to the reduction in viscosity as polymer concentration is now lesser and the presence of increasing number of mobile carriers from [C_4mquin][NTf_2] that provides the $[C_4mquin]^+$ and $[NTf_2]^-$ ions. At this composition, the highest ionic conductivity recorded was 2.26 mS cm^{-1}. Table 4.8 notes the conductivity of other GPE compositions.

Universiti Malaya

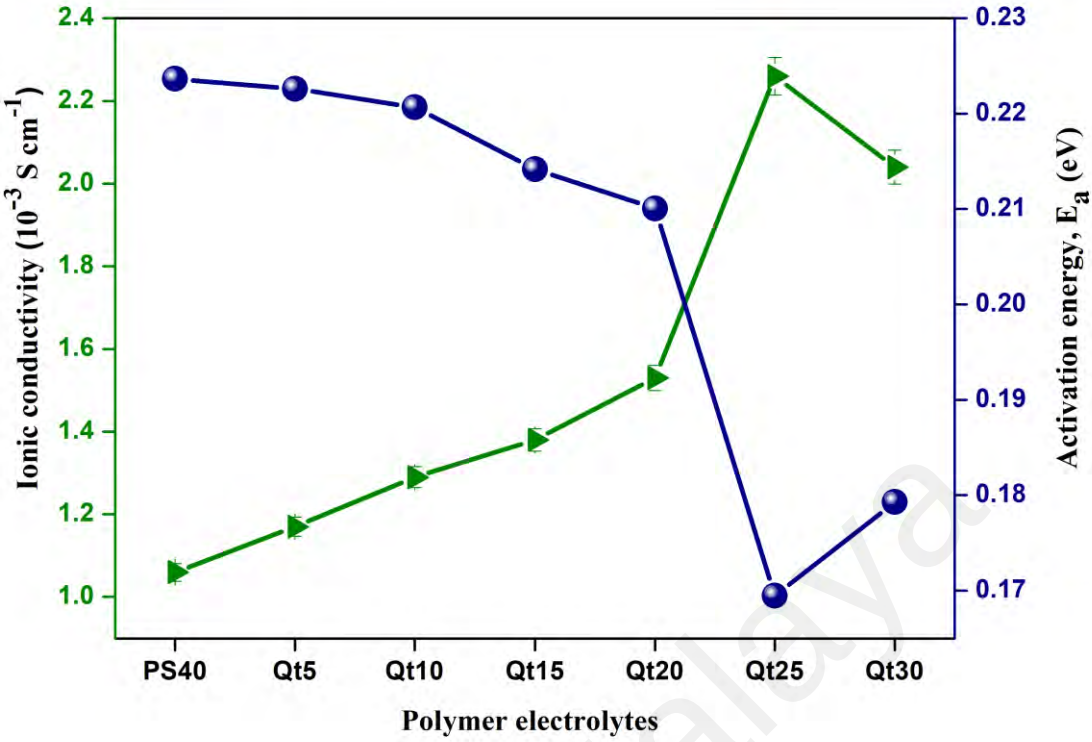

Figure 4.22: Variation in ionic conductivity and activation energy for [C_4mquin][NTf_2] containing GPEs.

Table 4.8 Ionic conductivity and corresponding activation energy values for Qt5-Qt30 GPEs at room temperature.

Electrolytes	Average R_b (Ω)	Ionic conductivity (mS cm^{-1})	Activation Energy (eV)
Qt5	108.3	1.17± 0.02	0.223
Qt10	98.5	1.29 ±0.02	0.221
Qt15	90.0	1.41± 0.02	0.214
Qt20	82.1	1.55 ±0.03	0.210
Qt25	56.2	2.26± 0.04	0.169
Qt30	62.3	2.04± 0.04	0.179

Figure 4.23 depicts a visible increase in flow properties as the wt. % ionic liquid was increased to 30 wt. %. However, a slight decrease in ionic conductivity is noted indicating a possibility of ion saturation whereby the extra charge carriers form neutral clusters. This

Universiti Malaya

dampens ion mobility with a likely reduction in polymer segmental motion as well. By theory, the ionic conductivity of electrolytes can be exemplified *Equation 2.6*. As the charge on the mobile ions are the same for samples Qt5- Qt30, henceforth omitted, ionic conductivity is governed mainly by the number of charge carriers and the mobility of ions present. Nevertheless, this is observed true only for systems with low ion concentration. Beyond an optimal point, ionic conductivity is a resultant of both ion movement as well as ionic conduction pathway (Asmara et al., 2011; Liew & Ramesh, 2012).

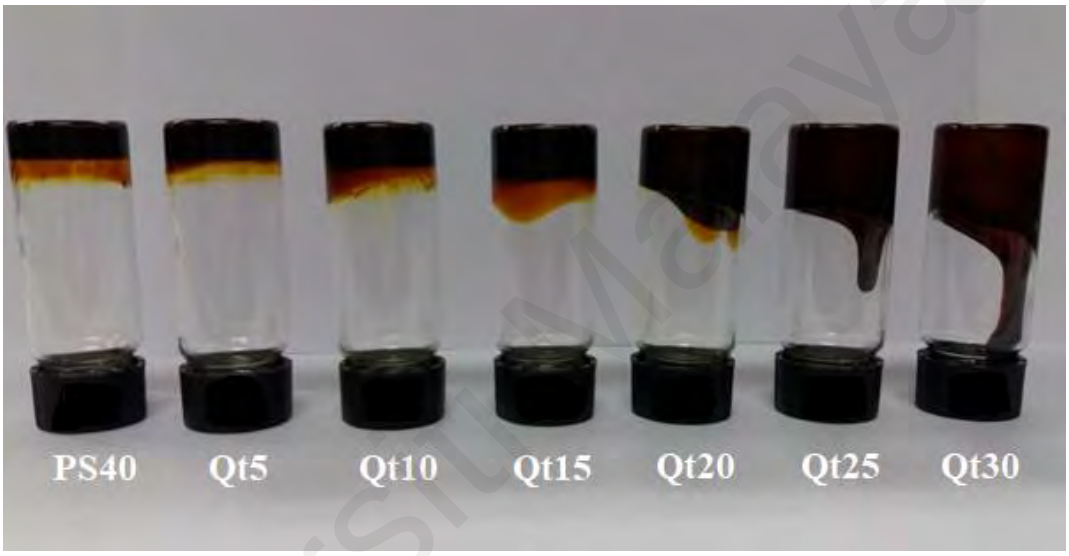

Figure 4.23: The ‘‘inverted’’ sample bottles technique confirms the gel nature of the electrolytes.

Indeed the addition of plasticizers like EC/PC improves the amorphous phase content of the polymer-salt-ionic liquid system and contributes to the increase in segmental mobility of the complex. Amid the list of plasticizers reported, EC and PC showed potential yield in improving ionic conductivity. The high dielectric constant of EC is crucial to achieve high ionic conductivity but EC alone as solvent tend to crystallize even at room temperature, which may cause phase separation between EC and the polymer composite matrix. The combined effect of EC and PC showed good improvement in ionic conductivity and a 1:1 wt.% possess long term stability and better light-to-electrical energy conversion efficiency compared to other ratio combination (Subramania et al.,

Universiti Malaya

2013; Vignarooban et al., 2014). Plus, all substrates used in making the GPEs has considerable solubility in EC/PC. However, a 50 wt. % of EC/PC was still maintained from the total sample mass as we deemed any further addition would weaken the mechanical strength of the GPE making it more liquid-like.

4.4.2 Temperature dependent ionic conductivity studies

Upon subjecting to an increase in temperature, the temperature dependent ionic conductivity plots are fitted with the thermal activated Arrhenius equation to study the ion mobility mechanism occurring within the GPEs. Figure 4.24 depicts the ionic conductivity of $[C_4mquin][NTf_2]$ containing polymer electrolytes on the basis of Arrhenius relationship for the temperature range of 30 ºC to 100 ºC. As temperature gradually increases, a temperate increase in ionic conductivity is noticed. The highest ionic conductivity of 7.28 mS cm^{-1} has been achieved by adding 25 wt. % of $[C_4mquin][NTf_2]$ at 100 °C. Essentially, heat supplied causes polymer molecules to vibrate faster which leads to substantial bond rotation within the polymer matrix. The rapid vibration mode makes cation decoupling easier. The cations coupled to polymer segments via coordinative bonding with the oxygen in PMMA are more easily detached as molecular vibration amplitude increases with temperature. Thus, free ions enhance ionic transportation at elevated temperatures. Besides, higher thermal decoupling rate is also anticipated between the $[C_4mquin]^+$ cations and its transiently coordinated anions. Increasing number of mobile cations with the polymer electrolyte generate more ionic conduction. So as anticipated, higher ionic conductivity with an increasing temperature is very much likely from this study. Apart from that, it is also possible for the polymer membranes to expand owing to higher vibration mode at high temperatures. The chain segmental expansion also create free spaces for ionic transportation to occur. Deriving from the linearity in graphs shown in Figure 4.24 with average regression lines

Universiti Malaya

approximating to unity for all of the samples, it appears that conductivity follows the Arrhenius relationship.

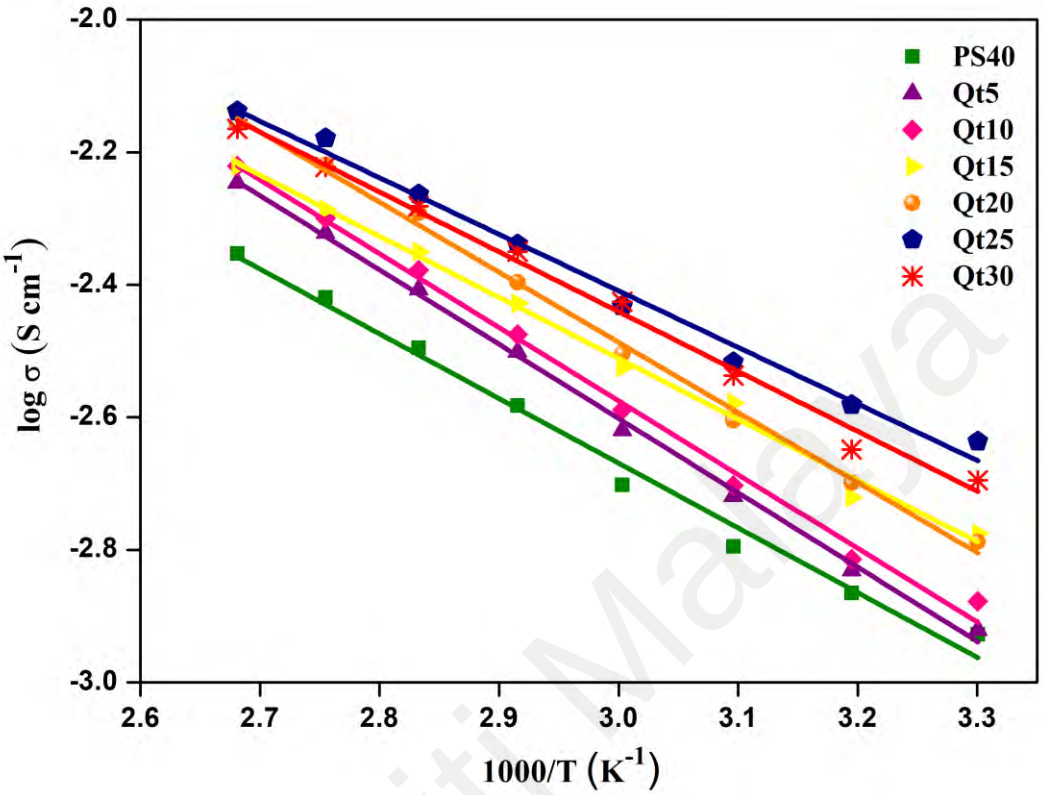

Figure 4.24: The variation of log σ plotted against the reciprocal absolute temperature for [C4mquin][NTf2] containing GPEs.

Ionic conduction in polymeric systems are generally a cooperative process whereby the ion hopping mechanism is conjoined with higher polymer segmental mobility in the amorphous phase. Thus, most polymeric systems have shown inclination towards the volume activated VTF- behaviour at elevated temperatures. However, obeying Arrhenius theory is also quite possible at higher temperatures. The increase in vibrational amplitude and dynamics on polymer backbone and sidechains can bring coordination sides closer together allowing ions to hop on to adjacent vacant sites with less energy requirement. Thus, a linear behaviour is still observed at higher temperatures due to simultaneous coupling and decoupling mechanism between the ionic and polymer segmental motion. Among all the [C4mquin][NTf2] containing samples, Qt25 shows the highest conductivity

Universiti Malaya

value signifying the maximum ion diffusion occurring in the polymer electrolyte. This indicates that there is considerably more number of charge carriers in Qt25 compared to other ionic liquid–added polymer electrolytes. Again, any wt. % addition of ionic liquid has proven enhance the ionic conductivity by providing more free charge carriers for ion transport than ionic liquid-free electrolytes (Martinelli, 2013; Aziz et al., 2018).

Referring to Figure 4.22 it is seen that the pseudo–activation energy is inversely proportional to the ionic conductivity indicative of an ease in ion hopping in response to the immediate surrounding of the freely moving ionic species that is constantly reorienting the local structure. The activation energy values corresponding to the Arrhenius plots are almost constant for the initial samples, Qt5-Qt20, with an average value of 0.22eV. Literature elucidation revealed that activation energy for a low or moderately concentrated salt mixture system becomes unresponsive to the salt-mixture concentration and type of salt used, however, is in fact dependent on the type of solvent used, particularly on the nature of the solvent heteroatom. With constant amount of EC/PC co-solvent present, it is possible to conclude that at initial stages, with little consecutive addition of ionic liquid, the ion transport involves a single activated process dominated by the solvent functional groups present causing dipole reorientation and therefore, results in similar activation energies.

Beyond Qt20, the activation energy was deemed to be somehow influenced by the ionic liquid added. As both cation, $[C_4mquin]^+$ and anion $[NTf_2]^-$ are bulky, these cations were expected to have high ionic dissociation in the electrolyte samples. With more liquid-like behaviour under an environment where the ionic liquid- salt mixture is dissolved in an organic polar co-solvent EC/PC entrapped in the P(MMA-co-MAA) matrix, a probable ease in ion transport is foreseen. Hence, the lower activation energy value recorded with higher ionic conductivity.

Universiti Malaya

4.4.3 FTIR

The result of cationic interaction of the salt components with plasticizers and copolymer was discussed in Section 4.3.3. This section highlights the interaction occurred upon adding novel [C_4mquin][NTf_2] ionic liquid in making the GPEs. Figure 4.2 shows the FTIR spectrum of pure [C_4mquin][NTf_2]. Peaks found between 3097-3000 cm^{-1} and 3000-2860cm^{-1} links to aromatic =C-H stretch and C-H stretch, respectively and peaks about 1600-1400 cm^{-1} correspond to C-C aromatic stretching. The peaks in the range 1300-1000 cm^{-1} denotes the in-plane C-H bending vibrations. In addition to this, the [C_4mquin][NTf_2] itself has some distinctive peaks that can be monitored to prove complexation within the GPEs. The initial S=O peaks appears at 1340 cm^{-1} while the subsequent S=O group can be found around 1134 cm^{-1}. A strong peak around 1191 cm^{-1} corresponds to the C-F functional group. S-N functional group can be associated with the strong peak at 1052 cm^{-1}. The complexation occurring between the materials shifts the polymer cage peak frequencies as FTIR is sensitive to such situation be it in the crystalline or amorphous phase. A noticeable shifting in peaks to another wavenumber can be seen upon inclusion of [C_4mquin][NTf_2] at different weight percentage. Overall, the graphically presented data in Figure 4.25 shows high congruency among the GPEs containing [C_4mquin][NTf_2].

Universiti Malaya

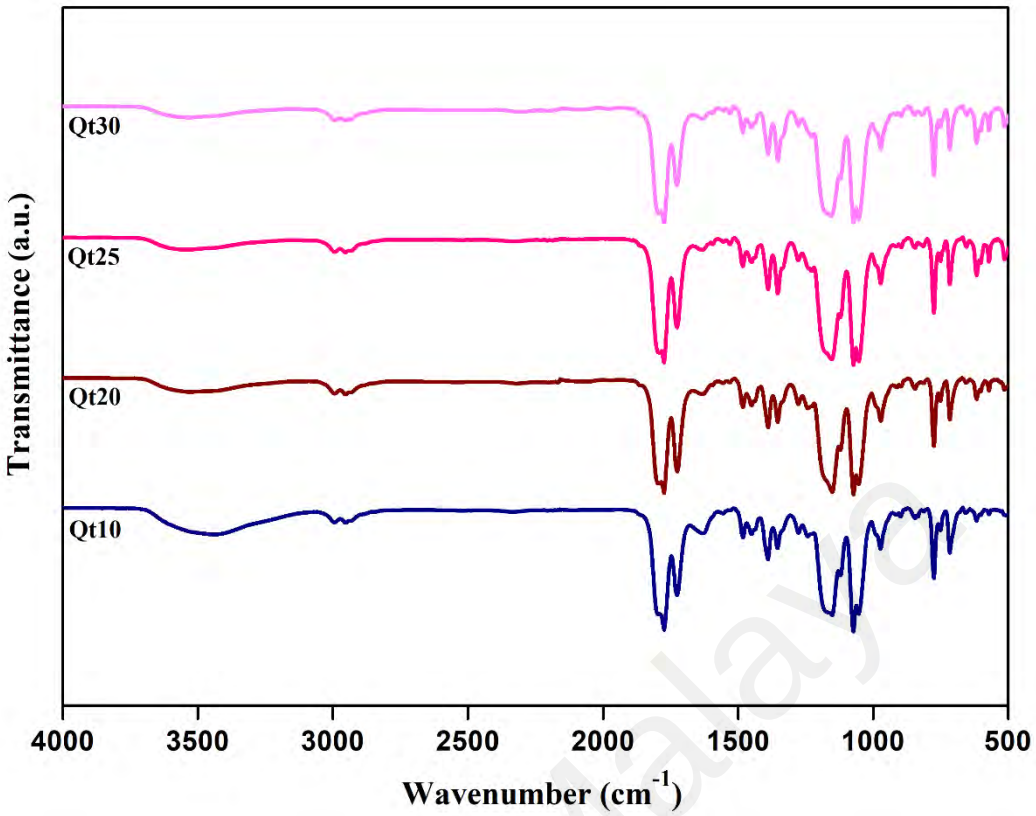

Figure 4.25: FTIR spectra of GPEs Qt10, Qt20, Qt25 and Qt30.

Once more, an important region to further study would be between wavenumbers 1000-1200 cm^{-1} and 1700-1850 cm^{-1}. Deconvolution revealed five individual peaks conjoined in the 1000-1200 cm^{-1} region with shifted wavenumber positions. At 1700-1850 cm^{-1}, three peaks were also found corresponding to interaction of cation with the carbonyl functional group of the copolymer and plasticizers with peaks shifting to higher wavenumbers. Generally, even the slightest shift to higher wavenumbers indicate the strengthening of a particular bond. Figure 4.26 highlights the variation in peak position, shape and intensity of PS40 and Qt25.

Universiti Malaya

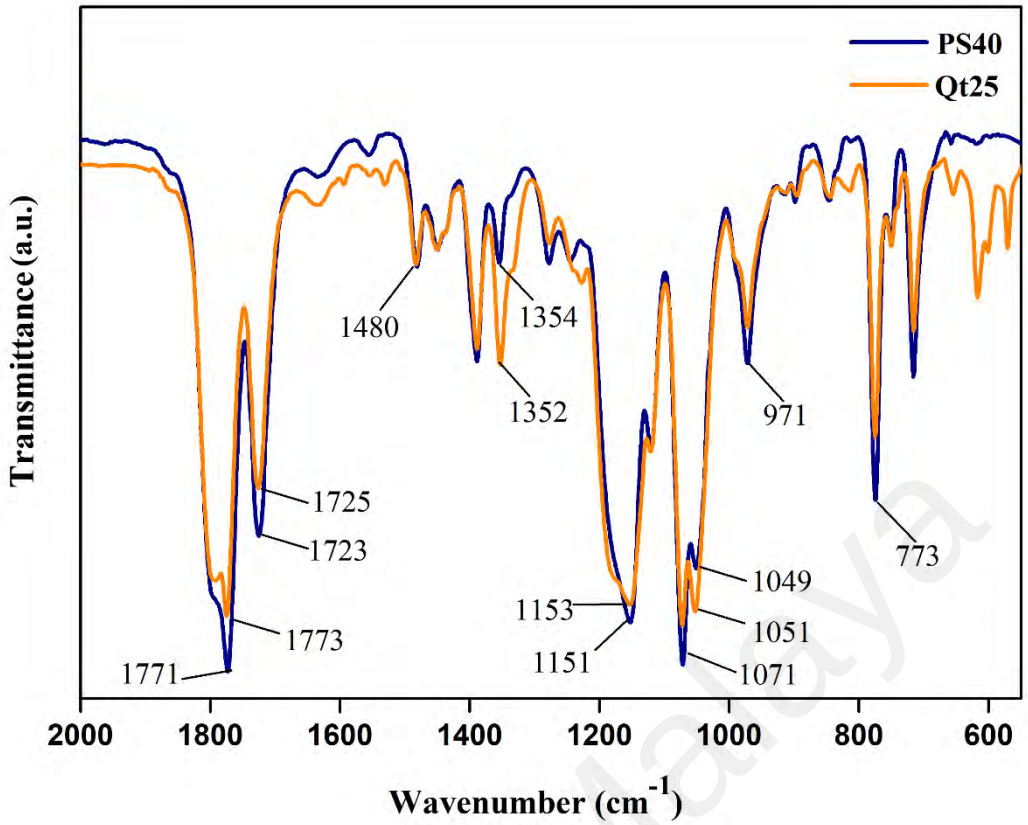

Figure 4.26: Comparative display of PS40 and Qt25 FTIR spectra.

Upon the incorporation of [C_4mquin][NTf_2], the ν(C=O) band is observed to shift from its original position of 1723 cm^{-1} to between 1725 and 1726 cm^{-1}. The trivial upward shift in ν(C=O) band to higher wavenumber can be due to a strengthening in C=O caused by a decrease in Na^+ coordination at the oxygen of C=O. This phenomena can be owed to a competing coordination of nitrogen from the [C_4mquin]$^+$ cation with oxygen of the same function group. Otherwise, it can be also due to the blocking effect induced by the presence of large ions of ionic liquid. The Na^+ ions can been deemed dispersed somewhat away from the polymer backbone. This trend was also noticed among the other peaks in the carbonyl functional group region.

The dual peak found between wavenumbers 1700-1850 cm^{-1} was deconvoluted to evaluate C=O interactions in the GPEs. Figure 4.27 displays the bar graph for the resulting peak area in percentage of three peaks found upon deconvolution. The characteristic C=O peak from P(MMA-co-MAA) at 1725 cm^{-1} shows a gradual decrease in peak intensity

Universiti Malaya

with increasing wt. % of ionic liquid which implies the known corresponding decrease in polymer content when making the GPEs. As for the other two peaks at wavenumbers 1773 cm^{-1} and 1800 cm^{-1}, there share an almost 1:1 ratio in peak percentage area for all [C_4mquin][NTf_2] containing sample indicative of good dissolution of ions in the plasticizing compounds.

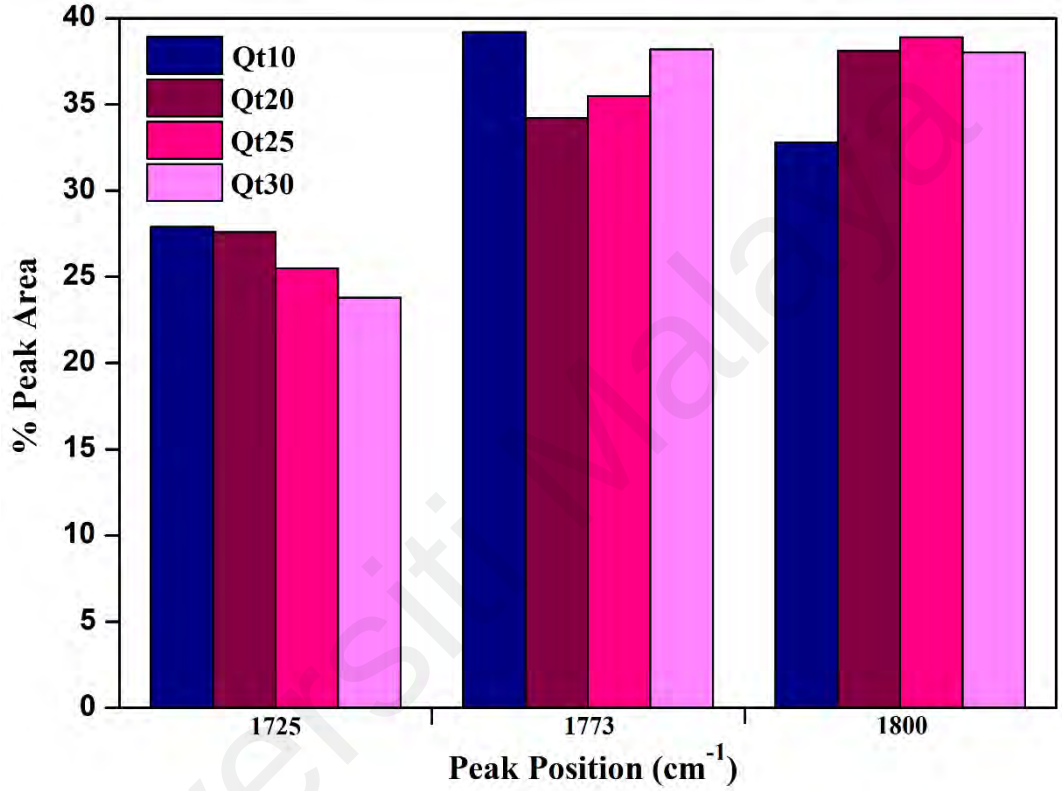

Figure 4.27: Relative FTIR band percentage area in the range of 1700 to 1850 cm^{-1} for Qt10, Qt20, Qt25 and Qt30.

On the other hand, deconvolution between wavenumbers 1000-1200 cm^{-1} revealed five peaks with significant variation in peak shifts at 1050 cm^{-1}, 1076 cm^{-1}, 1116 cm^{-1}, 1154 cm^{-1} and 1188 cm^{-1}. Despite the presence of five internal peaks, it was difficult to correctly identify the contributor of peaks owing to the cumulative effect from the ionic liquid functional groups and the ether interactions present. It can be noted from Figure 4.2 that peak at 1134 cm^{-1} belongs to the sulfoxide in NTf_2 group. However, in these polymer-salt-ionic liquid system it is unnoticeable. This suggest that the ionic liquid has solvated well into the polymer matrix. Overall, the other changes in shift observed

disclose the interaction between the polymer branches, sodium salt and [C_4mquin][NTf_2], hence validate the complexation.

4.4.4 XRD

The highly crystalline nature of pure [C_4mquin][NTf_2] was seen from the sharp peak patterns in Figure 4.7. Upon formation of GPEs containing [C_4mquin][NTf_2], majority of these peaks were found to have disappeared. This is an indication of complete dissolution of materials upon being mixed into the GPEs. Likewise, it also tells us that there were no excess salts or ionic liquids remaining in the gel polymer electrolytes. Figure 4.28 depicts the XRD diffractograms of [C_4mquin][NTf_2] containing GPEs. Using P(MMA-co-MAA) spectrum as reference, peak analysis revealed merging and shifting of peaks to a lower angle despite a similar overall pattern with two dominant peak. Table 4.10 lists down the exact shifting angle. The variation in peak heights whereby peak intensities are much lower than PS40 sample and the broadness of the peaks assure the improved amorphous nature of the GPEs upon successive [C_4mquin][NTf_2] addition. It should be also noted that two peaks are present in the [C_4mquin][NTf_2] containing spectra signifying changes in complexation. Hence, it is better to make direct comparison with XRD findings of pure P(MMA-co-MAA) instead with PS40. Besides, few sharp peaks observed along the spectra are mostly likely due to some undissolved NaI or [C_4mquin][NTf_2] with successive increase in ionic liquid content.

The presence of dual peaks is further verified by means to deconvolution as the intensity of the peaks can be utilized to calculate the degree of crystallinity. Regardless of two broad peaks in all the diffractograms, the first peak at the far left is noted as the crystalline peak and the following peak becomes the prominent amorphous peak. The peak tagging was necessary as we postulate the reduction in degree of crystallinity in these GPEs to be a positive contributor in enhancing the ionic conductivity with upon ionic liquid inclusion. The Hodge criterion can be utilized as calculating the area under

Universiti Malaya

the crystalline peak as a ratio of area under the curves of all the peak gives degree of crystallinity. P(MMA-co-MAA) polymer is a semi-crystalline compound with crystallinity about 66%. As for the GPEs, the percentage crystallinity has reduced to notable values ranging from 58.1% to 46.4% as shown in Table 4.9. XRD diffractogram of Qt25 revealed to be the most amorphous among the GPEs. On average, all [C_4mquin][NTf_2] containing GPE samples show a more or less equal share of crystallinity and amorphous nature in them with degree of crystallinity about 50%. The results obtained can prove the idea that the inclusion of large [C_4mquin][NTf_2] is able to retain more order in the GPE as well as leaving empty amorphous regions in between. A more guided charge carrier transportation via a hopping mechanism is highly probable. Hence, the quantity of free moving ions would regulate the ionic conductivity. By itself, Qt25 deemed to be the most conductive for the *"Qt"* system. With this, it can be concluded that more amorphous nature of polymer electrolytes at optimum mass loading of ionic liquid is the most conducting GPE with the lowest percentage of crystallinity.

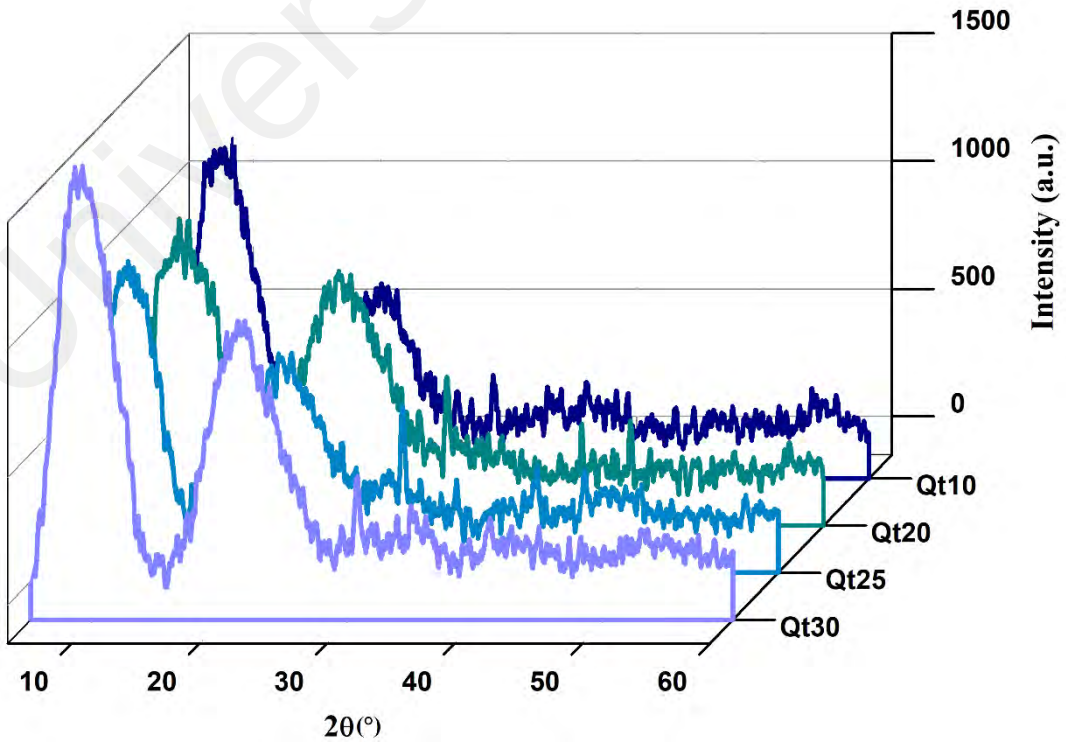

Figure 4.28: XRD diffractograms of GPEs Qt10-Qt30.

Universiti Malaya

Table 4.9: Parameters obtained from the curve fitting of XRD diffractograms in Qt system.

Electrolytes	Crystalline peak, 2θ (°)	Amorphous peak,2θ (°)	Area of crystalline peak, I_C	Total area under the curve, I_T	Percentage of crystallinity (%)
Qt10	9.59	21.78	6139	11205	54.6
Qt20	9.91	22.65	5989	12564	47.7
Qt25	9.31	22.80	4847	10449	46.4
Qt30	9.57	21.68	10335	17776	58.1

4.4.5 TGA

Figure 4.29 the thermogravimetric analysis of pure [C_4mquin][NTf_2] and ionic liquid added polymer electrolytes in comparison to PS40. Pure [C_4mquin][NTf_2] shows a single stage decomposition with onset decomposition temperature about 390 ºC and undergoes almost complete thermal decomposition at 441.8 ºC. High temperatures allow the defragmentation of the anion to smaller species like SO, SO_2, and $O_2S–CF_3$ (Keating et al., 2011). The thermal stability of an ionic liquid is often associated with the anion incorporated which emphases on the nucleophilicity of the ion. Thus, the hydrophobic $[NTf_2]^-$ anion containing better H-bonding ability is deemed to have high thermal stability (Maton et al., 2013). Inclusion of $[NTf_2]^-$ with other heterocyclic cations like alkylammonium cations and imidazolium cations have shown superior thermal stability with decomposition temperature above 200 ºC (Ghandi, 2014).

The initial thermal degradation of the ionic liquid containing polymer electrolytes is seen to follow a similar pattern with PS40 which contain no ionic liquid. As 50% of the polymer electrolytes are of EC: PC, the thermal degradations of plasticizers dominating up until 200 ºC comes with no surprise and the pattern observed is somehow predictable. This also signifies the probable anhydride formation occurring as discussed in section

Universiti Malaya

4.3.5. However, the noticeable increase in weight loss with addition of [C_4mquin][NTf_2] indicates the trapping of impurities in the ionic liquid, more likely moisture. Plus, gel like electrolytes also have higher ability to absorb and retain more solvents and moisture. Similar findings were also attained by Liew et al. also in their work on incorporating 1-butyl-3-methylimidazolium bis(trifluoromethylsulfonyl imide), BmImTFSI with poly(methyl methacrylate)-poly (vinyl chloride), PMMA-PVC blends (Liew & Ramesh, 2011).

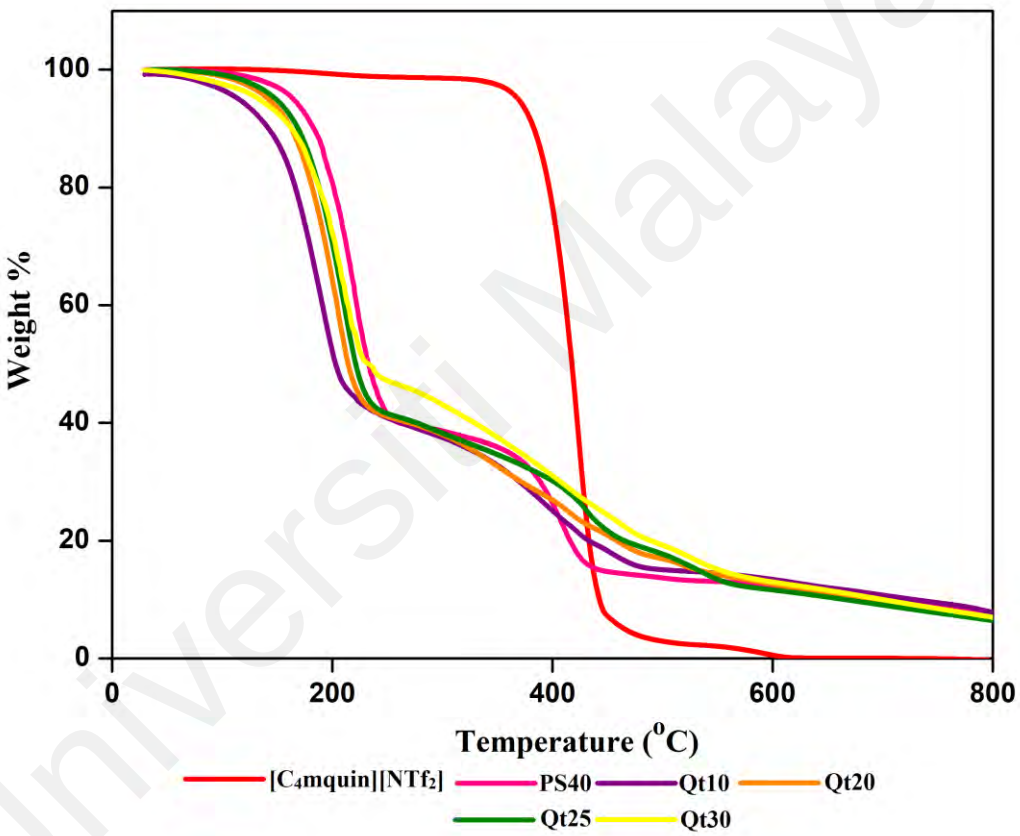

Figure 4.29: Comparative TGA analysis of PS40 with Qt10, Qt20, Qt25 and Qt30 along with pure [C_4mquin][NTf_2].

The second degradation region is a multistage drop, however stages are not discrete indicating no intermediaries formed. Continuous degradation of ionic liquid as discussed earlier can be a reason for this. As thermal degradation sees mass loss overlapping with pure polymer regions, another reason for no distinct degradation boundaries observed could be the good complexation between the polymers and ions present. The

Universiti Malaya

[C_4mquin][NTf_2] containing polymer electrolytes show a very accentuated total mass around 90 % which marks the decomposition of the sample and slowly continues up till 800 °C. Table 4.10 lists the thermally induced weight loss with corresponding temperature range for the GPEs. Finally, it is relevant to use [C_4mquin][NTf_2] containing polymers in electrochemical devices since the thermal stability is higher than 100°C and the optimum performance temperature of DSSCs is only 30- 40°C (Raga & Fabregat-santiago, 2013).

Table 4.10: The thermal induced weight loss with corresponding temperature range for [C_4mquin][NTf_2] containing GPEs.

Electrolytes	Qt10	Qt20	Qt25	Qt30
Initial weight loss temperature/ ^oC	137.7	148.5	156.3	157.7
Weight loss (%)	50.3	54.3	54.8	46.9
Intermediate weight loss temperature range/ ^oC	210.7- 482.3	227.6- 520.9	237.0-556.0	233.8-556.0
Weight loss (%)	30.4	28.0	29.7	34.5
Tailing weight loss temperature range/ ^oC	~500-800			
Weight loss (%)	~7			
Total weight loss (%)	87.7	91.2	92.5	88.4

4.4.6 Apparent diffusion study of I_3^-

Figure 4.30 shows the characteristic LSV curves for electrolytes containing different composition of [C_4mquin][NTf_2] ionic liquid. It can be seen that the saturation voltage

Universiti Malaya

attained by the samples are at about 0.1V. Besides, the anodic and cathodic plateaus are very much parallel and record similar limiting currents. Table 4.11 lists the J_{lim} and $D_{I_3^-}$ values elucidated based on LSV curves and *Equation 4.3*. Initial addition of ionic liquid, depreciated the value of $D_{I_3^-}$ from 1.51 x 10^{-8} cm^2 s^{-1} in PS40 to 1.12 x 10^{-8} cm^2 s^{-1} in Qt10. However, this behaviour was not seen in the conductivity of the electrolytes. Perhaps at low mass loading of ionic liquid, the conductivity relies on the higher number density of the iodide ions instead. Further increase in ionic liquid content escalated the $D_{I_3^-}$ values to a maximum of 2.19 x 10^{-8} cm^2 s^{-1} for Qt25. The addition of [C_4mquin][NTf_2] increased the total volume of sample by almost 40 % compared to that without ionic liquid. This contributes to a decrease in GPE viscosity and thus, explains the increase in triiodide diffusion coefficient. Besides, the slight decrease in $D_{I_3^-}$ value for Qt30 is parallel to the speculated idea of ion agglomeration whereby the interionic space is not sufficient for higher diffusion rate of the triiodide ions.

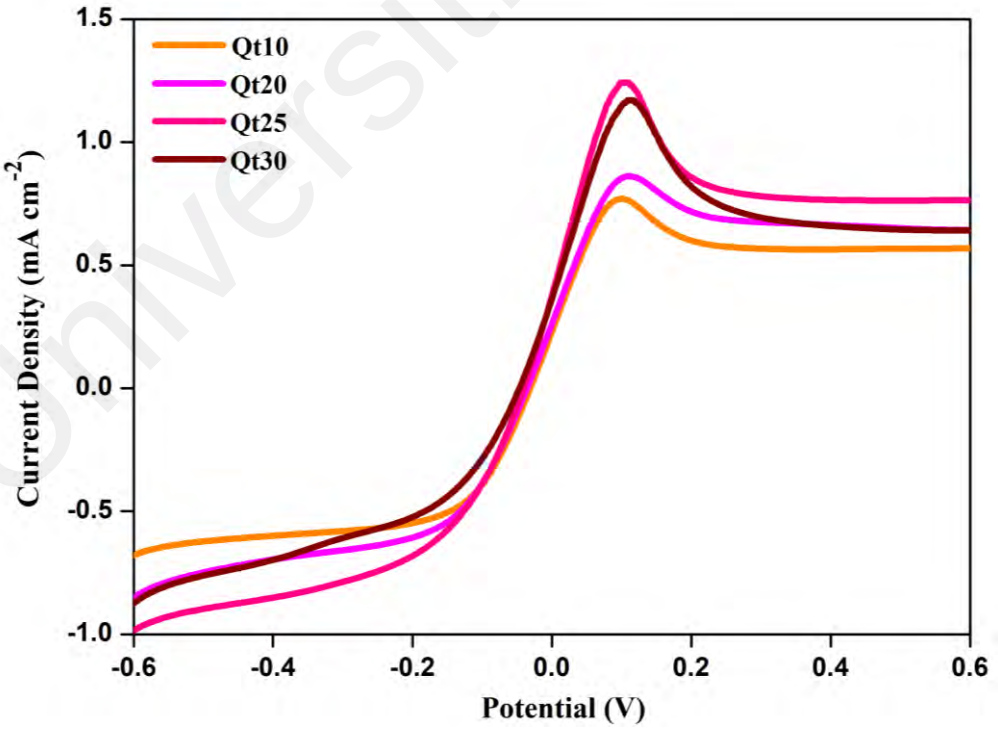

Figure 4.30: Linear sweep voltammograms of GPEs with different [C_4mquin][NTf_2] content.

Universiti Malaya

Table 4.11: J_{lim} and $D_{I_3^-}$ values obtained Qt10-Qt30 via steady state current measurements for corresponding GPEs.

Electrolyte	J_{lim} (mA cm^{-2})	$D_{I_3^-}$ (x 10^{-8} cm^{2}s^{-1})
Qt10	0.58	1.12
Qt20	0.68	1.65
Qt25	0.77	2.19
Qt30	0.71	2.16

4.5 P(MMA-co-MAA)-NaI-[C$_4$mquin][I]Gel Polymer Electrolyte.

4.5.1 Ambient temperature ionic conductivity studies

Figure 4.31 portrays the ionic conductivity of polymer electrolytes with respect to varying mass loadings of [C$_4$mquin][I] with exact values tabulated in Table 4.12. As predicted, the ionic conductivity of the polymer electrolytes increase with increasing ionic liquid concentration up to a certain mass loading after which shows a decline with further ionic liquid addition. Akin to the previous system added with [C$_4$mquin][NTf$_2$], the polymer-salt electrolyte ionic conductivity was enhanced by two folds in magnitude from 1.07 mS cm^{-1} to 2.64 mS cm^{-1} with addition of 25% of [C$_4$mquin][I], labelled as Qi25. Again, we related the augmented ionic conductivity to the strong plasticizing effect of quinolinium ionic liquids. The softening occurring on the polymer matrix may well dissociate charge carriers by abating bond coordination and thus promote fast ionic conduction. On top of softening the rigid PMMA containing backbone, addition of quinolinium based ionic liquids created more adherent polymer electrolytes which is necessary to provide better electrode- electrolyte contact. This is also deemed as a very vital feature to note in fabrication of sandwiched electrochemical devices like DSSCs in order to maintain the recyclability of the device. Surge in ionic conductivity noted in

Universiti Malaya

polymer electrolytes can be also interrelated to the crystallinity of the electrolytes. If the addition of ionic liquid is capable of reducing the crystallinity of polymer electrolytes, a boost in ionic conductivity is very much anticipated. Since the dissolution of salt, iodine and polymer was better with the addition of [C_4mquin][I] ,thus, the amorphous content of the polymer electrolytes must have increased equally. Large amorphous phase promotes ionic transportation. Undoubtedly, movement of charge carriers occurs with much ease in amorphous region than in rigid crystallinity phases .In the presence of large [C_4mquin] cation, it is proposed that both inter-atomic and –molecular interactions can be broken, hence, creating a more disordered chain structure. Increasing wt. % of the ionic liquid disrupts the ordered arrangement of macromolecules even higher. The creation of a random coil configuration may be a boon but with [C_4mquin][I] more than 25 wt.%, polymer electrolytes made become less conductive. Again, this depreciation is attributed to the formation of ion aggregates that clump up and dampen smooth ionic transportation within the polymer matrix as picturized before. It was also visible that upon optimum ionic liquid content, the polymer electrolytes show weakening mechanical properties that is above 30 wt. % of [C_4mquin][I]. When compared with the "*Qt"* system, GPEs containing [C_4mquin][I] ionic liquid fared better ionic conductivity for the same wt. % . This perhaps is a result of multiple polyiodide formation in the electrolyte. Higher iodide concentrations yield longer polyiodides chains like I_5^- and I_7^-. Multiple reports claim that an increase in ionic conductivity is possible through the formation of less-mobile polyiodides in the colloidal electrolyte because of the Grotthuss mechanism initiated by high concentrated packed polyiodide species. Thus, the results suggest the exchange between neutral iodine and polyiodides can be the more dominating mechanism than the physical drifting of I_3^- to promote conductivity (Thapa & Park, 2012; Shih, et.al., 2018).

Universiti Malaya

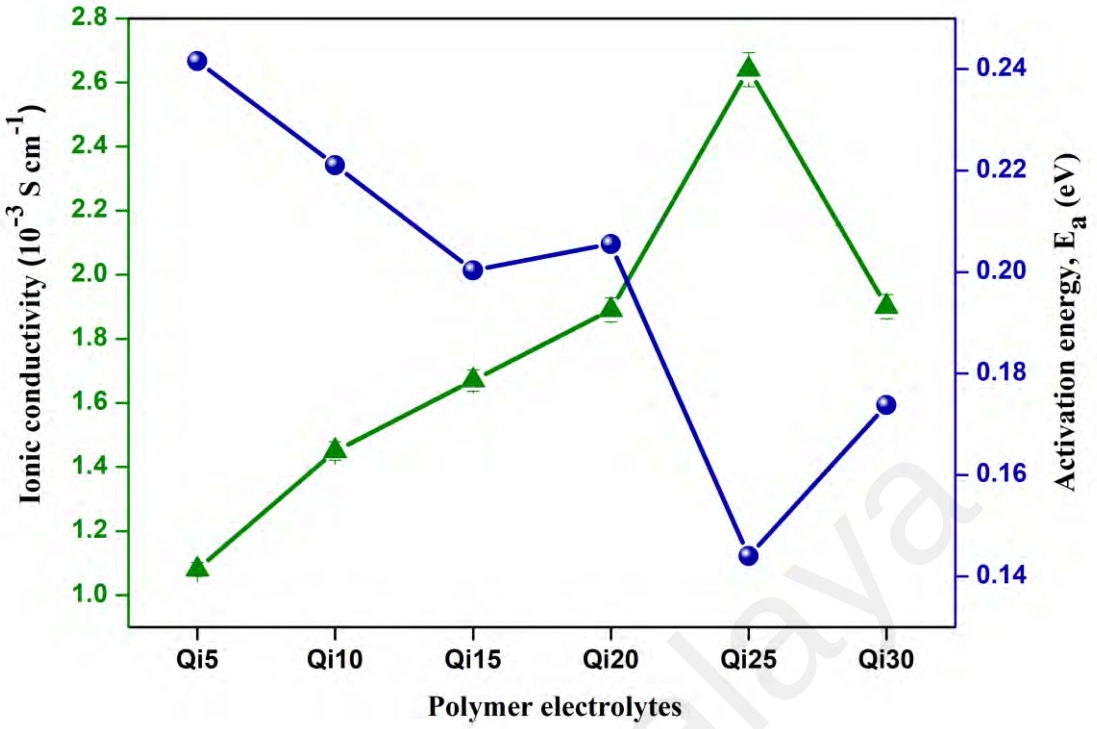

Figure 4.31 Variation in ionic conductivity and activation energy for [C4mquin][I] containing GPEs.

Table 4.12: Ionic conductivity and corresponding activation energy values for Qi5-Qi30 GPEs at room temperature.

Electrolytes	Average R_b (Ω)	Ionic conductivity (mS cm^{-1})	Activation Energy (eV)
Qi5	118.0	1.08 ±0.02	0.242
Qi10	87.8	1.45± 0.03	0.221
Qi15	76.1	1.67± 0.03	0.200
Qi20	67.0	1.89 ±0.03	0.206
Qi25	48.1	2.64±0.04	0.144
Qi30	66.8	1.90±0.04	0.174

Universiti Malaya

4.5.2 Temperature dependent ionic conductivity studies

The ion transport mechanism of P(MMA-co-MAA)-NaI-[C_4mquin][I] GPEs was also evaluated by measuring ionic conductivity over temperature ranging from ambient to 100^o C. Figure 4.32 shows the data presented on an Arrhenius plot. The linear variation obtained with average regression value of 0.99 reveal that even after the addition of the [C_4mquin][I] ionic liquid, ionic conduction mechanism obeys the Arrhenius theory. The dominance in the role of the quinolinium cation is very visible here as similar findings were reported using [C_4mquin][NTf_2] in Section 4.4.2. Furthermore, both [C_4mquin][I] and [C_4mquin][NTf_2] showed maximum ionic conductivity at 25 wt.% at 100 ^{o}C with values 7.60 mS cm^{-1} and 7.28 mS cm^{-1} respectively. It is noted that the conductivity of the iodide anion is slightly larger than the fluorinated anion. The iodide ion is capable of forming stronger hydrogen bonds with the hydrogens at two carbon positions namely the first and the seventh carbon counted anticlockwise from the nitrogen in the cation. Thus, making it less mobile compared to the fluorinated anion (Zhang et al., 2003). NTf_2 on the other hand, has lower charge density due to the negative charge spread over a larger volume (Leys et al., 2008). The cationic and anionic interaction is foreseen to be much weaker than between the iodide anion. Hence, a higher mobility should be noted that would directly reflect on the ionic conductivity at both room temperatures and higher. However, the opposite was noticed predominantly due to the presence of the polymeric network which made larger ions more difficult to move through the sample, causing much lower ionic conductivity.

The increase in ionic conductivity with the rise in temperature reflects on the increase in mobility of charge carriers due to the gain in energy upon heating. The pseudo-ion hopping from one coordination to another nature happens with more ease at higher temperature and it is reflected as activation energy values. The calculated E_a value from

Universiti Malaya

the slope of each respective Arrhenius plot is tabulated in Table 4.12 and Qi25 was found to have the lowest value.

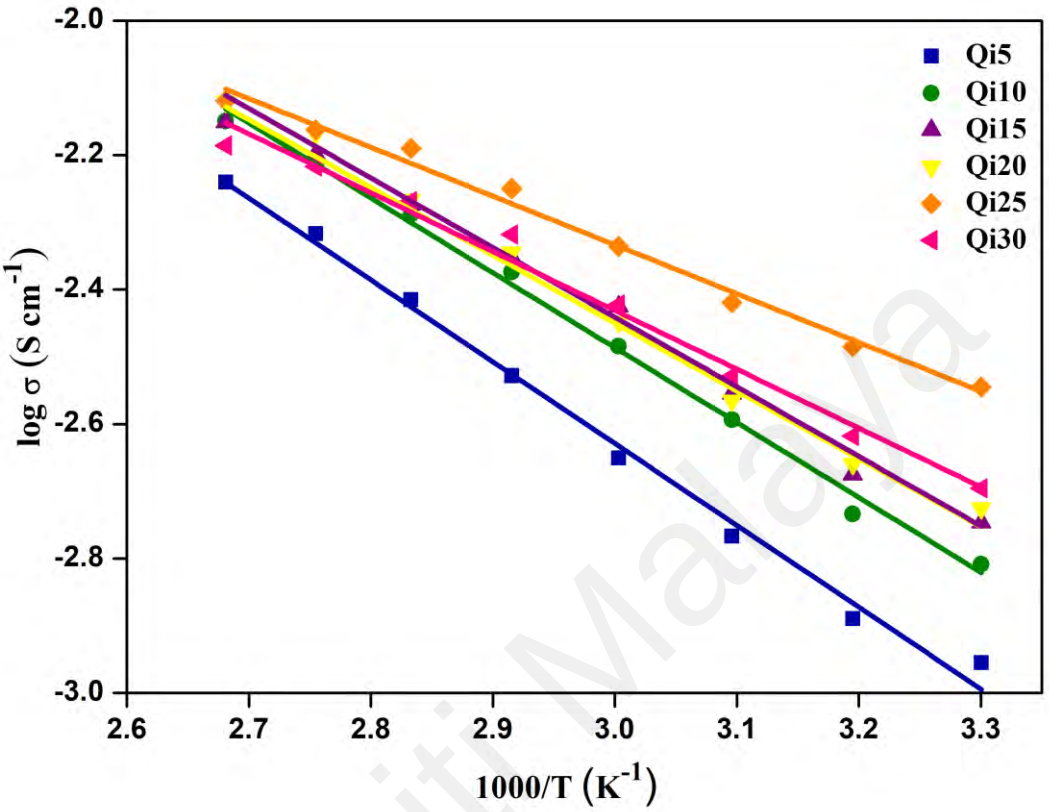

Figure 4.32: The variation of log σ plotted against the reciprocal absolute temperature for [C4mquin][I] containing GPEs.

4.5.3 FTIR

Figure 4.3 show the FTIR spectrum of pure [C4mquin][I]. As both novel ionic liquids studied in this research share the same cation, the spectra share similarity in peaks displayed. The corresponding peak regions and descriptions are as discussed in Section 4.4.3. In brief, the overlapping explanations include the O-H vibrations in water and aromatic C-H and C-C vibrations. Figure 4.33 displays FTIR spectra of GPEs upon inclusion of [C4mquin][I] at different weight ratio. The shifts in peaks at corresponding wavenumber are of close match irrespective of the different wt. % of ionic liquid added. However, variation in peak intensity were noticed as previous systems which were further analysed under deconvolution of peaks as shown in Figure 4.34 and 4.35.

Universiti Malaya

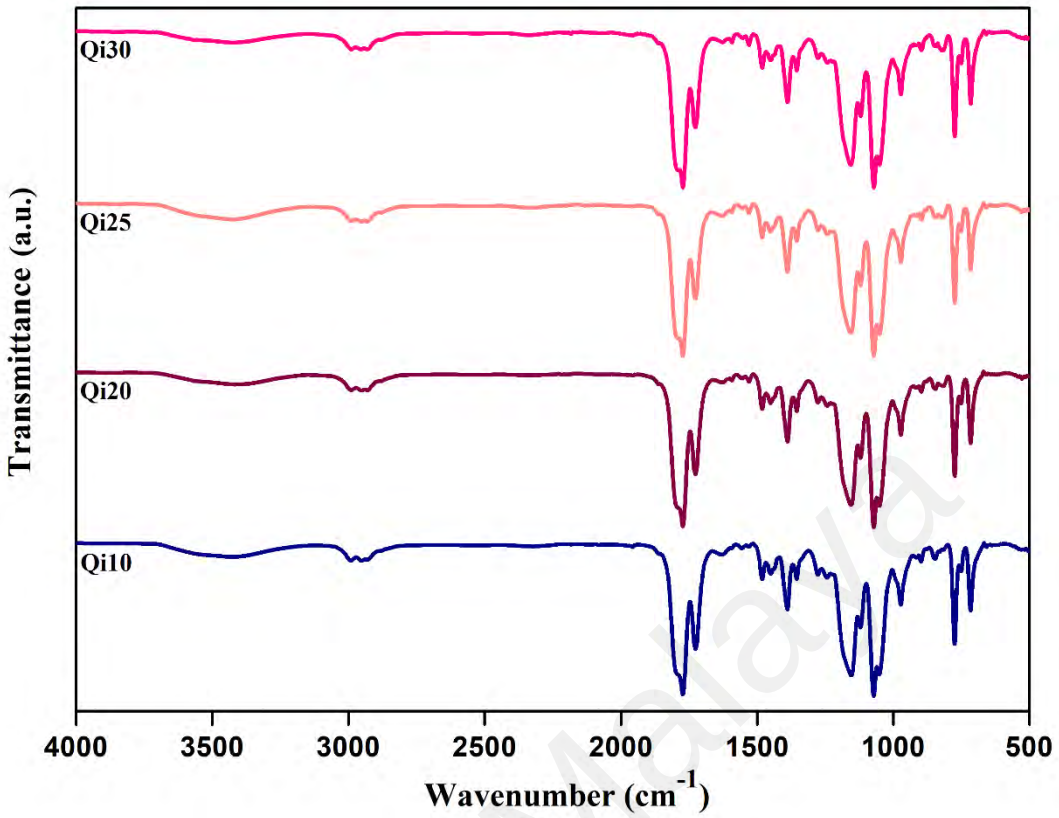

Figure 4.33: FTIR spectra of GPEs Qi10, Qi20, Qi25 and Qi30.

The shifting in the characteristic carbonyl peak of P(MMA-co-MAA) to 1727 cm^{-1} indicates the possibility of C=O bond strengthening, comparable to the $[C_4mquin][NTf_2]$ GPE systems. The reduction in intensity as ionic liquid wt. % increases in parallel to the composition of the GPE with decreasing wt. % of polymer- i.e lower concentration of polymer. Other two peaks found in the carbonyl region for Qi10 –Qi30 show minimal percentage area difference among each other, particularly peak at 1771 cm^{-1} which relates to C=O stretch in plasticizers. This validates agreeable ion solvation and complexation in samples.

Universiti Malaya

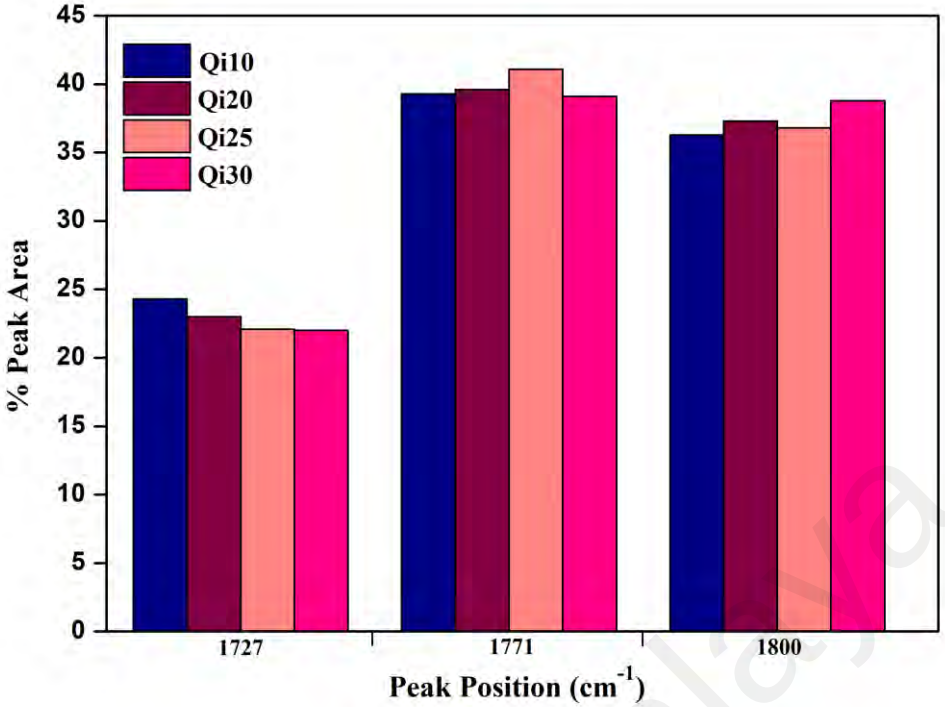

Figure 4.34: Relative FTIR band percentage area in the range of 1700 to 1850 cm^{-1} for Qi10, Qi20, Qi25 and Qi30.

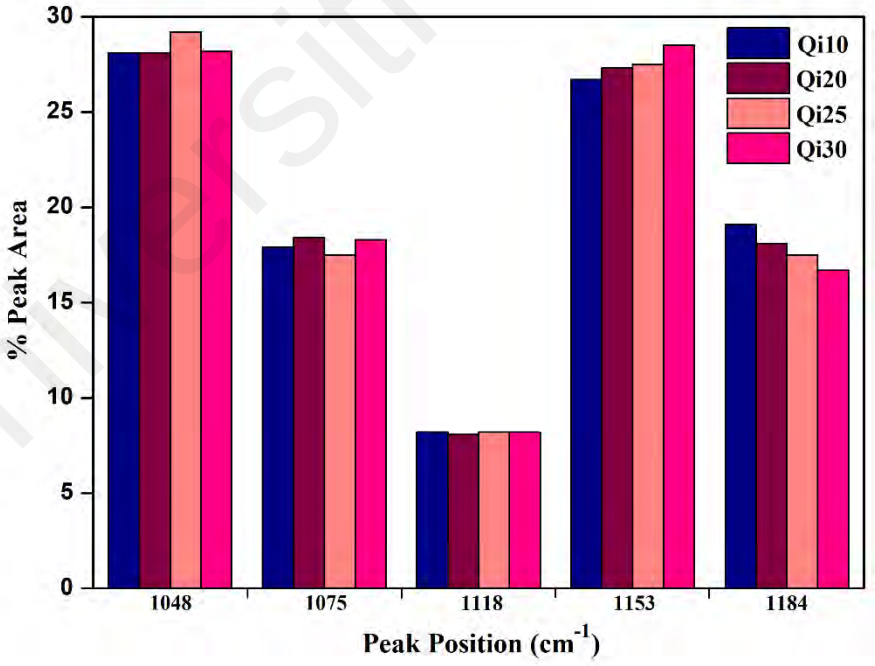

Figure 4.35: Relative FTIR band percentage area in the range of 1000 to 1200 cm^{-1} for Qi10, Qi20, Qi25 and Qi30.

Universiti Malaya

Besides, five deconvoluted peaks are obtained in the regions 1000-1200 cm^{-1}. This result is in good agreement with the suggested interaction depicted in Figure 4.14. For the four samples listed, Figure 4.35 shows the peak intensities noted do not vary much and this is another apparent prove of good ionic liquid- polymer interaction. The dominance of polymer and plasticizer functional group is evident from the congruity noticed in FTIR spectra before and after the addition of ionic liquids as depicted in Figure 4.36 with PS40 and Qi25. Both mentioned spectra share the presence of all functional groups but Qi25 has an additional $[C_4mquin]^+$ ion in it. Though the prominence of the $[C_4mquin]^+$ ion is not visible in the spectra, the solvation and complexation is evident from peak shifts and intensities.

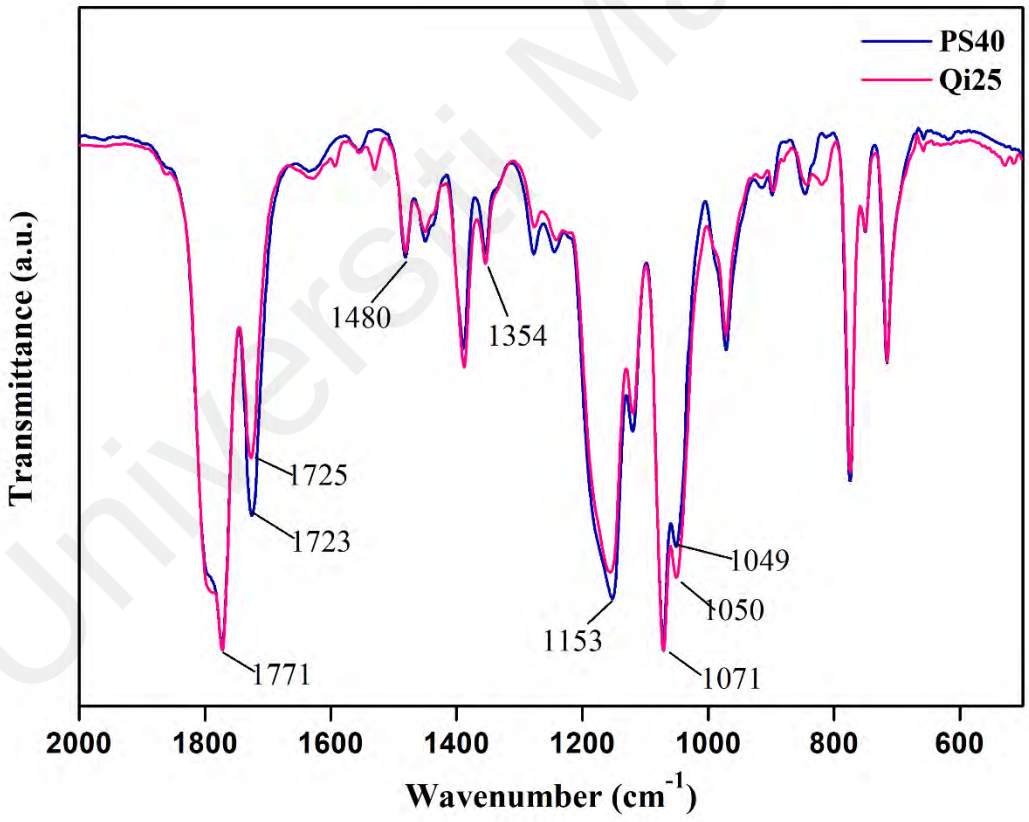

Figure 4.36 Comparative display of PS40 and Qi25 FTIR spectra.

Universiti Malaya

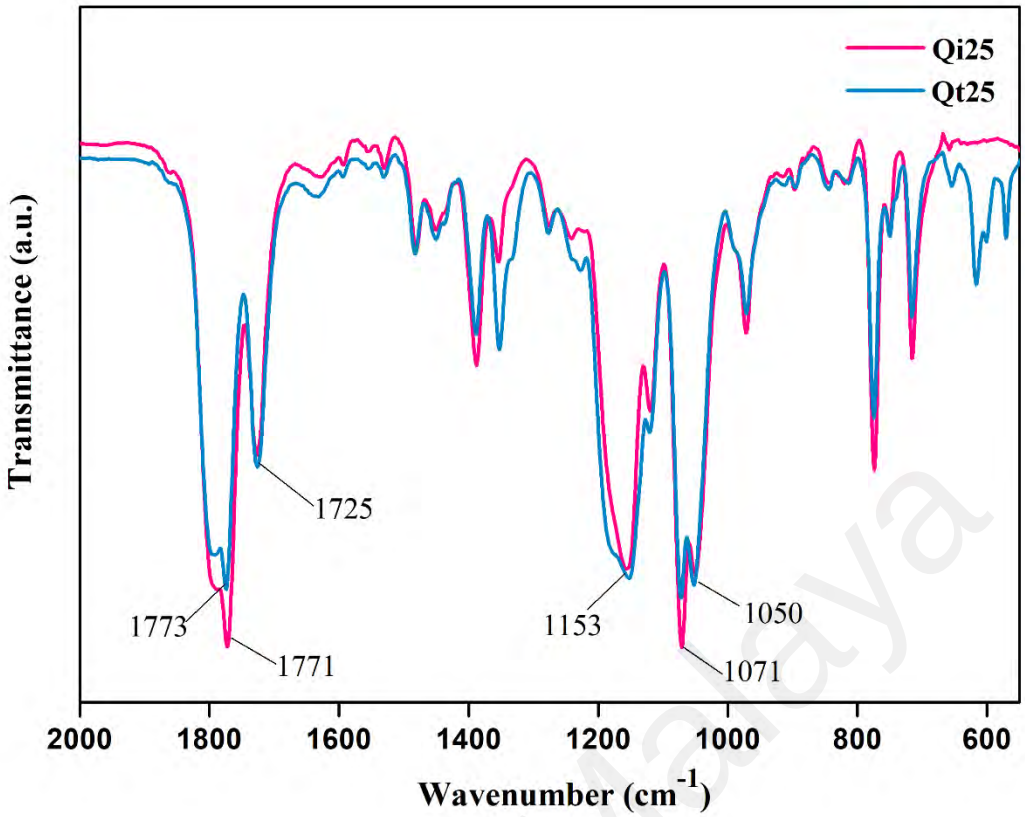

Figure 4.37: Comparative display of Qi25 and Qt25 FTIR spectra.

It was equally interesting to note that both [C_4mquin][I] and [C_4mquin][NTf_2] containing GPE spectra show vast similarity and this comparison is shown in Figure 4.37. The contrasting feature noticed lies at wavenumbers below 700 cm^{-1}. Peaks found at 653 cm^{-1}, 517 cm^{-1} denotes the symmetric and asymmetric deformation of the CF_3 bonds present in NTf_2 (Molla-abbassi et al., 2002). As for peak about 1355 cm^{-1}, the transmission is heightened in the Qt25 spectra compared to Qi25. This is attributed to the inclusion of S=O stretching vibrations occurring on top of commonly noted C-H bending vibrations in CH_3 and O-H bending vibrations occurring about that wavenumber (Bardak et al., 2007). Transmission peaks recorded in FTIR spectra can portray multiple effects from different functional groups which are additive. Likewise, comparing the 1000-1200 cm^{-1} region for both GPEs noted in Figure 4.37, a more intense C-O-C stretching is predicted to lie here for Qt25. This occurrence most probably swamped other peaks contributed by S=O stretching, N-S stretching and overtones.

Universiti Malaya

Thus, even with deconvolution it is difficult to perceive more information on ion-functional group interaction. Nevertheless, reasonable shifting in peaks, peak intensity and shape observed for each GPE containing [C_4mquin][I] concludes that complexation has occurred.

4.5.4 XRD

Figure 4.38 portrays the XRD diffractograms of GPEs Qi10, Qi20, Qi25 and Qi30. As shown in in Figure 4.7 in Section 4.2, the [C_4mquin][I] spectrum also exhibit sharp peaks indicating the highly crystalline nature of the solid state ionic liquid. However, the resulting XRD spectra of GPEs were mainly comprised of broader peaks at different 2θ values and a few sharp peaks most likely due to some undissolved NaI. As the ionic liquid content increases, better dissolution of the salt is also noticed as less intense sharp peaks are visible. In addition to the absence of peaks which is a proof of complexation between the components in the electrolyte, peak shifts and merging is another positive sign of a new complex formed. The ordered arrangement in NaI, [C_4mquin][I] and copolymer matrix are most likely disordered upon mixing and heat treatment causing a drop in crystallinity. All four GPEs possess similar XRD pattern and their respective humps are listed in Table 4.13 Visually, the diffractograms noted in Figure 4.38, have significantly lesser intensity as compared to PS40 sample which implies the more amorphous nature of the [C_4mquin][I] containing GPEs which helps in improving ion transport in the electrolyte. In the same way, two humps are also present in the [C_4mquin][I] containing spectra showing resemblance in complexation as [C_4mquin][NTf_2] containing samples.

To further emphasize complexation and amorphous nature of the GPEs, peak deconvolution method with curve fitting is done. Even though two broad humps are present, the first peak around 9° is denoted as a crystalline peak and the amorphous peak comes in as the latter around 24°. The variation in degree of crystallinity for Qi10 – Qi30 is quantified using area under the curve fitted under the Hodge criterion owing to the

Universiti Malaya

multi-peak spectra. Curve fitting allowed the calculation of degree of crystallinity present by dividing the area under the crystalline peak over total area of all the peaks. The relevant parameters obtained from curve fitting are also summarized in Table 4.13.

Again, the addition of [C_4mquin][I] along with salt and plasticizers have proven to reduce the crystallinity of the co-polymer substantially with increasing ionic liquid content which promotes conductive properties. A substantial decrease in the degree of crystallinity is seen from 66 % in pure co-polymer to 20.6 % in Qi25. This is evident to verify that one of the reason for the high conductivity attained by Qi25 is due to its low crystalline region in the electrolyte. Interestingly, Qi samples recorded much lower degree of crystallinity than their "*Qt*" counterparts at same ionic liquid mass loading. It is a good proof that mere inclusion of large anions in electrolyte system is able to retain much order and crystallinity. Highly ordered arrangement in a crystalline region restricts mobile charge carrier transportation and requires larger energy for hopping mechanism. Conversely, more empty spaces are available in the randomly arranged amorphous phase should allow ion transport at much ease. The lowest activation energy noted from Arrhenius fitting for Qi25 in section 4.5.2 is a good proof that high amorphous degree contributes to high ionic conductivity. In the face of Qi30 recorded to be the most amorphous among all four samples with degree of crystallinity at 16.9%, it was unable to produce the best conductivity and a slightly larger activation energy is also noted. Amorphous zones usually fill up inter crystalline sites and it is common for additives like salt and ionic liquid to occupy this region. Mobile charge carriers require enough contact with each other to form a conducting network. For the case of Qi30, the lowering polymer content and aggregation of ions can be deemed insufficient to sustain effective ion hopping despite the lower amorphous nature attained.

Universiti Malaya

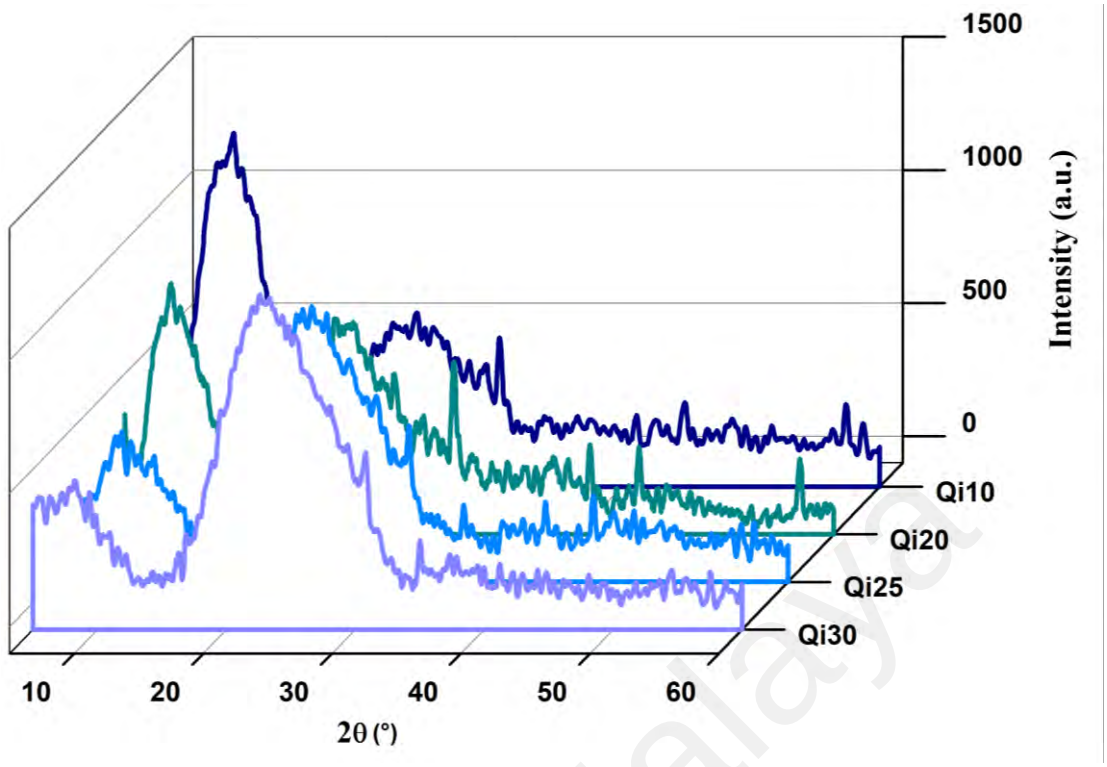

Figure 4.38: XRD Diffractograms of GPEs Qi10- Qi30.

Table 4.13: Significant parameters obtained from curve fitting the XRD diffractograms of GPEs in the Qi system.

Electrolytes	Crystalline peak,2θ (°)	Amorphous peak,2θ (°)	Area of crystalline peak, I_C	Total area under the curve, I_T	Percentage of crystallinity (%)
Qi10	9.71	24.37	6587	12564	52.4
Qi20	9.04	23.21	3637	10225	35.6
Qi25	8.83	23.83	2395	11614	20.6
Qi30	8.44	24.05	2429	14325	16.9

4.5.5 TGA

In order to further understand the role of halide ions in thermal stability of electrolytes, thermogravimetric analysis of N-butyl-6-methylquinolinium iodide containing polymer electrolytes is presented in Figure 4.39. Predictably, pure [C_4mquin][I] displays a single

University Malaya

stage decomposition with onset decomposition temperature about 220 ºC and undergo almost complete thermal decomposition at 248.9 ºC. By comparison, halide ions show lower thermal stability than non-halide anions and iodide in particular contains large electron delocalization and suffers from inability to hydrogen bond (Huddleston et al., 2001). Thus, the significant reduction in decomposition temperature. Despite the variation in weight percentage of [C_4mquin][I] added in the polymer electrolytes, the trends obtained from Qi20, Qi25 and Qi30 are very analogues and almost overlap with each other. The mass loss in the region of 220- 300 ºC was not observed for PS40. The thermal degradation in this phase arises from a chemical degradation process occurring on N-butyl-6-methylquinolinium cation which corresponds to a mass loss of 12% accounts for the fragment size, for the above mentioned three samples. The concerning fragment would be the -$CH_2CH_2CH_2CH_3$ chain. The chain scissoring between N-C bonds was found common observed around these temperature ranges (Efimova et al., 2013). Qi10 shows more resemblance towards the non-IL added graph, indicating at low concentration of IL not much affect thermal degradation pattern.

Universiti Malaya

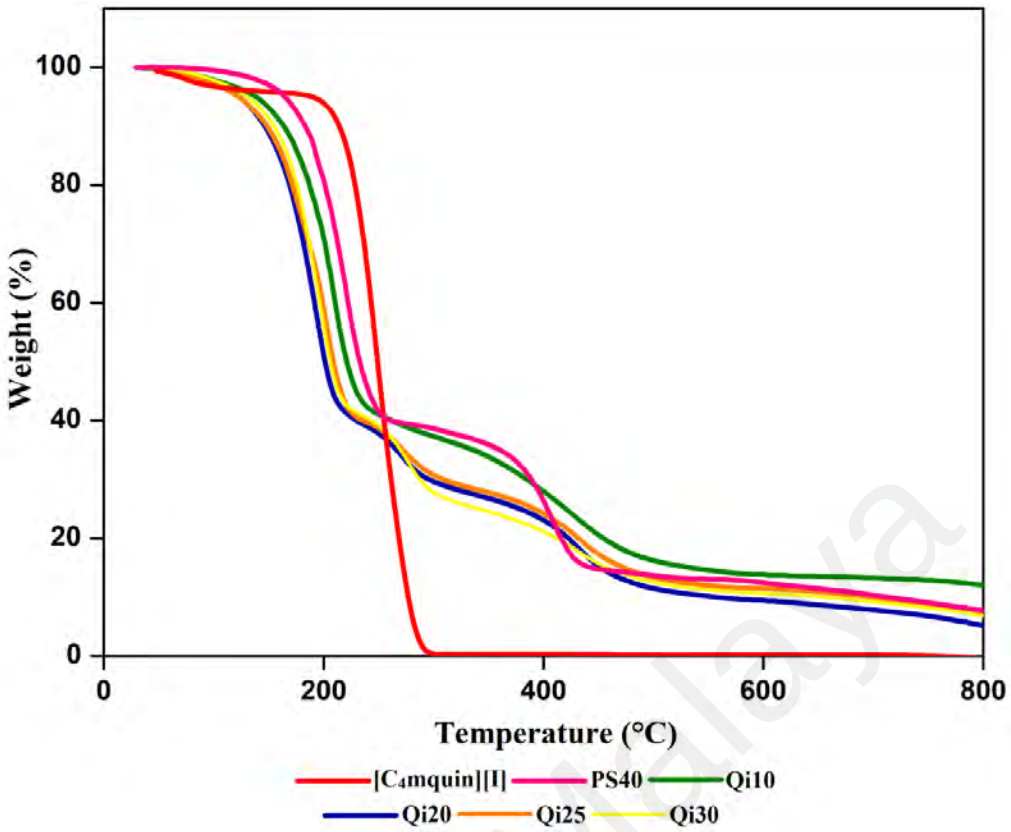

Figure 4.39: Comparative TGA analysis of PS40 with Qi10, Qi20, Qi25, Qi30 and pure [C4mquin][I].

As temperature go beyond 300 ºC, the polymer unzipping process occurs. Such degradation follows as random chain scissoring, depolymerisation and both inter- and intra-molecular transfer reactions. Eventually, the chemical absorbed monomers and oligomers entwined onto polymer matrix decomposes as temperature progresses. Clearly, the weight loss values at three marked regions as shown in Table 4.14 indicate similar complexation and thermal stability up to 155 ºC is good enough to perform as electrolytes in DSSCs.

Universiti Malaya

Table 4.14: The thermal induced weight loss with corresponding temperature range for [C_4mquin][I] containing GPEs.

Electrolytes	Qi10	Qi20	Qi25	Qi30
Initial weight loss temperature / ^oC	155.5	155.6	157.5	157.6
Weight loss (%)	55.1	53.1	51.2	51.4
Intermediate weight loss temperature range / ^oC	247.1- 488.3	215.3-290.0	215.3-290.0	221.5- 298.5
Weight loss (%)	23.4	11.5	10.7	15.0
Tailing weight loss temperature range / ^oC	~300-500			
Weight loss (%)	-	16.4	15.1	13.5
Total weight loss (%)	78.5	81.0	77.0	79.9

4.5.6 Apparent diffusion study of I_3^-

In order to correlate the higher ionic conductivity attained by the [C_4mquin][I] containing GPEs than their [C_4mquin][NTf_2] counterparts at equivalent mass loading, the triiodide diffusion coefficient is determined. Figure 4.40 illustrates the LSV curves with clear indication of ion saturation and limiting current values. Since the density of [C_4mquin][I] of 1.21 g ml^{-1} is marginally higher than [C_4mquin][NTf_2] of 1.07 g ml^{-1}, an increase in mass loading of ionic liquid increases the overall volume of the GPEs. Comparative ratio proof an increase in volume by 1.5 % for the same wt. % of ionic liquid added. Interestingly, the mere increase in volume had substantially increased the diffusion rate of triiodide ions. The saturation voltage attained by the samples are again at about

Universiti Malaya

0.1 V as [C_4mquin][NTf_2] samples, nevertheless, slight skewing to higher voltage is noted here indicating rapid electron transfer kinetics. The growing peak denote the inability of the reactant flux to reach the electrode fast enough owing to the growth of diffusion layer. Based on the voltagramms, Qi25 records the highest and more sustained limiting current of 1.05 mA cm^{-2} compared to Qi10, Qi20 and Qi30. Table 4.15 lists the values of limiting current and triiodide diffusion coefficient for Qi10- Qi30. Calculation of $\boldsymbol{D}_{I_3^-}$ values based on *Equation 4.3*, illustrates higher triiodide diffusion rate for Qi30 compared to Qi25. XRD findings as previously discussed also supports the existence of a more amorphous Qi30 compared to Qi25 which obviously aids the better triiodide movement Qi30. Nevertheless, this somehow did not translate as achievement in ionic conductivity. The exact reason to the phenomena is unclear on the basis of this result. It can be speculated that ionic conductivity observed is affected by the movement of cations as well as anions in the electrolyte and perhaps ion aggregation or increasing cationic interaction with the polymer backbone in the complex polymer matrix had led to a short fall in ionic conductivity seen in Qi30.

Comparatively, [C_4mquin][I] have shown to have better triiodide diffusion coefficient than the [C_4mquin][NTf_2] GPEs which translates into better ionic conductivity. A higher charge delocalization is expected from the $[NTf_2]^-$ anion which should bring about more amorphous nature when the cations utilized for the ionic liquids are the same. However, the opposite was true here. Yet, two of the [C_4mquin][NTf_2] GPEs manage to attain ionic conductivity higher than 2.0 mS cm^{-1} probably due to a Grotthuss style bond exchange on top of physical diffusion. Bentley el al. gauged this phenomena to be more common in bis(trifluoromethanesulphonyl)imide containing system (Bentley et al., 2014).

Universiti Malaya

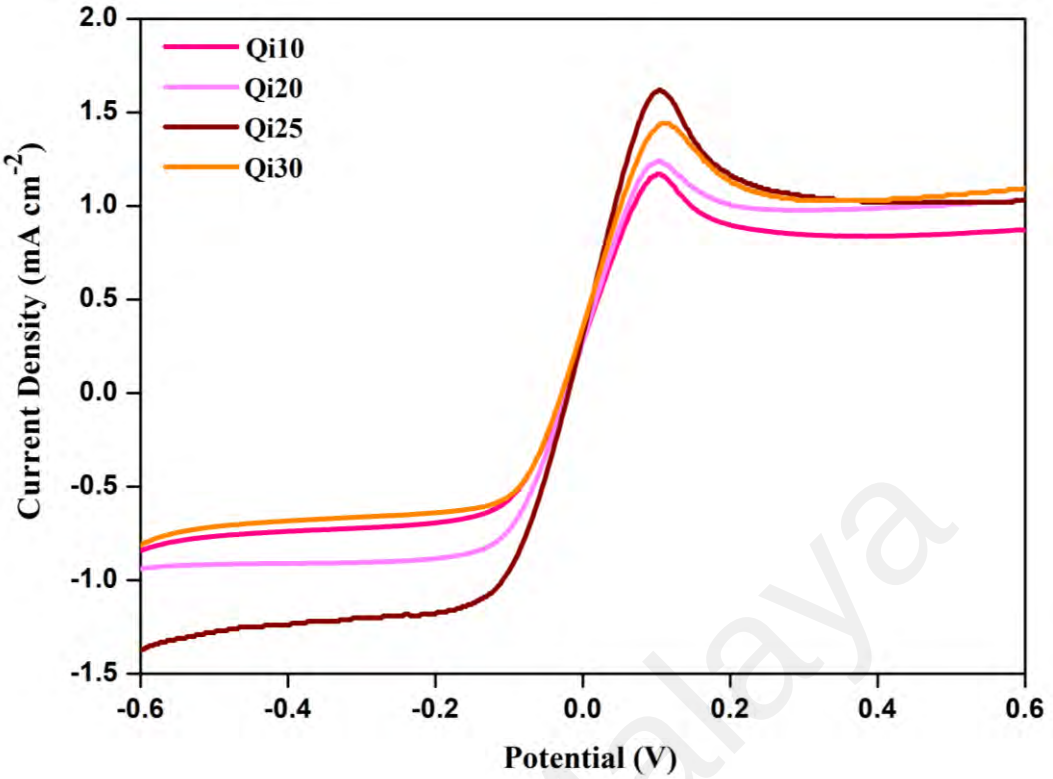

Figure 4.40 : LSV voltammograms for Qi10, Qi20, Qi25 and Qi30.

Table 4.15: J_{lim} and $D_{I_3^-}$ values obtained Qi10-Qi30 via steady state current measurements for corresponding GPEs.

Electrolyte	J_{lim} (mA cm^{-2})	$D_{I_3^-}$ (x 10^{-8} cm^{2}s^{-1})
Qi10	0.85	1.63
Qi20	0.99	2.34
Qi25	1.05	2.77
Qi30	1.01	2.97

4.6 P(MMA-co-MAA)-NaI-[C$_6$mim][I]Gel Polymer Electrolyte.

The inclusion of a commercially available ionic liquid was necessary to evaluate the overall efficiency of the polymer electrolyte itself in the basis of conductivity as well as emphasis the role of novel quinolinium based ionic liquids. Imidazolium ionic liquids have been vastly explored as ionic liquids in the DSSC field. Among the various choice

Universiti Malaya

of imidazolium-iodide ionic liquids present, the $[C_6mim]^+$ cation was chosen owing to several reasons. Research elucidation led to the inference that the hexyl group on imidazolium cation was the optimum length that promoted V_{oc} values without much compromising the J_{sc} values recorded. Any other larger alkyl chain was able to reproduce the V_{oc} values commonly obtained upon $[C_6mim]^+$ incorporation but depreciated the J_{sc} values significantly. The opposite was true for smaller alkyl chains, as better J_{sc} values are noted but unable to achieve higher V_{oc}. This was the reason why the $[C_6mim][I]$ ionic liquid containing samples do not have high conversion efficiencies compared to the ethyl, propyl and butyl counterparts. For the purpose of this research it was necessary to select an ionic liquid capable of supplying large electron cloud density as the quinolinium and possibly behave like a porous barrier between the dye and electrolytes. The hexyl chain length was repeatedly reported to create sufficient hydrophobic interaction forming barriers to prevent back electron transfers and produce large V_{oc} values.

4.6.1 Ambient temperature ionic conductivity studies

Figure 4.41 shows the variation in ionic conductivity of GPEs at different mass composition of ionic liquid with corresponding activation energy with exact values tabulated in Table 4.16. An obvious observations from the figure would be a gradual increase in ionic conductivity is seen with increasing wt.% of ionic liquid and ionic conductivity of the GPEs increases with temperature whereby the former can be attributed to the strong plasticizing effect of ionic liquid that indorses ion dissociation (Singh & Sekhon, 2003). With decreasing polymer concentration and increasing number of mobile carriers- $[C_6mim]^+$ and I^- ions, an apparent decrease in GPE viscosity is seen with consecutive increase in ionic liquid wt. % indicating improvement in the flow of ions achieving a maximum reading in ionic conductivity was achieved at 20 wt. % of $[C_6mim][I]$, 2.33 mS cm^{-1} at room temperature.

Universiti Malaya

However, there is a sudden drop in ionic conductivity when 25 wt. % of [C_6mim][I] added into the system. Although physically the 25 wt.% of [C_6mim][I] system showed good flow for a quasi-solid mixture, but the end-result can be an effect of excess ion accumulation instigating the mobile ions to form neutral pairs, thus, contributing to a reduction in ionic mobility in the GPEs as well as overall segmental motion of the polymeric chains. The ionic conductivity study of GPEs depend heavily on the mobility of ions in the redox couple I^-/ I_3^- which can be exemplified using *Equation 2.6* shown previously.

As the charge on the mobile ions are the same, and thus can be disregarded, ionic conductivity relies hugely on number of charge carriers and the mobility of ions incorporated. However, this is particularly true only for systems with low ion concentration. Upon reaching an optimal point, ionic conductivity is controlled dominantly by movement of ions as well as ionic conduction pathway (Yu et al., 2007). As the ionic liquid content increase to 20 wt. % , a decrease in R_b value is seen, most likely due to the influx in number density of mobile charge carriers. It is worthy of note that, amorphous phase content of the polymer salt- ionic liquid system is augmented by solvent cum plasticizers like EC/PC. EC alone is capable of crystallizing at room temperature, causing a probable phase separation between the polymer composite matrixes. Thus, addition of PC is crucial despite the high dielectric constant of EC would be sufficient to promote high ionic conductivity. Again, the use of plasticizers have highlighted the surplus in ionic conductivity, long term stability and improved power conversion efficiencies at a 1:1 wt. % of EC/PC in comparison to other blends in ratio.

When compared with samples containing the [C_4mquin][NTf_2] and [C_4mquin][I] ionic liquid, conductivity of [C_6mim][I] containing GPEs overrides by reaching a maximum value at just 20 wt. %. This was foreseen due to the inherent physiochemical properties of the ionic liquid itself whereby the lower viscosity owing to liquid physical state and

University Malaya

higher dielectric constant could be the contributors of the higher ionic conductivity achieved when added to the polymer electrolyte (Kumar et al., 2012). Nevertheless, the highest ionic conductivity was achieved with [C_4mquin][I], possibly due to better shielding of cation- anion in polymer matrix owing to the larger cation size but smaller anion which help in dissociating the cations from the attractive anionic bonding, hence, higher number of charge carriers would be present.

Table 4.16: Ionic conductivity and corresponding activation energy values for Hm5-Hm25 GPEs at room temperature.

Electrolytes	Average R_b (Ω)	Ionic conductivity (mS cm^{-1})	Activation Energy (eV)
Hm5	95.3	1.33 ± 0.02	0.215
Hm10	92.8	1.37 ± 0.02	0.211
Hm15	78.1	1.62 ± 0.03	0.205
Hm20	54.5	2.33 ± 0.04	0.182
Hm25	71.3	1.78 ± 0.04	0.188

Universiti Malaya

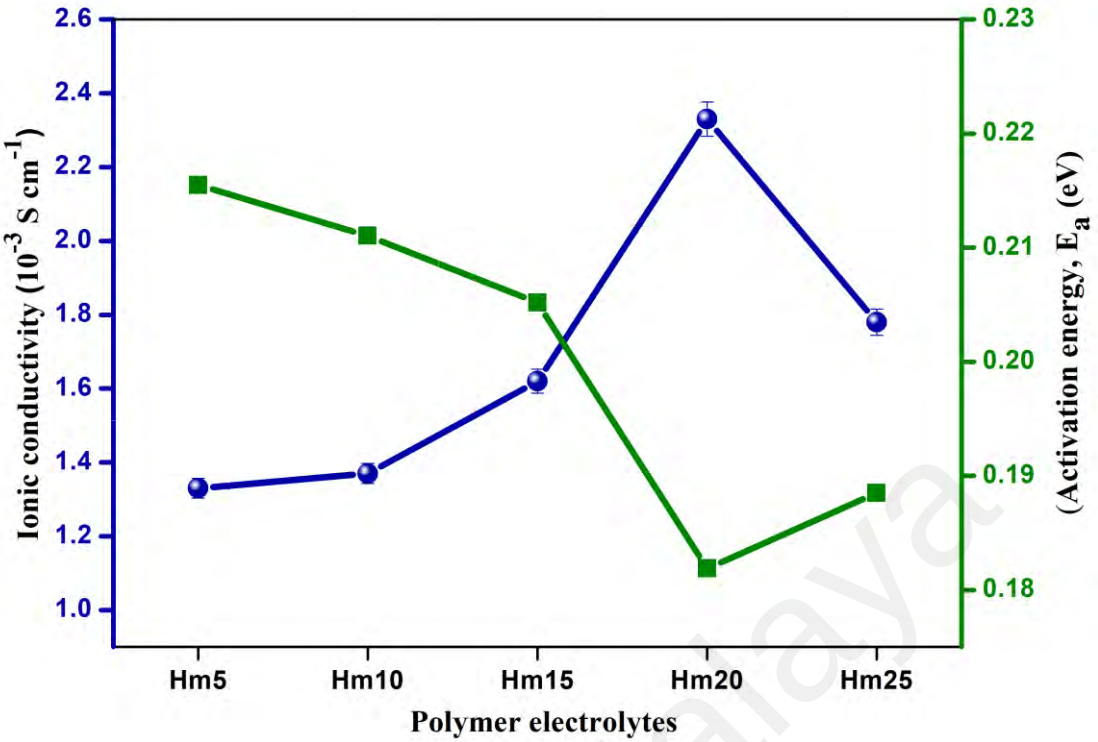

Figure 4.41: Variation in ionic conductivity and activation energy for [C_6mim][I] containing GPEs.

4.6.2 Temperature dependent ionic conductivity studies

Figure 4.42 depicts the ionic conductivity of each GPEs system made at different temperature with respect to a fitting rule. The temperature dependence analysis on ionic conductivity of [C_6mim][I] containing polymer electrolyte was also based on Arrhenius relationship. Illustrating the previous said, at 20 wt. % of [C_6mim][I], approximately 4 fold hike in the magnitude of ionic conductivity to 8.48 mS cm^{-1} is observed from room temperature to 100 ^{o}C. Principally, this is a result of faster ion movement arising from faster vibration modes and a probable thermal expansion in polymer electrolyte creating more free volume for conduction mechanism at higher temperatures. The temperature dependence plot in Figure 4.42 fitted with thermal activated Arrhenius relationship has regression value close to unity (R^2 = ~1) for all samples. The linearity of these lines indicate that the GPE samples are obeying Arrhenius behaviour whereby temperature and

Universiti Malaya

conductivity data highlights the nature of the hexyl-imidazolium cation migration occupying vacant neighbouring sites.

As we know, linearity also signifies that no phase transition occurring and is probable for any amorphous electrolyte. A temperature hike with no abrupt increase in conductivity confirms the amorphous structure present. Increment in temperature allows polymer expansion which creates free volume resulting an acceleration in overall mobility. The improved polymer segmental mobility steers a pathway for intermolecular ion hopping enhancing ionic movement.

Concurrently, activation energy data obtained from the gradient of the graphs implies the ease of ion hopping from one coordination to another. Evidently, the GPE sample with the lowest activation energy undoubtedly has the highest ionic conductivity i.e Hm20. At an optimum concentration, bulky $[C_6mim]^+$ cations are expected to have high ionic dissociation and undergo effortless ion transport mechanism inside the P(MMA-co-MAA) matrix. The distinctive plasticizing effects of the imidazolium ionic liquid reduces the energy required for bond reformation as the cations migrate, thus, lower activation energy.

Universiti Malaya

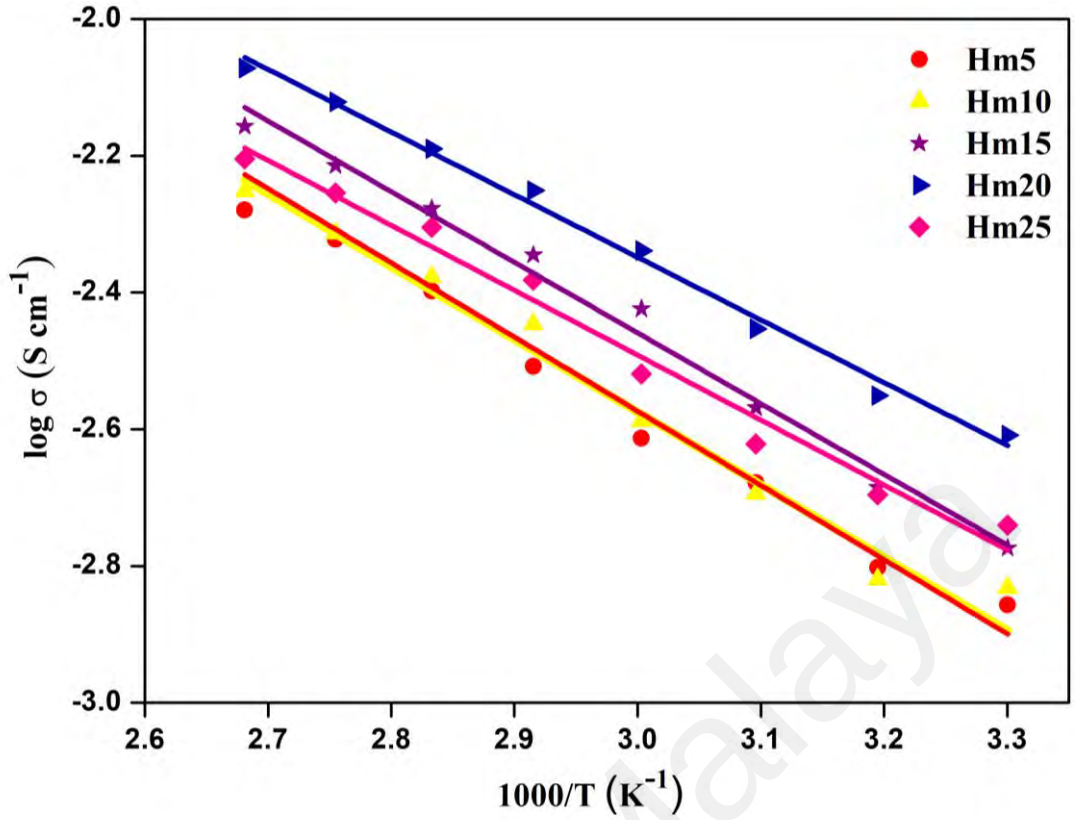

Figure 4.42: The variation of log σ plotted against the reciprocal absolute temperature for [C_6mim][I] containing GPEs.

4.6.3 FTIR

The interactions between the commercially available imidazolium ionic liquid and sodium iodide doped polymer electrolyte is also analysed in FITR studies. Figure 4.43 shows the FTIR spectrum of pure [C_6mim][I]. With reference to previous work done on imidazolium ionic liquids, the observed peak in the spectrum are as follows: 2926 cm^{-1} , 2856 cm^{-1} (C-H asymmetric and symmetric stretching of CH_3), 1568 cm^{-1} (C=N stretching), 1462 cm^{-1} (CH_3 and CH_2 asymmetric bending of alkyl substituent), 1378 cm^{-1} and 1340 cm^{-1} (C-H bending) and C-N stretching at 1162 cm^{-1} and 826 cm^{-1} (Lu, Chen, & Tao, 2016). Peak found in the 3300 to 3600 cm^{-1} range, is result of water molecules present.

Universiti Malaya

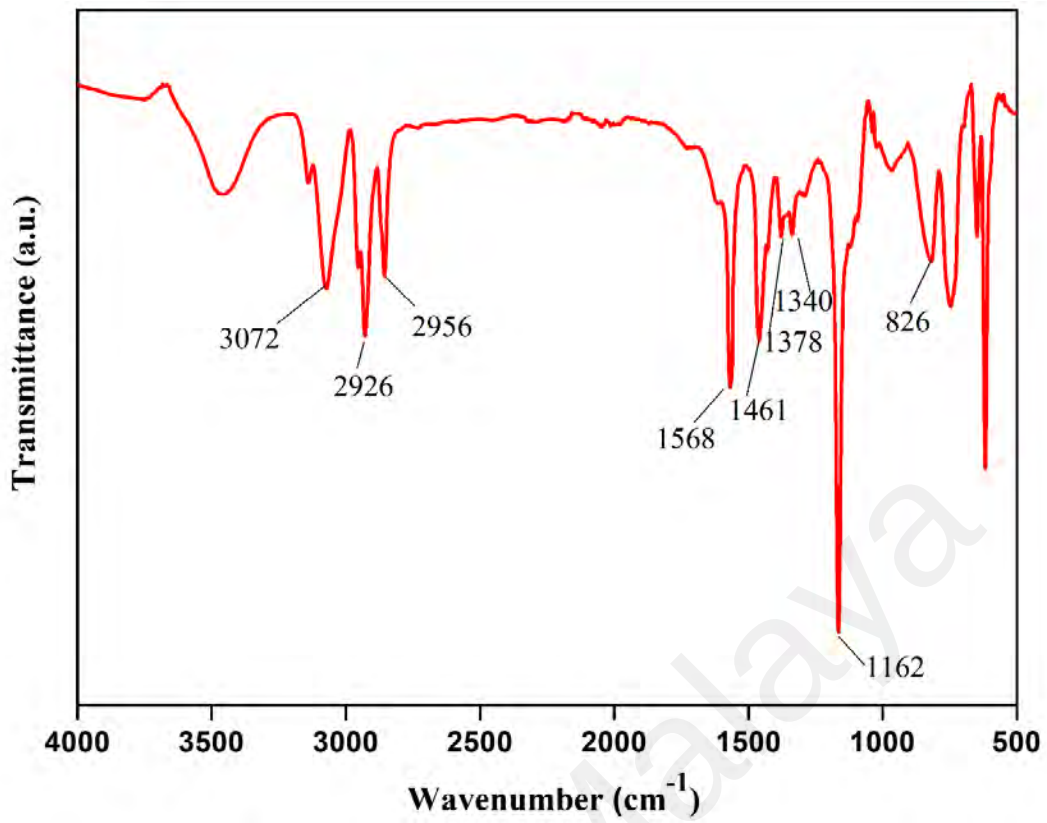

Figure 4.43: FTIR spectrum of pure [C_6mim][I] ionic liquid.

As for the FTIR spectra of the GPEs with varying [C_6mim][I] wt. % illustrated in Figure 4.44, the absence of [C_6mim][I] characteristic peaks stated above in all GPEs is suggestive of thorough dissolution of the ionic liquid. Apart from that, the presence of ionic liquid [C_6mim][I] resulted peak shifts from the original position which are seen around common vibration regions of C═O stretching and C─O stretching. This again is indicative of notable interaction occurring between the components of the GPE.

University Malaya

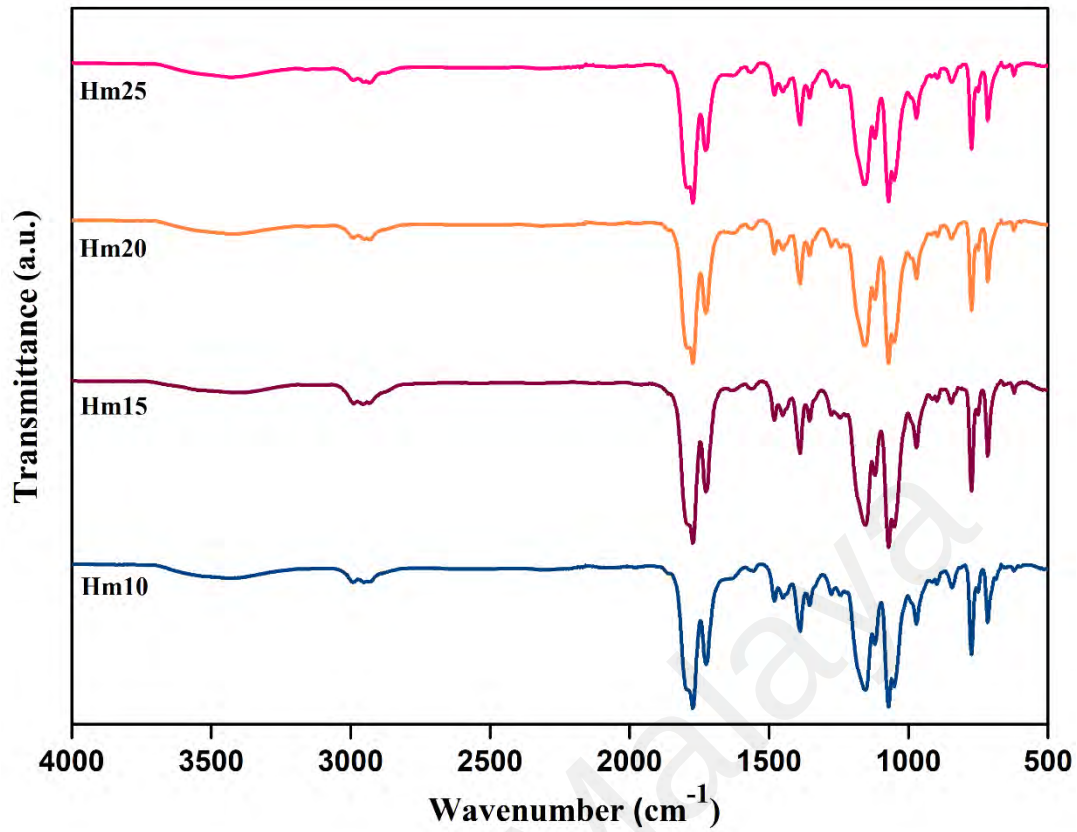

Figure 4.44: FTIR spectra of GPEs Hm10, Hm15, Hm20 and Hm25.

Shifting of carbonyl peaks to higher wavenumbers with respect to original carbonyl peaks found P(MMA-co-MAA) denotes the increasing basicity of the carbonyl groups in the presence of [C_6mim][I]. Interactions with [C_6mim]$^+$ ions are possible when C=O group acts as strong electron donor. The number of peaks noted upon deconvolution in the carbonyl region matched previous system with a matching peak position as shown in Figure 4.45. For instance, peak percentage area at 1726 cm^{-1}, previously at 1724 cm^{-1} in P(MMA-co-MAA) is shows a consistent decrease with decreasing wt. % of the copolymer. Then again a major peak area percentage is attributed for peaks at 1771 cm^{-1} and 1800 cm^{-1}, which clearly depicts the extent of cation interaction with the C=O group in plasticizers are more than that with polymer. This is an acceptable indication of good ion mobility along the polymer matrix as ions are more attracted to solvent functional group.

Universiti Malaya

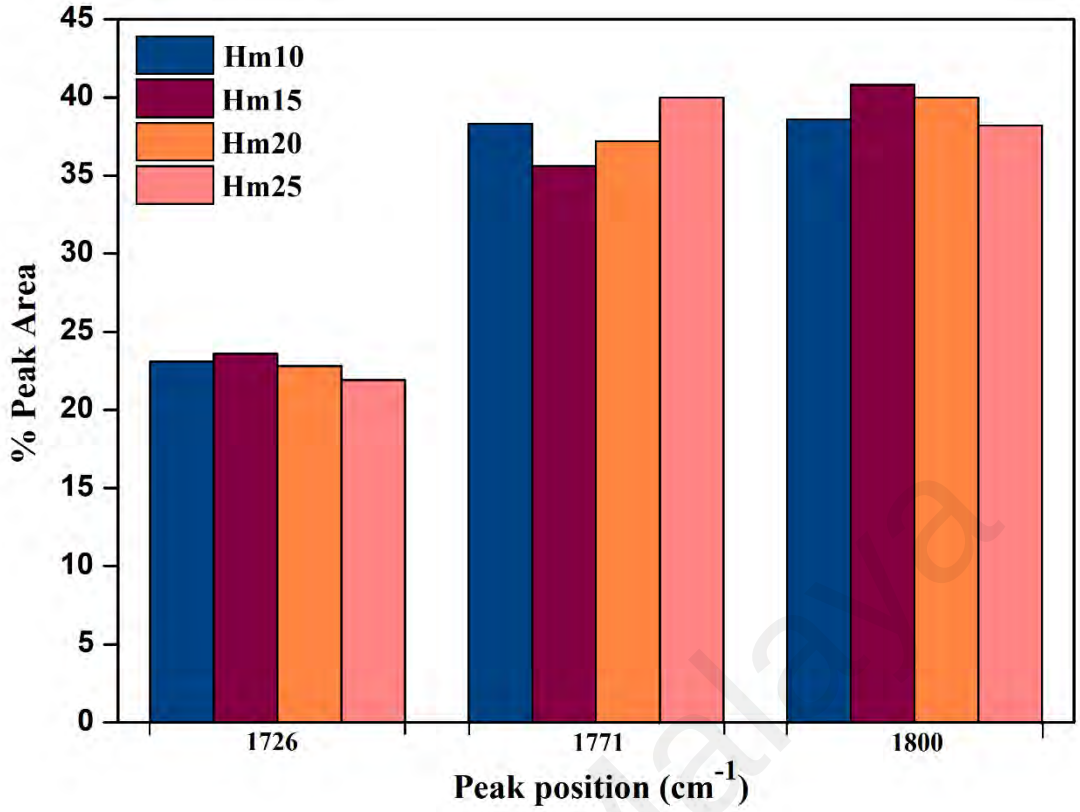

Figure 4.45: Relative FTIR band percentage area in the range of 1700 to 1850 cm^{-1} for Hm10, Hm15, Hm20 and Hm25.

Contrariwise, a more blue-shift is notice in peaks around 1000-1200 cm^{-1}. One distinguished shifting is seen here corresponds to C-O stretching frequency, originally found around 1145 cm^{-1} in the spectrum of pure copolymer and has shifted to lower frequency when incorporated into GPEs. This can be owed to the mesomeric effects on C-O stretching frequencies in esters which is more prevalent upon electrolyte formation (Siggel et al., 1988). Besides, the missing C-N stretching wavenumber, 1162 cm^{-1}, in GPE spectra can be deemed found at a lower wavenumber upon deconvolution. The peak can be noted at 1155 cm^{-1}. Though, this peak was also prevalent in sample PS40, it must be noted that for the GPEs containing [C_6mim][I] had higher intensity peaks , as shown in Figure 4.46, which implies a possible addition effect. Shifting to a lower wavenumber indicate some enhancement in the withdrawing characters of N atom in the imidazolium ring upon complexation in GPEs (Ramya et al., 2007).

Universiti Malaya

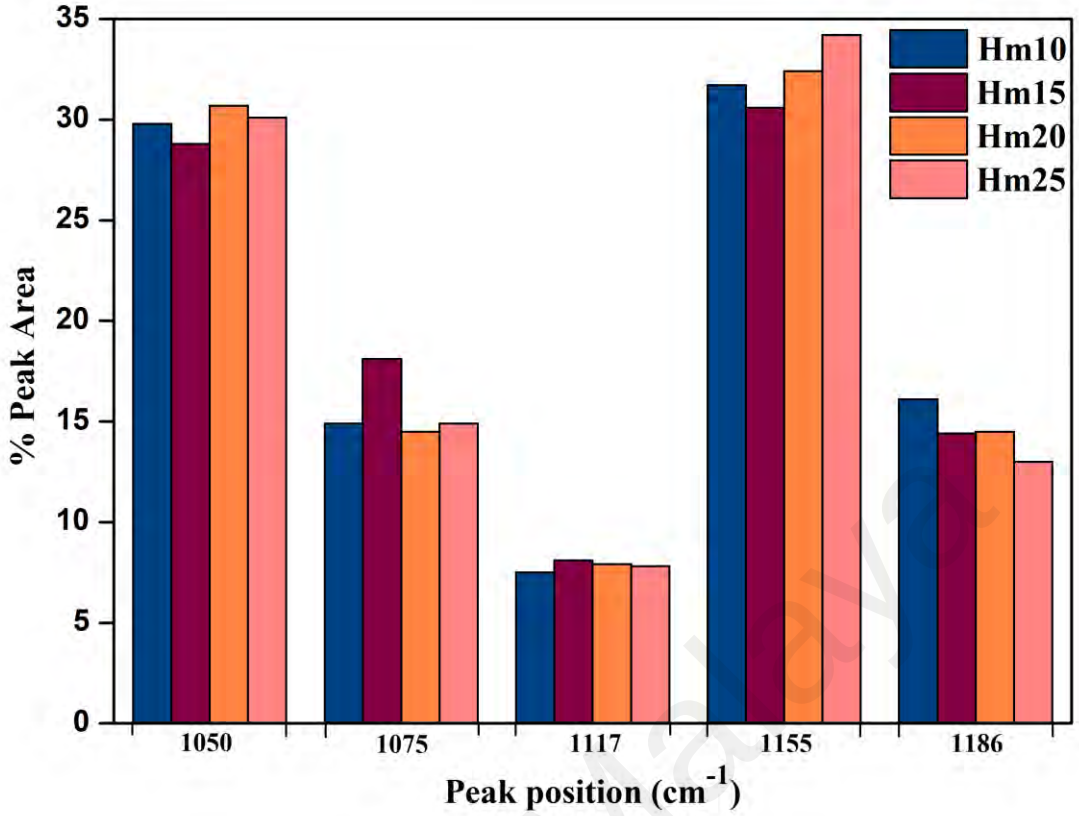

Figure 4.46: Relative FTIR band percentage area in the range of 1000 to 1200 cm^{-1} for Hm10, Hm15, Hm20 and Hm25.

With that, the increased percentage of iodide ions can be presumed to be more diffused rather than strongly bound in $[C_6mim]^+$ and I^- interaction. The unique fingerprint region from 1300 cm^{-1} to 500 cm^{-1} for all GPEs show similar pattern which also concludes no new interaction are present with varying ionic liquid content giving character to the P(MAA-co-MAA)-NaI-[C_6mim][I] complex.

4.6.4 XRD

Figure 4.47 reveals the XRD pattern for [C_6mim][I] whereas Figure 4.48 portrays diffractograms of GPEs Hm10, Hm15, Hm20 and Hm25. Pure [C_6mim][I] diffractogram shows three broad peaks at 2θ angle 9.55 °, 22.26° and 35.11°. As for the GPEs, the two characteristic peaks of ionic liquid at 9.55° and 35.11° have disappeared on the spectra. Nevertheless, the peaks observed in Figure 4.48 shows high possibility of merging between the ionic liquid and co-polymer characteristic peak at a corresponding position

along with peak shifting. Addition of [C_6mim][I] which is a liquid at room temperature have shown to improve the amorphous nature of the resulting GPEs. The obvious observation was the broader peaks with much lower intensity. On whole, the XRD patterns indicate near complete dissolution of ionic liquid and salt in making the electrolyte. However, minimal sharp peaks were also noted owing to the highly crystalline nature of NaI which seemingly did not undergo complete dissolution with increasing amount of [C_6mim][I]. Additionally, curve fitting and deconvolution methods are also applied to verify the peak formation. On whole, the inclusion of [C_6mim][I] have produced spectra with larger FWHM than the non- ionic liquid GPEs. As per earlier discussion, the Scherer formula was utilized to deduce degree of crystallinity for the electrolytes with one clear broad peak. Evidently, the considerable reduction in coherence length compared to non-ionic liquid samples denotes the more amorphous nature of the electrolytes which in turn aided in faster charger carrier movement. Table 4.17 tabulates FWHM and coherence length values. As for Hm15 and Hm20, the FWHM and coherence length values are not much far apart despite the values siding Hm15 to be more amorphous. Based on calculation, the most amorphous GPE did not translate to produce the highest ionic conductivity instead it was Hm20. Hm25 on the contrary with higher percentage of [C_6mim][I] and being more flowy physically suggestive of high amorphous nature has shown a more crystalline peak which corresponding to a drop in ionic conductivity. It can be concluded that ionic conductivity is influenced majorly by the quantity of free ions and lesser by the crystallinity of the Hm GPEs.

Universiti Malaya

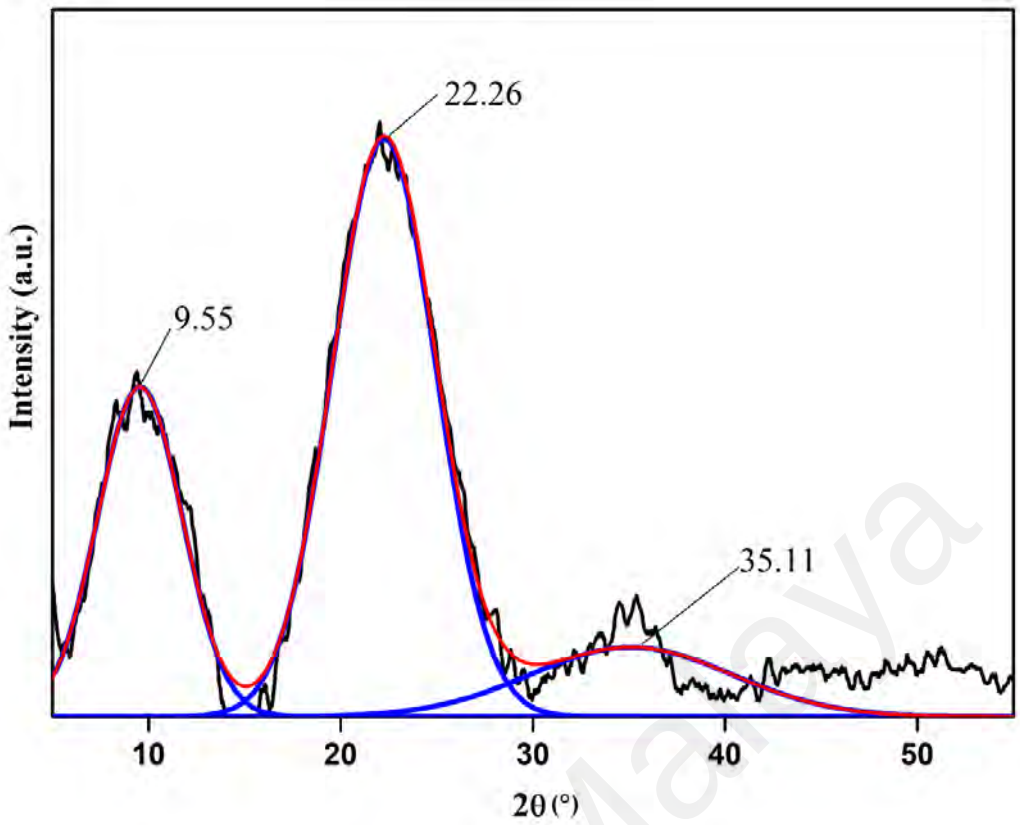

Figure 4.47 : Deconvoluted XRD diffractogram of pure [C_6mim][I].

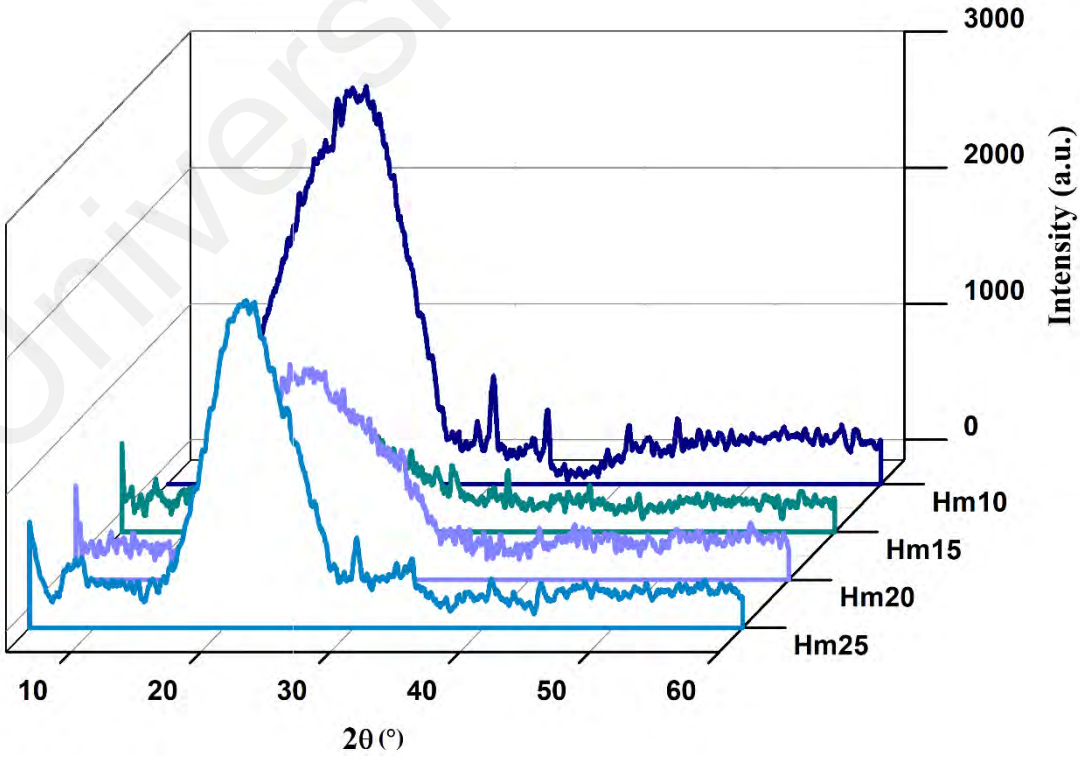

Figure 4.48: XRD diffractograms for GPEs Hm10- Hm25.

Universiti Malaya

Table 4.17: Significant parameters obtained from curve fitting the XRD diffractograms of GPEs in the Hm system.

Electrolytes	2θ (°)	FWHM (Å)	T (Å)
Hm10	18.88	9.61	0.146
Hm15	22.88	11.54	0.123
Hm20	19.54	10.86	0.130
Hm25	21.97	7.69	0.184

4.6.5 TGA

Thermal investigation on [C_6mim][I] containing GPEs reports the presence of sufficient thermal stability to be utilized in DSSCs. Literature revelation allows the confirmation of decomposition temperature of pure [C_6mim][I] in ranges less than 250 ºC as values for [C_6mim][BF_4], [C_6mim][PF_6], [C_6mim][NTf_2] coordinated with larger anions have shown decomposition temperatures from 260 - 300 ºC (Muhammad et al., 2008). Based on Figure 4.49, the initial decomposition temperature for the GPEs start about 105 ºC and a multistage decomposition is seen. Prior to that weight loss is associated with the evaporation of physically weak and chemically strong hydrogen bonding in H_2O.

Indeed, the decomposition begins at a temperature lesser than the non-ionic liquid GPEs, but by 400 ºC the mass loss can be accounted to be similar for both types of GPEs. All 4 GPEs show a much accentuated mass loss of 60 % which is a results of solvent and some ionic liquid decomposition and gradually continues as temperature increases up to 800 ºC. For these samples the second stage starts at 200 °C up till 400 ºC with an approximate weight loss percent of 27 %. This are due to the co-polymer and salt presence

Universiti Malaya

in the samples and the different interactions with ionic liquids. Table 4.18 details the thermally induced weight loss with the corresponding temperature range.

As to compare [C_4mquin][I] and [C_6mim][I] containing GPEs, the former shows slightly better thermal stability at similar mass loadings. This may be a result of the dispersion of the ionic liquids in the sample. Despite previous studies have noted the insignificance of cation contribution towards thermal stability but it is worth noting that the of longer alkyl chain length in the hexyl-ionic liquid that increases van der Waals forces but an overall intermolecular electrostatic interaction decreases. Thus, the thermal stability of the GPE also decreases from this contributing effect (Cao & Mu, 2014).

Comparatively, the more thermal sensitive [C_6mim][I] based GPEs are still relevant to be employed in DSSCs since the overall thermal stability is higher than 100 ^oC , however it seems unsuitable for under prolonged heat exposed circumstances.

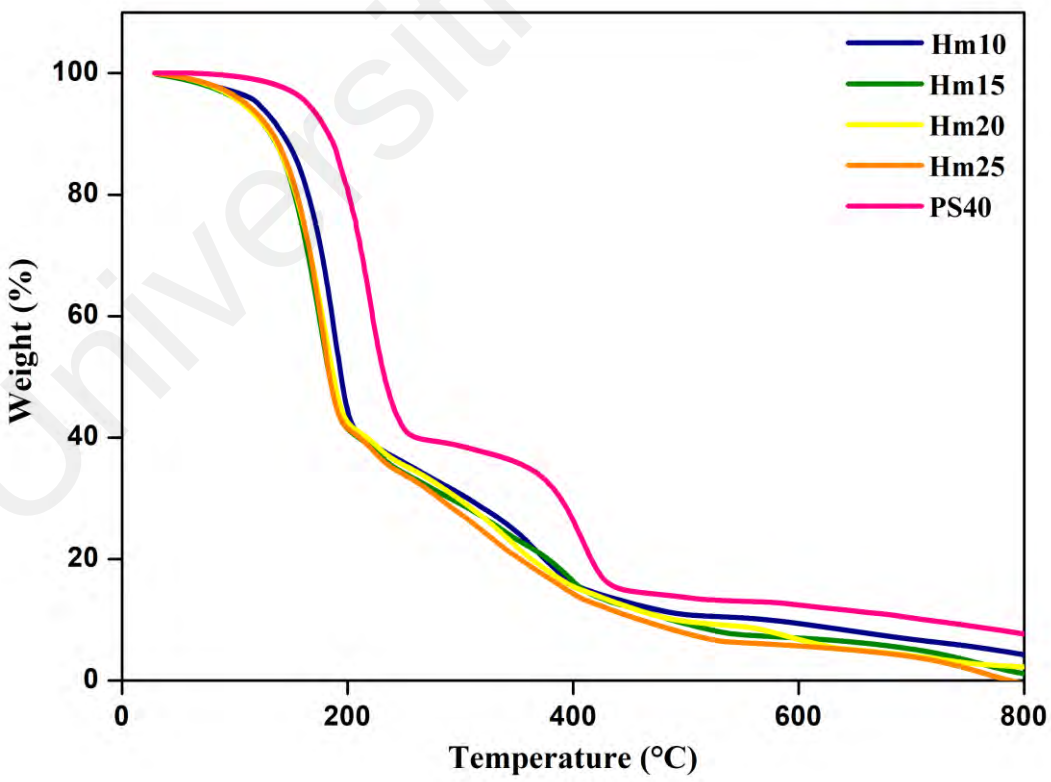

Figure 4.49: Comparative TGA analysis of PS40 with Hm10, Hm15, Hm20 and Hm25.

Universiti Malaya

Table 4.18: The thermal induced weight loss with corresponding temperature range for [C$_6$mim][I] containing GPEs.

Electrolytes	Hm10	Hm15	Hm20	Hm25
Initial weight loss temperature / ^{o}C	111.9	105.1	107.0	105.2
Weight loss (%)	55.0	53.7	52.5	54.2
Intermediate weight loss temperature range / ^{o}C	203.9-395.0	192.6-410.0	195.6-404.3	197.0-409.5
Weight loss (%)	25.1	28.0	28.0	28.3
Tailing weight loss temperature range / ^{o}C	~400- 600			
Weight loss (%)	7.2	6.9	8.1	8.4
Total weight loss (%)	87.3	88.6	88.6	90.9

4.6.6 Apparent diffusion study of I_3^-

Figure 4.50 depicts the LSV voltamgramms obtained for [C$_6$mim][I] GPEs – Hm10, Hm15, Hm20 and Hm25. Clearly, the steady-state current density obtained beyond 0.1V shows significant variation for consecutive increase in ionic liquid content. The spectra also notes a higher saturation voltage value compared to the quinolinium containing GPEs. On average, the value is about 0.12 V which points out the possibility of a tad better flux of reactant reaching the electrode or a slower growth of diffusion layer. The former reasoning is very much predictable as the $[C_6mim]^+$ cation is smaller comparative to $[C_4mquin]^+$ cation as is able to allow better flow of I_3^- before saturation. Table 4.19 list the J_{lim} and $D_{I_3^-}$ values for the corresponding GPEs. Hm20 recorded the highest limiting current value and this translated into the best triiodide diffusion coefficient

Universiti Malaya

calculated accordingly as previous systems. The $D_{I_3^-}$ values obtained in this work are comparable to that obtained in literature. The I_3^- diffusion coefficient of 7.9 x 10^{-8} cm^2s^{-1} for electrolyte composition containing only 3-hexyl-1-methylimidazoliumiodide and iodine has been reported by Kloo et al. (Kloo et al., 2006). It is apparent here that, the inclusion of polymer matrix had dampen the rate of I_3^- diffusion. Nevertheless, the amorphous nature of the GPE is able to maintain values in 10^{-8} order. The trend in $D_{I_3^-}$ values obtained emulates the trend in ionic conductivity attained for this system with Hm20 achieving the highest ionic conductivity.

Comparison between system containing ionic liquids of same anion but different cation, i.e. - [C_4mquin][I] and [C_6mim][I], revealed the role of stronger electrostatic interaction in determining the amorphous nature of the GPE. As such, the more amorphous [C_6mim][I] electrolytes showed better triiodide diffusion rate. At similar mass loading of ionic liquid both systems show comparable ionic conductivity despite saturation incurring at different percentage mass.

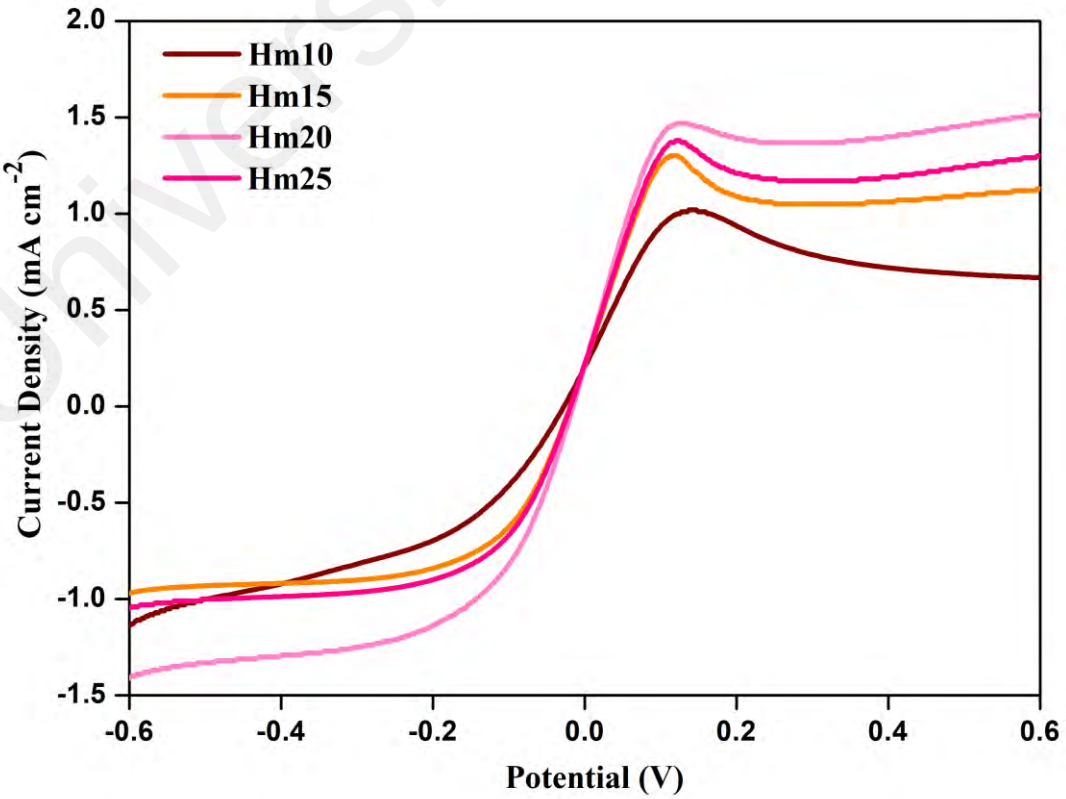

Figure 4.50: LSV voltammograms for Hm10, Hm15, Hm20 and Hm25.

Universiti Malaya

Table 4.19: J_{lim} and $D_{I_3^-}$ values obtained Hm10- Hm25 via steady state current measurements for corresponding GPEs.

Electrolyte	J_{lim} (mA cm^{-2})	$D_{I_3^-}$ (x 10^{-8} cm^{2}s^{-1})
Hm10	0.71	1.34
Hm15	1.04	2.16
Hm20	1.34	3.06
Hm25	1.16	2.94

4.7 Summary of systems

P(MMA-co-MAA) based polymer electrolytes with optimum conductivity in 10^{-3} S cm^{-1} range were successfully prepared for the fabrication of dye sensitized solar cells. In fact, we managed to achieve ionic conductivity as high as 2.64 x 10^{-3} S cm^{-1} at ambient temperature with the inclusion of 25 wt. % [C_4mquin][I] which faired superior than the maximum achieve by [C_4mquin][NTf_2] and of [C_6mim][I] containing samples. The ionic conductivity of all GPEs prepared increase with temperature and further portrays a compensated Arrhenius behaviour with some free volume contribution for the ion transportation process. Inclusion of the different ionic liquid not only improves ionic conductivity but also reduces the crystallinity of the polymer matrix by 20- 50% as proven in XRD studies. Moreover, the "*Qt"* and "*Qi"* GPEs also remained thermally stable up to 150 °C better than the "*Hm"* samples. The complexation between P(MMA-co-MAA), EC/PC, NaI and ionic liquids is established and proven in FTIR study. Cation interaction elucidated predominantly in the C=O, carbonyl, (1700-1850 cm^{-1}) region of polymer and plasticizers validates ion solvation in the polymer matrix for all GPEs. The apparent triiodide diffusion study revealed correlation of triiodide movement with the trend in ionic conductivity achieved. The GPEs containing ionic liquids with iodide anion- "*Qi"*and

Universiti Malaya

"*Hm*" samples, recorded higher values compared to [C_4mquin][NTf_2] included electrolytes which was apparent to the surplus of iodides present.

P(MMA-co-MAA) with *N*-butyl-6-methylquinolinium bis(trifluoromethanesulfonyl) imide and *N*-butyl-6-methylquinolinium iodide electrolytes portrays as promising materials to be used in DSSCs as it can achieve high ionic conductivity, triiodide diffusion rate, thermal stability and substantially gel-like to allow better contact between electrode as well as enhance safety.

Universiti Malaya

CHAPTER 5- RESULTS AND DISCUSSION 2: CHARACTERIZATION OF DYE SENSITIZED SOLAR CELLS (DSSCs)

Preparation and characterization of plasticized PMMA-co-MAA based polymer electrolytes which are ionic liquid free and with synthesized ionic liquids, [C_4mquin][NTf_2] and [C_4mquin][I], as well as commercially available [C_6mim][I] are discussed thoroughly in previous chapters. The highest conducting compositions for (PMMA-co-MAA)-NaI/I_2-(EC/PC), (PMMA-co-MAA)-NaI/I_2-[C_4mquin][NTf_2]-(EC/PC), (PMMA-co-MAA)-NaI/I_2-[C_4mquin][I]-(EC/PC) and (PMMA-co-MAA)-NaI/I_2-[C_6mim][I]-(EC/PC) systems have been determined as described in Chapter 4.

The redox active polymer electrolytes have been used to fabricate dye-sensitized solar cells with a standard dye sensitizer and their comparative performance is presented in this chapter. Comprehensively researched components like FTO, TiO_2, N719 dye and Pt coat were used in fabrication to solely understand the performance of the new electrolyte mixtures. This nascent investigation on quinolinium ionic liquids requires more supportive information to highlight their essential role in DSSCs, thus the testing with commonly used commercial ionic liquids in polymer electrolytes was necessary. Comparative photovoltaic performances of the gel polymer electrolytes are also disclosed.

5.1 Photocurrent-voltage (*J*-V) characteristics

The photocurrent density- voltage graphs for the DSSCs fabricated with optimized ionic liquid free electrolytes is shown in Figure 5.1. Table 5.1 shows the performance contributing parameters namely, the short-circuit current density (J_{sc}), open-circuit voltage (V_{oc}), fill factor (*FF*) and photovoltaic conversion efficiency (η) values for polymer electrolytes with different weight ratio of NaI. The minimal fluctuation of V_{oc} values with varying salt concentration as depicted in the figure can be attributed to the

Universiti Malaya

constant illumination of 100 mW cm^{-2} from the solar stimulator (Elumalai & Uddin, 2016). Meanwhile, what seems like a gradual increase for *FF* values denotes better contact between the TiO_2 layer and Pt electrode. Increase in *FF* values are also indicative of resistance reduction for the electron transport in the conducting films. As for J_{sc} and PCE values, a clear connection can be made with the relative ionic conductivity recorded for the samples which reached the maximum of 8.11 mA cm^{-1} and 2.34 % for PS40. This implies the presence of more ions jumping into the conduction band improves the rate of charge injection.

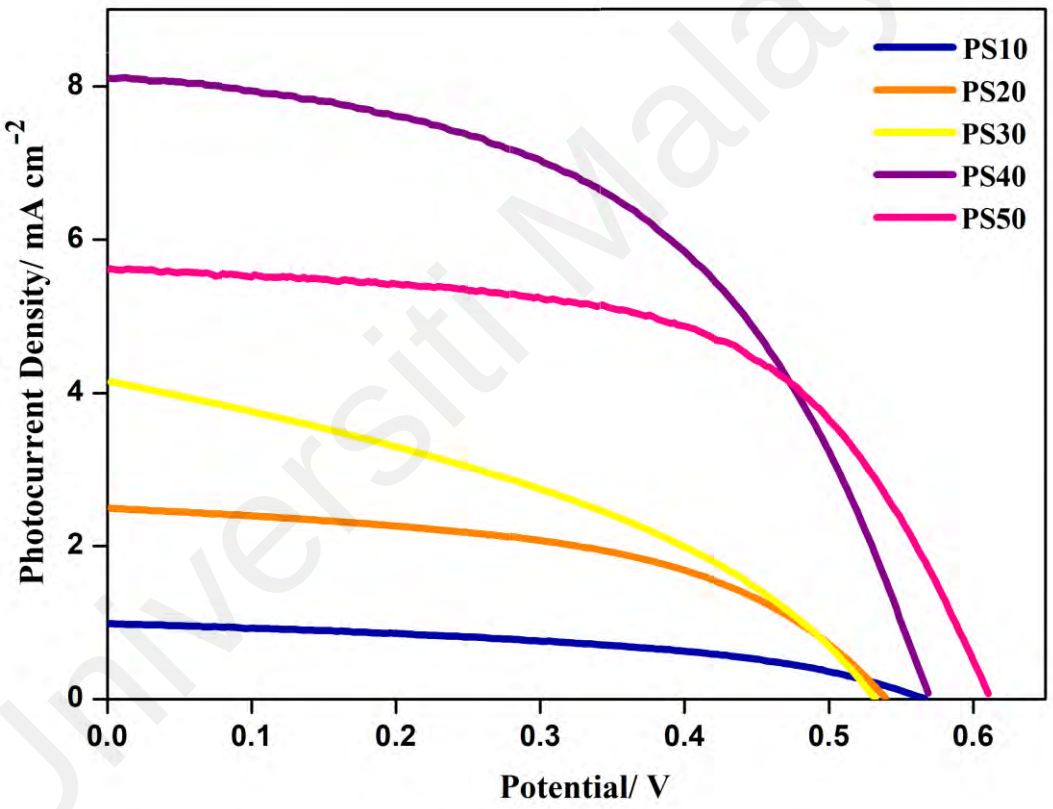

Figure 5.1 J-V characteristics of GPEs PS10 - PS50.

Universiti Malaya

Table 5.1: Photovoltaic parameters of GPEs containing different wt. % of NaI.

Electrolytes	J_{sc} (mA cm^{-2})	V_{oc} (V)	*FF* (%)	η (%)
PS10	1.02 ± 0.03	0.570 ± 0.003	48.5 ± 3.5	0.28 ± 0.03
PS20	2.70 ± 0.08	0.547 ± 0.090	45.6 ± 6.3	0.67 ± 0.01
PS30	4.15 ± 0.72	0.532 ± 0.025	38.1 ± 7.2	0.84 ± 0.02
PS40	8.11 ± 0.16	0.569 ± 0.008	50.7 ± 1.5	2.34 ± 0.06
PS50	5.58 ± 0.04	0.588 ± 0.022	59.9 ± 1.5	2.00 ± 0.01

Using PS40 data as baseline, the photovoltaic performances of polymer electrolytes containing different ionic liquids was evaluated. Optimization of samples containing ionic liquids yielded a maximum conversion efficiency of 5.67% for 25 wt. % of [C_4mquin][NTf_2] added. The *J*-V curves for DSSCs containing (PMMA-co-MAA)-NaI/I_2-[C_4mquin][NTf_2]-(EC/PC) samples are shown in Figure 5.2 and the corresponding V_{oc}, J_{sc}, *FF* and η of these DSSCs are tabulated in Table 5.2.

University Malaya

Table 5.2: Photovoltaic parameters of GPEs containing different wt. % of [C_4mquin][NTf_2].

Electrolytes	J_{sc} (mA cm^{-2})	V_{oc} (V)	*FF* (%)	η (%)
Qt5	7.97 ± 0.11	0.625 ± 0.005	58.8 ± 1.2	2.93 ± 0.06
Qt10	9.44± 0.45	0.613 ± 0.002	59.0 ± 1.1	3.41 ± 0.11
Qt15	10.50 ± 0.20	0.607 ± 0.021	58.6 ± 5.0	3.74 ± 0.27
Qt20	12.83 ± 0.26	0.612 ± 0.006	58.4 ± 2.4	4.59 ± 0.24
Qt25	15.37 ± 0.21	0.624 ± 0.011	59.1 ± 2.0	5.67 ± 0.02
Qt30	10.10 ± 0.27	0.608 ± 0.002	60.4 ± 1.4	3.71 ± 0.03

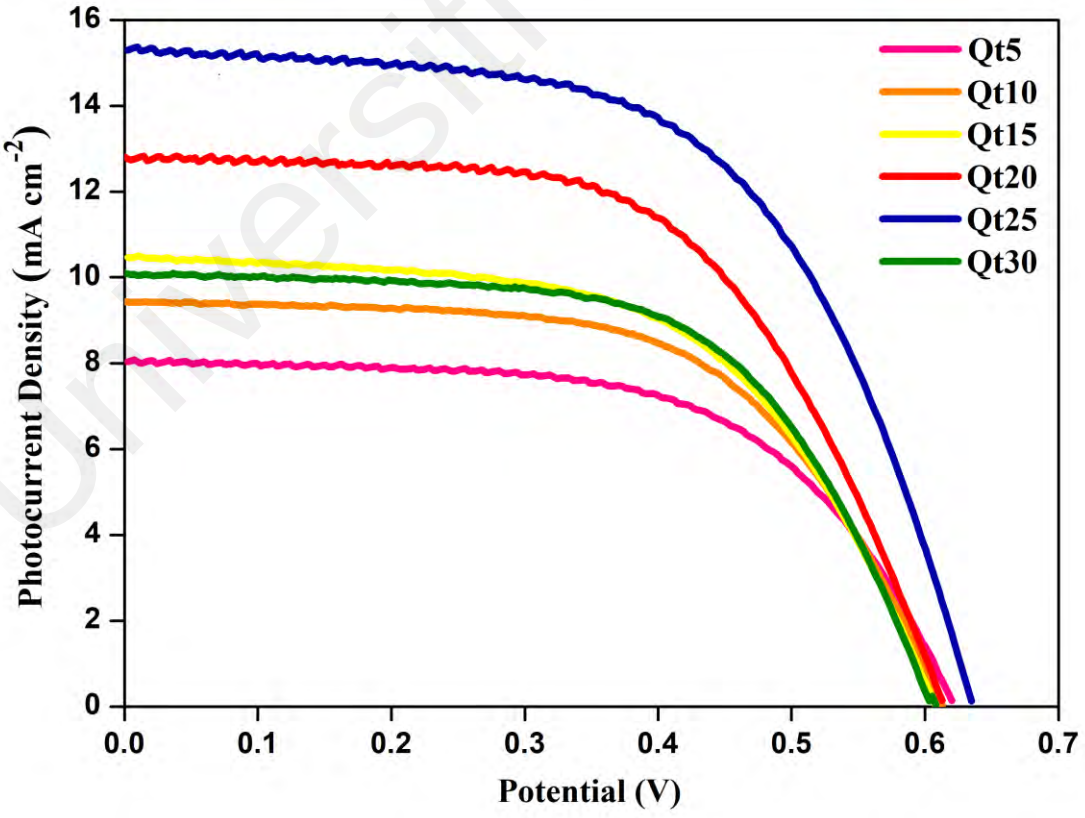

Figure 5.2: *J*-V characteristics of GPEs Qt5- Qt30.

University Malaya

The system with the maximum photovoltaic conversion efficiency was a cumulative result of maximum J_{sc}, V_{oc} and *FF* values of 15.37 mA cm^{-2}, 0.624 V and 59.1 %, respectively. Although the study on substituted quinolinium cation is limited, but the research on $[NTf_2]^-$ anion in lab-made ionic liquids is much more extensive. Armel et al. conducted a series of test with a number of imidazolium, quaternary ammonium and phosphonium cations containing NTf_2 anion and thus far have produced 4.2 % efficiencies with $[C_2mim][NTf_2]$ using porphyrin dyes (Armel et al., 2010). A more comparative data would be by C.P Lee et al. testing a range of different sulfonium and ammonium cation with TFSI, assembled with photoanode containing N719 dye and have produced about 4.6 % efficiency with $[S_{224}][NTf_2]$ (Lee et al., 2013). Earlier, Kawano et al. in 2003 utilized $[EMIm][NTf_2]$ and only yielded 2.4 % conversion efficiency (Kawano et al., 2004). It was believed that the weak interaction force between alkyl chain and quinolinium cation, and the flexibility of the substituted quinolinium enables electron to be transferred easily in the electrolyte similar to poly $[BVIm][HIm][NTf_2]^-$ based gel electrolyte as discussed by the Chen group (Chen et al., 2012). Thus, with the usage of $[C_4mquin][NTf_2]$, sample Qt25 could reach 5.67% which is a better efficiency compared to the discussed results (Sundararajan et al., 2017).

In accordance to *Equation 2.2*, it can be seen from Table 5.2 that the J_{sc} is the predominant contributing factor in determining the overall solar cell efficiency. Essentially, the J_{sc} numbers directly relate to the relative amount of ion conductivity in the P(MMA-co-MAA) based gel electrolyte. As the total ionic conductivity continues to increase from Qt5- Qt25, a parallel increase in J_{sc} is seen. Similarly, a drop in ionic conductivity for Qt30 resulted in a drop in J_{sc}. The drop beyond maximum can be also a result of competing effect between two cations having small and large charge density in this system, i.e. Na^+ and $[C_4mquin]^+$. With more wt. % of $[C_4mquin]^+$ present in Qt30 as compared to the wt. % of salt, the drop in J_{sc} is foreseeable. Despite NaI being the sole

Universiti Malaya

contributor of iodide ions in the system, the presence of other ions, particularly, the cation is deemed to have a profound effect on both the J_{sc} and V_{oc}. The samples containing quinolinium derivatives show higher open-circuit voltage. Even with a mere 8 % increment in V_{oc}, it is still crucial to indicate an increase in band gap between quasi-Fermi levels of electrons in the semiconductor and the redox electrolyte (Dissanayake et al., 2014; Aram et al., 2015).

This is a commonly seen trend upon introducing huge spectator ions into the system. The V_{oc} values recorded for the systems containing the quinolinum derivative do not differ much and there is not a specific inclination in the values, as shown in Table 5.2. This is sufficient to conclude that any further addition of ionic liquid only results in minimal alteration in the relative position of the flat band potential and the redox potential of the gel polymer electrolyte. Contrastingly, initial addition of quinolinium ionic liquid depreciated the short circuit photocurrent density value indicating a falloff in ionic conductivity. Previous literatures have noted that the cationic size can profoundly affect electron dynamics at the electrolyte/semiconductor boundary due to adsorption on the TiO_2 coated photoelectrode causing a negative shift in conduction band edge potential and decreasing the driving force of charge injection (Liu et al., 1998). Henceforth, the slight drop in J_{sc} is very much predictable. However, with further increase in $[C_4mquin][NTf_2]$ concentration, the system becomes less viscous and thus, a substantial increase in ionic conductivity is seen due to escalation in ion movement which dominates over band energy shift by cation adsorption, in other words, the rate determining mechanism is now the iodide ion transferences (Simon et al., 2016).

To further investigate the improved role of second generation non-halide ionic liquids in the performance of DSSCs, the (PMMA-co-MAA)-NaI/I_2-$[C_4mquin][I]$-(EC/PC) polymer electrolytes were tested under the same paramaters. The *J*-V curves for the best performing DSSC for each polymer electrolyte sample is shown in Figure 5.3 with

Universiti Malaya

detailed data tabulated in Table 5.3. As anticipated, large quinolinium cations have consistently improved the V_{oc} values and surprisingly slightly better than the non-iodide ionic liquid system. This can be related as a function of band gap whereby increasing band gap with an upshift in the conduction band edge can increase V_{oc} values.

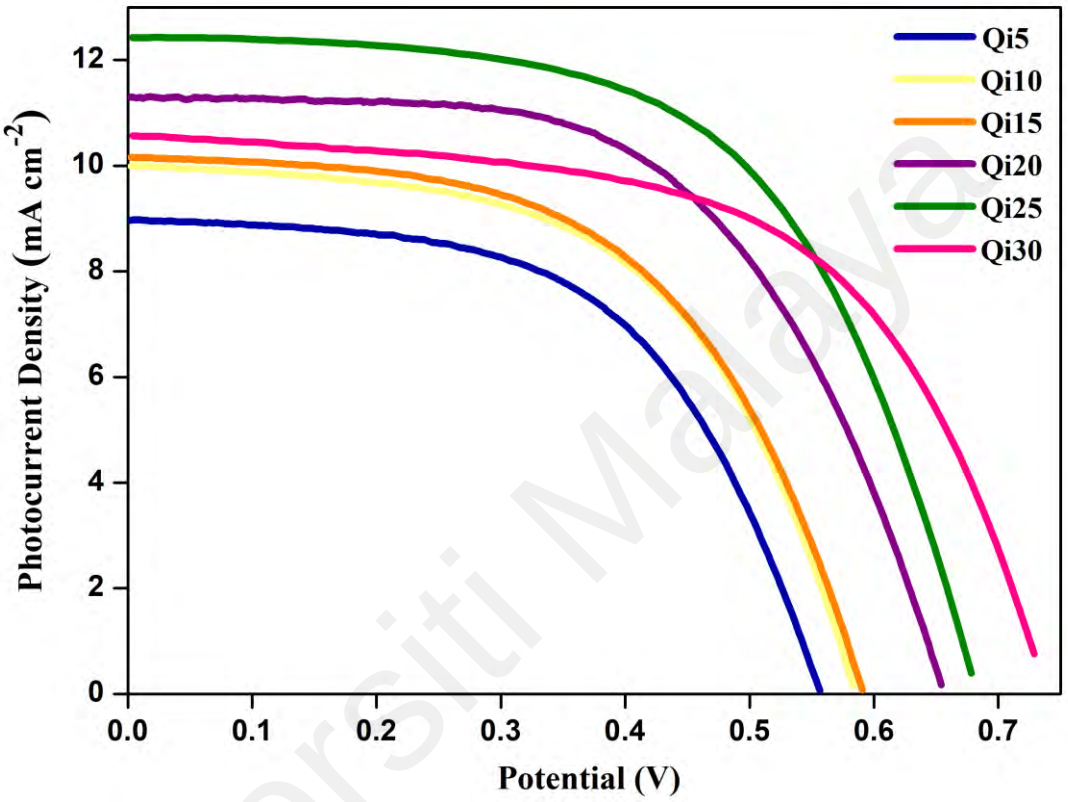

Figure 5.3: *J*-V characteristics of GPEs Qi5- Qi30.

Universiti Malaya

Table 5.3: Photovoltaic parameters of GPEs containing different wt. % of [C4mquin][I].

Electrolytes	J_{sc} (mA cm^{-2})	V_{oc} (V)	*FF* (%)	η (%)
Qi5	8.98 ± 0.84	0.556 ± 0.014	56.1 ± 6.0	2.80 ± 0.69
Qi10	10.00 ± 0.16	0.583 ± 0.022	56.2 ± 3.4	3.27 ± 0.02
Qi15	10.15 ± 0.57	0.591 ± 0.008	55.2 ± 1.4	3.31 ± 0.09
Qi20	11.30 ± 0.81	0.654 ± 0.009	57.8 ± 0.8	4.28 ± 0.09
Qi25	12.43 ± 0.52	0.678 ± 0.013	58.9 ± 0.7	4.98 ±0.03
Qi30	9.7 ± 0.80	0.718 ± 0.010	61.9 ± 2.6	4.32 ± 0.25

A higher V_{oc} recorded was for Qi25 sample, presumably because of the optimum introduction of additional steric bulk close to the semiconductor surface hindering electron transfer events much better than the [C4mquin][NTf2] ionic liquid at the same weight percentage. Ostensibly, the lack of hydrogen bonding between the ions in [C4mquin][I] would have allowed such occurrence and slow down recombination process between conduction band electrons and triiodide ions which led to an increase in V_{oc} values. After the addition of 25 wt. % of [C4mquin][I], an opposite trend in notice as the J_{sc} values decrease with a slight surge in V_{oc}. This affirms that the increasing ionic liquid quantity has increased conduction bandgap which makes it increasing difficult for electron injection process (Ogunsolu et al., 2017).

Albeit the same wt. % of ionic liquid used, [C4mquin][NTf2] have shown better J_{sc} value and conversion efficiencies despite [C4mquin][I] having a slim upper hand on ionic conductivity. On the basis of the results obtained, it is suggestive of the interfacial charge transfer reactions occurring at electrodes play a crucial role in determining the

Universiti Malaya

photovoltaic performances in the DSSC. Therefore, the role of anions present and their steric effects correlate with the different interfacial charge transfer behaviour and polymer electrolyte performance in DSSCs. As a consequence of larger molar weight of [C_4mquin][NTf_2] than that of [C_4mquin][I], the molar concentration of [C_4mquin][I] in "Qi" electrolyte is higher than of [C_4mquin][NTf_2] in "*Qt*" electrolyte at the same weight percentage. Moreover, the ionic radius of NTf_2 (325pm) is larger than of I^- (206 pm) (Lin, 2001). This leads to more cation adsorption at the surface of the electrode in "*Qt*" samples. Typically, the TiO_2 surface is relatively protonated and small Na^+ ion present plays a key role in determining the energetics of the TiO_2/electrolyte interface. Due to different ion affinities, the ability of iodide anion and [NTf_2] ion to attract Na^+ is also different, thus variation in conduction band shifts are observed. Since Na^+ ions have stronger attraction for iodide ions than the [NTf_2] ions, lesser surface intercalation from the Na^+ thus the higher V_{oc} values recorded for [C_4mquin][I] containing samples (Wang et al., 2013).

The origin of J_{sc} relates to how fast charge transport occurs in the electrolyte. This parameter is highly dependent on external contributions like light and temperature. In accordance to this, all experiments were conducted at 1 sun irradiation, hence, the resulting J_{sc} values are mainly contributed by the nature of the polymer electrolyte. As discussed earlier, the charge transport in the polymer electrolyte is based on a physical diffusion -the Grotthuss-type exchange. Since the polymer network is responsible for the diffusion process, the stronger repulsion between the anions and redox couple would facilitate better charge transport. As such, the polymer electrolyte samples containing the $[NTf_2]^-$ anion would experience bigger repulsion and allow better charge transfer, hence the higher J_{sc} values recorded. Higher J_{sc} value largely contributes towards higher power conversion efficiency.

Universiti Malaya

Alternatively, the key feature of the $[NTf_2]^-$ anion is the extensive charge delocalization making the ion very weakly coordinating. The bulky and asymmetrical configuration of the ions reduces their electrostatic interaction and prevents the ions from neatly packing together in the electrolyte. Thus, this creates space for facile ion transport which positively impacts the J_{sc}. As for the iodide functionalized ionic liquid, it provides a better opportunity for charge transfer through Grotthus mechanism as $I^- + I_3^- \leftrightarrow I_3^- + I^-$. It is important to note that in the absence of other anions in the electrolyte mixture, effective mass transport is favourable which suppresses mainly the back electron transfer.

Although there seems to be a discernible trend between the conductivity produced by the GPEs and the photocurrent produced, this is only partially true. The inter-system variations observed are contributed by the anions present. *FF* is another essential parameter that stems information on overall cell resistance and fluctuations in these readings are very common. On the whole the *FF* values recorded for both quinolinium containing electrolytes are largely within a range of 50- 60 %. Low diffusion resistance yield good *FF* values, nevertheless, the inter-electrode space, how well the electrolyte adheres with the electrode and evenness in the electrode films also greatly affect the values. The exact reason to *FF* variation is still uncertain at this point and the connection between the electrolytes is indiscernible.

The photocurrent density- voltage (*J*-V) curve for the working DSSC containing GPEs with different $[C_6mim][I]$ mass ratio is shown in Figure 5.4. Table 5.4 tabulates the four necessary parameter values for the respective polymer electrolytes. Prospectively, an increase in overall solar cell efficiency was seen upon addition of $[C_6mim][I]$. As speculated, ionic conductivity of $[C_6mim][I]$ containing GPE has a direct relationship with J_{sc} and also with the overall power efficiency of DSSCs. Comparing systems with and without ionic liquid, we see an increase in ionic conductivity about 55 %, reaching a peak of 5.30 % conversion efficiency, η (%), at 20 wt. % of $[C_6mim][I]$. The J_{sc}, V_{oc} and

University Malaya

FF values for this system was 14.70 mA cm^{-2}, 0.60 V and 60 %, respectively. Ionic liquids containing imidazolium cations are among the extensively studied cations as employed in DSSCs. Augmentation of these cations have been done with various anions namely, triflate, thiocyanate, bis(trifluoromethanesulfonyl) amide and most commonly iodide. Su'ait et al. reviewed that on average, systems incorporated with 1-alkyl-3-methylimidazolium iodides (alkyl chain: C_3–C_6) are capable of producing solar conversion efficiency about 5 % and some even higher depending on the constituent combinations and technique in making the polymer electrolytes (Su'ait et al., 2015).

$[C_6mim]^+$ cations have long alkyl chains with relatively higher Van Der Waals forces that would induce aggregation among cations and multi-layer adsorption of these aggregates at the semiconductor interface increases J_{sc} due to increase in diffusion coefficient. Kubo *et.al* highlighted that the dark current in DSSCs decreases with increasing alkyl chain length and is optimised about C_6 (Kubo et al., 2002). Upon analysis, a direct link between J_{sc} and overall solar cell efficiency is seen indicating the dominant contributor for solar cell efficiency is the short circuit current value. Equally, as the total ionic conductivity increases an upward trend in J_{sc} is also observed until Hm20. Likewise, a drop in ionic conductivity for Hm25 resulted in a decrease in J_{sc} and power conversion efficiency as well.

Based on previous studies, J_{sc} was initially predicted to fall short at 5 wt. % of $[C_6mim][I]$ due to a probable negative shift in conduction band edge potential which decreases the charge injection force. However, as the concentration of $[C_6mim][I]$ increased, viscosity of the GPE system decreased which resulted in considerable hike in ionic conductivity, indicating the fast ion movement is more significant over the negative shift in band energy by cation adsorption (Simon et al., 2016). Correspondingly, the increase in J_{sc} is also capable of elevating the quasi-Fermi level of the TiO_2, thus causing an increase in V_{oc} values as seen. However, the slight drop in initial V_{oc} values at Hm5

Universiti Malaya

and Hm10 compared to PS40 was initially rather unexpected but Park et al. had reported similar observation in a comparative study using LiI and 1,2-dimethyl-3-hexyl imidazolium iodide (Park et al., 2000). It can be considered that the first change in redox potential due to the increased iodide concentration is the cause for the slight decrease in V_{oc}. Another comparable explanation would be relating it to band edge movement. The competing effect between two different sized cations, whereby the smaller cation effect is dominating, causes band edge to shift towards a more positive potential due to the adsorption of Na^+ at the semiconductor surface. As a result, potential drop in the Helmholtz layer is foreseen, thus, V_{oc} is likely to decrease (Kang et al., 2004). Beyond Hm10, V_{oc} continues to increase and this upward trend is commonly observed when large cations area introduced into the system. Since the V_{oc} values do not escalate much between successive additions of ionic liquid, it would be valid to postulate that alteration in the position of flat band potential relative to the redox potential in the polymer electrolyte is minimal.

Table 5.4 also highlights the notable hike in *FF* values with the addition of $[C_6mim][I]$ suggestive of reduction in cell resistance. *FF* values remaining almost constant for samples containing ionic liquid surmises the influence of charge injection rate and recombination at contact surface along with the notion of how well the GPEs are adhering between the both electrodes. On a comparative basis, the results obtained shows, $[C_6mim][I]$ containing polymer electrolytes outperformed $[C_4mquin][I]$ polymer electrolytes in terms of maximum power conversion efficiencies achieved. This was solely due to the higher J_{sc} values obtained. The influence of cation size on V_{oc} values is again clearer here as larger cations boost V_{oc} values as explained before.

As a consequence of larger molar weight of $[C_4mquin][I]$ than that of $[C_6mim][I]$, the molar concentration of $[C_6mim][I]$ in "*Hm"* type electrolyte is higher than of $[C_4mquin][I]$ in "*Qi"* type electrolyte at the same weight percentage. Thus, saturation is

Universiti Malaya

ought to happen earlier leading to a probably peaking in DSSC values at lower wt. % of [C_6mim][I] also corresponding to the peak ionic conductivity value. Regardless of the same single anion present in both "*Hm"* and "*Qi"* electrolyte system, it is difficult to conclude more on which system has the better mass transport owing to maximum power conversion efficiency achieved at different wt. % of ionic liquid added.

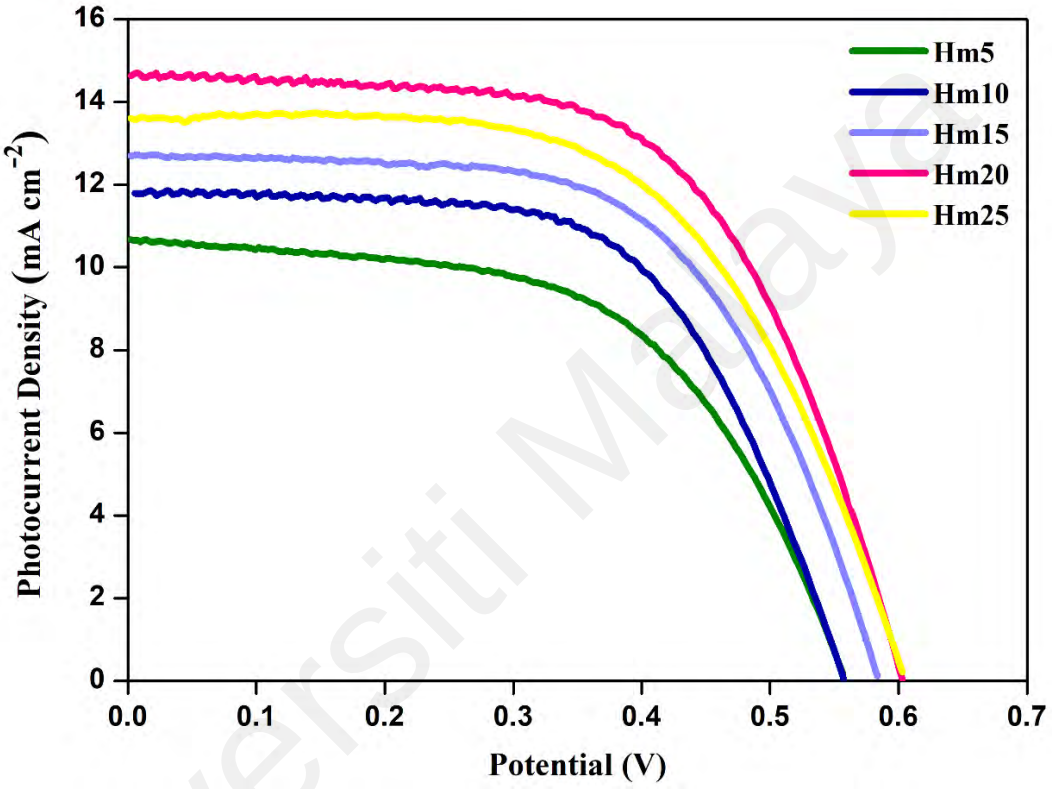

Figure 5.4: *J*-V characteristics of GPEs Hm5- Hm25.

Universiti Malaya

Table 5.4: Photovoltaic parameters of GPEs containing different wt. % of [C_6mim][I].

Electrolytes	J_{sc} (mA cm^{-2})	V_{oc} (V)	*FF* (%)	η (%)
Hm5	10.67 ± 0.05	0.557 ± 0.003	56.6 ± 3.4	3.36 ± 0.23
Hm10	11.86 ± 0.79	0.564 ± 0.032	58.6 ± 1.3	3.93 ± 0.04
Hm15	12.72 ± 0.22	0.578 ± 0.014	60.8 ± 4.6	4.48 ± 0.23
Hm20	14.70 ± 0.24	0.603 ± 0.007	59.8 ± 2.4	5.30 ± 0.12
Hm25	13.72 ± 0.46	0.595 ± 0.030	58.0 ± 4.3	4.83 ± 0.20

On a concluding note, it can been seen that the ionic liquids that innate high iodide concentration in electrolytes undergo faster reductive quenching of the excited state of the sensitizer. This electron deactivating mechanism depreciates the performance of the device. Thus, usage of second generation non-iodide ionic liquids can be as solution to overcome these limitations.

5.2 Electrochemical Impedance Spectroscopy (EIS) Studies

EIS is an essential technique to analyse the impedance variation occurred at different interfaces corresponding to electron transport properties in a DSSC. In order to investigate the impedance behaviour of the DSSCs fabricated containing the novel polymer electrolytes, the EIS data obtained was fitted with equivalent circuits. This was necessary to discuss quantitatively on the contribution of different elements like resistance and capacitance. Simulation of the real electrochemical system with an appropriately equivalent simple electrical circuit like Randles allowed the evaluation of charge transfer resistance occurring in the DSSC.

Universiti Malaya

Figure 5.5 shows the Nyquist plots of DSSC with "*PS*" polymer electrolytes, i.e- no ionic liquid electrolytes having different NaI concentration. Unlike the typical, only two distinct semicircle profiles are detected at 0.1−10 Hz (low frequency) and $10-10^5$ Hz (high frequency) representing the charge transfer resistance (R_{CT}) between the photoanode|electrolyte interface and charge-transfer resistance (R_{PT}) at the Pt|PE interface which led to triiodide reduction respectively. It must be noted that an imperceptible third semicircle appears on the spectra and some practical fitting was able to provide few rough data. The impedance curve starts at a non-zero value with intersection of the high frequency curve at the x-axis is taken as ohmic serial resistance (R_S) of the as-coated FTO substrate. The determined values of all parameters (R_{CT} and R_{PT}) for each tested device containing electrolytes are given in Table 5.5. As the salt concentration increased, the R_{PT} and R_{CT} values were noted to decrease substantially. The lower R_{PT} value of PS40 compared to other polymer electrolytes in this system, signified a higher charge transfer process occurring at the Pt|PE interface which supports the highest J_{sc} value obtained from DSSC performance analysis. In general, high R_{CT} values result in better V_{oc} values due to the suppression of back electron transfer. It was peculiar to noted that PS20 and PS30 samples recorded high R_{CT} values but this did not translate into high V_{oc} values. In the absence of relation to recombination, the low photocurrent and photovoltage noted can be caused by energy dissipation in the active layer due to poor penetration of the electrolyte. As PS20 and PS30 contain higher mass percentage of polymer, we speculate the probability of unfavourable polymer stacking that is hindering good charge transfer ability. Essentially, planar polymer confirmations are reasoned to allow strong intermolecular interactions promoting charge transport capacity and thus boost J_{sc} and V_{oc} values (Yahui Liu et al., 2016). Contrariwise, PS40 recorded a slightly lower R_{CT} value compared to its succeeding electrolyte PS50. This indicate faster recombination process between the photo-injected electrons and triiodide ions.

Universiti Malaya

Consistently, lower V_{oc} value was recorded for PS40 than PS50. In a different circumstances, Xu et al. claimed that lower recombination resistance imply that there is an improvement in the penetration of the GPEs into the photoelectrodes of the DSSCs without losing most portions of the dye absorbed in the TiO_2 layer (Xu et al., 2011). Thus, an enhancement in J_{sc} value is probable as noticed with PS40. The circuit used to fit the impedance data of the DSSCs is shown in Figure 5.6.

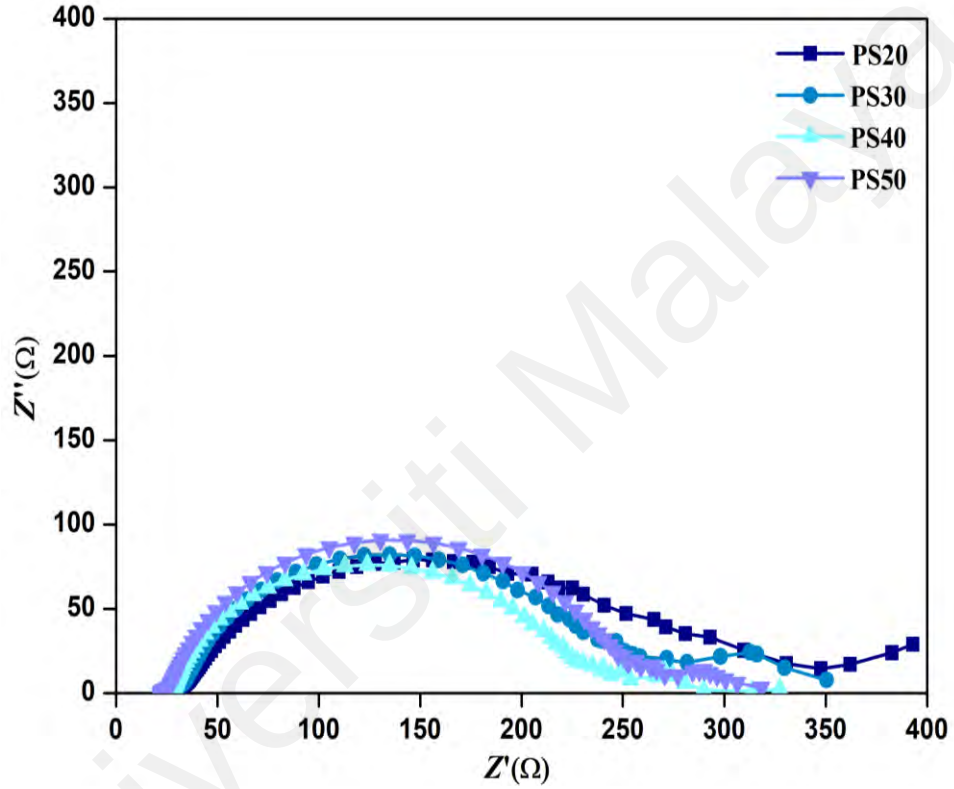

Figure 5.5 The electrochemical impedance spectra of DSSCs assembled with P(MMA-co-MAA)-NaI GPE samples in the form of Nyquist plots.

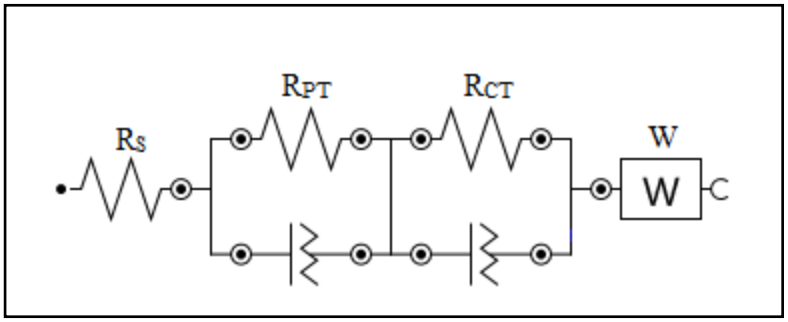

Figure 5.6: The equivalent circuits used to fit the data of the DSSCs.

Universiti Malaya

Table 5.5 The parameters of equivalent circuits used to fit the impedance data of P(MMA-co-MAA)-NaI based DSSCs.

Electrolytes	R_S (Ω)	R_{PT} (Ω)	R_{CT} (Ω)	W ($S^{1/2}\Omega$)	K_{eff} (s^{-1})	T_{eff} (s)	D_{eff} (cm^2s^{-1})
PS20	27.0	4.42	287	0.0749	1.000	0.159	2.08×10^{-6}
PS30	26.3	3.55	2.19	0.0292	2.143	0.159	2.11×10^{-6}
PS40	25.1	2.33	210	0.0537	5.458	0.159	3.00×10^{-6}
PS50	22.4	3.56	213	0.0970	2.927	0.054	2.85×10^{-6}

Following the addition of ionic liquids [C_4mquin][NTf_2] and [C_4mquin][I], a noticeable reduction of charge transfer resistance at the Pt and electrolyte interface is observed in the tested DSSCs. This implies the probable ease of triiodide ions receiving electrons to be reduced to iodide ions. Another way to perceive this is to note the availability of the electrons arriving at the counter electrode from the photoanode. Reduction in resistance would be only possible if sufficient triiodide ions are now present to receive the electrons arriving. The increase in flux of triiodide arriving at the cathode can be related to the triiodide diffusion rate as the inclusion of both quinolinium ionic liquids adequately improved D_{eff} values. The role triiodide diffusion in promoting conductivity is discussed in sections 4.4.6 and 4.5.6 and agrees with the resistance noted under DSSC impedance studies. In this investigation also, a third semicircle at low frequency region is vaguely present. A series of previous reports have concluded that small arcs in the low frequency range of 0.6-1 Hz was the finite Warburg impedance of triiodide in the electrolyte (Kern et al., 2002; Hauch & Georg, 2001). Wijeratne et al. claimed that when an electrolyte system becomes increasingly less viscous, electrolyte diffusion becomes less significant (Wijeratne et al., 2012).

Universiti Malaya

Addition of ionic liquids was found to depreciate Warburg values. This denotes an enhancement of I^-/I_3^- ions in the polymer electrolytes owing to better penetration of the electrolytes into the porous TiO_2 layer. This also reflects on the better *FF* values obtained with both quinolinium ionic liquids. [C_4mquin][I] containing electrolytes recorded lower Warburg impedance values than their [C_4mquin][NTf_2] counterparts probably due to less steric hindrance in the absence of large $[NTf_2]^-$ ions. Figures 5.7 and 5.8 depict the Nyquist plot obtained for electrolytes containing both novel ionic liquids with data tabulated in corresponding tables. The remarkably high J_{sc} value achieved by Qt25 syncs with the lowest R_{PT} recorded noting the ease in charge transfer process occurring at the platinum and electrolyte boundary. As shown in Table 5.6 and Table 5.7 the R_{CT} values were found to be higher for "*Qi"* samples than the "*Qt"* equivalents. Qi30 recorded a highest R_{CT} value of 171 Ω. R_{CT} relays information about the rate recombination process at the TiO_2/electrolyte interface whereby higher R_{CT} usually ramps up V_{oc} values. This was true for the case of Qi30. Similar to V_{oc}, the R_{CT} values did not follow a clear trend with successive increase in ionic liquid wt. %. Nevertheless, the samples with lower R_{CT} readings have found to have depreciated V_{oc} values except Qi25. The mismatch is intriguing, nonetheless, the superior sample quality may have improved pore penetration allowing efficient charge transfer to dominate.

The major recombination processes that occur within a DSSC are the recombination of the photo-injected electrons in the TiO_2 layer directly with the oxidized dye molecules or the oxidized form of the redox couple in the electrolyte. The charge transfer resistance arising from these recombination of electrons corresponds to the ω_{max} of the central arc which is equated as the recombination rate constant, k_{eff}. The reciprocal of k_{eff} is depicted as the effective lifetime of electron, T_{eff}. Ideally, lower recombination rate constant results in longer electron lifetime. The longer an electron can sustain in the TiO_2 conduction band, the higher its chances to reach the counter electrode. This is validated by the

Universiti Malaya

plausible time constants for charge transfer kinetics that occur within a working DSSC containing I_2/I^- redox couple whereby the back reaction of TiO_2 conduction band electrons with I_3^- occurs faster (~10^{-5} s) than the diffusion of electrons through the TiO_2 layer (~10^{-3} s) (Byranvand et al., 2012). Overall, samples with lower charge recombination rate would have higher electron lifetime and the results obtained are in agreement with the EIS data collected.

As for effective electron diffusion coefficient values, D_{eff}, it is highly dependent on the ratio of both electron transport resistance for the back and forward reaction. A favourable situation is when the recombination process is happening much slower than the diffusion of electrons through the TiO_2 layer. As such, the charge transfer resistance due to recombination, R_k becomes the main resistance. The relationship between R_k and the electron transport resistance in TiO_2, R_w is expressed as $R_k \approx R_w$ or sometimes $R_k = R_w$. Since the shape of the central arc is a true semi-circle, Adachi et al. recommends the estimation of R_k/R_w to be approximately 10. If such, the D_{eff} value estimated from *Equation 2.5* show high dependency of k_{eff} values which actually has contradicting purpose. Clearly, noting from the high D_{eff} values, "*Qt*" samples were able to sustain a high electron density in the conduction band which means a lower recombination rate and thus, high efficiency in general. However, the rate constant for recombination is also high which indicates an equal yet competing effect from the back reaction. This can be deemed as a reason for the fluctuation in V_{oc} values noted. Besides, from the works of Kern et al., k_{eff} values are also derived as a function of steady state electron density in the trap state, which means high k_{eff} value not necessary show the electron density in the conduction band. This might be an apparent reason why some k_{eff} value in the *PS* system noted higher than the samples in the "*Qt*" and "*Qi"* systems. Even so, the value did not reciprocate well in photovoltaic performances.

Universiti Malaya

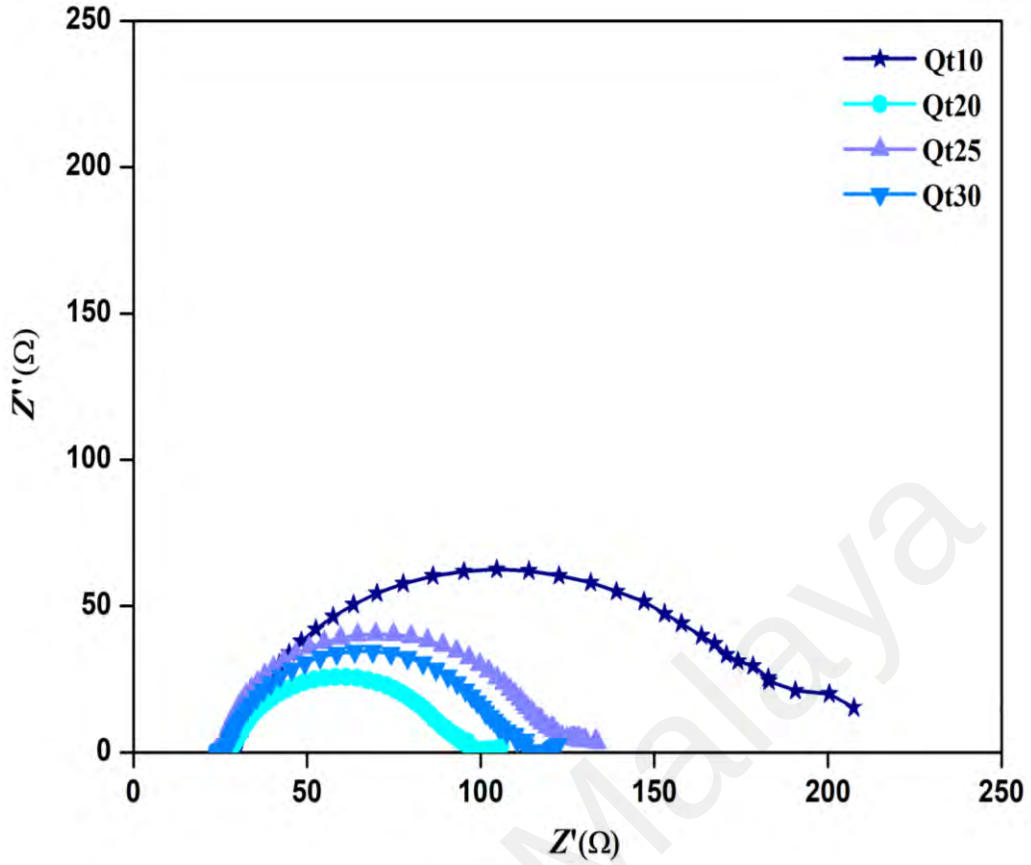

Figure 5.7: The electrochemical impedance spectra of DSSCs assembled with P(MMA-co-MAA)-NaI- [C4mquin][NTf2] GPE samples in the form of Nyquist plots.

Table 5.6: The parameters of equivalent circuits used to fit the impedance data of P(MMA-co-MAA)-NaI- [C4mquin][NTf2] based DSSCs.

Electrolytes	R_S (Ω)	R_{PT} (Ω)	R_{CT} (Ω)	W ($S^{1/2}\Omega$)	K_{eff} (s^{-1})	T_{eff} (s)	D_{eff} (cm^2s^{-1})
Qt10	26.3	2.08	164	0.574	2.143	0.074	2.59×10^{-6}
Qt20	25.2	3.10	65.8	0.667	2.955	0.054	2.90×10^{-6}
Qt25	23.6	1.60	94.4	0.390	1.968	0.081	2.74×10^{-6}
Qt30	24.6	2.24	82.8	0.483	2.735	0.058	3.48×10^{-6}

Universiti Malaya

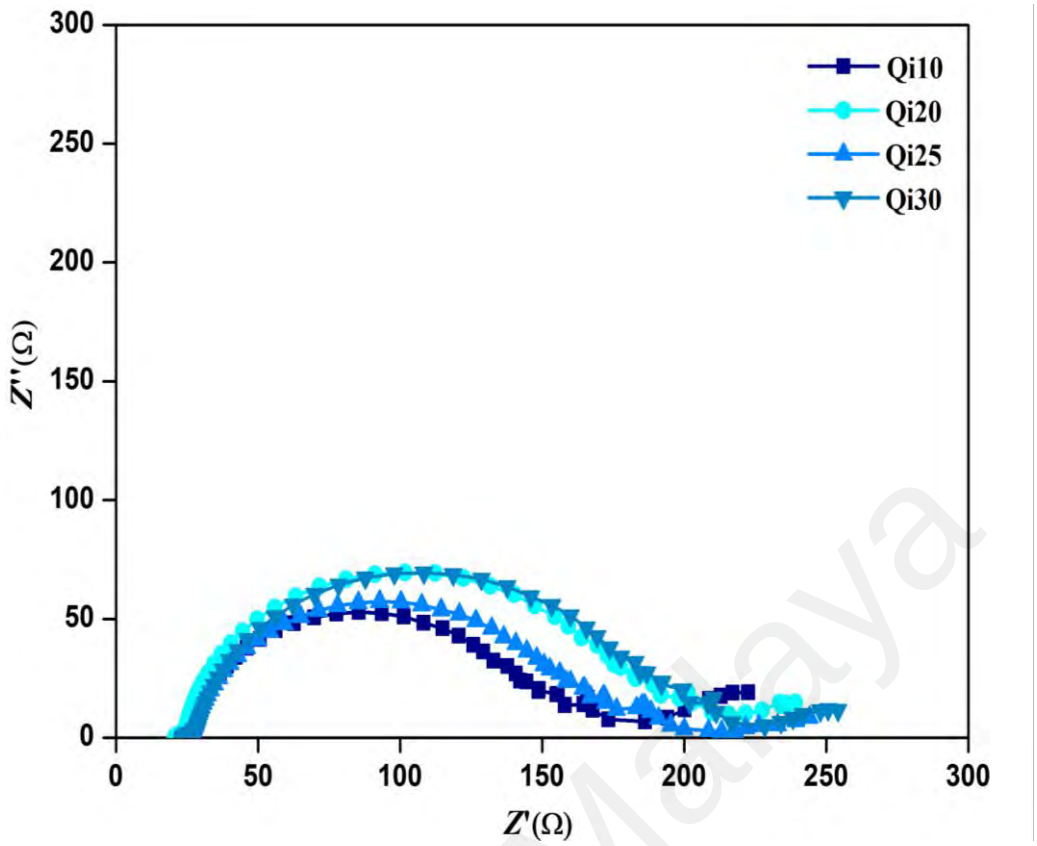

Figure 5.8: The electrochemical impedance spectra of DSSCs assembled with P(MMA-co-MAA)-NaI- [C4mquin][I] GPE samples in the form of Nyquist plots.

Table 5.7: The parameters of equivalent circuits used to fit the impedance data of P(MMA-co-MAA)-NaI- [C4mquin][I] based DSSCs.

Electrolytes	R_S (Ω)	R_{PT} (Ω)	R_{CT} (Ω)	W ($S^{1/2}\Omega$)	k_{eff} (s^{-1})	T_{eff} (s)	D_{eff} (cm^2s^{-1})
Qi10	22.7	2.72	128	0.081	1.834	0.087	2.16×10^{-6}
Qi20	25.8	2.59	165	0.093	1.569	0.101	2.70×10^{-6}
Qi25	24.1	1.92	149	0.135	2.143	0.074	3.19×10^{-6}
Qi30	23.9	3.49	171	0.105	1.719	0.093	3.07×10^{-6}

Figure 5.9 shows the data obtained for DSSCs containing electrolytes with varying [C6mim][I] ionic liquid content. As previous, the data was fitted with equivalent circuits and all parameters obtained were tabulated in Table 5.8. In this system, the R_S and R_{PT}

Universiti Malaya

values are noted to be in similar range with the no ionic liquid system. However, GPEs with [C_6mim][I] show higher T_{eff} values showing longer retention of electron in the conduction band, hence resulting in high J_{sc} values collectively. Besides, the marginal difference in R_{CT} values are recorded aligns well with the minimal fluctuation in the V_{oc} values. Unlike the incongruity observed in quinolinium containing samples, [C_6mim][I] containing samples portray the commonly discussed relationship between R_{CT} and $V_{oc.}$ Hm20 recorded the highest R_{CT} value which in turn has the highest V_{oc} value owing to higher driving force for recombination which suppresses the back electron transfer. On the other hand, despite the highest J_{sc} values and efficiency achieved for sample Hm20, T_{eff} is noted to be slightly lower than Hm15 and Hm25. T_{eff} is a product of recombination resistance and chemical capacitance. There seems to be a slight mismatch between the effective electron lifetime and recombination resistance based on usual descriptions. However, it must be minded that very often recombination arc does not singly dominate the contribution towards the impedance spectra and a significant portion of capacitance may affect the effective electron lifetime (Bisquert & Fabregat-Santiago, 2009). For the case of Hm20, it can be speculated that the capacitance contribution for this electrolyte is poor, hence, the lower lifetime recorded.

Table 5.8: The parameters of equivalent circuits used to fit the impedance data of P(MMA-co-MAA)-NaI- [C6mim][I] based DSSCs.

Electrolytes	R_S (Ω)	R_{PT} (Ω)	R_{CT} (Ω)	W ($S^{1/2}\Omega$)	k_{eff} (s^{-1})	T_{eff} (s)	D_{eff} (cm^2s^{-1})
Hm10	29.0	3.42	182	0.040	2.187	0.073	2.22×10^{-6}
Hm15	25.2	11.2	185	0.405	1.311	0.121	2.71×10^{-6}
Hm20	24.9	2.24	215	0.092	1.560	0.101	3.29×10^{-6}
Hm25	26.4	4.18	170	0.118	1.299	0.123	2.60×10^{-6}

Universiti Malaya

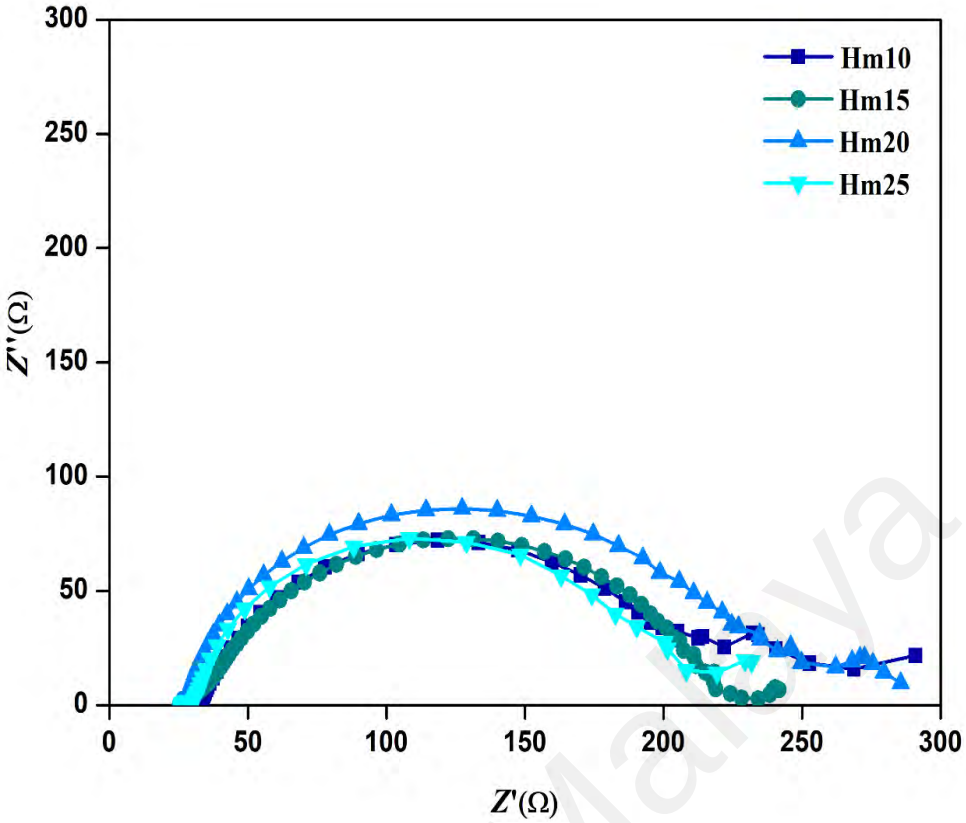

Figure 5.9: The electrochemical impedance spectra of DSSCs assembled with P(MMA-co-MAA)-NaI- [C_6mim][I] GPE samples in the form of Nyquist plots.

In brief with EIS investigation, it is shown that low k_{eff}, high T_{eff} and high D_{eff} are necessary combinatory conditions to attain higher solar cell performance. The enhanced electron transport properties, reduced charge recombination and increased electron lifetime which are imperative for highly efficient DSSCs could be achieved using pristine quinolinium based ionic liquids.

Universiti Malaya

CHAPTER 6- CONCLUSION AND FUTURE WORK

6.1 Conclusion

A series of P(MMA-co-MAA) based polymer electrolytes were prepared along with two novel ionic liquids, [C_4mquin][I] and [C_4mquin][NTf_2] which were synthesized and characterised. The polymer electrolytes were able to form gel- consistency both in the absence and presence of ionic liquids. Prior to discussing the valuable information obtained from this research, the purpose of ionic liquid integration with co-polymers are discussed as to address the direction of research. The necessity of quasi-solid features together with conduction occurring in polymer electrolytes were also highlighted. Groundwork on the polymer electrolytes were also for the employment in DSSCs. Thus, the relevance and functionality of DSSCs were also emphasized.

The synthesis of high purity ionic liquid shows the prospects of quaternization and metathesis reaction with yield at 82 % and 87 % for [C_4mquin][I] and [C_4mquin][NTf_2], respectively. Structural and thermal characterization of the ionic liquids using NMR, FTIR, XRD, TGA and DSC analysis confirmed the desired product formation as well as accentuated the suitability in employing the ionic liquids in polymer electrolytes. Despite the solidification of both ionic liquids at room temperature, their melting temperatures below 80 ºC makes them ideal incorporation to develop quasi-solid polymer electrolytes. The effect of adding ionic liquids with anionic and cationic variation is investigated throughout the research. In fact, the ionic conductivity of polymer electrolytes surged to high levels of 10^{-3} S cm^{-1} with increasing mass fraction of ionic liquid up to a maximum after which was followed by a decrease in ionic conductivity owing to ion agglomeration possibly hindering ion conduction path. The ionic conductivity reached a maximum of 2.26 mS cm^{-1} and 2.64 mS cm^{-1} for [C_4mquin][NTf_2] and [C_4mquin][I] containing electrolytes respectively, and both at 25 wt. % of ionic liquid mass loading. The ionic

Universiti Malaya

conductivity for the P(MMA-co-MAA) electrolytes also increased with temperature which reveals a compliance between polymer backbone segmental motion with ion hopping mechanism a rule for high conduction. The increase in ionic conductivity indicated a low degree of crystallinity which was supported by XRD findings. The drop in crystallinity also revealed the ease of triiodide diffusion throughout the electrolyte via LSV studies. Herewith, the complexation between P(MMA-co-MAA), EC/PC and ionic liquid were substantiated in FTIR studies. Impregnation of ionic liquids have shown to improve the electrochemical properties in DSSCs. Significant increment in J_{sc} and V_{oc} values were noted upon inclusion of the novel [C_4mquin][NTf_2] and [C_4mquin][I] ionic liquids. Thus, high power conversion efficiencies were also achieved compared to ionic liquid-free polymer electrolytes. The best conversion efficiency in this research was 5.67% from 25 wt. % of [C_4mquin][NTf_2] added. Despite not being the highest conducting sample, the maximum PCE was possible owing to role of anions present and their steric effects correlating with the different interfacial charge transfer behaviour. With that, a clear correlation between short circuit current and power conversion efficiency was also established through this research. The excellent electrochemical performances were also proven in EIS studies. Inclusion of quinolinium derived ionic liquids in polymer electrolytes were able to show enhanced electron transport properties with reduction in back-electron transfers and sustain a higher electron lifetime. This was done via the evaluation of charge transfer resistance from Nyquist plots obtained. Of three different polymer electrolyte system, one comprising of [C_6mim][I] was prepared to determine the effect of counter-cation and -anion of ionic liquid onto ionic conduction and power conversion efficiency in DSSCs. Overall the pristine quinolinium based ionic liquids deemed promising to be used in polymer electrolytes as they have improved ionic conductivity, increase the amorphous region through the polymer complex and enhance electrochemical properties in DSSCs.

Universiti Malaya

6.2 Future work

This study had highlighted the advantages and limitations inherited by quinolinium ionic liquids by incorporating it in gel polymer electrolytes for DSSCs. Work should be continued to improve the overall efficiency of the DSSC with newer and better cell preparation and assembly techniques as this research was done with conventional standard approach. Since the photovoltaic conversion efficiency of DSSC containing these ionic liquid-added polymer electrolytes can be escalated quickly, thus I would like to employ these polymer electrolytes in other application like in supercapattery as my further research and see how well they fair. Feasibly, some composition changes can be also done to suit the needs. The electrolytes can be tested with alternative electrode materials like graphite on nickel foams to see their energy storing ability. Perhaps, the electrolytes can perform equally well in other electrochemical devices too.

Universiti Malaya

REFERENCES

Abarna, S., & Hirankumar, G. (2017). Electrical , dielectric and electrochemical studies on new Li ion conducting solid polymer electrolytes based on polyethylene glycol p - tert -octylphenyl ether. *Polymer Science, Series A*, *59*(5), 1–9.

Abraham, K. M. (1996). A polymer electrolyte - based rechargeable lithium/ oxygen battery. *Journal of the Electrchemical Society*, *143*(1), 1–5.

Adachi, M., Sakamoto, M., Jiu, J., Ogata, Y., & Isoda, S. (2006). Determination of parameters of electron transport in dye-sensitized solar cells using electrochemical impedance spectroscopy. *The Journal of Physical Chemistry B*, *110*(28), 13872–80.

Aghazada, S., & Nazeeruddin, M. K. (2018). Ruthenium complexes as sensitizers in dye-sensitized solar cells. *Inorganics*, *6*(52), 1–34.

Ahmed, M. I., Habib, A., & Javaid, S. S. (2015). Perovskite solar cells: Potentials, challenges, and opportunities. *International Journal of Photoenergy*, *2015*, Article#592308. https://doi.org/10.1155/2015/592308

Ali, A. M. M., Yahya, M. Z. A., Bahron, H., & Subban, R. H. Y. (2007). Impedance studies on plasticized PMMA-LiX [X: $CF_3SO_3^-$, N $(CF_3SO_2)_2^-$] polymer electrolytes. *Materials Letters*, *61*(10), 2026–2029.

Ali, U., Juhanni, K., Abd, B., & Buang, N. A. (2015). A Review of the properties and applications of poly(methyl methacrylate) (PMMA). *Polymer Reviews*, *55*(4), 678–705.

Alireza, S., Gharagheizi, F., Ilani-kashkouli, P., & Farahani, N. (2012). Determination of the glass transition temperature of ionic liquids : A molecular approach. *Thermochimica Acta*, *543*, 88–95.

Aram, E., Ehsani, M., & Khonakdar, H. A. (2015). Improvement of ionic conductivity and performance of quasi-solid-state dye sensitized solar cell using PEO/PMMA gel electrolyte. *Thermochimica Acta*, *615*, 61–67.

Armel, V., Pringle, J. M., Forsyth, M., & Macfarlane, D. R. (2010). Ionic liquid electrolyte porphyrin dye sensitised solar cells. *Chemical Communications*, 3146–3148.

Asmara, S. N., Kufian, M. Z., Majid, S. R., & Arof, A. K. (2011). Preparation and characterization of magnesium ion gel polymer electrolytes for application in electrical double layer capacitors. *Electrochimica Acta*, *57*, 91–97.

Universiti Malaya

Aziz, S. B., & Abidin, Z. H. Z. (2013). Electrical conduction mechanism in solid polymer electrolytes : New concepts to Arrhenius equation. *Journal of Soft Matter*, *2013,* Article#323868. https://doi.org/10.1155/2013/323868

Aziz, S. B., Al-zangana, S., Woo, H. J., Kadir, M. F. Z., & Abdullah, O. G. (2018). The compatibility of chitosan with divalent salts over monovalent salts for the preparation of solid polymer electrolytes. *Results in Physics*, *11*, 826–836.

Aziz, S. B., Woo, T. J., Kadir, M. F. Z., & Ahmed, H. M. (2018). A conceptual review on polymer electrolytes and ion transport models. *Journal of Science: Advanced Materials and Devices*, *3*(1), 1–17.

Bandara, T. M. W. J., Fernando, H. D. N. S., Furlani, M., Albinsson, I., Dissanayake, M. A. K. L., & Mellander, B.-E. (2016). Performance enhancers for gel polymer electrolytes based on LiI and RbI for quasi-solid-state dye sensitized solar cells. *RSC Advances*, *6*(105), 103683–103691.

Bardakchi, B. (2007). FTIR-ATR spectroscopic characterization of monochlorophenols and effects of symmetry on vibrational frequencies. *Cankaya University Journal of Arts and Science*, *1*(7), 13–19.

Baskoro, F., Wong, H. Q., & Yen, H. (2019). Strategic structural design of a gel polymer electrolyte toward a high efficiency lithium-ion battery. *ACS Applied Energy Materials*, *2*(6), 3937–3971.

Bella, F., Galliano, S., Falco, M., Viscardi, G., Barolo, C., Gratzel, M., & Gerbaldi, C. (2016). Unveiling iodine-based electrolytes chemistry in aqueous dye- sensitized solar cells. *Chemical Science*, *7*(8), 4880–4890.

Bella, F., Pugliese, D., Zolin, L., & Gerbaldi, C. (2017). Paper-based quasi-solid dye-sensitized solar cells. *Electrochimica Acta*, *272*, 87–93.

Bentley, C. L., Bond, A. M., Hollenkamp, A. F., Mahon, P. J., & Zhang, J. (2014). Electrode reaction and mass-transport mechanisms associated with the iodide/triiodide couple in the ionic liquid 1-ethyl-3-methylimidazolium bis(trifluoromethanesulfonyl)imide. *The Journal of Physical Chemistry C*, *118*(39), 22439–22449.

Bhattacharya, B., Lee, J. Y., Geng, J., Jung, H.-T., & Park, J.-K. (2009). Effect of cation size on solid polymer electrolyte based dye-sensitized solar cells. *Langmuir*, *25*(5), 3276–3281.

Bisquert, J. (2010). Theory of the impedance of charge transfer via surface states in dye-sensitized solar cells. *Journal of Electroanalytical Chemistry*, *646*(1–2), 43–51.

Universiti Malaya

Bisquert, J., & Fabregat-Santiago, F. (2009). Electron lifetime in dye-sensitized solar cells: theory and interpretation of measurements. *The Journal of Physical Chemistry C*, *113*(40), 17278–17290.

Boschloo, G., & Hagfeldt, A. (2009). Characteristics of the iodide/triiodide redox mediator in dye-sensitized solar cells. *Accounts of Chemical Research*, *42*(11), 1819–1826.

Broström, M., Enestam, S., Backman, R., & Mäkelä, K. (2013). Condensation in the KCl – NaCl system. *Fuel Processing Technology*, *105*, 142–148.

Buraidah, M. H., Shah, S., Teo, L. P., Chowdhury, F. I., Careem, M. A., Albinsson, I., Mellander, B., & Arof, A. K. (2017). High efficient dye sensitized solar cells using phthaloylchitosan based gel polymer electrolytes. *Electrochimica Acta*, *245*, 846–853.

Buraidah, M. H., Teo, L. P., Majid, S. R., Yahya, R., Taha, R. M., & Arof, A. K. (2010). Characterizations of chitosan-based polymer electrolyte photovoltaic cells. *International Journal of Photoenergy*, *2010*, Article#805836. https://doi.org/10.1155/2010/805836

Byranvand, M. M., Kharat, A. N., Badiei, A., & Bazargan, M. H. (2012). Electron transfer in dye-sensitized solar cells. *Journal of Optoelectronics and Biomedical Materials*, *4*(3), 49–57.

Cao, Y., & Mu, T. (2014). Comprehensive investigation on the thermal stability of 66 ionic liquids by thermogravimetric analysis. *Industrial & Engineering Chemistry Research*, *53*(20), 8651–8664.

Chen, C. L., Teng, H., & Lee, Y. L. (2011). Preparation of highly efficient gel-state dye-sensitized solar cells using polymer gel electrolytes based on poly(acrylonitrile-co-vinyl acetate). *Journal of Materials Chemistry*, *21*(3), 628–632.

Chen, X., Zhao, J., Zhang, J., Qiu, L., Xu, D., Zhang, H., Han, X., Sun, B., Fu, G., Zhang, Y., & Yan, F. (2012). Bis-imidazolium based poly(ionic liquid) electrolytes for quasi-solid-state dye-sensitized solar cells. *Journal of Materials Chemistry*, *22*(34), 18018–18024.

Cherry, B. W., Stachurski, Z. H., & Wright, P. H. (1972). Ionic conduction in polymers. *Journal of Macromolecular Science: Part A-Chemistry: Pure and Applied Chemistry*, *6*(4), 797–809.

Universiti Malaya

Chu, M. M. (2019, May 14). Malaysia can generate more electricity if all roofs use solar panels, says Yeo. The Star. Retrieved from https://www.thestar.com.my/news/nation/2019/05/14/malaysia-can-generate-more-electricity-if-all-roofs-use-solar-panels-says-yeo/.

Costa, L. T., Lavall, R. L., Borges, R. S., Rieumont, J., Silva, G. G., & Ribeiro, M. C. C. (2007). Polymer electrolytes based on poly(ethylene glycol) dimethyl ether and the ionic liquid 1-butyl-3-methylimidazolium hexafluorophosphate: preparation, physico-chemical characterization, and theoretical study. *Electrochimica Acta*, *53*, 1568–1574.

Costache, M. C., Wang, D., Heidecker, M. J., Manias, E., & Wilkie, C. A. (2006). The thermal degradation of poly(methyl methacrylate) nanocomposites with montmorillonite, layered double hydroxides and carbon nanotubes. *Polymers for Advanced Technologies*, *17*(4), 272–280.

Deepa, M., Agnihotry, S. A., Gupta, D., & Chandra, R. (2004). Ion-pairing effects and ion – solvent–polymer interactions in LiN $(CF_3SO_2)_2$ –PC–PMMA electrolytes: a FTIR study. *Electrochimica Acta*, *49*(3), 373–383.

Denizalti, S., Ali, A. K., Ela, C., & Ekmekci, M. (2018). Dye-sensitized solar cells using ionic liquids as redox mediator. *Chemical Physics Letters*, *691*, 373–378.

Dissanayake, M. A. K. L., Jayathissa, R., Seneviratne, V. A., Thotawatthage, C. A., Senadeera, G. K. R., & Mellander, B. E. (2014). Polymethylmethacrylate (PMMA) based quasi-solid electrolyte with binary iodide salt for efficiency enhancement in TiO_2 based dye sensitized solar cells. *Solid State Ionics*, *265*, 85–91.

Efimova, A., Hubrig, G., & Schmidt, P. (2013). Thermal stability and crystallization behavior of imidazolium halide ionic liquids. *Thermochimica Acta*, *573*, 162–169.

Elumalai, N. K., & Uddin, A. (2016). Open circuit voltage of organic solar cells: An in-depth review. *Energy & Environmental Science*, *9*, 391–410.

Farhana, N. K., Khanmirzaei, M. H., Ramesh, S., & Ramesh, K. (2017). Exploration on poly(propylene) carbonate polymer for gel polymer electrolyte preparation and dye-sensitized solar cell application. *Journal of Applied Polymer Science*, *134*(29), Article#45091.

Farhana, N. K., Ramesh, S., & Ramesh, K. (2019). Efficiency enhancement of dye-sensitized solar cell based gel polymer electrolytes using poly(vinyl butyral-co-vinyl alcohol-co-vinyl acetate)/ tetrapropylammonium iodide. *Materials Science in Semiconductor Processing*, *91*, 414–421.

Universiti Malaya

Feng, H., Lu, X., Wang, W., Kang, N. G., & Mays, J. W. (2017). Block copolymers: Synthesis, self-assembly, and applications. *Polymers*, *9*(10), Article#494.

Fenton, D. E., Parker, J. M., & Wright, P. V. (1973). Complexes of alkali metal ions with poly(ethylene oxide). *Polymers*, *14*(11), Article#589.

Gadjourova, Z., Andreev, Y. G., Tunstall, D. P., & Bruce, P. G. (2001). Ionic conductivity in crystalline polymer electrolytes. *Nature*, *412*(6846), 520–523.

GCell (n.d.). Efficiency of DSSC, Retrieved from https://gcell.com/dye-sensitized-solar-cells/advantages-of-dscc/efficiency.

Genova, K. M., Selvasekarapandian, S., Rajeswari, N., Devi, S., Karthigeyan, S., & Raja, C. (2013). Lithium ion polymer electrolyte based on PVA-PAN. *In Solid State Ionics: Ionics for Sustainable World*, 63–71.

Ghandi, K. (2014). A review of ionic liquids , their limits and applications. *Green and Sustainable Chemistry*, *4*(1), 44-53.

Hagfeldt, A., Boschloo, G., Sun, L., Kloo, L., & Pettersson, H. (2010). Dye-sensitized solar cells. *Chemical Reviews*, *110*(11), 6595–6663.

Hamed, N., Ahmad, M., Urus, N., Mohamad, F., Nafarizal, N., Ahmad, N., & C.F, S. (2017). Performance comparison between silicon solar panel and dye-sensitized solar panel in Malaysia. *AIP Conference Proceedings* (Vol. 1883), Article#020029.

Handy, S. T. (2005). Room temperature ionic liquids : Different classes and physical properties. *Current Organic Chemistry*, *9*, 959–988.

Hauch, A., & Georg, A. (2001). Diffusion in the electrolyte and charge-transfer reaction at the platinum electrode in dye-sensitized solar cells. *Electrochimica Acta*, *46*(22), 3457–3466.

Hodge, R. M. (1996). Water absorption and states of water in semicrystalline poly(vinyl alcohol) films. *Polymer*, *37*(8), 1371–1376.

Hoffmann, M. R., Martin, S. T., Choi, W., & Bahnemannt, D. W. (1995). Environmental applications of semiconductor photocatalysis. *Chemical Reviews*, *95*, 69–96.

Huang, M., Yang, H., Wu, J., Lin, J., Lan, Z., Li, P., Hao, S., Han, P., & Jiang, Q. (2007). Preparation of a novel polymer gel electrolyte based on N-methyl-quinoline iodide and its application in quasi-solid-state dye-sensitized solar cell. *Journal of*

Universiti Malaya

Sol-Gel Science and Technology, *42*(1), 65–70.

Huddleston, J. G., Visser, A. E., Reichert, W. M., Willauer, H. D., Broker, G. A., & Rogers, R. D. (2001). Characterization and comparison of hydrophilic and hydrophobic room temperature ionic liquids incorporating the imidazolium cation. *Green Chemistry*, *3*(4), 156–164.

Ikezawa, Y., & Nishi, H. (2008). In situ FTIR study of the Cu electrode/ethylene carbonate + dimethyl carbonate solution interface. *Electrochimica Acta*, *53*(10), 3663–3669.

Islam, M. R. (2009). Renewable energy research in Malaysia. *Engineering e-Transaction*, *4*(2), 69–72.

Ito, S. (2011). Investigation of dyes for dye-sensitized solar cells: Ruthenium-complex dyes, metal-free dyes, metal-complex porphyrin dyes and natural dyes. In L. A. Kosyachenko (Ed.), *Solar Cells - Dye-Sensitized Devices*. InTech, 19–48.

Jacoby, M. (2016). The future of low-cost solar cells. *Chemical & Engineering News*, *94*(18), 30–35.

Jayakumar, N., & Srinivasan, V. (2015). Morphological characterization of poly methyl methacrylate for surface coating of metals. *International Journal of Mechanical Engineering and Technology*, *6*(8), 139–143.

Kakiage, K., Aoyama, Y., Yano, T., Oya, K., Fujisawa, J., & Hanaya, M. (2015). Highly-efficient dye-sensitized solar cells with collaborative sensitization by silyl-anchor and carboxy-anchor dyes. *Chemical Communications*, *51*(88), 15894–15897.

Kambe, S., Nakade, S., Kitamura, T., Wada, Y., & Yanagida, S. (2002). Influence of the electrolytes on electron transport in mesoporous TiO_2 - electrolyte systems. *The Journal of Physical Chemistry B*, *106*(11), 2967–2972.

Kanamura, K., Umegaki, T., Ohashi, M., & Toriyama, S. (2001). Oxidation of propylene carbonate containing $LiBF_4$ or $LiPF_6$ on $LiCoO_2$ thin film electrode for lithium batteries. *Electrochimica Acta*, *47*(3), 433–439.

Kang, M. G., Ryu, K. S., Chang, S. H., & Park, N. G. (2004). A new ionic liquid for a redox electrolyte of dye-sensitized solar cells. *ETRI Journal*, *26*(6), 647–652.

Kawano, R., Matsui, H., Matsuyama, C., Sato, A., Susan, M. A. B. H., Tanabe, N., & Watanabe, M. (2004). High performance dye-sensitized solar cells using ionic liquids as their electrolytes. *Journal of Photochemistry and Photobiology A: Chemistry*, *164*(1–3), 87–92.

Universiti Malaya

Keating, M. Y., Gao, F., & Ramsey, J. B. (2011). TGA-MS study of the decomposition of phosphorus-containing ionic liquids trihexyl (tetradecyl) phosphonium decanoate and trihexyltetradecylphosphonium bis [(trifluoromethyl) sulfonyl] amide. *Journal of Thermal Analysis and Calorimetry*, *106*(1), 207–211.

Kern, R., Sastrawan, R., Ferber, J., Stangl, R., & Luther, J. (2002). Modeling and interpretation of electrical impedance spectra of dye solar cells operated under open-circuit conditions. *Electrochimica Acta*, *47*(26), 4213–4225.

Khanmirzaei, M. H., Ramesh, S., & Ramesh, K. (2015). Polymer electrolyte based dye-sensitized solar cell with rice starch and 1-methyl-3-propylimidazolium iodide ionic liquid. *Materials and Design*, *85*, 833–837.

Khiar, A. S. A., & Arof, A. K. (2010). Conductivity studies of starch-based polymer electrolytes. *Ionics*, *16*(2), 123–129.

Kloo, L., Hagfeldt, A., & Boschloo, G. (2006). Electron transport and recombination in dye-sensitized solar cells with ionic liquid electrolytes. *Journal of Electroanalytical Chemistry*, *586*(1), 56–61.

Kovash, C. S., Hoefelmeyer, J. D., & Logue, B. A. (2012). Electrochimica Acta TiO_2 compact layers prepared by low temperature colloidal synthesis and deposition for high performance dye-sensitized solar cells. *Electrochimica Acta*, *67*, 18–23.

Kubo, W., Kitamura, T., Hanabusa, K., Wada, Y., & Yanagida, S. (2002). Quasi-solid-state dye-sensitized solar cells using room temperature molten salts and a low molecular weight gelator. *Chemical Communications (Cambridge, England)*, *2002*(4), 374–375.

Kubo, W., Murakoshi, K., Kitamura, T., Yoshida, S., Haruki, M., Hanabusa, K., Shirai, H., Wada, Y., & Yanagida, S. (2001). Quasi-solid-state sye-sensitized TiO_2 solar cells : Effective charge transport in mesoporous space filled with gel electrolytes containing iodide and iodine. *The Journal of Physical Chemistry B*, *105*(51), 12809–12815.

Kumar, E. N., Jose, R., Archana, P. S., Vijila, C., Yusoff, M. M., & Ramakrishna, S. (2012). High performance dye-sensitized solar cells with record open circuit voltage using tin oxide nanoflowers developed by electrospinning. *Energy & Environmental Science*, *5*(1), Article#5401.

Kumar, R, Singh, B., & Sekhon, S. S. (2005). Effect of dielectric constant of solvent on the conductivity behavior. *Journal of Materials Science*, *40*(5), 1273–1275.

Universiti Malaya

Kumar, Rajiv, & Sekhon, S. S. (2013). Conductivity, FTIR studies, and thermal behavior of PMMA-based proton conducting polymer gel electrolytes containing triflic acid. *Ionics*, *19*(11), 1627–1635.

Kumaran, V. S., Ng, H. M., Ramesh, S., Ramesh, K., Vengadaesvaran, B., & Numan, A. (2018). The conductivity and dielectric studies of solid polymer electrolytes based on poly (acrylamide-co-acrylic acid) doped with sodium iodide. *Ionics*, *24*(7), 1947–1953.

Kumari, J. M. K. W., Senadeera, G. K. R., & Dissanayake, M. A. K. L. (2017). Dependence of photovoltaic parameters on the size of cations adsorbed by TiO_2 photoanode in dye-sensitized solar cells. *Ionics*, *23*(10), 2895–2900.

Lau, S. T. C., Dayou, J., Sipaut, C. S., & Mansa, R. F. (2014). Development in photoanode materials for high efficiency dye sensitized solar cells. *International Journal of Renewable Energy Research*, *4*(3), 665-674.

Lee, C.-P., Li, C.-T., & Ho, K.-C. (2017). Use of organic materials in dye-sensitized solar cells. *Materials Today*, *20*(5), 267–283.

Lee, C. P., Peng, J. De, Velayutham, D., Chang, J., Chen, P. W., Suryanarayanan, V., & Ho, K. C. (2013). Trialkylsulfonium and tetraalkylammonium cations-based ionic liquid electrolytes for quasi-solid-state dye-sensitized solar cells. *Electrochimica Acta*, *114*, 303–308.

Lee, S. A., Jackson, A. S., Hess, A., Fei, S., Pursel, S. M., Basham, J., … Pennsyl, V. (2010). Influence of different iodide salts on the performance of dye-sensitized solar cells containing phosphazene-based nonvolatile electrolytes. *Journal of Physical Chemistry C*, *114*(35), 15234–15242.

Lenzmann, F., Krueger, J., Burnside, S., Brooks, K., Gra, M., Gal, D., Ru, S., & Cahen, D. (2001). Surface photovoltage spectroscopy of dye-sensitized solar cells with TiO_2, Nb_2O_5 , and $SrTiO_3$ nanocrystalline photoanodes : Indication for electron injection from higher excited dye states. *The Journal of Physical Chemistry B*, *105*(27), 6347–6352.

Leys, J., Wübbenhorst, M., Menon, C. P., Rajesh, R., & Thoen, J. (2008). Temperature dependence of the electrical conductivity of imidazolium ionic liquids. *The Journal of Chemical Physics*, *128*(6), Article#064509.

Li, B., Liduo, W., Kang, B., Wang, P., & Qiu, Y. (2006). Review of recent progress in solid-state dye-sensitized solar cells. *Solar Energy Materials & Solar Cells*, *90*, 549–573.

Universiti Malaya

Li, P. J., Wu, J. H., Huang, M. L., Hao, S. C., Lan, Z., Li, Q., & Kang, S. (2007). The application of P (MMA- co -MAA)/ PEG polyblend gel electrolyte in quasi-solid state dye-sensitized solar cell at higher temperature. *Electrochimica Acta*, *53*, 903–908.

Liew, C., & Ramesh, S. (2012). Impact of low viscosity ionic liquid on PMMA – PVC – LiTFSI polymer electrolytes based on AC -impedance , dielectric behavior, and HATR – FTIR characteristics. *Journal of Materials Research*, *27*(23), 2996–3004.

Lin, H. (2001). A new sight towards dye-sensitized solar cells: Material and theoretical. In *Key Engineering Materials volume 451*. Switzerland: Tras Tech Publications Ltd, 1–133.

Liu, Y, Li, G., Zhang, Z., Wu, L., Chen, J., Xu, X., Chen, X., Ma, W., & Bo, Z. (2016). An effective way to reduce energy loss and enhance open-circuit voltage in polymer solar cells based on a diketopyrrolopyrrole polymer containing three regular alternating units. *Journal of Materials Chemistry A*, *4*(34), 13265–13270.

Liu, Yao, Hagfeldt, A., Xiao, X.-R., & Lindquist, S.-E. (1998). Investigation of influence of redox species on the interfacial energetics of a dye-sensitized nanoporous TiO_2 solar cell. *Solar Energy Materials and Solar Cells*, *55*(3), 267–281.

Lu, W. F. Y., Chen, Y., & Tao, Y. L. (2016). Thermal stability of imidazolium-based ionic liquids investigated by TG and FTIR techniques. *Journal of Thermal Analysis and Calorimetry*, *125*(1), 143–154.

M. Freemantle. (2010). *An Introduction to Ionic Liquids.* Cambridge, UK: Royal Society of Chemistry.

Martinelli, A. (2013). Ionic liquids for green energy applications - local structure and dynamics by advanced spectroscopic techniques. In *Ionic Liquids: New Aspects for the Future*, 233.

Mas Harris, R., Kathiresan, S., & Mohan, S. (2010). FT-IR and FT-Raman spectra and normal coordinate analysis of poly methyl methacrylate. *Der Pharma Chemica*, *2*(4), 316–323.

Mathew, C. M., Kesavan, K., & Rajendran, S. (2015). Structural and electrochemical analysis of PMMA based gel electrolyte membranes. *International Journal of Electrochemistry*, *2015*, 1–7.

Maton, C., De Vos, N., & Stevens, C. V. (2013). Ionic liquid thermal stabilities: Decomposition mechanisms and analysis tools. *Chemical Society Reviews*, *42*(13), 5963–5977.

Universiti Malaya

Molla-abbassi, A., Eriksson, L., Lindqvist-Reis, P., Mink, J., & Persson, I. (2002). Supplementary material structure and bonding of bisaquamercury (II) and trisaquathallium (III) trifluoromethanesulfonate. *Journal of the Chemical Society, Dalton Transactions*, *2002*(23), 4357–4364.

Mozaffari, S., Nateghi, M. R., & Zarandi, M. B. (2017). An overview of the challenges in the commercialization of dye sensitized solar cells. *Renewable and Sustainable Energy Reviews*, *71*, 675–686.

Muhammad, A., Mutalib, A., Wilfred, C. D., Murugesan, T., & Shafeeq, A. (2008). Thermophysical properties of 1-hexyl-3-methyl imidazolium based ionic liquids with tetrafluoroborate , hexafluorophosphate and bis (trifluoromethylsulfonyl) imide anions. *The Journal of Chemical Thermodynamics*, *40*(9), 1433–1438.

Nadia, S. R., Khanmirzaei, M. H., Ramesh, S., & Ramesh, K. (2016). Quasi-solid-state agar-based polymer electrolytes for dye-sensitized solar cell applications using imidazolium-based ionic liquid. *Ionics*, 1–6.

Ng, H. M., Ramesh, S., & Ramesh, K. (2015). Exploration on the P(VP-co-VAc) copolymer based gel polymer electrolytes doped with quaternary ammonium iodide salt for DSSC applications: Electrochemical behaviors and photovoltaic performances. *Organic Electronics*, *22*, 132–139.

Ng, H. M., Ramesh, S., & Ramesh, K. (2017). A quasi solid polymer electrolyte composed of poly(1-vinylpyrrolidone-co-vinyl acetate) copolymer and the influence of its composition on electrochemical properties and the performances of the dye sensitized solar cells. *Polymer-Plastics Technology and Engineering*, *57*(2), 98–107.

Noor, M. M., Buraidah, M. H., Yusuf, S. N. F., Careem, M. A., Majid, S. R., & Arof, A. K. (2011). Performance of dye-sensitized solar cells with (PVDF-HFP)-KI-EC-PC electrolyte and different dye materials. *International Journal of Photoenergy*, *2011*, Article#960748. https://doi.org/10.1155/2011/960487

Ogunsolu, O. O., Wang, J. C., & Hanson, K. (2017). Increasing the open-circuit voltage of dye-sensitized solar cells via metal-ion coordination. *Inorganic Chemistry*, *56*(18), 11168–11175.

Oregan, B., & Gratzel, M. (1991). A low-cost, high-efficiency solar-cell based on dye-sensitized colloidal TiO_2 films. *Nature*, *353*(6346), 737–740.

Palomar, J., Torrecilla, J., Lemus, J., Ferroa, V., & Rodriguez, F. (2010). A COSMO-RS based guide to analyze/quantify the polarity of ionic liquids and their mixtures with organic cosolvents. *Physical Chemistry Chemical Physics*, *12*(8), 1991–2000.

Universiti Malaya

Pandey, K., Asthana, N., Dwivedi, M. M., & Chaturvedi, S. K. (2013). Effect of plasticizers on structural and dielectric behaviour of [PEO + $(NH_4)_2C_4H_8(COO)_2$] polymer electrolyte. *Journal of Polymers, 2013*, Article#752596. https://doi.org/10.1155/2013/752596

Pandikumar, A. & Ramaraj, R. (Ed.). (2018). *Rational Design of Solar Cells for Efficient Solar Energy Conversion*. New Jersey, USA: John Wiley & Sons.

Park, J. H., Lee, M. A., Park, B. J., & Choi, H. J. (2007). Preparation and electrophoretic response of poly (methyl methacrylate-co-methacrylic acid) coated TiO_2 nanoparticles for electronic paper application. *Current Applied Physics*, *7*(4), 349–351.

Park, N. G., Chang, S. H., Van de Lagemaat, J., Kim, K. J., & Frank, A. J. (2000). Effect of cations on the open-circuit photovoltage and the charge-injection efficiency of dye-sensitized nanocrystalline rutile TiO2 films. *Bulletin of the Korean Chemical Society*, *21*(10), 985–988.

Park, N., & Kim, K. (2008). Transparent solar cells based on dye-sensitized nanocrystalline semiconductors. P*hysica Status Solidi (a)*, *205*(8), 1895–1904.

Parker, A. J. (1969). Protic-dipolar aprotic solvent effects on rates of bimolecular reactions. *Chemical Reviews*, *69*(1), 1–32.

Petkovic, M., Seddon, K. R., Rebelo, N., & Silva, C. (2011). Ionic liquids : A pathway to environmental acceptability. *Chemical Society Reviews*, *40*(3), 1383–1403.

Petrowsky, M., & Frech, R. (2009). Temperature dependence of ion transport: The compensated arrhenius equation. *Journal of Physical Chemistry B*, *113*(17), 5996–6000.

Phuong, T., Pham, T., Cho, C., & Yun, Y. (2010). Environmental fate and toxicity of ionic liquids : A review. *Water Research*, *44*(2), 352–372.

Ponrouch, A., Marchante, E., Courty, M., Tarascon, J., & Palac, M. R. (2012). In search of an optimized electrolyte for Na-ion batteries. *Energy & Environmental Science*, *5*(9), 8572–8583.

Prabavathy, N., Shalini, S., Balasundaraprabhu, R., Velauthapillai, D., Prasanna, S., & Muthukumarasamy, N. (2017). Enhancement in the photostability of natural dyes for dye-sensitized solar cell (DSSC) applications: A review. *International Journal of Energy Research*, *41*(10), 1372–1396.

Universiti Malaya

Przytuski, J., & Wieczorek, W. (1992). Copolymer electrolytes. *Solid State Ionics*, *56*, 1071–1076.

Raga, S. R., & Fabregat-santiago, F. (2013). Temperature effects in dye-sensitized solar cells. *Physical Chemistry Chemical Physics*, *15*(7), 2328–2336.

Raghavan, V. (2011). *Materials Science and Engineering: A First Course, 5th ed.* Prentice-Hall of India Pvt.Ltd.

Rajendran, S., Ramesh Prabhu, M., & Usha Rani, M. (2008). Characterization of PVC/PEMA based polymer blend electrolytes. *International Journal of Electrochemical Science*, *3*(3), 282–290.

Ramesh, S., & Bing, K. N. (2012). Conductivity , mechanical and thermal studies on poly (methyl methacrylate) -based polymer electrolytes complexed with lithium tetraborate and propylene carbonate. *Journal of materials engineering and performance*, *21*(1), 89–94.

Ramesh, S., & Liew, C. (2013). Dielectric and FTIR studies on blending of [x PMMA – (1À x) PVC] with LiTFSI. *Measurement*, *46*(5), 1650–1656.

Ramesh, S., Liew, C., & Ramesh, K. (2011). Evaluation and investigation on the effect of ionic liquid onto PMMA-PVC gel polymer blend electrolytes. *Journal of Non-Crystalline Solids*, *357*(10), 2132–2138.

Ramesh, S., Liew, C. W., & Arof, A. K. (2011). Ion conducting corn starch biopolymer electrolytes doped with ionic liquid 1-butyl-3-methylimidazolium hexafluorophosphate. *Journal of Non-Crystalline Solids*, *357*(21), 3654–3660.

Ramya, C. S., Selvasekarapandian, S., Savitha, T., Hirankumar, G., & Angelo, P. C. (2007). Vibrational and impedance spectroscopic study on PVP-NH4SCN based polymer electrolytes. *Physica B: Condensed Matter*, *393*(1–2), 11–17.

Roslan, N., Ya, M. E., Radzi, M. A. M., Hashimoto, Y., Jamaludin, D., & Chen, G. (2018). Dye Sensitized Solar Cell (DSSC) greenhouse shading : New insights for solar radiation manipulation. *Renewable and Sustainable Energy Reviews*, *92*, 171–186.

Rudhziah, S., Ahmad, A., Ahmad, I., & Mohamed, N. S. (2015). Biopolymer electrolytes based on blend of kappa-carrageenan and cellulose derivatives for potential application in dye sensitized solar cell. *Electrochimica Acta*, *175*, 162–168.

Universiti Malaya

Salvador, G. P., Pugliese, D., Bella, F., Chiappone, A., Sacco, A., Bianco, S., & Quaglio, M. (2014). New insights in long-term photovoltaic performance characterization of cellulose-based gel electrolytes for stable dye-sensitized solar cells. *Electrochimica Acta*, *146*, 44–51.

Schild, H. G. (1993). Thermal degradation of poly (methacrylic acid): Further studies applying TGA/ FTlR. *Journal of Polymer Science Part A: Polymer Chemistry*, *31*(9), 2403–2405.

Sekar, N., & Gehlot, V. Y. (2010). Metal complex dyes for dye-sensitized solar cells: Recent developments. *Resonance*, *15*(9), 819–831.

Selamat, M. H., Zakaria, R., & Ahmad, A. H. (2017). Effects of sodium iodide (NaI) on electro-conductivity with polyurethane-diol organic electrolyte for dye-sensitized solar cell (DSSC). *Solid State Phenomena*, *268*, 358–362.

Selvanathan, V., Nasir, M., Halim, A., Azzahari, A. D., Rizwan, M., Shahabudin, N., & Yahya, R. (2018). Effect of polar aprotic solvents on hydroxyethyl cellulose-based gel polymer electrolyte. *Ionics*, *24*(7), 1955–1964.

Selvaraj, G. (2017). *Quinolinium based ionic liquids as electrolyte for dye sensitised (DSSC)* (Master's thesis, Universiti Teknologi Petronas). Retrieved from https://www.researchgate.net/publication/349172572_QUINOLINIUM_BASED_IONIC_LIQUIDS_AS_ELECTROLYTE_FOR_DYE_SENSITIZED_SOLAR_CELLS_DSSC/stats

Shalini, S., Balasundaraprabhu, R., Satish Kumar, T., Prabavathy, N., Prasanna, S., & Senthilarasu, S. (2016). Status and outlook of sensitizers/dyes used in dye sensitized solar cells (DSSC): A review. *International Journal of Energy Research*, *40*(10), 1303–1320.

Sharma, K., Sharma, V., & Sharma, S. S. (2018). Dye-sensitized solar cells : Fundamentals and current status. *Nanoscale Research Letters*, *13*(1), Article#381.

Shashkov, M. V., & Sidelnikov, V. N. (2019). New stationary ionic liquid phases with quinolinium cations for capillary gas chromatography new stationary ionic liquid phases with quinolinium cations for capillary gas chromatography. *Analytical Letters*, *53*(1), 84–101.

Shih, C., Wu, Y., Wang, Y., Kumar, S. R., Tung, Y., Yang, C., & Jessie, S. (2018). Ionic transport and interfacial interaction of iodide / iodine redox mechanism in agarose electrolyte containing colloidal titanium dioxide nanoparticles. *Journal of Photochemistry & Photobiology, A: Chemistry*, *356*, 565–572.

Universiti Malaya

Siggel, M. R. F., Streitwieser, A., & Thomas, T. D. (1988). The role of resonance and inductive effects in the acidity of carboxylic acids. *Journal of the American Chemical Society*, *110*(24), 8022–8028.

Simon, S. J. C., Parlane, F. G. L., Swords, W. B., Kellett, C. W., Du, C., Lam, B., … Berlinguette, C. P. (2016). Halogen bonding promotes higher dye-sensitized solar cell photovoltages. *Journal of the American Chemical Society*, *138*(33), 10406–10409.

Singh, H. P., & Sekhon, S. (2003). Conductivity behaviour of proton conducting polymer gel electrolytes with PVdF-HFP. *European Polymer Journal*, *39*(1), 93–98.

Singh, M., Singh, V. K., Surana, K., Bhattacharya, B., Singh, P. K., & Rhee, H. (2013). New polymer electrolyte for electrochemical application. *Journal of Industrial and Engineering Chemistry*, *19*(3), 819–822.

Singh, R., Jadhav, N. A., Majumder, S., Bhattacharya, B., & Singh, P. K. (2013). Novel biopolymer gel electrolyte for dye-sensitized solar cell application. *Carbohydrate Polymers*, *91*(2), 682–685.

Singh, R., Polu, A. R., Bhattacharya, B., Rhee, H. W., Varlikli, C., & Singh, P. K. (2016). Perspectives for solid biopolymer electrolytes in dye sensitized solar cell and battery application. *Renewable and Sustainable Energy Reviews*, *65*, 1098–1117.

Sinha, D., De, D., Goswami, D., & Ayaz, A. (2018). Fabrication of DSSC with nanostructured ZnO photoanode and natural dye sensitizer. *Materials Today: Proceedings*, *5*(1), 2056–2063.

Souquet, J., Luis, M., Nascimento, F., Candida, A., Rodrigues, M., Souquet, J., Luis, M., & Nascimento, F. (2010). Charge carrier concentration and mobility in alkali silicates Charge carrier concentration and mobility in alkali silicates. *The Journal of Chemical Physics*, *132*(3), Article#034704. https://doi.org/10.1063/1.3271154

Sridhar, N., & Freeman, D. (2011). A study of dye sensitized solar cells under indoor and low level outdoor lighting: comparison to organic and inorganic thin film solar cells and methods to address maximum power point trackin. *European Photovoltaic Solar Energy Conference*, 232–236.

Su'ait, M. S., Rahman, M. Y. A., & Ahmad, A. (2015). Review on polymer electrolyte in dye-sensitized solar cells (DSSCs). *Solar Energy*, *115*, 452–470.

Subramania, A., Vijayakumar, E., Sivasankar, N., Sathiya Priya, A. R., & Kim, K. J. (2013). Effect of different compositions of ethylene carbonate and propylene carbonate containing iodide/triiodide redox electrolyte on the photovoltaic performance of DSSC. *Ionics*, *19*(11), 1649–1653.

Universiti Malaya

Sundararajan, V., Selvaraj, G., Ng, H. M., Ramesh, S., Ramesh, K., Wilfred, C. D., & Bashir, S. (2017). Exploring the effect of novel N-butyl-6-methylquinolinium bis(trifluoromethylsulfonyl)imide ionic liquid addition to poly(methyl methacrylate-co-methacrylic) acid electrolyte system as employed in gel-state dye sensitized solar cells. *Electrochimica Acta*, *240*, 361–370.

Syairah, A., Khanmirzaei, M. H., Saidi, N. M., Farhana, N. K., Ramesh, S., Ramesh, K., & Ramesh, S. (2018). Effect of different imidazolium-based ionic liquids on gel polymer electrolytes for dye-sensitized solar cells. *Ionics*, *25*(5), 2427–2435.

Tan, C. Y., Farhana, N. K., Saidi, N. M., Ramesh, S., & Ramesh, K. (2018). Conductivity, dielectric studies and structural properties of P(VA-co-PE) and its application in dye sensitized solar cell. *Organic Electronics*, *56*, 116–124.

Thakur, Y., Zhang, B., Dong, R., Lu, W., Iacob, C., Runt, J., Bernholc, J., & Zhang, Q. M. (2016). Generating high dielectric constant blends from lower dielectric constant dipolar polymers using nanostructure engineering. *Nano Energy*, *32*, 73–79.

Thapa, R., & Park, N. (2012). First-principles identification of iodine exchange mechanism in iodide ionic liquid. *The Journal of Physical Chemistry Letters*, *3*(20), 3065–3069.

Tommasini, F. J., Ferreira, L. da C., Tienne, L. G. P., Angular, V. de O., & Silva, H. P. (2018). Poly (methyl methacrylate)-SiC nanocomposites prepared through in situ polymerization. *Materials Research*, *21*(6), Article#20180086.

Ulu, A., Koytepe, S., & Ates, B. (2016). Design of starch functionalized biodegradable P(MAA-co-MMA) as carrier matrix for l-asparaginase immobilization. *Carbohydrate Polymers*, *153*, 559–572.

Venkatesan, S., Hidayati, N., Liu, I., & Lee, Y. (2016). Highly efficient gel-state dye-sensitized solar cells prepared using propionitrile and poly(vinylidene fluoride-co-hexafluoropropylene). *Journal of Polymers*, *336*, 385–390.

Vignarooban, K., Dissanayake, M. A. K. L., Albinsson, I., & Mellander, B. (2014). Effect of TiO2 nano-filler and EC plasticizer on electrical and thermal properties of poly(ethylene oxide) (PEO) based solid polymer electrolytes. *Solid State Ionics*, *266*, 25–28.

Wang, X., Deng, R., Kulkarni, S. A., Wang X., Pramana, S. S., Wong, C. C., … Mhaisalkar, S. (2013). Investigation of the role of anions in hydrotalcite for quasi-solid state dye-sensitized solar cells application. *Jounal of Materials Chemistry A*, *1*(13), 4345–4351.

Universiti Malaya

Wang, P., Zakeeruddin, S. M., & Gr, M. (2002). High efficiency dye-sensitized nanocrystalline solar cells based on ionic liquid polymer gel electrolyte. *Chemical Communications*, *24*, 2972–2973.

Wasserscheid, P., & Welton, T. (2008). *Ionic Liquids in Synthesis* (Vol. 1). Wiley online library.

Watanabe, M., & Ogata, N. (1988). Ionic conductivity of polymer electrolytes and future applications. *British Polymer Journal*, *20*(3), 181–192.

Wei, Z. (2011). *Fabrication of dye sensitized solar cells with enhanced energy conversion efficiency*. National University of Singapore.

Wen, L. C. (2011). *Investigations on Lithium ion conductivity and characterization of PMMA-PVC based polymer electrolytes incorporating ionic liquid and nano-filler*. Universiti Tunku Abdul Rahman.

Wijeratne, K., Akilavasan, J., Thelakkat, M., & Bandara, J. (2012). Enhancing the solar cell efficiency through pristine 1-dimentional SnO2 nanostructures : Comparison of charge transport and carrier lifetime of SnO2 particles vs . nanorods. *Electrochimica Acta*, *72*, 192–198.

Wilkinson, A. D. M. and A. (1997). *Compendium of chemical terminology vol. 1669*. Blackwell Science Oxford.

William E. Acree, Jr., J. S. C. (n.d.). Infrared Spectra. In P. J. L. and W. G. Mallard (Ed.), *NIST Chemistry WebBook, NIST Standard Reference Database Number 69*. National Institute of Standards and Technology, Gaithersburg MD.

Wu, J., Lan, Z., Hao, S., Li, P., Lin, J., Huang, M., Fang, L., & Huang, Y. (2008). Progress on the electrolytes for dye-sensitized solar cells. *Pure and Applied Chemistry*, *80*(11), 2241–2258.

Wu, J., Lan, Z., Lin, J., Huang, M., Huang, Y., Fan, L., & Luo, G. (2015). Electrolytes in dye-sensitized solar cells. *Chemical Reviews*, *115*(5), 2136–2173.

Wu, J., Lan, Z., Lin, J., Huang, M., Huang, Y., Fan, L., Luo, G., Lin, Y., Xie, Y., & Wei, Y. (2017). Counter electrodes in dye-sensitized solar cells. *Chemical Society Reviews*, *46*(19), 5975–6023.

Xia, L., Yu, L., Hu, D., & Chen, G. Z. (2017). Electrolytes for electrochemical energy storage. *Materials Chemistry Frontiers*, *1*(4), 584–618.

Universiti Malaya

Xu, S., Hu, H., Sebo, B., Chen, B., Tai, Q., & Zhao, X. (2011). Modification of nanocrystalline porous films by poly(ethyleneglycol) for quasi-solid dye-sensitized solar cells. *Journal of Power Sources*, *196*(24), 10817–10821.

Yang, C., Ho, W., Yang, H., & Hsueh, M. (2010). Approaches to gel electrolytes in dye-sensitized solar cells using pyridinium molten salts. *Journal of Materials Chemistry*, *20*(29), 6080–6085.

Yang, F. (2008). *Thin film solar cells grown by organic vapor phase deposition*. Princeton University.

Yang, H., Huang, M., Wu, J., Lan, Z., Hao, S., & Lin, J. (2008). The polymer gel electrolyte based on poly(methyl methacrylate) and its application in quasi-solid-state dye-sensitized solar cells. *Materials Chemistry and Physics*, *110*(1), 38–42.

Ye, Y., Rick, J., & Hwang, B. (2013). Ionic liquid polymer electrolytes. *Journal of Materials Chemistry A*, *8*(1), 2719–2743.

Yu, B., Zhou, F., Wang, C., & Liu, W. (2007). A novel gel polymer electrolyte based on poly ionic liquid 1-ethyl 3-(2-methacryloyloxy ethyl) imidazolium iodide. *European Polymer Journal*, *43*(6), 2699–2707.

Yusuf, S. N. F., Azzahari, a. D., Yahya, R., Majid, S. R., Careem, M. a., & Arof, a. K. (2016). From crab shell to solar cell: a gel polymer electrolyte based on N-phthaloylchitosan and its application in dye-sensitized solar cells. *RSC Advances*, *6*(33), 27714–27724.

Zallen, R., Mahan, G. D. M., & Douglas, R. W. (2008). *The Physics of Amorphous Solids*. Weinheim, Germany: *John Wiley & Sons*.

Zebardastan, N., Khanmirzaei, M. H., Ramesh, S., & Ramesh, K. (2017). Performance enhancement of poly (vinylidene fluoride-co-hexafluoro propylene)/polyethylene oxide based nanocomposite polymer electrolyte with ZnO nanofiller for dye-sensitized solar cell. *Organic Electronics*, *49*, 292–299.

Zhang, D., Zhu, H., Xu, W., Shuai, Z., & Zhu, D. (2003). Structural and magnetic studies of quinoline and N -methyl quinolinium-substituted nitronyl nitroxides. *Synthetic Metals*, *139*(2), 479–483.

Zhang, Q., & Cao, G. (2011). Nanostructured photoelectrodes for dye-sensitized solar cells. *Nano Today*, *6*(1), 91–109.

Universiti Malaya

Zistler, M., Wachter, P., Wasserscheid, P., Gerhard, D., Hinsch, A., Sastrawan, R., & Gores, H. J. (2006). Comparison of electrochemical methods for triiodide diffusion coefficient measurements and observation of non-Stokesian diffusion behaviour in binary mixtures of two ionic liquids. *Electrochimica Acta*, *52*, 161–169.

BP Statistics. (2019). BP Statistical Review of World Energy 2019. Retrieved from https://www.bp.com/content/dam/bp/business-sites/en/global/corporate/pdfs/energy-economics/statistical-review/bp-stats-review-2019-full-report.pdf.

Universiti Malaya

LIST OF PUBLICATION AND PAPERS PRESENTED

List of publications

1. **Sundararajan, V**., Selvaraj, G., Ng, H. M., Ramesh, S., Ramesh, K., Wilfred, C. D., & Bashir, S. (2017). Exploring the effect of novel N-butyl-6-methylquinolinium bis(trifluoromethylsulfonyl)imide ionic liquid addition to poly(methyl methacrylate-co-methacrylic) acid electrolyte system as employed in gel-state dye sensitized solar cells. *Electrochimica Acta*, *240*, 361–370.

2. **Sundararajan, V**., Saidi, N.M., Ramesh, S., Ramesh, K., Selvaraj, G., & Wilfred, C.D. (2019). Quasi solid-state dye-sensitized solar cell with P(MMA-co-MAA)-based polymer electrolytes. *Journal of Solid State Electrochemistry*. *23*(4), 1179-1189.

3. **Sundararajan, V**., Farhana, N.K., Ng, H.M., Ramesh, S., & Ramesh, K. (2019). Efficiency enhancement study on addition of 1-hexyl-3-methylimidazolium iodide ionic liquid to the poly (methyl methacrylate-co-methacrylic acid) electrolyte system as applied in dye-sensitized solar cells. *Journal of Physics and Chemistry of Solids*, *129*, 252-260.

Papers Presented

1. **Sundararajan, V.**, Ng, H.M., Ramesh, S., & Ramesh, K. (2016). Efficiency enhancement using ionic liquid in PMMA-co-MAA based gel polymer electrolytes for dye sensitized solar cells (DSSCs), presented in National Physics Conference 2016 (PERFIK 2016), 21-22 December 2016, Kuala Lumpur Malaysia.

Universiti Malaya